8-2013

SYNTHESIS AND CHARACTERIZATION OF THERMALLY RESPONSIVE POLYMER LAYERS

Michael Seeber
Clemson University, mseeber@g.clemson.edu

SYNTHESIS AND CHARACTERIZATION OF THERMALLY RESPONSIVE POLYMER LAYERS

A Dissertation
Presented to
the Graduate School of
Clemson University

In Partial Fulfillment
of the Requirements for the Degree
Doctor of Philosophy
Materials Science and Engineering

---

by
Michael Seeber
August 2013

Accepted by:
Dr. Igor Luzinov, Committee Chair
Dr. Konstantin Kornev
Dr. Olin Mefford
Dr. Scott Husson
Dr. Bogdan Zdyrko

ABSTRACT

Future devices such as biomedical and microfluidic devices, to a large extent, will depend on the interactions between the device surfaces and the contacting liquid. Further, biological liquids containing proteins call for controllable interactions between devices and such proteins, however the bulk material must retain the inherent mechanical properties from which the device was fabricated from. It is well known that surface modification is a suitable technique to tune the surface properties without sacrificing the bulk properties of the substrate.

In the present study, surface properties were modified through temperature responsive polymer layers. After the modification, the surfaces gained switchability toward protein interaction as well as surface wettability properties. Poly(*N*-isopropylacrylamide) (PNIPAM), a well studied thermo-responsive polymer was utilized in the subsequent work.

Firstly, thermally responsive brushes made from well defined block copolymers incorporating NIPAM and the surface reactive monomer, glycidyl methacrylate (GMA) were fabricated in a single step process. Reaction of the PGMA block with surface hydroxyl groups anchors the polymers to the surface yet allows PNIPAM to assemble at the interface at high enough concentration to exhibit thermally responsive properties in aqueous solutions. Surface properties of the resulting brushes prepared the 1-step process are compared to characteristics of PNIPAM brushes synthesized by already established methods.

The thickness, swelling, and protein adsorption of the PNIPAM films were studied by ellipsometry. Chemical composition of the layer was studied by angle-resolved x-ray photoelectron spectroscopy. Film morphologies and forces of adhesion to fibrinogen were examined using atomic force microscopy (AFM) tapping mode and colloidal probe technique. Block copolymer (BCP) and conventional brush films were abraded and subsequently examined for changes in thermally responsive behavior. The results show that deposition of PNIPAM-*b*-PGMA provides an effective route to create thermally responsive brushes via a 1-step process, with properties equaling and surpassing that of traditional brushes obtained in multiple steps.

Further, the 1-step deposition of reactive BCPs can be extended to fabricate mixed block copolymer films. Well defined BCP containing ethylene glycol and GMA were deposited from a joint solution with PNIPAM-*b*-PGMA. Mixed brush films were also fabricated via a 2-step process for comparison of the resulting properties. PNIPAM BCP layers were utilized as the grafted primary layer with which end-functionalized PEG was grafted in a second step. Protein adhesion and adsorption of the resulting mixed brush films were studied by AFM colloidal probe technique and ellipsometry.

In the next part of the work reported, monolayers of PNIPAM containing nanogels were anchored to the surface of silicon wafers, glass slides, polyvinylidene fluoride (PVDF) fibers, and tungsten wires using a "grafting to" approach. The particles of were synthesized with different diameters by free radical precipitation polymerization and reversible addition chain transfer polymerization (RAFT) techniques. The behavior of the synthesized grafted layers with the behavior of PNIPAM brushes (densely end-

grafted) is compared. Indeed, the grafted monolayer swells and collapses reversibly at temperatures below and above the transition temperature of PNIPAM. AFM in aqueous environment was utilized to study the actuation behavior of the nanogel films. Wettability studies of the grafted layers were performed using various contact angle measurement methods to determine the contact angle changes on different substrates.

New methods for the development of thermally responsive polymer films are described. The methods enable the grafting of films with tunable film thickness, temperature response, and well defined biological interaction. The complete grafting of the responsive polymer films require no organic rinsing after grafting step.

DEDICATION

This work is dedicated to my parents Doug and Colleen Seeber, who have supported and believed in me and been there through all the happy and tough times throughout my entire life. Thank you for all the sacrifices you have made to make this happen. I would also like to dedicate this to my girlfriend Christy, who was also extremely supportive and never left my side through the last three years of my PhD journey.

ACKNOWLEDGMENTS

Firstly, I would like to thank my advisor, Dr. Igor Luzinov for his guidance in both scientific and life settings, patience, and encouragement during my research work and writing progression.

I also appreciate the time and helpful suggestions from my committee members, Dr. Konstantin Kornev, Dr. Olin Mefford, Dr. Scott Husson, and Dr. Bogdan Zdyrko.

I also owe a special ode of gratitude to Dr. Ruslan Burtovvy for his patience and willingness to teach and improve me as a scientist. He spent many hours sitting with me discussing, and helping me with various topics.

I also owe a debt of gratitude to Mr. and Mrs. Dr. Lickfield for all the help and fruitful discussions throughout my 5 years of work. The Lickfields taught me a lot towards becoming a scientific professional.

I would like to acknowledge Kimberly Ivey, who was always there for a great conversation, as well to teach and educate me on all her instruments. She was always willing to discuss and help me with my work no matter the time or situation.

I am grateful to Mr. Bob Bowen who originally made my enrollment to Clemson possible through his recruiting efforts. I also am very thankful for all the events and cookouts Bob hosted which created a family atmosphere at Clemson and within the Material Science department.

I am thankful to Dr. Michael Kilbey II and Dr. Bradley Lokitz at Oak Ridge National Lab for helping to make my work possible, and allowing me to work in their wonderful laboratory, along with their fruitful discussions and suggestions.

A special thanks to Yuriy Galabura, Taras Andrukh, and Sasha Tokarev, whom I shared an office area with the last two years of my studies. We had great times together all throughout our studies.

I would like to acknowledge my research group; Yuriy Galabura, Fehime Vatansever, James Giammarco, Jake Townsend, Tugba Demir, AP Soliani, Bernice Nizioki, Dr. Marius Chyasnavichyus, and Dr. Olga Hoy, whom made the last 5 years of life an amazing experience. Thank you for all the encouragement, support, and helpful suggestions that you provided me throughout my graduate studies.

I am grateful to the Department of Material Science and Engineering at Clemson University for the possibility and opportunity to achieve my PhD degree. Clemson will always feel like home to me.

TABLE OF CONTENTS

Page

Table of Contents (Continued)

Page

Table of Contents (Continued)

Page

Table of Contents (Continued)

Page

Table of Contents (Continued)

Page

LIST OF FIGURES

Figure Page

List of Figures (Continued)

Figure Page

List of Figures (Continued)

Figure Page

List of Figure (Continued)

Figure Page

List of Figures (Continued)

Figure Page

List of Figures (Continued)

Figure Page

List of Figures (continued)

Figure Page

LIST OF TABLES

Table Page

List of Tables (Continued)

Table Page

CHAPTER 1:INTRODUCTION

Many current medical and biological devices used in medicine are made from polymeric materials.[1] It is well known that inserting materials into the human body or in contact with bodily fluids with incompatible properties will cause a surge of detrimental biological processes, such as, protein and platelet adsorption to medical devices. Such reactions will cause a potential failure of the device. Therefore, coatings that can control the amount of protein adsorption are of the utmost importance. To this end, stimuli-responsive polymer coatings have attracted an immense amount of attention due to their intrinsic ability to undergo adsorption property changes when exposed to environmental stimuli. Due to the ease and straightforwardness of temperature control, temperature responsive polymer systems have been one of the most widely studied subset of stimuli-responsive polymers. The progress of current medical and biological technologies has caused an immense amount of research directed towards Poly(*N*-isopropylacrylamide) (PNIPAM).

PNIPAM is a temperature responsive polymer that undergoes a conformational transition near physiological conditions (~32°), and is tunable by copolymerization. Therefore, modifications of the bulk substrate with polymers such as PNIPAM are extremely important for today's emerging complex applications. PNIPAM has been successfully utilized to control protein adsorption in an on and off manner, as well as cell

---

[1] *See Chapter 2 for in-depth references.*

attachment-detachment. Additionally, PNIPAM modified substrates enable the harvesting of confluent cell sheets, as well as the release of such cell sheets with the simple control over the environment temperature. However, the current methods used to create such coatings are complex and require multiple steps. Additionally, despite the diverse methods available to modify substrates, only a few have been implemented into industry. There is a continuing demand for a simple, cost effective, and universal method to modify bulk material with known controllable properties over, among other things, biological interaction.

The ultimate goal of this work is to develop modified surface grafting procedures for the synthesis of thermally responsive layers. The grafting procedures are based off the classical "grafting to" procedure in order to preserve the robust and simplistic experimental approach for future possibilities of large scale and continuous substrate modification processes in industrial settings. The fabricated layers containing PNIPAM are equal and in some formulations, surpass that of conventional PNIPAM coatings surface property switchability. I also have aimed to overcome a well documented limitation of the "grafting to" approach. That is, the maximum film thickness that can be created using such a technique. I further extend such techniques, and lay the foundational work towards the fabrications of mixed polymer brush layers concerning the construction of intelligent delivery surfaces that can activate a biological process or reaction on demand.

Two different strategies were employed to create surfaces with defined thermally responsive surface properties. These were the fabrication of responsive surfaces via a

single-step process through reactive block copolymers. Moreover, I also utilized PNIPAM nanoparticles capable of robust covalent attachment to various substrate surfaces.

In this dissertation, **Chapter 2** provides an overview of polymer brush properties, and synthetic techniques utilized to create polymer brush films. It will also provide an overview of the thermally responsive subset of polymer brushes and their unique aqueous solution behavior, including an in depth overview of reported work concerning PNIPAM. **Chapter 3** gives a description of the experimental methods used in this work.

Chapter 4 deals with the synthesis and characterization of thermally responsive layers by a modified "grafting to" approach via reactive block copolymers. The active layers were fabricated in a single-step method, thus eliminating the need for post treatment with organic solvents. The ability to tune the thickness of the polymeric layers was demonstrated. The uniformity of the resulting films was studied by atomic force microscopy (AFM) imaging. The chapter details the systematic study of the surface properties and actuation behavior of the responsive layers as a function of temperature and block copolymer segment length.

Chapter 5 describes for polymer layer-protein interaction. Protein interaction with the block copolymer films was studied as a function of temperature and block copolymer segment length. The work of adhesion values were determined for brush-protein contact via the AFM colloidal probe technique in an aqueous environment. The extent of protein adsorption to polymer grafted substrates was studied as a function of temperature and block copolymer molecular weight. However, such coatings implanted

into the body would undergo long term wear due to contact with other surfaces. Therefore, a method to study the change of properties after wearing was developed. The switchable protein adhesion ability of the block copolymer films was studied as a function of the temperature and the amount of abrasion. Finally, the changes in the protein interaction properties as a function of temperature was evaluated in comparison to conventional PNIPAM brush films.

The extension of the 1-step method for the fabrication of polymer brush films was confirmed by the fabrication of more complex layers in **Chapter 6**, namely mixed polymer brush films. I aimed to create the foundational work towards creation of an on-demand delivery coating, where active ligands can be delivered or hidden from a biocompatible matrix. Hence, our choice to utilize the biocompatible, non-toxic, and protein repelling polymer, poly(ethylene glycol) (PEG). Firstly, PEG based films were synthesized by the 1-step method via reactive block copolymers. The resulting surface properties and protein interaction were characterized by methods previously utilized with PNIPAM containing films. Further, mixed brush films were constructed by two different procedures containing PNIPAM and PEG. In the first method, mixed brush films were created in a single-step method by creating a mixed solution of both reactive block copolymers. In a second method, primary grafted layers were deposited from PNIPAM reactive block copolymers and subsequently modified with end-functionalized PEG. Both methods were compared for the activity towards protein adsorption behavior as a function of temperature.

Chapter 7 is devoted to an alternative method for the fabrication of relatively thick thermally responsive polymer layers. PNIPAM containing thermoresponsive nanogels were synthesized with carboxy functionalities by copolymerization with acrylic acid. Monolayers of nanogel particles were grafted onto various substrates including silicon wafers, PVDF fibers, glass slides, and tungsten wires by the "grafting to" procedure using poly(glycidyl methacrylate) (PGMA) anchoring layers. The composition of the resulting particles was analyzed by NMR spectroscopy. The layers were characterized for their thermoresponsive surface properties and compared to conventional brush films. AFM was utilized to characterize the swelling and collapse of the microgel layers as a function of temperature and acrylic acid content. Various contact angle measurement techniques were employed to study the surface wettability changes as a function of temperature on silicon wafers as well as more complex surfaces of tungsten wire.

Chapter 8 is devoted towards the synthesis of the thermoresponsive nanogel with decreased diameter as compared to the ones reported in **Chapter 7**. Nanogels polymerization was conducted by a surfactant free polymerization in water by utilization of macroRAFT chain transfer polymerization. The macroRAFT agent used was functionalized with acrylic acid units to ensure graftability of the resulting nanogels. The thermoresponsive properties of the particles in aqueous solution were characterized by dynamic light scattering (DLS) studies. Interestingly, the resulting thickness of the nanogels films could be tuned by the solvent chosen for deposition. Finally, the particles

were evaluated for their ability to attach to non flat surfaces such as electrospun PVDF fibers.

In conclusion, this dissertation provides the fundamentals for the grafting of thermally responsive polymer films using modified "grafting to" procedures. The reactive block copolymer methods were characterized for their surface properties as a function of temperature as well as their interaction with protein. The nanogel layers were characterized for their thermo-responsive properties in water as well as their ability to be grafted to complex surfaces and retain their wettability switching properties.

CHAPTER 2:LITERATURE REVIEW

Current research is devoted to the synthesis, characterization and application of thermally responsive polymer brushes. The study requires the understanding of polymer brushes, grafting concepts, and polymer solution behavior. Herein, this chapter gives an overview of polymer brushes, polymer brush preparation by various grafting techniques, unique polymer solution behavior, and an introduction to polymer brushes with respect to a known thermally responsive polymer, poly(*N*-isopropylacrylamide) (PNIPAM).

2.1:Polymer Brushes. Definition and General Properties:

Polymer assemblies at interfaces have long fascinated scientists for nearly a half century within both basic and applied research. Thin polymer films are most intensely used for modification of surfaces in order to alter properties of the bulk material. Dating back, much interest towards polymer molecules at surfaces originated due to importance within different technologies such as; wetting[6], corrosion[7], colloidal stability[7-9], adhesion[10], lubrication[11], and chromatographic devices.[12] Historically, polymer brush science was propelled by the discovery in the 1950's, that grafting of polymer brush films could prevent aggregation of colloidal particles. Van der Waarden utilized hydrocarbon based polymers to stabilize carbon black particles.[9]

Polymer brushes are defined as polymeric assemblies tethered to a substrate by one end.[2, 7, 13] The term "brush" is considered when end-tethered molecules are attached at close proximity where the distance between "grafting' sites is less than two radii of gyration.[13] Such proximity of the polymer molecules forces overlap between the

neighboring chains and alters the conformational dimension. The deformation of the anchored chains is, therefore, governed by a balance between the segment-segment interaction and elastic free energy of the system. As grafting density is decreased, the segment-segment interaction increases, subsequently increasing the interaction energy. As a result, the polymer molecules extend and stretch in order to avoid thermodynamic unfavorable conditions, decreasing the monomer-monomer interaction and increasing the layer thickness, forming "brush" conditions.[14]

Alexander first considered this balance between interaction and elastic free energy.[15-16] He considered monodisperse polymer chains tethered to nonadsorbing surfaces. The final minimization of the polymer chain energy with respect to the layer thickness yielded the following scaling **Equation (2.1)**:

$$L / a \approx N(a / d)^{2/3} \tag{2.1}$$

Table 2.1: Polymer chain size in the brush and solution.[5] *Reprinted with permission from Elsevier.*

	Polymer Brush	**Free Polymer Chain**
Good Solvent	$L/a \sim N(a/d)^{2/3}$	$R_g \sim N^{3/5}$
Theta Solvent	$L/a \sim N(a/d)$	$R_g \sim N^{1/2}$
Bulk State	$L \sim N^{2/3}$	$R_g \sim N^{1/2}$

where L is the layer thickness, a is the average segment diameter, d is the distance between grafting sites, and N is the degree of polymerization. Therefore, as described by **Equation (2.1)**, the thickness of the polymer "brush" layer scales linearly with the degree of polymerization. This was a significant finding within polymer science because it was previously determined that the same relationship as determined by Flory for polymer chains in a good solvent scaled non-linearly with degree of polymerization, $R \sim N^{3/5}$.[17] The balance between interaction and free elastic energy has been described within a range of environments such as theta solvents, bad solvents, and the bulk state. The relationship and comparison between degree of polymerization N, and the dimensions of the brush and free polymer chains is described in **Table 2.1.**

As observed from **Table 2.1** the behavior of polymer brushes and polymer coils in solution is much different. It was this novel discovery that has lead to many new and unique properties that have been generated by polymer brush films.[18] To date, polymer brushes have found numerous interesting applications in adhesives[10], control of protein and cell adsorption[19-21], flocculation control[9], and stimuli responsive surfaces to such factors as, pH[22], light[23], redox potential[24], and temperature.[25-27]

2.2:Formation of Polymer Brushes:

Physisorption and covalent attachment are the two major methods for the fabrication of polymer brushes. Consequently, attachment of the polymer chains can be reversible or irreversible.[5] In general, the reversible formation of polymer tethered films is created through preferential adsorption of block copolymers. Specifically, one block

strongly interacts with the surface while the second block weakly interacts creating polymer chains in an end tethered nature. Moreover, there are two major techniques used to fabricate irreversible polymer brush layers via covalent attachment, referred to as "grafting to" and grafting from".[5, 28-29] The "grafting to" technique is carried out via the covalent reaction of pre-synthesized polymer molecules that are end functionalized with complimentary functional groups to ones present on the surface deemed for modification. On the other hand, "grafting from" methods are conducted by polymerizing monomer from surfaces modified with initiator species. Initiator species attached to the surface are activated in the presence of monomer and sacrificial initiator in solution or bulk states. Polymer chains are subsequently grown from the substrates surface. All of the above mentioned procedures are illustrated in **Figure 2.1**.

2.2.1:Physisorption

Early studies of polymer brushes were carried out using the physisorption process. This leads to polymer brush films that are reversibly attached by nature with which the process is primarily directed by thermodynamics.[18, 30-31] Physisorption causes polymer chains to bind to a surface through physical forces such as; hydrogen bonding, van der Waals, and electrostatic interactions.[31] Typically, a diblock or graft copolymer is used for the fabrication of polymer brush layers by physisorption. The surface is selected to maximize the selective adsorption of one block, while the other block forms a stretched brush structure due to selective solvation.[18] The resulting polymer brush structure is dependent on a variety of factors such as; selectivity of solvent and surface, copolymer

molecular weight, chemical composition, architecture, and interaction strengths of the individual block towards the solvent and surface.[31]

An example of utilizing a selective solvent for the preferential deposition of block copolymers towards the generation of polymer brush films was carried out by Parsonage

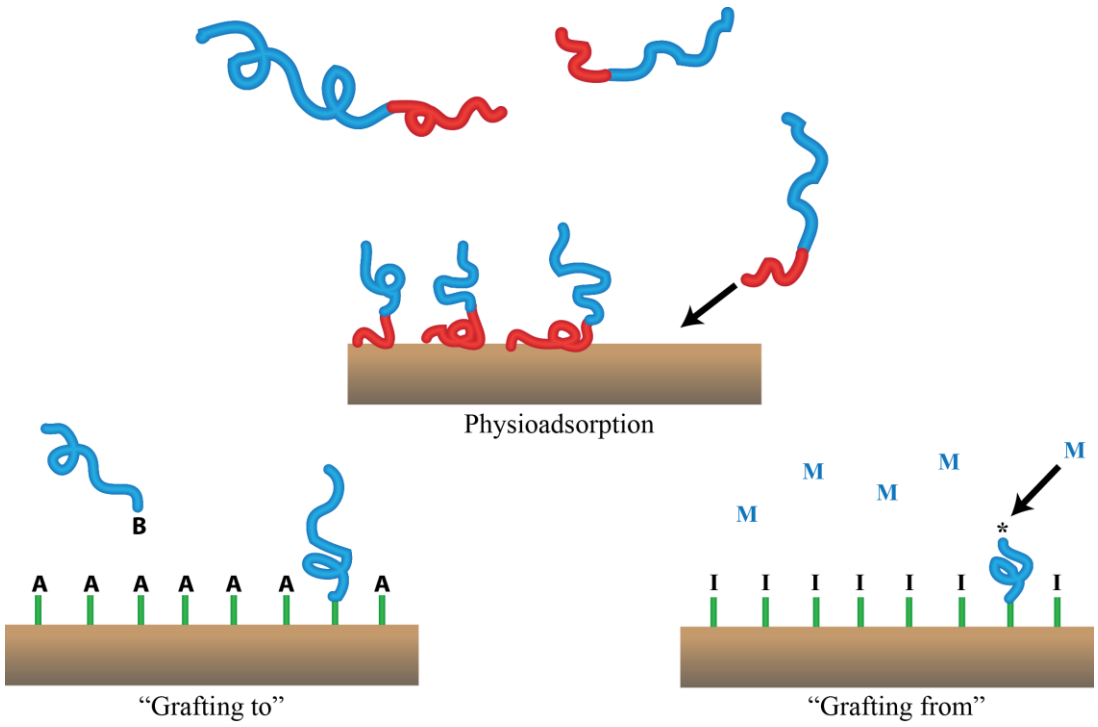

Figure 2.1: Formation of polymer brushes by physioadsorption, "grafting to" and "grafting from" methods.[2, 5] *Reprinted with permission from Elsevier*.

et al.[32] by deposition of poly(2-vinylpyridine) (PVP)-b-poly (styrene) (PS) from toluene onto silicon and mica surfaces. Various molecular weights and block copolymer composition were studied to determine the adsorbed amount on the substrate surface. They found that for copolymers consisting of "moderate asymmetry" the surface density of the adsorbed copolymer was more strongly influenced by the adsorbing block (PVP).

However, for higher degrees of asymmetry (smaller PS block), they found the surface density was reflected by the molecular weight of the solvated block, PS.

On the other hand, surfaces can be selected that preferentially adsorb one component of the block copolymer while the non-adsorbing segment forms a polymer brush. Guzonas et al.[33] utilized mica surfaces to selectively adsorb one segment of PS-poly ethylene oxide (PEO) block copolymers at different asymmetry ratios by surface force measurements. They found distinct differences in the thickness of the resulting films when the non-adsorbing block size approached the size of the adsorbing block or larger, respectively.

One can see that physisorption is a facile and convenient approach towards the fabrication of polymer brush layers. However, physioadsorption suffers from low stability of the resulting modified surfaces. Such instabilities can appear due to thermal and/or solvent treatments.[31] Upon treatment with a good solvent, polymer molecules can be removed from the surface. Additionally, molecules with a higher affinity for the surface can displace the adsorbed macromolecules.[34] Moreover, Sharma et al.[35] found that thermal treatment of such physisorbed polymer brush layers dewetted above the glass transition behavior by growth of cylindrical holes and rim patterns. The ascertained drawbacks of the physisorption process can be readily overcome by the covalent attachment by one end of macromolecules.

2.2.2:"Grafting from" Technique

The "grafting from" technique is carried out via the polymerization of monomer species from functionalized surfaces containing initiating groups. Surface functionalization with initiating species can be prepared by variety of methods including, self-assembled mono layers with incorporated initiators, and thin reactive polymer films.[36] Plasma or glow discharge can also be utilized to generate free radical species on the surface succeeded by polymerization reactions. With the recent advances in polymerization technology, both free radical and controlled free radical, cationic and anionic polymerizations have been successfully conducted from functionalized surfaces yielding polymer brushes via the "grafting from" procedure.

For instance, Boven et al.[37] formed SAM layers with 3-aminopropyltriethyoxysilane (APS) to obtain reactive amino groups on surfaces. Azo bearing initiators were reacted to the APS layer through an acid chloride-amino reaction creating surface bound initiating groups. Poly(methyl methacrylate) molecules were then formed via the conventional radical polymerization in the presence of monomer.

Various controlled or "living" free radical polymerizations were used to generate polymer brushes via the "grafting from" method.[38-42] Husseman et al.[43] prepared a wide variety of polymer brush structures utilizing atom transfer radical polymerization (ATRP) from surface bound alkoxyamines and R-halo esters in the presence of a catalyst. They observed that molecular weight and polydispersity (PDI) could be accurately controlled.

Moreover, they successfully synthesized more complex structures such as end-tethered block copolymers by the sequential addition of different monomers.

On the other hand, reversible addition-fragmentation chain transfer (RAFT) polymerization mechanisms were also utilized to grow polymer brushes via the "grafting from" technique. The living polymerization mechanism is based off a transfer of an active free radical to a di or trithioester moiety, creating dormant and active species. The dynamic equilibrium between the two states affords the uniform control over polymer chains. Thus time can be varied in order to control brush length in a linear relationship.[44] For example, Baum et al.[45] utilized RAFT polymerization by first immobilizing a RAFT azo initiator on the surface of silicon wafers. Polymer brushes with controlled thickness were produced of PS, PMMA, and *N,N*-dimethylacrylamide (DMA). Also, to display the living nature of the reaction, they synthesized block copolymer brushes of PS-PDMA and PDMA-PMMA that displayed responsive properties based on solvent treatment.

"Grafting from" reactions provide the opportunity to synthesize polymer brushes with high grafting density resulting in thick films, due to high diffusion rates of monomer to reactive sites. The major limitations of the technique are initiator surface coverage and initiator efficiency.[46] Further, a large concentration of growing chains, and therefore active radicals, cause termination side reactions to become apparent. Therefore, a broadening of molecular weight of the resulting polymer brushes is evident, as compared to carrying out the same reaction in solution.[13] Lastly, the synthesis of polymer brushes

requires more elaborate polymerization conditions than "grafting to", which is described in the next section.

2.2.3:Preparation of Polymer Brushes by "Grafting to" Technique:

Contrary to "grafting from", the "grafting to" method provides a simplistic procedure for the creation of polymer brush layers as there is are no elaborate synthetic methods required. The "grafting to" approach utilizes already synthesized end-functionalized polymers that react with complementary functional groups present on a substrate. End-functionalized polymers can be synthesized by any available synthetic technique. However, the major advantage of "grafting to" is that the polymers can be fully characterized prior to attachment. Therefore, many researchers choose living polymerizations that create polymers with low polydispersity (PDI) such as RAFT, ionic, and ATRP. Therefore, by attaching polymers with low PDI, well defined grafted layers are formed.[47]

Literature suggests that the use of SAM has been used most frequently for the preparation of polymer brush films by "grafting to". Silane[48-52] and thiol[53-56] chemistries are most commonly employed for the modification of silicon containing oxide layers and gold surfaces respectively for the formation of end-tethered polymer chains.[47] For example, Karim et al. grafted trichlorosilane end-functionalized PS chains to silicon wafers.[49] The grafting was done in poor solution conditions to circumvent weak surface interaction from good solvent conditions. Interestingly, they found three different regimes of layer formation. At small exposure time, grafted layers formed patchy island

like structures. At intermediate exposure times, a surface coverage resembling morphologies of spinodal decomposition in bulk samples was noticed. Finally, at long induction periods, homogenous layers were observed.

Mansky[57] and coworkers utilized thiol chemistry for the preparation of polymer brushes by the "grafting to" method. Random copolymers with differing ratios of PS and PMMA were synthesized by "living" radical polymerization. The end functionalized polymers were grafted to silicon wafers through silanol groups located on the surface. They found that when copolymers contain less than 70% styrene, copolymers rapidly dewetted when annealed over the glass transition temperature. It was determined when copolymer composition was nearly equivalent, the interfacial energies were such that no preferential affinity of the surface to PS or PMMA was found. Therefore by controlling the copolymer composition they could effectively modulate domain orientation of the resulting polymer brush films.

"Grafting to" through a macromolecular anchoring layer has been extensively studied as well.[31, 47, 58-62] Epoxy containing polymers, specifically poly (glycidyl methacrylate) (PGMA), provide reactive groups that self-cross link and attach itself to the surface, while also containing intact epoxy rings for further reaction with end-functionalized polymer molecules. Thin homogenous layers of PGMA have been successfully attached to surfaces via spin-coating, dip-coating and adsorption.[47] PGMA layers have been attached to inorganic surfaces such as silicon and titanium, and organic substrates such as polyethylene, polypropylene, nylon, and polyvinylidene fluoride

(PVDF), and further modified with polymer brushes.[29, 47, 63-64] Additionally, PGMA has been successfully grafted to non-flat surfaces such as nano-particles and PVDF fibers.[65-67]

Iyer et al.[68] fabricated dense and homogenous layers of polymer brushes onto PGMA anchoring layers attached to silicon wafers. They grafted polymer molecules by utilizing carboxy and anhydride terminated PS of different molecular weights towards the creation of hydrophobic surfaces. It was found that the method lead to stable films as they did not dewet or desorb at elevated temperatures and in good solvents, respectively. Further, they found that grafting PS to PGMA or epoxysilane monolayers were very similar. However, the grafting of PS to PGMA layers was more effective. Higher efficiency and grafting density was attributed to the formation of an interpenetrating region between the polystyrene chains and thin PGMA layer.

On the other hand, Zdyrko et al.[69] utilized PGMA anchoring layers for the grafting of high density poly(ethylene glycol) (PEG) layers via the "grafting to" procedure to form hydrophilic coatings. They attached carboxylic end-functionalized PEG molecules of different molecular weights to the PGMA anchoring layers from the melt. Grafting from melt led to complete and homogenous PEG brushes with very high grafting densities. It was found that the resulting thickness of the polymer brush films was dependent on the molecular weight of the PEG chains. The maximum grafting efficiency found was indeed close to the critical entanglement molecular weight for PEG. Contact angle measurements verified (~30°) that indeed the modified substrate was hydrophilic.

However, the major shortcomings of the "grafting to" procedure are the low maximum thickness of grafted layers. By grafting large macromolecular chains, the process becomes self-limiting in nature. The large polymer chains must diffuse through the existing end-tethered chains in order to reach a reactive site.[31, 47] This "excluded volume" effect becomes increasingly stronger as thickness of the layer increases. However, "grafting to" carried out in the melt or theta solvents can somewhat combat this effect by screening the excluded volume effect producing films as thick as 30nm.[47] Examples of new methods to combat this effect are discussed in the body of this thesis.

2.3:Thermally Responsive Polymer Brushes:

Due to the ease and straightforward control of temperature, thermoresponsive polymers and polymer brushes have been studied at length throughout the physical sciences in the last few decades. A thermoresponsive polymer is defined as a polymer that undergoes property changes upon small changes in the temperature of the environment. Thermally responsive water soluble polymers are the most attractive polymer-solvent pairs due to water being environmentally friendly and applications in biological and medicinal fields.[1] Polymers that exhibit changes in affinity to water are separated into two general classes of phase behavior. Polymers that display solubility upon heating have an upper critical solution temperature (UCST), and macromolecules that exhibit solubility in water upon cooling, are deemed to have a lower critical solution temperature (LCST) in their phase diagrams. There are however, systems that can exhibit both UCST and LCST behavior simultaneously.[70-72] Therefore, UCST and LCST type polymer systems and thus polymer brush films have led to numerous publications

and research applicable to a wide range of technologies. As Seuring[1] et. al recently stated, research in the field of UCST and LCST polymer systems have led to the development of "smart" materials in applications such as; wettability switchable surfaces[73-75], separation[76], drug delivery[77], gene therapy[78-79], bioseperation[80-82], and cell sheet engineering[83-84].

2.3.1:Polymers Governed by UCST Solution Behavior:

For polymers exhibiting UCST phase behavior, above the UCST the polymer is fully miscible with the solvent. However, by decreasing the temperature one would reach a miscibility gap throughout certain compositional fractions where phase separation and creation of polymer and solvent rich regions would occur.[85-86] An idealized phase diagram depicting a UCST behavior between polymer-solvent is depicted in **Figure 2.2**. As observed in **Figure 2.2**, at T_1, the polymer and solvent are miscible at all compositions. As temperature is decreased to T_2, and subsequently laying on the binodal tie line, phase separation occurs into c1a and c2b polymer and solvent rich phases. Upon further decrease to T_3, the phase compositions become c2a and c2b. The hydrophobic-hydrophilic change with small fluctuations in temperature is what has captured many scientists interest in generating responsive polymer brush films from such polymers. In general polymers need to contain polar groups that can interact with water by dipole-dipole and hydrogen bonding interactions to be soluble. A general list of polymers exhibiting UCST phase behavior in water is listed in **Table 2.2**[1].

Various types of polymers have been studied for their unique UCST behavior, a few examples being, zwitterionic polymers[87-88], polyelectrolytes in the presence of multivalent counterions[89], carboxylic containing polymers as a function of pH and ionic strength[78], poly(N-acryloylglycinamide) copolymers and derivatives[81, 90], ureido modified polymers[91-92], and acrylamide based polymers[80]. For example Shimada et al.[91] demonstrated the synthesis of ureido modified polymers that exhibited UCST phase behavior in water around physiological conditions. They found that poly(allylurea) copolymers exhibited UCST behavior at pH 7.5 in 150 mM NaCl solutions at low polymer concentration. Interestingly, they showed control of the UCST up to 65°C. This

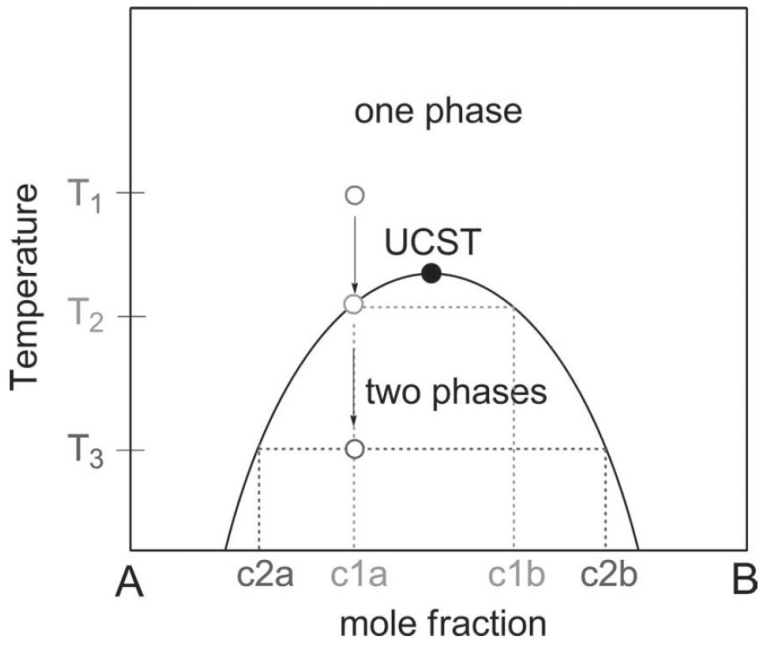

Figure 2.2: Idealized phase diagram of a polymer solvent mixture exhibiting a UCST miscibility behavior.[1] *Reprinted with permission from Wiley.*

was the first demonstration of non vinyl polymers exhibiting a UCST at physiological relevant conditions.

Liu et al.[92] demonstrated the synthesis of poly(N-acryloglycinamide) by RAFT polymerization technique. In order to preserve the UCST behavior of the monomer, they determined that non ionic initiators had to be employed for the synthesis. Interestingly, they found that the polymer end groups played a distinct role on the cloud point, the lower the degree of polymerization the higher the effect the chosen end group had.

Table 2.2: A general list of polymers that exhibit UCST phase behavior with water.[1] *Reprinted with permission from Wiley.*

Polymer	Inter-polymer interactions	UCST Behavior		Remarks
		Pure Water	Physiological Conditions	
PEO (1)	Dipole + bridged HB	Yes	Yes	Loop-shaped miscibility gap LCST < 200°C <UCST
PVME (2)	Dipole + bridged HB	Yes	Yes	2 UCSTs <0°C + bimodal LCST
Hydrophobically Modified PVA(3)	Weak HB	Yes	Yes	Loop-shaped miscibility gap LCST < 80°C <UCST; tunable UCST for graft copolymers
PHEMA (4)	Weak HB	Yes	Yes	Loop-shaped miscibility gap for polymers with Mn < 6kg mol-1, UCST >100°C
Zwitterionic (5-7)	Zwitterionic Interaction	Yes	No	
Polyelectrolyte in the presence of multivalent counterions	Bridged ionic interaction	No	Depends on System	Strongly dependent on pH, ionic strength, and ion valency
PAA and copolymers (8)	HB	No	No	UCST behavior at c(NaCl) > 400 x 10-3 m or pH < 4
PAU (10)	HB	Yes	Yes	Hysteresis of PNAGA and copolymers about 10C while only 0.5 - 0.8 C for the derivative PNAAAm
PNAGA and derivatives and copolymers (11-14)	HB	Yes	Yes	hysteresis of 1-2°C
Ureido functionalized polymers (15,16)	HB	Yes	Yes	Slow hydrolysis, hysteresis of 1-2°C
Poly(acrylamide-co-acrylonitrile) (17)	HB	Yes	Yes	
Poly(methacrylamide) (9)	HB	Yes	?	
Copolymers of N-acetylacrylamide (18)	HB	Yes	?	Broad Transition and strong hysteresis; slow hydrolysis

2.3.2:Polymers Governed by LCST Behavior:

When water soluble polymers precipitate into polymer and solvent rich phases upon increasing temperature, the said phase behavior is described by a LCST miscibility gap in the polymer-solvent phase diagram. For binary mixtures, the LCST is the maximum point on the binodal tie line with which polymer and water will phase separate. The effect is due primarily to association of hydrophobic or non-polar segments within the polymer.[3] The intra-molecular association causes collapse of the individual polymer chains. In fact, Heskins et al. described the first known existence of LCST type polymers in 1968 with poly(N-isopropylacrylamide) (PNIPAM) and water, prescribed primarily due to an entropic effect.[93]

Various types of polymer exhibit LCST type properties including: N-substituted acrylamides such as; PNIPAM[94-95], poly(2-carboxyisopropylacrylamide) (PCIPAM) [96],[97-98], poly(N-(L)-(1-hydroxymethyl) propylmethacrylamide)[99], poly(N-acryloyl-*N*-alkypiperazine[100], other vinyl polymers such as; poly(vinylmethyl ether)[101], poly(N-vinylcaprolactam)[102], and poly(dimethylaminoethyl methacrylate)[103]. Amphiphilic type polymers such as the triblock copolymer of poly(ethylene-oxide)-poly(propylene oxide)-poly(ethylene oxide) (PEO-PPO-PEO) have also shown LCST micellization behavior.[104-105] Further, certain biopolymers have also shown LCST behavior (gelatin[106] and agarose.[107]).

Maeda et al.[101] investigated the phase transitions of poly(vinyl methyl ether) (PVME) in H_20 and D_20 as a function of temperature utilizing Fourier transform infrared

spectroscopy (FTIR). They found that by heating the solution above the LCST, it leads to shifts in the C-H and C-O stretching bands to lower and higher wavenumbers, respectively. They also determined that the methyl peak is composed of two adsorption bands associated with the hydrated and dehydrated methyl species. From these peak assignments, it was found that the molar fraction of the "hydrated" methyl species was close to 100% percent below 36°C, and nearly 0% above 40°C, validating that indeed most methyl groups are in the dehydrated state above the LCST, whereas the C-O band indicated partial dehydration of the ether moiety above the LCST. In conclusion, they state that in general, the dehydration of the methyl and ether group initiates at different water/monomer ratios, but they do indeed simultaneous proceed in the phase separation.

The combination of multiple species exhibiting LCST type properties can be combined to create dually responsive materials as well. Inoue et al.[102] studied the LCST behavior of oligo(N-vinylacprolactam) (oVCL) and oligo-NIPAM among others. They thus created hydrogels that demonstrated two different LCSTs. They fabricated such systems by utilizing carboxy terminated version of the oligomers and carried out the reaction with glycidyl methacrylate. Acrylamide was utilized as the base monomer of the hydrogels, copolymerized with glycidyl methacrylate and cross-linker. The properties of the hydrogels were compared with properties of the oligo functionalized hydrogels. Indeed, the non modified hydrogels show a lack of temperature response; however the corresponding modified versions displayed two LCSTs corresponding to oNIPAM and oVCL.

Polymers exhibiting LCST properties are useful in industrial applications as well. Poloxamers is a general term used to coin non-ionic copolymers composed of a centrally hydrophobic poly(propylene oxide) chain with terminal chains composed of hydrophilic poly(ethylene oxide) segments (PEO-PPO-PEO). You can find various versions of the surfactant like polymer PEO-PPO-PEO in industrial applications such as cosmetics and pharmaceuticals. The study of PEO-PPO-PEO is also well studied in academic settings. For example, Mortensen et al.[105] studied the behavior of PEO-PPO-PEO triblock copolymers in an aqueous environment as function of temperature and polymer concentration using small-angle neutron scattering. They found that at low temperatures, the polymer was fully dissolved and took on a Gaussian type chain conformation with a radius of gyration of 1.7nm. However close to room temperature, the hydrophobic PPO segment caused aggregation of the macromolecules into spherical micelles, with core sizes measured at approximately 4-5nm in diameter. Further increasing the temperature, researchers found that the micellar structure changed from spherical to ellipsoidal, leading to a diminished micelle-micelle interaction. Finally, upon increasing the temperature to nearly 95°C, large agglomerates of polymers formed ordered lamellae, leading to a translucent suspension.

2.4:Poly (*N*-isopropylacrylamide) Brushes

PNIPAM has been the most extensively studied polymer exhibiting LCST phase behavior for various reasons. Firstly, the hydrophobic to hydrophilic phase change for pure PNIPAM occurs at approximately 32°C, well within physiological conditions.[26, 108-111].

Further, polymers exhibiting temperature responsive phase behavior have been classified into three categories by Berghmans and Van Mele.[3] Type I polymers such as PVCL, follow classical theory by Flory and Huggins. By changing the polymer concentration, the LCST of the system shifts. The critical point is found for infinite molar mass at zero concentration.[1] Type II systems such as PNIPAM, exhibit very stable

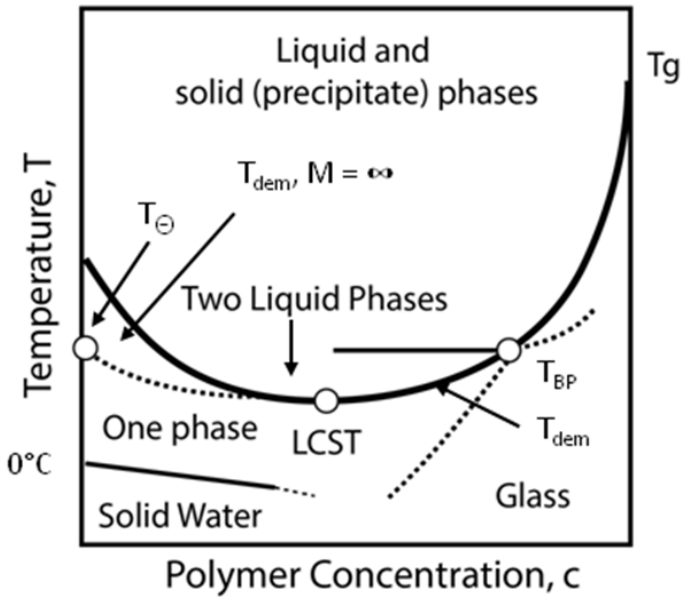

Figure 2.3: Phase diagram of PNIPAM in water. Phase separation temperature is marked T_{dem}. T_Θ is the theta temperature of the system and T_{BP} is the temperature corresponding to Berghmans point.[2-3] Redrawn from Ref. [2]

LCST temperatures as a function of polymer molecular weight. Lastly, Type III exhibit two minimums in their phase diagram, which creates two different critical points for low and high polymer concentrations.

Therefore, a major advantage of PNIPAM over other systems exhibiting temperature responsive phase behavior is that the various architectures of PNIPAM chains have negligible effects on the magnitude of the LCST of PNIPAM. A typical phase diagram of free PNIPAM chains in solution is displayed in **Figure 2.3**. Broad applications of PNIPAM have found pertinence due to the critical point being independent of molar mass, and the influence of temperature on the phase separation is very small due to the very flat LCST curve.[1] The simulation of PNIPAM molecule in solution as a function of temperature is shown in **Figure 2.4**. The conformational change

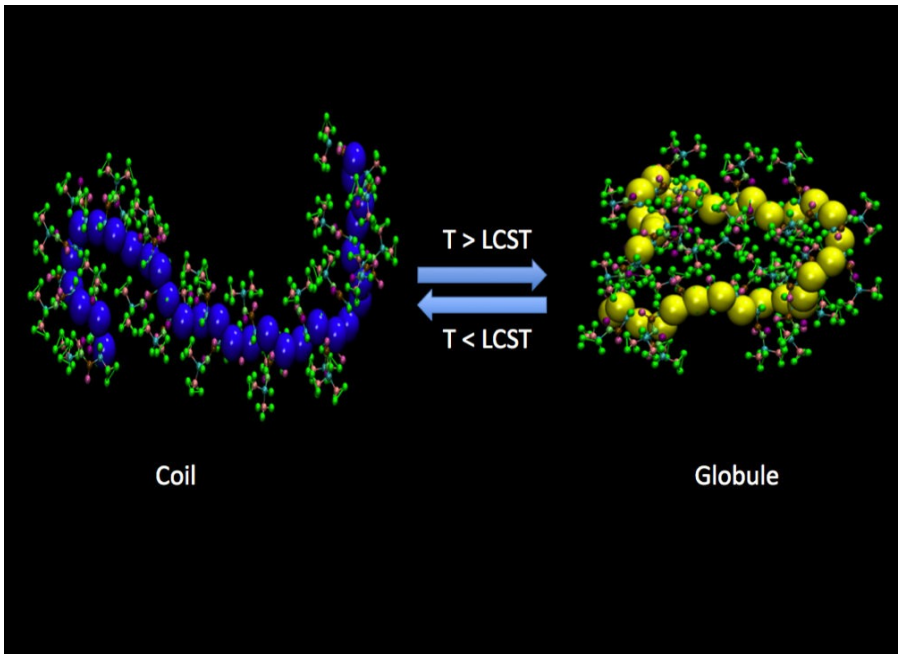

Figure 2.4: Coil to globule transition of PNIPAM chains in solution as a function of temperature as simulated at Argonne National Laboratory.[4]

through the LCST occurs due to a chain to globule transition.[19, 94, 109, 112] However, for UCST systems, it is unlikely that type II behavior like that of PNIPAM can occur because

UCST systems are based on intermolecular interactions and positive combinatorial entropies of mixing.[1]

Polymer brushes containing PNIPAM are extremely attractable to scientists due to the ability to create modified surfaces while retaining the LCST properties of the system within feasible biological conditions, therefore creating robust switchable surfaces that undergo a hydrophilic to hydrophobic change with small deviations in temperature. The switching of PNIPAM brush films is accompanied by extension and collapse in water at temperatures above and below the LCST as seen in **Figure 2.5**. At temperatures below

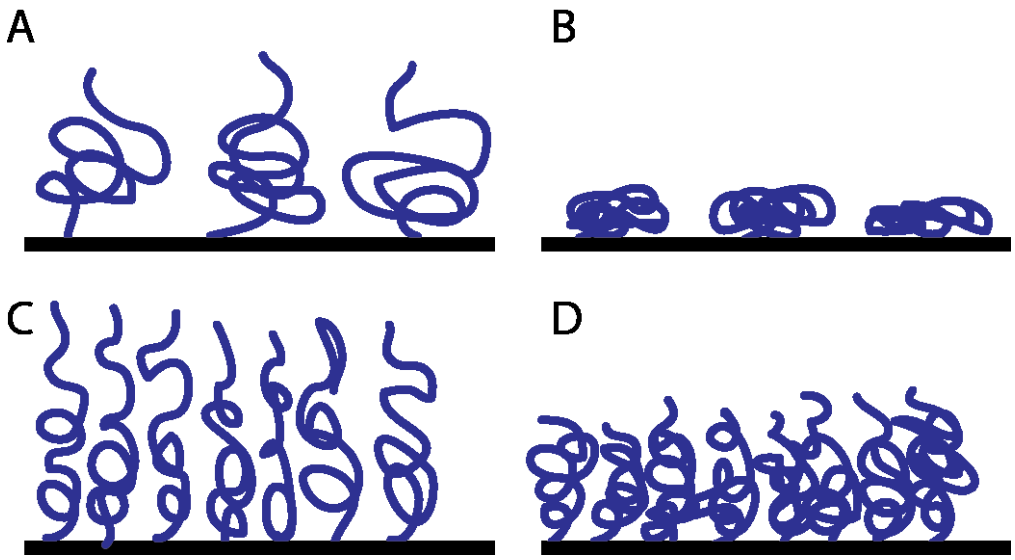

Figure 2.5: Schematic representation of PNIPAM end-tethered in A-B) mushroom regime and C-D) brush regime. At temperatures below the LCST, PNIPAM chains form an extended structure (A,C). When temperature is increased above the LCST, PNIPAM chains collapse (B,D).

the LCST, PNIPAM chains are extended, which translates to an increase in thickness of the polymer brush film. However, upon increasing the temperature above the LCST, PNIPAM chains collapse and thickness of the layer subsequently decreases. The

hydrophilic to hydrophobic transition is related to the reorientation of the non-polar isopropyl groups and polar amide groups in the polymer side chain.

PNIPAM end-tethered macromolecules have found pertinence within a wide variety of applications calling for switchable surfaces such as; cell-sheet culturing[113-114], drug delivery[115-117], tissue engineering[118], and bio-separation.[76, 119-120]. In fact, PNIPAM brush systems have been thoroughly characterized theoretically and experimentally. Specifically, Halperin et al. proposed theoretical considerations for design of PNIPAM brush films towards control of protein adsorption[121] and development of cell culture harvesting platforms.[122-123]

PNIPAM brush films are utilized to culture tissue in order to harvest confluent cell sheets for tissue engineering. Clinical use calls for a cell culture medium that is free of bovine serum albumin, therefore implying the need for conjugation with adhesion peptides that contain the RGD recognition sequence.[122] Halperin and Kroger utilized self-consistent field theory (SCF) to determine the optimum position for placement of the RGD ligands within the brush films. Their results determined that placement of RGDs should be at the grafting surface or immediate vicinity. The random placement of the RGD groups did not enable detachment of cells due to a large fraction of the RGD bonds not sufficiently available when the PNIPAM was in the swollen and extended state. This was confirmed experimentally.[124]

On the other hand Halperin and Kroger[121] also theoretically modeled protein adsorption onto PNIPAM brush films as a function of temperature utilizing SCF theory.

They found that for relatively small particles (i.e. proteins), the free energy penalty incurred upon protein penetration (Fins) into the brush film is related to the work against osmotic pressure of the un-perturbed brush. They found that the Fins decreased with brush thickness, < z >. This was true because the value of osmotic pressure at the grafting surface (Pi(0)) was similar to < z > independent of the interaction free energy. Further, PNIPAM in the collapsed state favors adsorption because it reduces Fins by lowering the osmotic pressure within the brush layer, and a decrease of the volume available for the protein to penetrate in.

Experimentally, the surface energy switchability has been well documented in literature.[125-127] Interestingly, Plunkett et al.[94] found that the magnitude of the thermally induced collapse of end-tethered PNIPAM brushes depended on the grafting density and molecular weight of the brush layer. In order to study the effects of grafting density and molecular weight on the behavior of the PNIPAM brush films, PNIPAM was grafted from SAM layers utilizing ATRP polymerization techniques by the "grafting from" method. By varying the reaction time and monomer concentration they could effectively control the molecular weight of the brushes. By altering the initiator concentration on the surface, control over grafting density was obtained. Through surface force measurements of the polymer films the authors showed that the chain collapse above the LCST decreased with decreased grafting density and molecular weight. The advancing water contact angle increased sharply at T > LCST when brushes were comprised of higher molecular weight chains and increased grafting density. The change was less pronounced for lower grafting density and molecular weight. Finally, force distance profiles of the

PNIPAM brush films displayed non-ideal polymer behavior which they attributed to the polymer brush chain density increasing from the surface outer edge to the grafting site.

Protein adsorption to PNIPAM brush layers has been well documented in literature.[74, 108, 128-130] Xue et al.[128] studied the protein adsorption and reversible cell attachment as a function of grafting density. They determined the dependence of reversible, protein-mediated cell adhesion was in fact affected by polymer chain density. At temperatures above the LCST of PNIPAM, PNIPAM brushes grafted from a protein repelling surface exhibited maximum protein adsorption. They found nearly no cells attached to either dilute or densely grafted PNIPAM films above 32°C, however, cells and proteins reversibly adsorbed at intermediate chain density. They attributed this phenomenon to penetration of the proteins into the brush layers at intermediate grafting densities under poor solvent conditions.

Yu et al.[74] also investigated protein adsorption (human serum albumin HSA) as a function of grafted layer thickness, by polymerizing PNIPAM brushes from the surface using ATRP. They studied the brush behavior at differing temperatures using water contact angle, x-ray photoelectron spectroscopy (XPS), and atomic force microscopy (AFM). Firstly, at layer thickness less than 15nm, they did not find a significant change in adsorption levels as a function of temperature. When thickness of the layer was increased to 38nm, the adsorption results showed a stronger change in the amount of protein adsorbed as a function of temperature. This is clearly contradictory results to that of Xue. Yu and coworkers found increased adsorption of protein at high temperatures for

densely grafted surfaces while Xue. et al. found increased adsorption for intermediate to low grafting densities.

Of the large variety of methods available to synthesize thermally responsive polymer brushes, current methods require multi-step procedures. The "grafting to" procedure is feasible on a large scale from a procedural standpoint, however, limiting film thickness and grafting density is a major limitation. "Grafting from" however, can yield polymer brush films that are thicker and of higher grafting density. Nevertheless, the procedure requires multiple steps and treatments with organic solvents. The current work aims towards a modification of the "grafting to" procedure that fills the gaps between the two major polymer brush fabrication techniques. We aim towards procedures that can create robust thermally responsive polymer brush coatings with tunable thickness and grafting density towards manipulation of biological interaction while maintaining the simplistic procedure of the "grafting to" approach.

PNIPAM has shown to be an active polymer that demonstrates LCST phase behavior in aqueous environments within physiological conditions. PNIPAM has been demonstrated to display broad binodal decomposition at its miscibility gap region, leading to predictable and stable phase separation at a wide polymer concentration range. Additionally, PNIPAM has been shown to exhibit type II phase behavior. Therefore, molecular weight and chain architecture has limited effects on the LCST temperature. The above benefits of PNIPAM have led to the investigation of novel grafting techniques of PNIPAM containing films. The present work aims towards a universal method that can

be applied to a wide range of substrates and deliver tunable surface properties with small changes in temperature, and thus parallel control over interaction with biological material.

2.5:References

1. Seuring, J.; Agarwal, S., Polymers with upper critical solution temperature in aqueous solution. *Macromolecular Rapid Communications* **2012,** *33* (22), 1898-1920.

2. Arnauts, J.; Berghmans, H., Amorphous thermoreversible gels of atactic polystyrene. *Polymer Communications* **1987,** *28* (3), 66-68.

3. Aseyev, V.; Tenhu, H.; Winnik, F. M., Non-ionic thermoresponsive polymers in water. In *Self organized nanostructures of amphiphilic block copolymers ii*, Muller, A. H. E.; Borisov, O., Eds. Springer-Verlag Berlin: Berlin, 2011; Vol. 242, pp 29-89.

4. Sankaranarayanan Argonne leadership computing facility. https://www.alcf.anl.gov/projects/dynamics-conformational-transition-thermo-sensitive-polymers-and-hydrogels.

5. Zhao, B.; Brittain, W. J., Polymer brushes: Surface-immobilized macromolecules. *Prog. Polym. Sci.* **2000,** *25* (5), 677-710.

6. Takei, Y. G.; Aoki, T.; Sanui, K.; Ogata, N.; Sakurai, Y.; Okano, T., Dynamic contact-angle measurement of temperature-responsive surface-properties for poly(n-isopropylacrylamide) grafted surfaces. *Macromolecules* **1994,** *27* (21), 6163-6166.

7. Azzaroni, O., Polymer brushes here, there, and everywhere: Recent advances in their practical applications and emerging opportunities in multiple research fields. *Journal of Polymer Science Part A: Polymer Chemistry* **2012,** *50* (16), 3225-3258.

8. Clayfiel.Ej; Lumb, E. C., Detachment of adhered colloidal particles by non-aqueous surfactant solutions. *Discussions of the Faraday Society* **1966,** (42), 285-&.

9. Wan der Waarden, M. J., *Colloid Science* **1950,** *5*, 535.

10. Hong, J.; Degennes, P. G., Adhesion via connector molecules - the many-stitch problem. *Macromolecules* **1993,** *26* (3), 520-525.

11. Joanny, J. F., Lubrication by molten polymer brushes. *Langmuir* **1992,** *8* (3), 989-995.

12. van Zanten, J. H., Terminally anchored chain interphases: Their chromatographic properties. *Macromolecules* **1994,** *27* (23), 6797-6807.

13. Brittain, W. J.; Minko, S., A structural definition of polymer brushes. *Journal of Polymer Science Part a-Polymer Chemistry* **2007,** *45* (16), 3505-3512.

14. Szleifer, I.; Carignano, M. A., Tethered polymer layers. *Advances in Chemical Physics, Vol Xciv* **1996,** *94*, 165-260.

15. Alexander, S., Polymer adsorption on small spheres - scaling approach. *Journal De Physique* **1977,** *38* (8), 977-981.

16. Alexander, S., Adsorption of chain molecules with a polar head a-scaling description. *Journal De Physique* **1977,** *38* (8), 983-987.

17. Flory, P. J., *Principles of polymer chemistry*. Cornell University Press: Ithaca NY, 1981.

18. Halperin, A.; Tirrell, M.; Lodge, T. P., Tethered chains in polymer microstructures. *Advances in Polymer Science* **1992,** *100*, 31-71.

19. Akiyama, Y.; Kikuchi, A.; Yamato, M.; Okano, T., Ultrathin poly(n-isopropylacrylamide) grafted layer on polystyrene surfaces for cell adhesion/detachment control. *Langmuir* **2004,** *20* (13), 5506-5511.

20. Gan, D.; Lyon, L. A., Synthesis and protein adsorption resistance of peg-modified poly(n-isopropylacrylamide) core/shell microgels. *Macromolecules* **2002,** *35* (26), 9634-9639.

21. Saeki, S.; Kuwahara, N.; Nakata, M.; Kaneko, M., Upper and lower critical solution temperatures in poly (ethylene glycol) solutions. *Polymer* **1976,** *17* (8), 685-689.

22. Ito, Y.; Park, Y. S.; Imanishi, Y., Visualization of critical ph-controlled gating of a porous membrane grafted with polyelectrolyte brushes. *Journal of the American Chemical Society* **1997,** *119* (11), 2739-2740.

23. Ito, Y.; Ochiai, Y.; Park, Y. S.; Imanishi, Y., Ph-sensitive gating by conformational change of a polypeptide brush grafted onto a porous polymer membrane. *Journal of the American Chemical Society* **1997,** *119* (7), 1619-1623.

24. Ito, Y.; Nishi, S.; Park, Y. S.; Iminishi, Y., Oxidoreduction-sensitive control of water permeation through a polymer brushes-grafted porous membrane (vol 30, pg 5858, 1997). *Macromolecules* **1997,** *30* (25), 8096-8096.

25. Balamurugan, S.; Mendez, S.; Balamurugan, S. S.; O'Brien, M. J.; Lopez, G. P., Thermal response of poly(n-isopropylacrylamide) brushes probed by surface plasmon resonance. *Langmuir* **2003,** *19* (7), 2545-2549.

26. Bittrich, E.; Burkert, S.; Muller, M.; Eichhorn, K. J.; Stamm, M.; Uhlmann, P., Temperature-sensitive swelling of poly(n-isopropylacrylamide) brushes with low molecular weight and grafting density. *Langmuir 28* (7), 3439-3448.

27. Alarcon, C. D. H.; Pennadam, S.; Alexander, C., Stimuli responsive polymers for biomedical applications. *Chemical Society Reviews* **2005,** *34* (3), 276-285.

28. Zdyrko, B.; Luzinov, I., Polymer brushes by the "grafting to" method. *Macromolecular Rapid Communications 32* (12), 859-869.

29. Liu, Y.; Klep, V.; Zdyrko, B.; Luzinov, I., Synthesis of high-density grafted polymer layers with thickness and grafting density gradients. *Langmuir* **2005,** *21* (25), 11806-11813.

30. Bug, A. L. R.; Cates, M. E.; Safran, S. A.; Witten, T. A., Theory of size distribution of associating polymer aggregates .1. Spherical aggregates. *Journal of Chemical Physics* **1987,** *87* (3), 1824-1833.

31. Zdyrko, B. Thin polymer films for biomedical applications: Synthesis and characterization. Clemson University, 2005.

32. Parsonage, E.; Tirrell, M.; Watanabe, H.; Nuzzo, R. G., Adsorption of poly(2-vinylpyridine)-poly (styrene) block copolymers from toluene solutions. *Macromolecules* **1991,** *24* (8), 1987-1995.

33. Guzonas, D.; Boils, D.; Hair, M. L., Surface force measurements of polystyrene-block-poly(ethylene oxide) adsorbed from a nonselective solvent on mica. *Macromolecules* **1991,** *24* (11), 3383-3387.

34. Dijt, J. C.; Stuart, M. A. C.; Fleer, G. J., Kinetics of polymer adsorption and desorption - poly(ethylene oxide) on silica. *Acs Symposium Series* **1993,** *532*, 14-22.

35. Sharma, A.; Reiter, G., Instability of thin polymer films on coated substrates: Rupture, dewetting, and drop formation. *Journal of Colloid and Interface Science* **1996,** *178* (2), 383-399.

36. Luzinov, I.; Minko, S.; Tsukruk, V. V., Responsive brush layers: From tailored gradients to reversibly assembled nanoparticles. *Soft Matter* **2008,** *4* (4), 714-725.

37. Boven, G.; Folkersma, R.; Challa, G.; Schouten, A. J., Radical grafting of poly(methyl methacrylate) onto silicon-wafers, glass slides and glass-beads. *Polymer Communications* **1991,** *32* (2), 50-53.

38. Zengin, A.; Yildirim, E.; Caykara, T., Raft-mediated synthesis and temperature-induced responsive properties of poly(2-(2-methoxyethoxy)ethyl methacrylate) brushes. *Journal of Polymer Science Part a-Polymer Chemistry* **2013,** *51* (4), 954-962.

39. Price, A. D.; Huber, D. L., Controlled polymer monolayer synthesis by radical transfer to surface immobilized transfer agents. *Polymer Chemistry* **2013,** *4* (5), 1565-1574.

40. Kitano, H.; Liu, Y.; Tokuwa, K.-i.; Li, L.; Iwanaga, S.; Nakamura, M.; Kanayama, N.; Ohno, K.; Saruwatari, Y., Polymer brush with pendent glucosylurea groups constructed on a glass substrate by raft polymerization. *European Polymer Journal* **2012,** *48* (11), 1875-1882.

41. Choi, J.; Schattling, P.; Jochum, F. D.; Pyun, J.; Char, K.; Theato, P., Functionalization and patterning of reactive polymer brushes based on surface reversible addition and fragmentation chain transfer polymerization. *Journal of Polymer Science Part a-Polymer Chemistry* **2012,** *50* (19), 4010-4018.

42. Matsuzaka, N.; Takahashi, H.; Nakayama, M.; Kikuchi, A.; Okano, T., Effect of the hydrophobic basal layer of thermoresponsive block co-polymer brushes on thermally-induced cell sheet harvest. *Journal of Biomaterials Science-Polymer Edition* **2012,** *23* (10), 1301-1314.

43. Husseman, M.; Malmstrom, E. E.; McNamara, M.; Mate, M.; Mecerreyes, D.; Benoit, D. G.; Hedrick, J. L.; Mansky, P.; Huang, E.; Russell, T. P.; Hawker, C. J., Controlled synthesis of polymer brushes by "living" free radical polymerization techniques. *Macromolecules* **1999,** *32* (5), 1424-1431.

44. Olivier, A.; Meyer, F.; Raquez, J. M.; Damman, P.; Dubois, P., Surface-initiated controlled polymerization as a convenient method for designing functional polymer brushes: From self-assembled monolayers to patterned surfaces. *Prog. Polym. Sci.* **2012,** *37* (1), 157-181.

45. Baum, M.; Brittain, W. J., Synthesis of polymer brushes on silicate substrates via reversible addition fragmentation chain transfer technique. *Macromolecules* **2002,** *35* (3), 610-615.

46. Hoy, O. Synthesis and characterisation of polymer brushes for controlled protein adsorption. Clemson University 2008.

47. Zdyrko, B.; Luzinov, I., Polymer brushes by the "grafting to" method. *Macromolecular Rapid Communications* **2011,** *32* (12), 859-869.

48. Jones, R. A. L.; Lehnert, R. J.; Schonherr, H.; Vancso, J., Factors affecting the preparation of permanently end-grafted polystyrene layers. *Polymer* **1999,** *40* (2), 525-530.

49. Karim, A.; Tsukruk, V. V.; Douglas, J. F.; Satija, S. K.; Fetters, L. J.; Reneker, D. H.; Foster, M. D., Self-organization of polymer brush layers in a poor solvent. *Journal De Physique Ii* **1995,** *5* (10), 1441-1456.

50. Zhao, W.; Krausch, G.; Rafailovich, M. H.; Sokolov, J., Lateral structure of a grafted polymer layer in a poor solvent. *Macromolecules* **1994,** *27* (11), 2933-2935.

51. Luzinov, I.; Julthongpiput, D.; Tsukruk, V. V., Thermoplastic elastomer monolayers grafted to a functionalized silicon surface. *Macromolecules* **2000,** *33* (20), 7629-7638.

52. Motornov, M.; Sheparovych, R.; Lupitskyy, R.; MacWilliams, E.; Hoy, O.; Luzinov, I.; Minko, S., Stimuli-responsive colloidal systems from mixed brush-coated nanoparticles. *Advanced Functional Materials* **2007,** *17* (14), 2307-2314.

53. Taylor, W.; Jones, R. A. L., Producing high-density high-molecular-weight polymer brushes by a "grafting to" method from a concentrated homopolymer solution. *Langmuir* **2010,** *26* (17), 13954-13958.

54. Corbierre, M. K.; Cameron, N. S.; Lennox, R. B., Polymer-stabilized gold nanoparticles with high grafting densities. *Langmuir* **2004,** *20* (7), 2867-2873.

55. Corbierre, M. K.; Cameron, N. S.; Sutton, M.; Laaziri, K.; Lennox, R. B., Gold nanoparticle/polymer nanocomposites: Dispersion of nanoparticles as a function of capping agent molecular weight and grafting density. *Langmuir* **2005,** *21* (13), 6063-6072.

56. Liu, G. M.; Cheng, H.; Yan, L. F.; Zhang, G. Z., Study of the kinetics of the pancake-to-brush transition of poly(n-isopropylacrylamide) chains. *Journal of Physical Chemistry B* **2005,** *109* (47), 22603-22607.

57. Mansky, P.; Liu, Y.; Huang, E.; Russell, T. P.; Hawker, C. J., Controlling polymer-surface interactions with random copolymer brushes. *Science* **1997,** *275* (5305), 1458-1460.

58. Chyasnavichyus, M.; Tsyalkovsky, V.; Zdyrko, B.; Luzinov, I., Tuning fluorescent response of nanoscale film with polymer grafting. *Macromolecular Rapid Communications 33* (3), 237-241.

59. Lokitz, B. S.; Wei, J.; Hinestrosa, J. P.; Ivanov, I.; Browning, J. F.; Ankner, J. F.; Kilbey, S. M., II; Messman, J. M., Manipulating interfaces through surface confinement of poly(glycidyl methacrylate)-block-poly(vinyldimethylazlactone), a dually reactive block copolymer. *Macromolecules* **2012,** *45* (16), 6438-6449.

60. Luzinov, I. A.; Swaminatha Iyer, K. L.; Klep, V. Z.; Zdyrko, B. V. Surface graft modification of substrates, us patent 7,026,014 b2, apr. 11, 2006.

61. Luzinov, I.; Minko, S.; Tsukruk, V. V., Adaptive and responsive surfaces through controlled reorganization of interfacial polymer layers. *Progress in Polymer Science* **2004,** *29* (7), 635-698.

62. Zdyrko, B.; Klep, V.; Luzinov, I., Universal platform for surface modification employing grafted polymer layers. *Material Matters* **2008,** *3* (2), 44-47.

63. Zdyrko, B.; Klep, V.; Luzinov, I., Synthesis and surface morphology of high-density poly(ethylene glycol) grafted layers. *Langmuir* **2003,** *19* (24), 10179-10187.

64. Liu, Y.; Klep, V.; Zdyrko, B.; Luzinov, I., Polymer grafting via atrp initiated from macroinitiator synthesized on surface. *Langmuir* **2004,** *20* (16), 6710-6718.

65. Seeber, M.; Zdyrko, B.; Burtovvy, R.; Andrukh, T.; Tsai, C. C.; Owens, J. R.; Kornev, K. G.; Luzinov, I., Surface grafting of thermoresponsive microgel nanoparticles. *Soft Matter 7* (21), 9962-9971.

66. Tsyalkovsky, V.; Burtovyy, R.; Klep, V.; Lupitskyy, R.; Motornov, M.; Minko, S.; Luzinov, I., Fluorescent nanoparticles stabilized by poly(ethylene glycol) containing shell for ph-triggered tunable aggregation in aqueous environment. *Langmuir* **2010,** *26* (13), 10684-10692.

67. Tsyalkovsky, V.; Klep, V.; Ramaratnam, K.; Lupitskyy, R.; Minko, S.; Luzinov, I., Fluorescent reactive core-shell composite nanoparticles with a high surface concentration of epoxy functionalities. *Chemistry of Materials* **2008,** *20* (1), 317-325.

68. Iyer, K. S.; Zdyrko, B.; Malz, H.; Pionteck, J.; Luzinov, I., Polystyrene layers grafted to macromolecular anchoring layer. *Macromolecules* **2003,** *36* (17), 6519-6526.

69. Zdyrko, B.; Varshney, S. K.; Luzinov, I., Effect of molecular weight on synthesis and surface morphology of high-density poly(ethylene glycol) grafted layers. *Langmuir* **2004,** *20* (16), 6727-6735.

70. Rana, D.; Bag, K.; Bhattacharyya, S. N.; Mandal, B. M., Miscibility of poly(styrene-co-butyl acrylate) with poly(ethyl methacrylate): Existence of both ucst and lcst. *Journal of Polymer Science Part B-Polymer Physics* **2000,** *38* (3), 369-375.

71. Roth, P. J.; Davis, T. P.; Lowe, A. B., Comparison between the lcst and ucst transitions of double thermoresponsive diblock copolymers: Insights into the behavior of poegma in alcohols. *Macromolecules* **2012,** *45* (7), 3221-3230.

72. Tian, H. Y.; Yan, J. J.; Wang, D.; Gu, C.; You, Y. Z.; Chen, X. S., Synthesis of thermo-responsive polymers with both tunable ucst and lcst. *Macromolecular Rapid Communications* **2011,** *32* (8), 660-664.

73. Yamada, N.; Okano, T.; Sakai, H.; Karikusa, F.; Sawasaki, Y.; Sakurai, Y., Thermoresponsive polymeric surfaces - control of attachment and detachment of cultured-cells. *Makromolekulare Chemie-Rapid Communications* **1990,** *11* (11), 571-576.

74. Mori, N.; Horikawa, H.; Furukawa, H.; Watanabe, T., Temperature-induced changes in the surface wettability of sbr plus pnipa films. *Macromolecular Materials and Engineering* **2007,** *292* (8), 917-922.

75. Muthiah, P.; Hoppe, S. M.; Boyle, T. J.; Sigmund, W., Thermally tunable surface wettability of electrospun fiber mats: Polystyrene/poly(n-isopropylacrylamide) blended versus crosslinked poly[(n-isopropylacrylamide)-co-(methacrylic acid)]. *Macromolecular Rapid Communications* **2011,** *32* (21), 1716-1721.

76. Kanazawa, H.; Yamamoto, K.; Matsushima, Y.; Takai, N.; Kikuchi, A.; Sakurai, Y.; Okano, T., Temperature-responsive chromatography using poly(n-isopropylacrylamide)-modified silica. *Analytical Chemistry* **1996,** *68* (1), 100-105.

77. Bulmus, V.; Patir, S.; Tuncel, S. A.; Piskin, E., Stimuli-responsive properties of conjugates of n-isopropylacrylamide-co-acrylic acid oligomers with alanine, glycine and serine mono-, di- and tri-peptides. *Journal of Controlled Release* **2001,** *76* (3), 265-274.

78. Hinrichs, W. L. J.; Schuurmans-Nieuwenbroek, N. M. E.; van de Wetering, P.; Hennink, W. E., Thermosensitive polymers as carriers for DNA delivery. *Journal of Controlled Release* **1999,** *60* (2-3), 249-259.

79. Dincer, S.; Tuncel, A.; Piskin, E., A potential gene delivery vector: N-isopropylacrylamide-ethyleneimine block copolymers. *Macromolecular Chemistry and Physics* **2002,** *203* (10-11), 1460-1465.

80. Chen, J. P.; Hoffman, A. S., Polymer protein conjugates .2. Affinity precipitation separation of human immuno-gamma-globulin by a poly(n-isopropylacrylamide)-protein-a conjugate. *Biomaterials* **1990,** *11* (9), 631-634.

81. Kondo, A.; Kaneko, T.; Higashitani, K., Development and application of thermosensitive immunomicrospheres for antibody purification (vol 44, pg 1, 1994). *Biotechnology and Bioengineering* **1994,** *44* (3), 395-395.

82. Anastase-Ravion, S.; Ding, Z.; Pelle, A.; Hoffman, A. S.; Letourneur, D., New antibody purification procedure using a thermally responsive poly(n-isopropylacrylamide)-dextran derivative conjugate. *Journal of Chromatography B* **2001,** *761* (2), 247-254.

83. Fukumori, K.; Akiyama, Y.; Kumashiro, Y.; Kobayashi, J.; Yamato, M.; Sakai, K.; Okano, T., Characterization of ultra-thin temperature-responsive polymer layer and its polymer thickness dependency on cell attachment/detachment properties. *Macromolecular Bioscience* **2010,** *10* (10), 1117-1129.

84. Takahashi, H.; Nakayama, M.; Yamato, M.; Okano, T., Controlled chain length and graft density of thermoresponsive polymer brushes for optimizing cell sheet harvest. *Biomacromolecules* **2010,** *11* (8), 1991-1999.

85. A. D. McNaught, A. W., *Iupac compendium of chemical terminology (the gold book)*. Blackwell Sceintific Publications: Oxford, 1997.

86. Yuan, J. J.; Jin, R. H., Fibrous crystalline hydrogels formed from polymers possessing a linear poly(ethyleneimine) backbone. *Langmuir* **2005,** *21* (7), 3136-3145.

87. Lowe, A. B.; McCormick, C. L., Synthesis and solution properties of zwitterionic polymers. *Chemical Reviews* **2002,** *102* (11), 4177-4189.

88. Kudaibergenov, S.; Jaeger, W.; Laschewsky, A., Polymeric betaines: Synthesis, characterization, and application. In *Supramolecular polymers polymeric betains oligomers*, Donnio, B.; Guillon, D.; Harada, A.; Hashidzume, A.; Jaeger, W.; Janowski, B.; Kudaibergenov, S.; Laschewsky, A.; Njuguna, J.; Pielichowski, J.; Pielichowski, K.; Takashima, Y., Eds. 2006; Vol. 201, pp 157-224.

89. Jia, X.; Chen, D. Y.; Jiang, M., Preparation of peo-b-p2vph(+)-s2o82- micelles in water and their reversible ucst and redox-responsive behavior. *Chemical Communications* **2006,** (16), 1736-1738.

90. Haas, H. C.; Moreau, R. D.; Schuler, N. W., Synthetic thermally reversible gel systems .2. *Journal of Polymer Science Part a-2-Polymer Physics* **1967,** *5* (5PA2), 915-&.

91. Shimada, N.; Ino, H.; Maie, K.; Nakayama, M.; Kano, A.; Maruyama, A., Ureido-derivatized polymers based on both poly(allylurea) and poly(l-citrulline) exhibit ucst-type phase transition behavior under physiologically relevant conditions. *Biomacromolecules* **2011,** *12* (10), 3418-3422.

92. Liu, F. Y.; Seuring, J.; Agarwal, S., Controlled radical polymerization of n-acryloylglycinamide and ucst-type phase transition of the polymers. *Journal of Polymer Science Part a-Polymer Chemistry* **2012,** *50* (23), 4920-4928.

93. Heskins, M.; Guillet, J. E., Solution properties of poly(n-isopropylacrylamide). *Journal of Macromolecular Science: Part A - Chemistry* **1968,** *2* (8), 1441-1455.

94. Plunkett, K. N.; Zhu, X.; Moore, J. S.; Leckband, D. E., Pnipam chain collapse depends on the molecular weight and grafting density. *Langmuir* **2006,** *22* (9), 4259-4266.

95. Kaholek, M.; Lee, W. K.; Ahn, S. J.; Ma, H. W.; Caster, K. C.; LaMattina, B.; Zauscher, S., Stimulus-responsive poly(n-isopropylacrylamide) brushes and nanopatterns prepared by surface-initiated polymerization. *Chemistry of Materials* **2004,** *16* (19), 3688-3696.

96. Gil, E. S.; Hudson, S. M., Stimuli-reponsive polymers and their bioconjugates. *Prog. Polym. Sci.* **2004,** *29* (12), 1173-1222.

97. Aoyagi, T.; Ebara, M.; Sakai, K.; Sakurai, Y.; Okano, T., Novel bifunctional polymer with reactivity and temperature sensitivity. *Journal of Biomaterials Science-Polymer Edition* **2000,** *11* (1), 101-110.

98. Ebara, M.; Aoyagi, T.; Sakai, K.; Okano, T., Introducing reactive carboxyl side chains retains phase transition temperature sensitivity in n-isopropylacrylamide copolymer gels. *Macromolecules* **2000,** *33* (22), 8312-8316.

99. Aoki, T.; Muramatsu, M.; Torii, T.; Sanui, K.; Ogata, N., Thermosensitive phase transition of an optically active polymer in aqueous milieu. *Macromolecules* **2001,** *34* (10), 3118-3119.

100. Gan, L. H.; Deen, G. R.; Loh, X. J.; Gan, Y. Y., New stimuli-responsive copolymers of n-acryloyl-n '-alkyl piperazine and methyl methacrylate and their hydrogels. *Polymer* **2001,** *42* (1), 65-69.

101. Maeda, Y., Ir spectroscopic study on the hydration and the phase transition of poly(vinyl methyl ether) in water. *Langmuir* **2001,** *17* (5), 1737-1742.

102. Inoue, T.; Chen, G. H.; Nakamae, K.; Hoffman, A. S., Temperature sensitivity of a hydrogel network containing different lcst oligomers grafted to the hydrogel backbone. *Polymer Gels and Networks* **1997,** *5* (6), 561-575.

103. Okubo, M.; Ahmad, H.; Suzuki, T., Synthesis of temperature sensitive micron sized monodispersed composite polymer particles and its application as a carrier for biomolecules. *Colloid and Polymer Science* **1998,** *276* (6), 470-475.

104. Zhang, K. W.; Khan, A., Phase-behavior of poly(ethylene oxide)-poly(propylene oxide)-poly(ethylene oxide) triblock copolymers in water. *Macromolecules* **1995,** *28* (11), 3807-3812.

105. Mortensen, K.; Pedersen, J. S., Structural study on the micelle formation of poly(ethylene oxide) poly(propylene oxide) poly(ethylene oxide) triblock copolymer in aqueous-solution. *Macromolecules* **1993,** *26* (4), 805-812.

106. Kuijpers, A. J.; Engbers, G. H. M.; Feijen, J.; De Smedt, S. C.; Meyvis, T. K. L.; Demeester, J.; Krijgsveld, J.; Zaat, S. A. J.; Dankert, J., Characterization of the network structure of carbodiimide cross-linked gelatin gels. *Macromolecules* **1999,** *32* (10), 3325-3333.

107. Ramzi, M.; Rochas, C.; Guenet, J. M., Structure-properties relation for agarose thermoreversible gels in binary solvents. *Macromolecules* **1998,** *31* (18), 6106-6111.

108. Xue, C. Y.; Yonet-Tanyeri, N.; Brouette, N.; Sferrazza, M.; Braun, P. V.; Leckband, D. E., Protein adsorption on poly(n-isopropylacrylamide) brushes: Dependence on grafting density and chain collapse. *Langmuir 27* (14), 8810-8818.

109. Zhu, X.; Yan, C.; Winnik, F. M.; Leckband, D., End-grafted low-molecular-weight pnipam does not collapse above the lcst. *Langmuir* **2007,** *23* (1), 162-169.

110. Cheng, X. H.; Canavan, H. E.; Stein, M. J.; Hull, J. R.; Kweskin, S. J.; Wagner, M. S.; Somorjai, G. A.; Castner, D. G.; Ratner, B. D., Surface chemical and mechanical properties of plasma-polymerized n-isopropylacrylamide. *Langmuir* **2005,** *21* (17), 7833-7841.

111. Halperin, A.; Kroger, M., Collapse of thermoresponsive brushes and the tuning of protein adsorption. *Macromolecules 44* (17), 6986-7005.

112. Rzaev, Z. M. O.; Dincer, S.; Piskin, E., Functional copolymers of n-isopropylacrylamide for bioengineering applications. *Progress in Polymer Science* **2007,** *32* (5), 534-595.

113. Cole, M. A.; Voelcker, N. H.; Thissen, H.; Griesser, H. J., Stimuli-responsive interfaces and systems for the control of proteinâ€“surface and cellâ€“surface interactions. *Biomaterials* **2009,** *30* (9), 1827-1850.

114. Ratner, B. D.; Bryant, S. J., Biomaterials: Where we have been and where we are going. *Annual Review of Biomedical Engineering* **2004,** *6* (1), 41-75.

115. Alexander, C.; Shakesheff, K. M., Responsive polymers at the biology/materials science interface. *Advanced Materials* **2006,** *18* (24), 3321-3328.

116. Kikuchi, A.; Okano, T., Pulsatile drug release control using hydrogels. *Advanced Drug Delivery Reviews* **2002,** *54* (1), 53-77.

117. Kost, J.; Langer, R., Responsive polymeric delivery systems. *Advanced Drug Delivery Reviews* **2001,** *46* (1â€“3), 125-148.

118. Jagur-Grodzinski, J., Polymers for tissue engineering, medical devices, and regenerative medicine. Concise general review of recent studies. *Polymers for Advanced Technologies* **2006,** *17* (6), 395-418.

119. Kanazawa, H.; Kashiwase, Y.; Yamamoto, K.; Matsushima, Y.; Kikuchi, A.; Sakurai, Y.; Okano, T., Temperature-responsive liquid chromatography .2. Effects of hydrophobic groups in n-isopropylacrylamide copolymer-modified silica. *Analytical Chemistry* **1997,** *69* (5), 823-830.

120. Kanazawa, H.; Sunamoto, T.; Matsushima, Y., Temperature-responsive chromatographic separation of amino acid phenylthiohydantoins using aqueous media as the mobile phase. *Analytical Chemistry* **2000,** *72* (24), 5961-5966.

121. Halperin, A.; Kroeger, M., Collapse of thermoresponsive brushes and the tuning of protein adsorption. *Macromolecules* **2011,** *44* (17), 6986-7005.

122. Halperin, A.; Kroeger, M., Thermoresponsive cell culture substrates based on pnipam brushes functionalized with adhesion peptides: Theoretical considerations of mechanism and design. *Langmuir* **2012,** *28* (48), 16623-16637.

123. Halperin, A.; Kroeger, M., Theoretical considerations on mechanisms of harvesting cells cultured on thermoresponsive polymer brushes. *Biomaterials* **2012,** *33* (20), 4975-4987.

124. Ebara, M.; Yamato, M.; Aoyagi, T.; Kikuchi, A.; Sakai, K.; Okano, T., Immobilization of cell-adhesive peptides to temperature-responsive surfaces facilitates both serum-free cell adhesion and noninvasive cell harvest. *Tissue Engineering* **2004,** *10* (7-8), 1125-1135.

125. Chen, T.; Ferris, R.; Zhang, J. M.; Ducker, R.; Zauscher, S., Stimulus-responsive polymer brushes on surfaces: Transduction mechanisms and applications. *Prog. Polym. Sci.* **2010,** *35* (1-2), 94-112.

126. Sun, T. L.; Wang, G. J.; Feng, L.; Liu, B. Q.; Ma, Y. M.; Jiang, L.; Zhu, D. B., Reversible switching between superhydrophilicity and superhydrophobicity. *Angewandte Chemie-International Edition* **2004,** *43* (3), 357-360.

127. Schild, H. G., Poly (n-isopropylacrylamide) - experiment, theory and application. *Prog. Polym. Sci.* **1992,** *17* (2), 163-249.

128. Xue, C. Y.; Choi, B. C.; Choi, S.; Braun, P. V.; Leckband, D. E., Protein adsorption modes determine reversible cell attachment on poly(n-isopropyl acrylamide) brushes. *Advanced Functional Materials 22* (11), 2394-2401.

129. Burkert, S.; Bittrich, E.; Kuntzsch, M.; Mueller, M.; Eichhorn, K.-J.; Bellmann, C.; Uhlmann, P.; Stamm, M., Protein resistance of pnipaam brushes: Application to switchable protein adsorption. *Langmuir 26* (3), 1786-1795.

130. Huber, D. L.; Manginell, R. P.; Samara, M. A.; Kim, B. I.; Bunker, B. C., Programmed adsorption and release of proteins in a microfluidic device. *Science* **2003,** *301* (5631), 352-354.

CHAPTER 3:EXPERIMENTAL[1]

3.1:Chemical Reagents Used

3.1.1: Hydrogen peroxide [H_2O_2]:

Company Identification: Acros Organics.

MSDS Name: Hydrogen Peroxide (30% in Water) (Without Stabilizer), Reagent ACS.

Catalog Numbers: AC411880000, AC411881000, AC411885000.

3.1.2: Sulfuric acid [H_2SO_4] 98%:

Company Identification: Acros Organics.

MSDS Name: Sulfuric acid, reagent ACS.

Catalog Numbers: 13361-0000, 13361-0010, 13361-0025.

3.1.3: Toluene:

Company Identification: Acros Organics.

MSDS Name: Toluene, reagent ACS.

Catalog Numbers: 424500-0000, 42455-0010, 42455-0250, 42455-5000.

3.1.4: Methyl ethyl ketone:[2]

Company Identification: Acros Organics.

MSDS Name: 2-Butanone, 99+%.

---

[2] *Experimental procedures and chemical reagents that are specific to a particular chapter are outlined in the chapter's experimental section.*

Catalog Numbers: 14967-0000, 14967-0010, 14967-0025, 14967-0250.

3.1.5: Chloroform:

Company Identification: Acros Organic

MSDS Name: Chloroform ACS reagent

Catalog Numbers: 423550040

3.1.6: Dimethyl Sulfoxide (DMSO):

Company Identification: Acros Organics.

MSDS Name: Methyl sulfoxide, ACS reagent

Catalog Numbers: 414880010, 414880025

3.1.7: Bovine serum fibrinogen

Company Identification: Sigma-Aldrich.

MSDS Name: Fibrinogen form bovine plasma, factor I

Catalog Numbers: F4753

3.1.8: Succinic anhydride (99%):

Company Identification: Acros Organics.

MSDS Name: Succinic anhydride, 99%.

Catalog Numbers: 158760010

3.1.9: Rhodamine-B-isothiocyanate (99%):

Company Identification: Research Organics.

MSDS Name: Rhodamine-B-Isothiocyanate.

Catalog Numbers: 0808R

3.1.10: Methanol

Company Identification: Sigma-Aldrich

MSDS Name: Methanol Chromasolv for HPLC

Catalog Numbers: 34860-4XL-R

3.2.11 PBS TABLETS

Company Identification: Amresco

MSDS Name: Phosphate Buffered Saline Tablets, 100mL

Catalog Numbers: E404

3.2.12 Tetrahydrofuran

Company Identification: Sigma-Aldrich

MSDS Name: Tetrahyrofuran, anhydrous,

Catalog Numbers: 401757

3.2.13 2',2-Azobisisobutyronitrile, 98% (AIBN)

Company Identification: Sigma-Aldrich

MSDS Name: 2,2'-Azobis(2-methylpropionitrile)

Catalog Numbers: 441090

3.2.14 N,N'-Methylenebisacrylamide (BIS)

Company Identification: Sigma-Aldrich

MSDS Name: N,N'-Methylenebisacrylamide

Catalog Numbers: M7279

3.2.15 N-isopropylacrylamide (NIPAM)

Company Identification: Trade TCI

MSDS Name: N-isopropylacrylamide

Catalog Numbers: A39DOOA

3.2.16 Acrylic Acid

Company Identification: Alfa Aesar

MSDS Name: Acrylic Acid

Catalog Numbers: 43359

3.2.17 Dodecyltrimethylammonium chloride (DTAC)

Company Identification: Fluka

MSDS Name: Dodecyltrimethylammonium chloride

Catalog Numbers: 44242

3.2.18 2,2'-Azobis(2-methylpropionamidine) dihydrochloride (AAPH)

Company Identification: Aldrich

MSDS Name: 2,2'-Azobis(2-methylpropionamidine) dihydrochloride

Catalog Numbers: 440914

3.2.19 2Glycidyl Methacrylate (GMA)

Company Identification: Aldrich

MSDS Name: Glycidyl Methacrylate

MSDS Name: *Catalog Numbers*: 151238

3.2.20 Diethyl Ether

Company Identification: Aldrich

MSDS Name: Glycidyl Methacrylate

MSDS Name: *Catalog Numbers*: 151238

3.2:Polymer Used for Surface Modification

3.2.1: Poly(glycidyl methacrylate) (PGMA) (Structure 3.1):

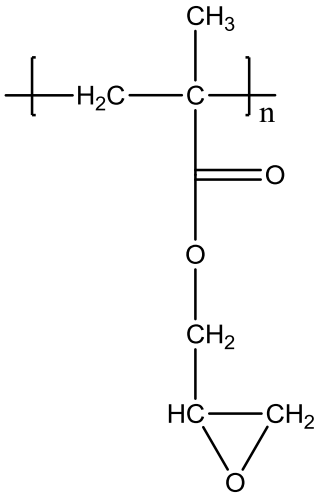

PGMA (Mn = 176,000 g/mol with polydispersity 2.70, determined by GPC using polystyrene standards) was synthesized by solution free radical polymerization and purified by multiple precipitations in diethyl ether.[1]

3.2.2: Poly(ethylene glycol) (PEG) (Structure 3.2):

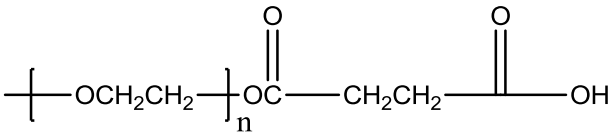

Poly(ethylene glycol) monomethyl ether, with Mn = 5,000 g/mol was modified with succinyl anhydride to form a carboxylic acid terminated derivative.[2]

3.2.3: Carboxy terminated polystyrene (PS) (Structure 3.3):

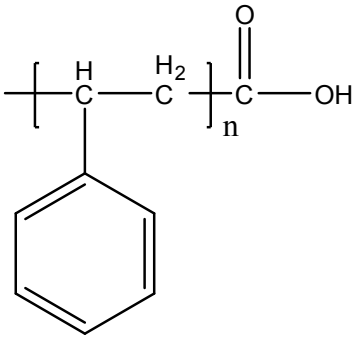

Carboxy terminated polystyrene with molecular weight Mn = 2,000 g/mol was obtained from Polymer Source Inc., Canada.

3.2.4: PGMA-*b*-PNIPAM diblock copolymer (Structure 3.4):

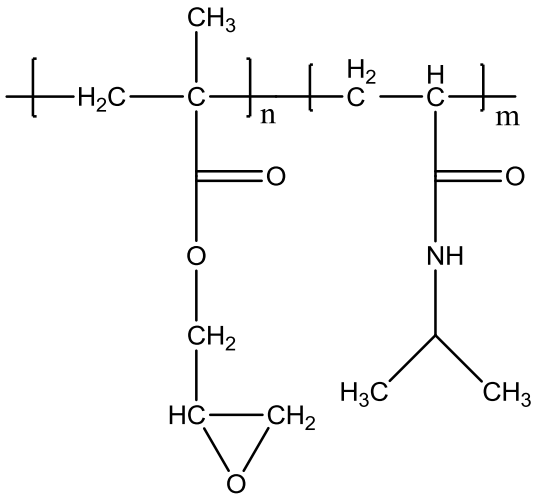

PGMA-*b*-PNIPAM block copolymers were synthesized via reversible addition fragmentation chain transfer polymerization by Dr. Bradley Lokitz at Oak Ridge National Laboratory, Oak Ridge TN. See **Table 4.1** for molecular weight.

3.2.5: PGMA-*b*-PEG diblock copolymer (Structure 3.5):

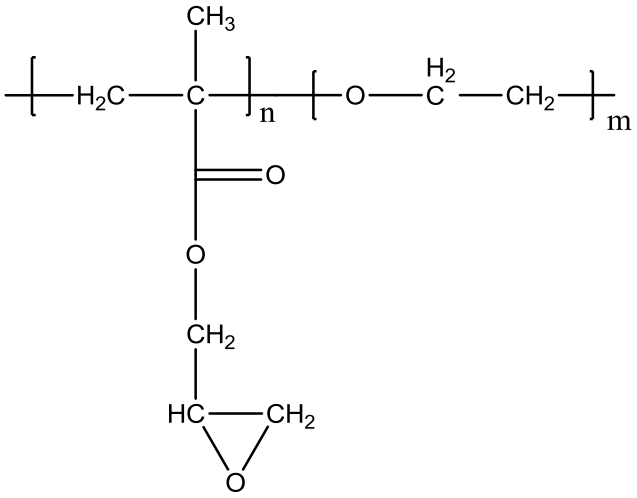

PGMA-*b*-PEG block copolymers were synthesized via reversible addition fragmentation chain transfer polymerization by Dr. Bradley Lokitz at Oak Ridge National Laboratory, Oak Ridge TN. See **Table 6.1** for molecular weight.

3.2.6: Acrylic Acid (AAc) MacroRAFT agent (Structure 3.6):

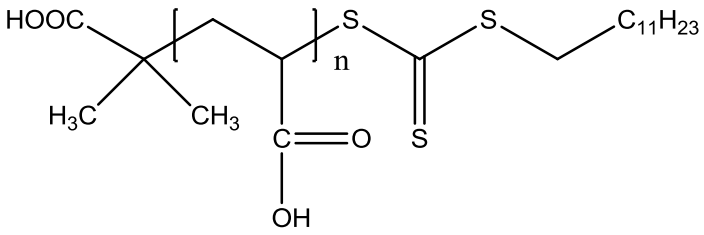

The AAc MacroRAFT (7,800 g/mol) agent was synthesized by Jutta Rieger via reversible fragmentation chain transfer polymerization at UPMC University Paris, Paris France.

3.3:Principal Experimental Characterization Techniques

3.3.1:Dip-Coating:

Dip-coating was the method used for the preparation of the thin polymer films on silicon substrates. Therefore, the substrate is immersed into the polymer solution and withdrawn at a constant speed. The resulting uniformity and thickness of the deposited film depend on the speed and any vibration of the substrate or coating solution. All polymer samples were dip-coated using a Mayer Fientechnik D-3400 dip-coater located in a clean room to avoid contamination of the clean substrates with dust particles. The operating speed was set to approximately 4 mm/sec. Therefore, in order to generate films of different thicknesses, substrates were dip-coated into solutions of different concentrations.

3.3.2:Atomic Force Microscopy (AFM):

AFM was utilized to image the resulting morphologies of the polymer and particle modified substrates. Morphological imaging was done on a Dimension 3100 and MultiMode AFM equipped with a Nanoscope 3A controller in tapping mode in ambient air, and under water. Silicon tips from Micromasch with spring constants of 50 N/m were used. All imaging was done at a scan rate of 1 Hz. Nanoscope III 5.12r3 was used for image processing.

3.3.3:Ellipsometry:

3.3.3.1:Dry State Measurements

In general, ellipsometry measures the change in polarization of light reflected off the sample surface. Measurements in the dry state for all grafted substrates were carried

out using a COMPEL automatic ellipsometer (InOmTech, Inc) at an angle of incidence of 70°. For all samples with thickness less than 11nm, the compensator was turned on. For samples with thicknesses greater than 14 nm, the compensator was turned off. Substrates with thicknesses in between these ranges, an average value was taken for measurements with the compensator on and off.

3.3.3.2:In-situ Ellipsometry

Swelling and collapse of the SSB brush layers were measured at ORNL as was reported previously.[3] Dry and solvated layer thickness and refractive index measurements were conducted on a Beaglehole Picometer Phase Modulated Ellipsometer that employs a photoelastic birefringence modulator to modulate polarization state of the incident light beam (λ=632.8nm). Ψ and Δ values were measured by changing the angle of incidence from 50 to 80° in 1° steps. These values were fit using a Cauchy model (Igo Pro. software package) to determine thickness and refractive index. Before solvated layer thickness changes were measured, each sample was measured in the dry state. A refractive index of 1.5 for all PNIPAM SSB was used, and values were fit only for thickness.

To investigate the response of the PNIPAM BCP film at different water temperatures, in situ-ellipsometry was used. All measurements were conducted inside a cylindrical liquid flow cell. The surface modified silicon wafers were clamped onto a Teflon stage which was mounted inside the glass cell. Water at approximately 25 and 60°C was continuously circulated through the cell using a peristaltic pump. All samples were scanned dry, and solvated in the same position on the wafer, while also remaining in

the cell while water at different temperatures was exchanged in order to alleviate any lateral heterogeneity of the films. The standard deviation was calculated from successive cycles of water at the two different temperatures for each sample.

3.3.4:Contact Angle Measurements:

Advancing and receding contact angle measurements were performed on a Kruss (DSA10) contact angle goniometer fitted with a temperature-controlled sample cell. Samples were run at 23°C and 41°C. Modified silicon wafers were allowed to equilibrate to the temperature of the sample cell before any measurements were taken. The water contact angle was determined using recorded video images as the drop was allowed to advance and recede while water was added and removed from the drop with an automatic syringe. At least 3 locations were measured from each sample. Still images were taken from the video using VideoDub freeware. ImageJ freeware was used to calculate the angles from the still images. Receding angles were determined using the angle tool function, while advancing contact angles were found using the Drop Shape Analysis plug-in for ImageJ.

3.3.5:AFM Colloidal Probe Technique:

All adhesion measurements were performed employing AFM colloidal probe technique. First, a force constant of AFM cantilevers (N-P series, Veeco Inc.) were determined by cantilever vs. cantilever calibration method.[4] The force constant was found to be 0.093 ±0.005 Nm^{-1}. Then, a 20 μm hollow glass bead modified firstly with PGMA and subsequently fibrinogen, was attached to the cantilevers. The procedure used was as follows. The beads (Potter Industries) were kept in piranha solution (3:1 volume ratio of

concentrated sulfuric acid (BMD) and 30 % solution of hydrogen peroxide) at 70^{o}C for 1 hour (*As a precaution, it is important to note that the cleaning solution is highly corrosive and extremely reactive to organic substances)*. The solution was decanted and the beads were rinsed several times with deionized (DI) water dried in a stream of ultra-high pure nitrogen. The beads were stirred in a 1 % wt/vol solution of PGMA (M_n = 176K) in MEK for 24 hours and rinsed several times with pure MEK. This treatment creates a thin (about 2 nm) PGMA film on the glass surface. Then, the beads were glued to the cantilevers applying the procedure described elsewhere.[5] Modified cantilevers were immersed in 1 mg/mL solution of fibrinogen in PBS for 30 min, rinsed with pure buffer solution and DI water and dried at room temperature. PGMA has very high affinity to fibrinogen and the protein is adsorbed irreversibly on the polymer's surface.

3.3.6:Protein Adsorption:

Phosphate buffered saline (PBS) solution (pH 7.4) was prepared from PBS tablets (Amresco) and deionized water as directed from the manufacturer. Bovine Fibrinogen (Sigma Aldrich) was dissolved in 0.1 M PBS at a concentration of 1.0 mg mL^{-1}. SSB (1-3) diblock copolymers were tested for adsorption at temperatures of 23 ± 2°, and 41 ± 1°C. For the latter, adsorption was achieved using an incubator. In order to guarantee homogenous adsorption conditions, vials of pure PBS, PBS protein solution, and deionized water were left to equilibrate for 1 hour at their respective temperatures. Modified wafers were then immersed in pure PBS solutions for 1 hour. Brush modified wafers were immediately transferred into their appropriate protein solution for 30 min. The samples were gently agitated. Following, wafers were rinsed in fresh PBS buffer and

deionized water (at their respective temperature) for 10 minutes each and left to dry at ambient temperatures. The thickness of the adsorbed protein was measured by ellipsometry assuming the refractive index of the protein to be 1.5.

3.3.7:Characterization of the Polymer Brush Films:

To characterize the polymer layers, several parameters have been evaluated.[6] The surface coverage (adsorbed amount), Γ (mg/m^2), was calculated from the ellipsometry thickness of the layer h (nm) using **Equation (3.1)**

$$\Gamma = h\rho \tag{3.1}$$

where ρ is the density of attached macromolecules. The density was taken as 1.05 g/cm^3 for PNIPAM, 1.13 g/cm^3 for PEG, and 1.27 g/cm^3 for PGMA. Densities were calculated by Polymer Design Tools, version 1.1 (DTW Associates, Inc) by Bicerano methods.

The chain density, σ (chain/nm^2), i.e, the inverse of the average area per adsorbed chain, was determined by **Equation (3.2)**:

$$\sigma = \Gamma * N_A * 10^{-21} / \mathrm{M}_n = (6.023 * \Gamma * 100) / M_n \tag{3.2}$$

where N_A is Avogadro's number and Mn (g/mol) is the number average molar mass of the grafted polymer.

The distance between grafting sites, D (nm), was calculated using the following **Equation (3.3)**:

$$D = \left(4 / \pi\sigma\right)^{\frac{1}{2}} \tag{3.3}$$

The radius of gyration for the macromolecules was estimated using **Equation (3.4)** :

$$6Rg^2 = L^2 \tag{3.4}$$

where L is the end to end distance.

The end-to-end distance for PNIPAM and PGMA were calculated using **Equation (3.5)** :

$$L^2 = nl^2C_\infty \tag{3.5}$$

where n is the number of C-C bonds in the polymer backbone, l is the bond length (0.154nm)[7], and C_∞ is the characteristic ratio for the polymer. C_∞ was calculated as 9.9 and 9.8 for PNIPAM and PGMA respectively utilizing the Polymer Design Tools software as mentioned above.

The work of adhesion ($\Delta\gamma$) per unit contact area was estimated using the Johnson Kendal Roberts (JKR) method for PNIPAM (See **Chapter 4** for Derjaguin-Muller-Toporov (DMT) method) and PEG films using the **Equation (3.6)**:

$$F_{JKR} = \frac{3}{2}\pi R_{tip}\omega \tag{3.6}$$

where F_{JKR} is the pull off force measured by AFM, R_{tip} is the radius of the tip, and ω is the work of adhesion.

To estimate the area of PEG and PGMA present in the grafted films in **Chapter 6**, the Cassie relation was utilized as (**Equation(3.7)**):

$$\cos\theta_{CB} = f\cos\theta_{PEG} + (1-f)\cos\theta_{PGMA} \tag{3.7}$$

where θ_{CB} is the Cassie apparent contact angle, f and $(1-f)$ are the fractional area of PEG and PGMA respectively, θ_{PEG} and θ_{PGMA} is the contact angle of pure PEG and PGMA.

3.4:References

1. Liu, Y.; Klep, V.; Zdyrko, B.; Luzinov, I., Synthesis of high-density grafted polymer layers with thickness and grafting density gradients. *Langmuir* **2005,** *21* (25), 11806-11813.

2. Zdyrko, B.; Klep, V.; Luzinov, I., Synthesis and surface morphology of high-density poly(ethylene glycol) grafted layers. *Langmuir* **2003,** *19* (24), 10179-10187.

3. Rahane, S. B.; Floyd, J. A.; Metters, A. T.; Kilbey, S. M., Swelling behavior of multiresponsive poly(methacrylic acid)-block-poly (n-isopropylacrylamide) brushes synthesized using surface-initiated photoiniferter-mediated photopolymerization. *Advanced Functional Materials* **2008,** *18* (8), 1232-1240.

4. Torii, A.; Sasaki, M.; Hane, K.; Okuma, S., A method for determining the spring constant of cantilevers for atomic force microscopy. *Measurement Science & Technology* **1996,** *7* (2), 179-184.

5. Jones, R.; Pollock, H. M.; Cleaver, J. A. S.; Hodges, C. S., Adhesion forces between glass and silicon surfaces in air studied by afm: Effects of relative humidity, particle size, roughness, and surface treatment. *Langmuir* **2002,** *18* (21), 8045-8055.

6. Henn, G.; Bucknall, D. G.; Stamm, M.; Vanhoorne, P.; Jerome, R., Chain end effects and dewetting in thin polymer films. *Macromolecules* **1996,** *29* (12), 4305-4313.

7. Sperling, L. H., *Polymeric multicomponent materials*. Wiley-Interscience Publication: New York, 1998.

CHAPTER 4:SYNTHESIS AND CHARACTERIZATION OF THERMALLY RESPONSIVE FILMS FORMED FROM REACTIVE BLOCK COPOLYMERS

4.1:Introduction

Recent studies in the area of active/responsive surfaces have importance for a variety of prospective applications such as; bio-separation[1-3], regulated cell attachment/detachment[4-6], tissue engineering[7-9], and controlled drug delivery[10]. Polymers offer diverse opportunities to design stimuli-responsive surfaces due to the ability of the polymer chains to alter their confirmation in the response to environmental stimuli. The response can be tuned by regulating chain length, chemical composition, topology, and chain architecture of macromolecules.[10]

Precise and easy methods of temperature control have drawn significant attention towards temperature responsive polymer molecules. Furthermore, among the thermally responsive class of macromolecules, considerable attention has been given to poly(*N*-isopropylacrylamide) (PNIPAM). [6-7, 11-20] PNIPAM undergoes a temperature-sensitive phase transition at its lower critical solution temperature (LCST) within the tolerances (~32°C) of the human metabolism.[21-22] A coil-to-globule conformational change is attributed to the transition of PNIPAM.[10, 23] At temperatures below the LCST, PNIPAM macromolecules arrange into an extended and hydrated layer. However, when temperatures overcome the LCST, PNIPAM chains collapse into a relatively non-hydrated conformation.

A straightforward way to fabricate the active surfaces is via polymer grafting. Polymer grafting provides robust covalent attachment of polymer chains to a substrate boundary. Controlled conformational transformation of the polymer chains have been governed by external stimuli such as; temperature[24-26], pH and ionic strength[27-30], light[31-33], ultrasound[34], and electromagnetic fields.[35-37]

Well-defined brush films have emerged as encouraging candidates for temperature manipulated surfaces used in applications such as control of protein absorption and cell adhesion. [7, 10, 38-39] In general, the covalent grafting of polymer brushes, including PNIPAM, is carried out via the "grafting from" or "grafting to" techniques. [40-43] The "grafting from" technique is conducted through polymerization that is initiated from surface bound initiating groups. Alternatively, "grafting to" technique involves the reaction of end-functionalized macromolecules with complimentary functional groups located on the substrate surface, resulting in tethered polymer chains.

Experimentally, "grafting to" provides a simplistic procedure for the construction of polymer brush films in contrast to "grafting from" as "grafting from" requires more elaborate synthetic steps. Furthermore, an additional advantage of the "grafting to" technique is the straightforward method of producing well defined polymer brush layers. Well defined layers are produced because the polymers are synthesized and characterized before attachment. However, a major drawback of this technique is low thickness (1-30nm) of the resulting films due to the self limiting characteristics of the procedure.[44] Polymer chains are hindered by diffusion of large chains through the existing polymer film to the reactive sites on the surface boundary layer. This effect becomes more

prominent as film thickness increases. [45] Equally important are the limitations of "grafting from" techniques. While increased thickness of the grafted layers can be achieved via "grafting from", the control over these characteristics of the grafted macromolecules is lost at high thickness. As a consequence, it has proven a difficult task to fabricate thick films and subsequently control the grafting density.

Covalently bound PNIPAM brushes have been routinely synthesized by a variety of effective techniques, including surface-initiated photoiniferter-mediated photopolymerization[20], surface-initiated atom transfer radical polymerization[46-48], electron beam irradiation[7], and plasma polymerization[49]. "Grafting to" of PNIPAM has been previously carried out by reaction of carboxy-terminated PNIPAM to a macromolecular anchoring layer of poly(glycidyl methacrylate) (PGMA) on silicon substrates as well.[10] It is necessary to point out that covalent attachment of polymer brushes is routinely done minimally in three experimental steps; surface treatment with complimentary functional groups or initiator groups, attachment or growth of polymer chains, and post modification extraction of non-covalently attached chains via multiple rinsing with a solvent.

Physisorption of PNIPAM block copolymers has been utilized to fabricate thin responsive brush films as well. To our knowledge only a handful of reports have been published using these conditions. [50-52] Loh et al. utilized PNIPAM-b-poly[(R)-3-hydroxybutyrate]-b-PNIPAM triblock copolymer to coat bare substrates. Although stable coatings were made, a roughly 10% by mass of the original coating was lost after incubation in water as monitored by ellipsometry.[52] Nakayama and coworkers employed

a diblock copolymer for the formation of polymer brushes by physisorption. Scientists utilized a hydrophobic second component with PNIPAM to anchor it to the surface. They determined that little to no loss of the layer was seen after cycling in cold and hot water rinses. However, for other applications where increased thickness is desirable (30-100nm for example), scientists did not demonstrate coatings of increased thickness without layer thickness loss using this technique.[51]

To this end, the primary focus of the work reported in **Chapter 4** is the single step robust fabrication of thermally responsive thin films with accurate control over surface properties. To the best of our knowledge, fabrication of this type of grafted layer has not yet been reported in the scientific literature. Traditionally, polymer brushes are synthesized via multiple steps. Additionally, the proposed technique allows the formation of tunable thickness (5-250nm) of PNIPAM-grafted layer, much thicker than traditional "grafting to" technique allows.

By deposition of thermally responsive/reactive block copolymers (BCP), the advantages of the "grafting to" procedure were seen. A PGMA anchoring layer has been employed to modify various polymeric and inorganic surfaces.[22, 53-54] Therefore, we foresee procedures demonstrated in this work to be readily adapted to various substrate types.

For this purpose, PNIPAM containing BCPs with varying molecular weights of PGMA were used. Conditions for synthesis and preparation of thermally responsive polymer layers with varying block copolymer symmetry were identified. PGMA was selected as the complimentary reactive block to PNIPAM block to serve as the anchoring

layer attaching the block copolymer to the substrate.[10, 22, 43-44, 53, 55] Therefore, PNIPAM brush synthesis via "grafting to" was made possible through the reaction between epoxy groups from the PGMA anchoring block and the substrates natural oxide layer.[44, 55-57] We compare the thermally responsive behavior of the grafted single step PNIPAM block copolymers brush (SSB) films with varying block symmetry to that of conventional PNIPAM brush methods in terms of their surface properties. Conventional brushes were fabricated utilizing methods developed in our laboratory and published elsewhere.[10, 57] Thin films (5-8nm) of PGMA (Mn-176k) were dip-coated and annealed on silicon wafers. Carboxy terminated PNIPAM (Mn-25k) was subsequently deposited and grafted in a second step. Multiple rinsing in organic solvent was utilized to remove any un-reacted polymer from the layer.

Herein, the morphology of the resulting polymer films was investigated using atomic force microscopy (AFM). The thermally responsive behavior of the grafted SSB layers was investigated by advancing contact angle measurements as a function of temperature and pre-solvent treatment. Actuation of the brush layers were monitored via in-situ ellipsometric measurements in aqueous environments as a function of temperature. Lateral chemical composition of the grafted layers was studied by angle resolved-X-ray photon spectroscopy (AR-XPS).

4.2:Experimental

4.2.1:Synthesis of Block Copolymers at ORNL by Bradley Lokitz

PGMA MacroCTA: Reactions were formulated in a single-neck 100 mL Airfree® round bottom reaction flask equipped with a Teflon-coated magnetic stir bar. In a typical

reaction, GMA (7.11 g, 5.00 x 10^{-2} mol) was combined with CPDT (245.71 mg, 7.11 x 10^{-4} mol; GMA: CPDT = 352), V-70 (43.85 mg; molar ratio of CPDT:V-70 = 5:1) and benzene (50.0 mL). The reaction vessel was capped with a rubber septum and the solution was sparged with dry argon for approximately 30 min. The reaction vessel was then placed in a heated oil bath thermostatted at 30°C and allowed to react for a predetermined time, after which the reaction vessel was immersed in liquid nitrogen to quench the polymerization.

PGMA-b-PNIPAM. Reactions were formulated in a single-neck 50 mL Airfree® round bottom reaction flask equipped with a Teflon-coated magnetic stir bar. In a typical reaction, NIPAM (1.13 g, 1.00 x 10^{-2} mol) was combined with the PGMA-macroCTA (433.78 mg, 3.77 x 10^{-5} mol; PNIPAM:PGMA-macroCTA = 265), V-70 (11.63 mg; molar ratio of PGMA-macroCTA:V-70 = 1:1) and benzene (20.0 mL). The reaction vessel was capped with a rubber septum and the solution was sparged with dry argon for approximately 30 min. The reaction vessel was then placed in a heated oil bath thermostatted at 30°C and allowed to react for a predetermined time, after which the reaction vessel was immersed in liquid nitrogen to quench the polymerization. PGMA-*b*-PNIPAM was subsequently reconstituted in THF and precipitated in a 10-fold excess of hexanes (repeated 3x) and dried *in vacuo*.

4.2.2:Grafting of Block Copolymers to Silicon Substrates

Silicon wafers were used as a model substrate. Highly polished single-crystal silicon wafers (Semiconductor Processing Co.) were first cleaned in an ultrasonic bath for 30 minutes, placed in a hot (80°C) “piranha” solution (3:1 conc. H_2SO_4 : 30% H_2O_2) for

1 hour, and then rinsed several times with high-purity DI water. (*As a precaution, it is important to note that the cleaning solution is highly corrosive and extremely reactive to organic substances.)* PNIPAM block co-polymers were dissolved in MEK (0.75% w/v) and thin films (30 ± 5nm) were deposited on the substrate by dip-coating (Mayer Feintechnik D-3400, speed 240 mm/min) and annealed at 130°C for 16 hours. To be consistent with all experiments, all samples were rinsed three times in fresh MEK for 30 min.

Two step conventional PNIPAM (TSB) brushes were fabricated as follows. A 5-8nm thin film of PGMA (Mn=176,000) was dipcoated from 0.1 wt/vol% solution in MEK and annealed at 130°C for 1 hour. Subsequent modified wafers were dipped into a 1% wt/vol solution of PNIPAM (Mn=25,000) in MEK. Dipcoated films were annealed in vacuum at 130°C for 16 hours. Unbound PNIPAM chains were removed by three subsequent rinses in fresh MEK for 30 minutes each upon completion of annealing.

4.2.3:Characterization of Block Copolymer Films

Dry grafted layer thickness was determined by ellipsometry measurements as discussed in **Section 3.3.3.1** Advancing and receding contact angle data was performed as mentioned in **Section 3.3.4.** To investigate the response of the PNIPAM SSB films at variable water temperature, in situ-ellipsometry was used (**Section 3.3.3.2)**.

Angle Resolved X-ray Photoelectron Spectroscopy (AR-XPS) was performed by Niz Naoki at Georgia Tech University using a Kratos AXIS Ultra system, with an Al Kα x-ray source. Survey scans were performed at 0º, 30º, and 60º with respect to the normal to the surface, and the compositions were compared to obtain qualitative depth profiles.

Measurements can be affected by adventitious carbon and shards of Si contaminating the surface during handling, making precise quantitative analysis challenging. However, a quantitative approximation can still be instructive. Given that the attenuation length of the polymer is expected to be on the order of 10 nm, samples of approximately 30 nm were used to obtain approximate depth profiles of the films.

4.2.4:Equations used to Characterize Block Copolymers

To characterize the polymer layers, several parameters have been evaluated.[58] The surface coverage (adsorbed amount), Γ (mg/m^2), was calculated from the ellipsometry thickness of the layer h (nm) using **Equation (3.1)** The chain density, σ (chain/nm^2) was determined by **Equation (3.2)** The distance between grafting sites, D (nm), was calculated using **Equation (3.3):** The radius of gyration for the macromolecules was estimated using **Equation (3.4)** The end-to-end distance for PNIPAM and PGMA were calculated using **Equation (3.5)**.

In order to determine the amount of water entering the films, and also back check thickness change with the measured refractive index during swelling and collapse of the films monitored by *in-situ* ellipsometry, Bruggemans effective medium approximation applies for ideal mixtures as represented by **Equation (4.1)** [59]:

$$0 = v_1 \frac{n_1^2 - \langle n \rangle^2}{n_1^2 + 2\langle n \rangle^2} + v_2 \frac{n_2^2 - \langle n \rangle^2}{n_2^2 + 2\langle n \rangle^2} + \ldots \qquad (4.1)$$

where $\langle n \rangle$ is the refractive index of the mixture, n_1, n_2 are the refractive indexes of the components (water and polymer) of the mixture, and v_1, v_2 are the volume fractions of the components in the mixture.

This approximation has been widely used in organic and inorganic coatings to model refractive index. [60-61] In our case, we assume no lateral direction changes in the film upon swelling in aqueous environments. Therefore, $v_1 = v_p$ (polymer) = h_o/h and $v_2 = v_s$ (solvent) = $(h-h_o)/h$. Here, h is the measured swollen or collapsed film thickness and h_o is the thickness of the film in the dry state. Therefore, we can approximate the volume fraction of water within the polymer films at varying temperatures as a function of block copolymer composition. **Equation (4.1)** can be rewritten as (**Equation (4.2)**:

$$\frac{h}{h_o} = 1 - \left(\frac{n_o^2 - n^2}{n_o^2 + 2n^2} / \frac{n_s^2 - n^2}{n_s^2 + 2n^2} \right) \tag{4.2}$$

where n_o is the refractive index of the dry polymer film, n_s is the refractive index of the solvent, and n is measured refractive index of the film in the swollen or collapsed state.

4.3:Results and Discussion

4.3.1:Block Co-Polymer Synthesis and Characterization

Block copolymers were synthesized via reversible-addition fragmentation chain transfer (RAFT) polymerization at Oak Ridge National Laboratory by Bradley Lokitz. Diblock co-polymers are consisting of two blocks: PNIPAM segment, and a PGMA segment with varying molecular weights.

A PGMA macro chain transfer agent was synthesized and employed in the ensuing co-polymer synthesis. The co-polymers were specifically designed in order to vary the molecular weight of the PGMA block, while the PNIPAM block was held constant. Moreover, the PGMA block was designed as such that, PGMAs degree of

polymerization was much less than PNIPAM, approximately equal, and finally synthesized to a greater degree of polymerization than that of PNIPAM.

Table 4.1: Molecular weight characteristics of SSB PNIPAM block copolymers.

	Block Copolymer Mn	Mw	PDI	PGMA Mn	Mw	PDI	PNIPAM Mw
BCP-1	35,700	45,900	1.28	11,500	13,500	1.17	32,400
BCP-2	47,800	53,900	1.13	21,200	24,200	1.14	29,700
BCP-3	65,500	74,100	1.16	36,600	43,900	1.20	30,200

The targeted molecular weights and degrees of polymerization were chosen as such in order to study the effects of an increasing PGMA block on thermally responsive brush behavior fabricated by deposition of bi-functional block copolymers (BCP 1-3). The BCPs where characterized by gel permeation chromatography (GPC). GPC was performed to estimate the molecular weight of the individual block segments. **Table 4.1** displays the molecular weights and polydispersities of the resulting polymers. The block co-polymers exhibit relatively low polydispersity (< 1.20). Moreover **Table 4.1** verifies that a series of three block co-polymers were synthesized consisting of a PGMA segment with varying degrees of polymerization. From BCP-1 the PGMA degree of polymerization was found to be in a 1:3 ratio with PNIPAM, BCP-2 2:3 ratio, and finally BCP-3 was found to be 2.5:2. The PGMA block co-polymers here on out will be referred to by sample names given in **Table 4.1**.

4.3.2:Synthesis and Morphology of Polymer Brush Layers formed from Block Copolymers

4.3.2.1:Synthesis of Polymer Brush Layers

The series of PNIPAM block copolymer layers (SSB 1-3) bearing different molecular weights of PGMA block segments were deposited on silicon wafer substrates via dip-coating from MEK. The surface attachment of the BCPs arises from an epoxy functionality located in every repeat unit of PGMA. PGMA homopolymers has been extensively used as macromolecular anchoring layer for the grafting of various polymers to surfaces.[22, 44, 53-54, 57, 62-63] For homopolymer PGMA thin films, the epoxy units that react with surfaces are found in the train portion of the deposited film. It has been shown that, for high molecular weight polymers, roughly 0.15 to 0.25 accounts for the train fraction adsorbed at the surface.[64] At maximum, 60% of epoxy groups may be lost due to self cross-linking of PGMA.[55, 64] It was expected that SSB 1-3 films would successfully graft to silicon wafers similar to results shown by Lokitz et al.[65]

A solvent with high affinity for both blocks was chosen in order to achieve total solvation of the BCPs, in order to inhibit micellization of the blocks. Methyl ethyl ketone (MEK) was used as the solvent for deposition.

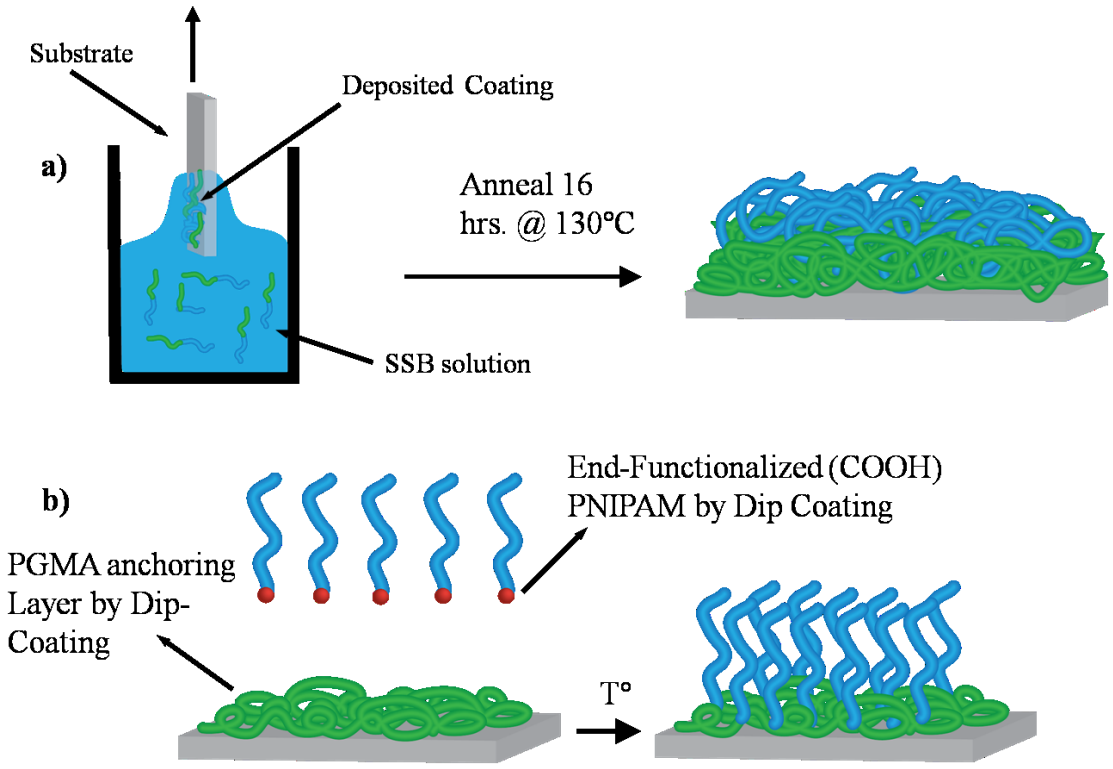

Figure 4.1: Schematic of film formation techniques for a) SSB films and b) TSB type films.

Figure 4.1a displays an overall schematic of the film formation technique for the SSB generated films. After the deposition by dip-coating, block copolymer layers were annealed under vacuum at 130°C for various amounts of time. After annealing, samples were vigorously rinsed in solvents with varying polarities (water, MEK, THF) to confirm that indeed SSB layers were formed. **Figure 4.2** displays the percentage of thickness of anchored polymer layer vs. annealing time at 130°C. Initial deposited layers shown in **Figure 4.2** were measured to be 25-35nm. The percentage of layer retention was measured by dividing the ellipsometric layer thickness before and after rinsing in MEK

after grafting at the appropriate temperature. It is evident at shorter times (30 min), roughly 92% of the initial deposited layer is attached at the annealing conditions of 130°C. At annealing times approaching 16 hours, the percent of grafted SSB layers reach ~100%. This indicates that the amount of initial polymer deposited is fully retained on the surface at 16 hours of annealing. Moreover, layers with increased (to deposit films with increased thickness, the BCP concentration of the dip-coating solution was increased) thickness (100, 250nm) were also annealed at 16 hours. Complete grafting was observed independent of initial layer thickness. Therefore, polymeric films with desired thicknesses can be deposited and attached to the surface in a single step. Thus, this is a promising advantage of the technique over conventional "grafting to" methods, as diffusion limitations effectively prohibit fabrication of such thick films.

4.3.2.2:Characterization of Polymer Brush Layers

However, to substantiate the SSB end tethered systems as brush surfaces, the distance between grafting sites should be smaller than two radii of gyration.[66] Therefore the prepared PNIPAM assemblies can be assigned to "brush" or "mushroom" regimes based on the plot shown in **Figure 4.3a**. The dashed line in **Figure 4.3a** corresponds to the border point between the "brush" and "mushroom" regimes for the SSB block copolymers and TSB assembly. The radius of gyration, end-to-end distance, and grafting density were calculated where PNIPAM chains are end grafted to a PGMA scaffold.

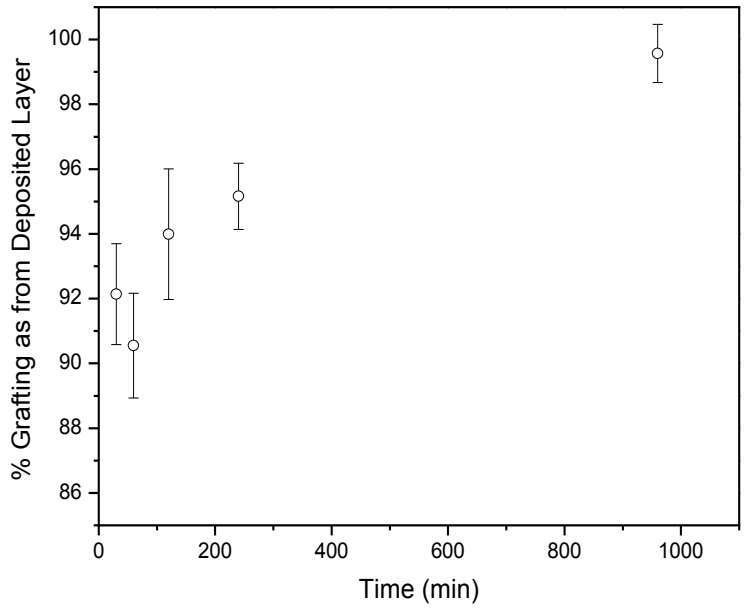

Figure 4.2: Anchoring of SSB films as a function of time at 130°C.

Radius of gyration for the SSB PNIPAM fractions of the films was calculated as; 4.1 (SSB-1), 4.3 (SSB-2), and 4.5nm (SSB-3) with 2Rg approximately 8.5nm for all three fractions. Macromolecules in the dry state are collapsed on the surface when in the amorphous state. But when in solution, the prepared films are all in the "brush" regime, as the effective distance between grafting sites (1.6-2.1nm) is much less than 2Rg of the polymer coil. To compare the new developed SSB method, TSB PNIPAM films were also evaluated for the regime of surface tethering. Radius of gyration, R_g, for polymer molecular weight (Mn = 25,000) is 4.2nm, with 2Rg of 8.4nm. Thus, the TSB film is also in the brush regime as the grafting density (0.3 chains/nm^2) is much less than its two radii of gyration.

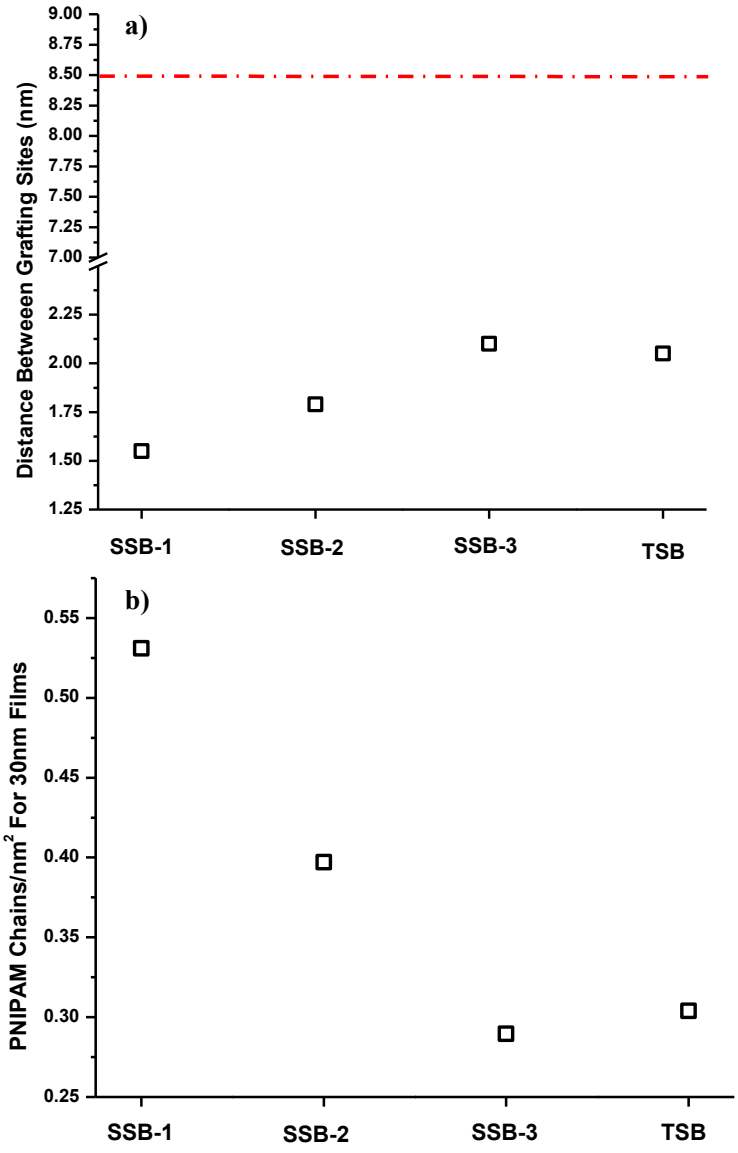

Figure 4.3: Parameters of SSB and TSB brushes. a) Distance between grafting sites vs. temperature. Dashed line corresponds to the border between the mushroom (above line) regime and brush (below) regime. b) Grafting density (chains/nm^2) for PNIPAM films normalized for 30nm films.

For the incorporated PGMA fragments, the radius of gyration varies from 2.5 (SSB-1) to 4.5nm (SSB-3), as a second component yielding an apparent overall radius of gyration for the block copolymer system as; 6.6 (SSB-1), 7.7(SSB-2) and 8.9 nm (SSB-3). The creation of symmetric and asymmetric block copolymers by varying the block length of PGMA creates a simple and effective method to fabricate surfaces with known and controllable effective grafting densities. As **Figure 4.3b** shows, the PNIPAM grafting density of SSB films decrease with increasing PGMA content for films normalized at constant surface coverage (30nm thick films). SSB-1 effective grafting density was calculated to be 0.5 chains/nm^2, decreasing to 0.4 (SSB-2) and 0.3 chains/nm^2 for SSB-3. The TSB layer grafting density was calculated to be 0.3 chains/nm^2 for comparison.

30 nm films were chosen specifically in order to study the brush behavior of "single" layer films of the SSB layers. Block copolymers can phase separate into spheres, cylinders, or alternating lamellae depending on the length of the blocks. Lamellae are formed when the block segments are close to the same length, which we suppose is our case. Therefore we calculated the thickness of the lamellae size of each PNIPAM and PGMA component of SSB 1-3 depending on the molecular weights of the block substituents.[67] To do so, we used the **Equation (4.3)**:

$$R = 1.4\alpha \bar{K} M^{1/2} \qquad (4.3)$$

where $\bar{K}$ is the experimental constant relating the root mean square end-to-end distance to the molecular weight and is taken as 0.565 (poly (methyl methacrylate), R is the half thickness of the lamellae, α values were taken as 1.25 since α varies between 1.0 and

1.5 for most polymers and M is the number average molecular weight.[67] **Table 4.2** displays the calculated values for the full thickness of the resulting lamellae structures found from PGMA PNIPAM phase separation. As observed, with increasing PGMA molecular weight, the total lamellae formation for one complete layer ranges approximately from 52-71nm for SSB1-3 respectively. If SSB layers were deposited at thicknesses above values listed in **Table 4.2**, multi-layer structures will form (Ex. grafting of 250nm SSB films). Therefore, we can conclude that the film thickness studied in this chapter is not multi-layer structures, and more closely resemble a single layer system much like conventional brush films.

Table 4.2: Calculated thickness values for lamellae's formed from resulting PNIPAM-PGMA BCPs.

	PNIPAM Lamellae Thickness (nm)	**PGMA Lamellae Thickness (nm)**	**Total Thickness (nm)**
SSB-1	30.8	21.2	52.0
SSB-2	32.3	28.8	61.0
SSB-3	33.6	37.8	71.4

4.3.2.3:Determination of Lateral Chemical Composition of Grafted Layers

To validate the changes in surface properties in relation to the amount of PGMA present in the block copolymer, angle resolved x-ray photon spectroscopy (ARXPS) was performed in order to elucidate the lateral chemical composition in the outer 10 nm region of the PNIPAM grafted films. The measurements were conducted at Georgia Tech

with Naoki Nitta under Prof. Gleb Yushin's guidance. Specifically, ARXPS was recorded for all PNIPAM grafted brush films. Spectra were also recorded for pure PNIPAM and PGMA films as reference samples. **Table 4.3** displays the carbon and nitrogen percentages as a function of take off angle. The carbon and nitrogen content was determined at take-off angles of 0 (perpendicular to film surface), 30 and 60°. Depth of probing for the measured angles is approximately 10, 6 and 2nm respectively according to literature.[68-69] The amount of PNIPAM at the outermost nano region of the film was estimated based on theoretical values for nitrogen content.

Table 4.3: Carbon and nitrogen content as a function of take off angle.

	0°	**30°**	**60°**
Take Off Angle	**C%/N%**	**C%/N%**	**C%/N%**
SSB-1	72.9/8.9	74.1/8.7	74.5/10.0
SSB-2	72.7/8.7	72.8/8.6	74.7/10.4
SSB-3	71.4/6.8	72.6/7.5	73.1/9.0
Conv. Brush	73.7/10.8	75.2/11.0	75.7/11.8
PNIPAM Reference	75.2/12.5	76.5/11.9	77.0/12.0
PGMA Reference	69.5/0	71.4/0	73.6/0

As evident in **Table 4.3** carbon and nitrogen values determined for the PNIPAM and PGMA reference samples at the highest depth (0°) of probing were within 0.5% of theoretical values. However as probing depth decreased, the values for carbon and nitrogen deviate from theoretical values for atomic ratios of PNIPAM and PGMA. In both cases the carbon ratios for PGMA and PNIPAM increased with increasing take off angle. It is also observed that the nitrogen content in PNIPAM reference sample decreases with decrease depth of probing. We attribute this to the fact that at the very most outer region of the film, the increased carbon and decreased nitrogen content is due to the rearrangement of the polymer chain backbone. It is evident that the carbon containing backbone of PNIPAM and PGMA is in higher concentration in the 1nm depth range in comparison to their more polar side chains.

The TSB film was found to have 10.8% nitrogen content at a takeoff angle of 0°. It was estimated that 10.8% nitrogen is equivalent to approximately 87% PNIPAM content. This is due to the probing of the interpenetrating region between the top most layer of PNIPAM and the grafted under layer of PGMA. However, at take off angle of 60°, the percentage of nitrogen increased, thus the PNIPAM composition was estimated as 95%. This is roughly 1% less than the measured reference value at a 0° take off angle of PNIPAM. Rearrangement of the polymer backbone and side chain was attributed to the increase carbon and decreased nitrogen percentages at the outermost region of the film. Therefore, TSB PNIPAM conventional films have a polymer-air interface that is solely dominated by PNIPAM.

The series of SSB diblock copolymers were subjected to the same ARXPS measurements. At take off angle of 0°, all PNIPAM BCP contained nitrogen ratios less than that of the pure PNIPAM and traditional PNIPAM films. As the amount of PNIPAM in the block copolymer decreased, the nitrogen ratio decreased from roughly 9% to 6.8%, while the carbon ratio remained relatively stable (72.9-71.4%). This is indicative of the increased ratio of PGMA contained in the block copolymers. Interestingly, as the probing depth decreased, the amount of nitrogen contained in the film increased for all PNIPAM BCPs. This indicates slight preferential organization of PNIPAM at the outermost region of the films. The SSB films were estimated for the percent composition of PNIPAM at the outermost nano region of the BCP films; SSB-1 80%, SSB-2 83%, and SSB-3 71%. SSB-1 and -2 showed the greatest amount of PNIPAM at the interface, correlating with the largest change in properties verified by in-situ ellipsometry and contact angle measurements. SSB-3 displayed the least amount of PNIPAM at the interface, validating the diminished switchability of the PNIPAM-3 layers as seen with contact angle and in-situ ellipsometry measurements (Discussed in **Section 4.3.4, 4.3.5**). This is confirmed by the theoretical calculation for the random distribution of the block copolymers based on their compositional molar ratio. They were calculated based on the degree of polymerization (number of PNIPAM molecules present). The ratio predicts the amount of PNIPAM that would be present if the layer was completely random and no preferential arrangement was observed. The % PNIPAM values for the SSB layers were calculated as, 72.5 (SSB-1), 61.2(SSB-2), and 49.8% (SSB-3). Indeed, the experimentally determined PNIPAM percentages increase above

the statistical percentage of PNIPAM present when no preferential order is assumed. Further, the preferential arrangement lends evidence against any cylindrical layer formation and indicates a lamellae type layer formation.

4.3.2.4:Morphology of Polymer Brush Layers

To investigate to the effect of PGMA block length on film formation and morphology, AFM imaging (**Figure 4.4a-e**) was utilized to image the top most surface of the film. **Figure 4.4a-e** shows an AFM topography image of the PNIPAM block copolymers after deposition and annealing at 130°C for 16 hours, as well as PNIPAM conventional brush films and PNIPAM-PGMA homopolymer blend films after annealing. Homopolymer carboxy terminated PNIPAM (Mn-25K) and PGMA (Mn-176k) were mixed in equal wt fractions in MEK and dip-coated to evaluate if blending was a possible alternative route to synthesize thermally responsive brushes in a single step. However, **Figure 4.4e** displays that there is macroscopic phase separation making the PNIPAM-PGMA homopolymer blend an implausible technique for creating smooth and homogenous layers.

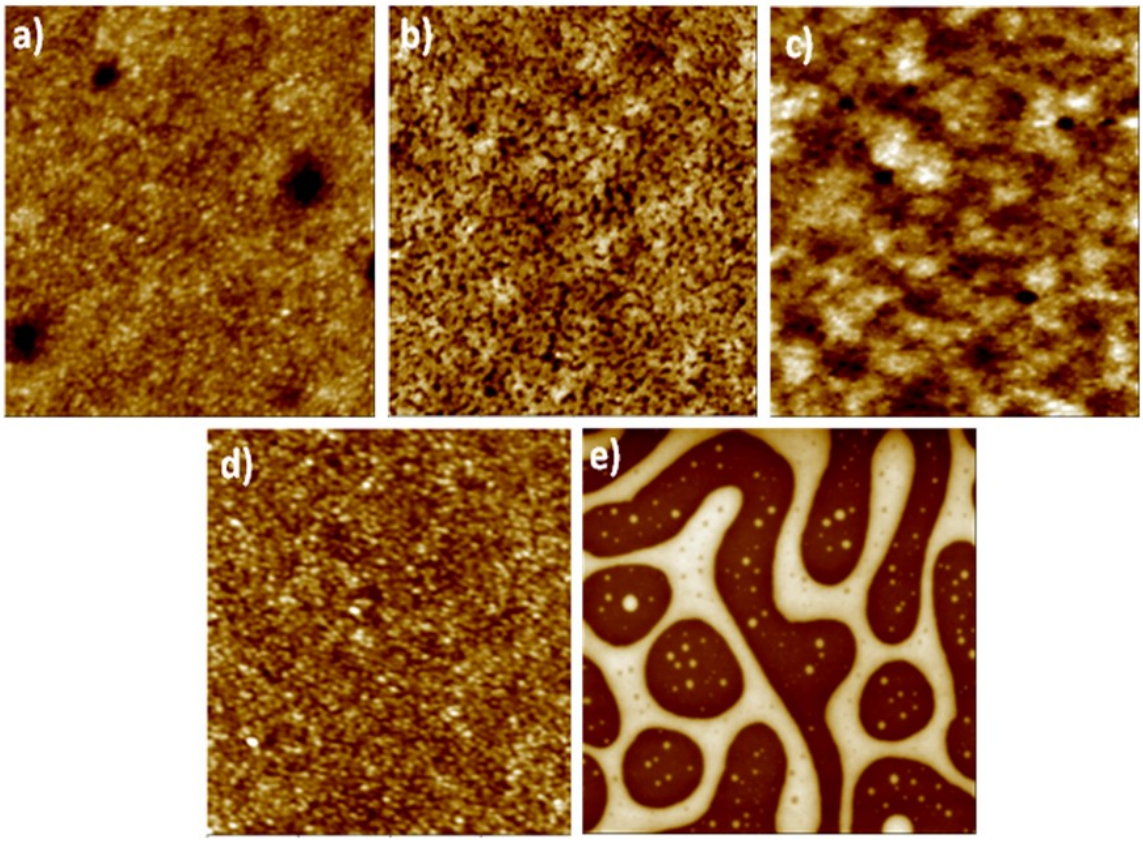

Figure 4.4: AFM topographical images (a-d: 1 x 1 μm, e: 10 x 10 μm) of grafted PNIPAM layers on silicon wafers, vertical scale for a-d: 7nm, e: 40nm a) SSB-1 b) SSB-2 c) SSB-3 d) TSB e) PNIPAM and PGMA homopolymer blend.

Figure 4.4a-c depicts films with increasing PGMA block molecular weight from left to right. **Figure 4.4d** display morphology of conventional PNIPAM brushes. The block copolymers and homopolymer brush films formed smooth and homogenous surfaces. The root mean square (RMS) roughness, evaluated for each 1x1 μm image was calculated to be <1 nm for all PNIPAM (excluding the blend) surfaces, indicating smooth layer formation and complete coverage. Morphology of the block copolymer films and conventional brush films appear similar.

In order to enhance the contrast of the resulting SSB films, grafted layers were scanned via AFM tapping mode in the presence of 25°C water vapor. Layers were scanned in water vapor because at temperatures below the LCST of PNIPAM, it is a selective solvent for the SSB films as water is a non-solvent for PGMA. Phase contrast from AFM imaging arises due to energy dissipation from contact between the tip and the material. The energy dissipation depends on the materials characteristics such as viscoelasticity, adhesion, and contact area. Therefore, differences of properties within a mixed or heterogeneous films induces a phase shift in the oscillation of the AFM cantilever.[70]

Figure 4.5a-e displays 1 x 1 μm AFM phase images of the SSB films. **Figure 4.5a** displays the soft and swollen nature of SSB-1 films when utilizing a increased set-point value permitting low force, termed "soft" tapping. Utilizing low forces, we can image the morphology of the top most region of the film. As observed, the layer is smooth and homogenous with no apparent phase contrast, indicating that PNIPAM is swollen and concentrated at the film interface. However, when utilizing a lower set-point value ("hard" tapping, **Figure 4.5b-e**), an increased phase contrast is seen. "Hard" tapping can allow the observation of phase separation that is formed underneath the swollen soft outmost layer.[71] However, we cannot estimate the exact surface coverage of the PGMA or PNIPAM because there is a very apparent gradual change between domains of PGMA and PNIPAM.

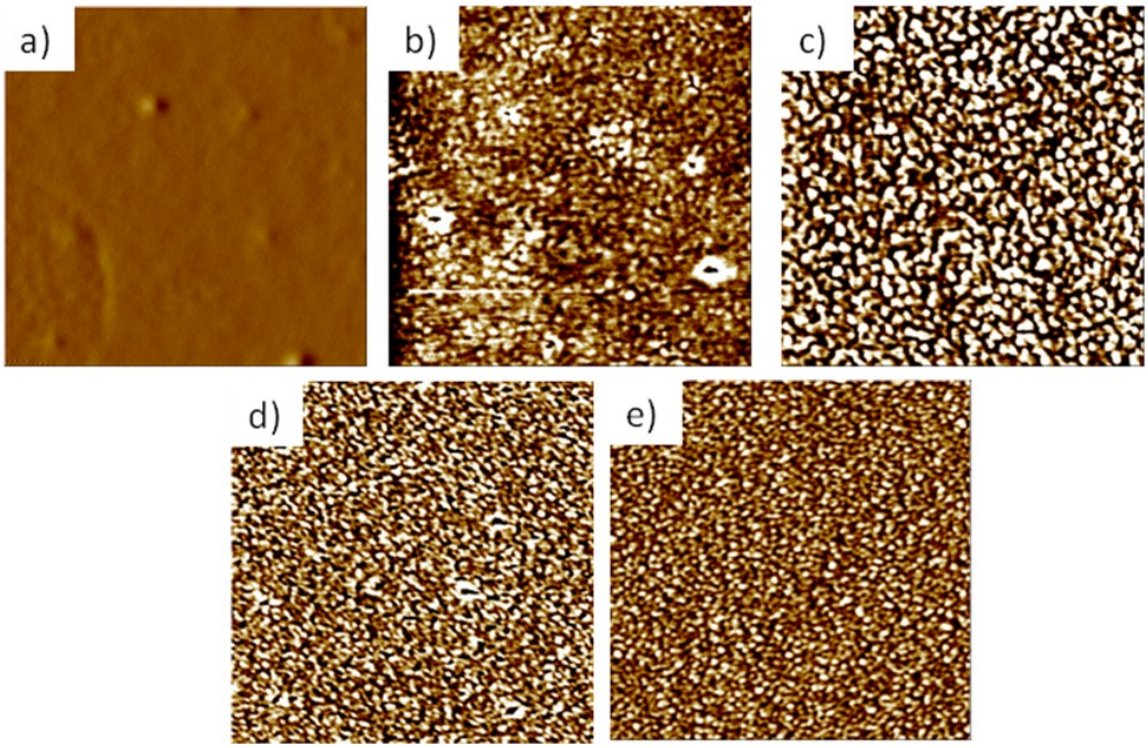

Figure 4.5: 1 x 1 μm phase images of PNIPAM block copolymers in the presence of room temperature water vapor. a) SSB-1 soft tapping b) SSB-1 hard tapping c) SSB-2 hard tapping d) PNIPAM-3 hard tapping e) Traditional brush hard tapping.

4.3.3:Contact Angle of PNIPAM Brush Layers

An important property of PNIPAM brushes is the ability to demonstrate temperature induced wettability changes.[22, 48, 72-73] The temperature dependent wettability properties of PNIPAM have been extensively reported in literature.[22, 47-48, 51, 72, 74-75] Literature has shown that the switchability of PNIPAM layers can vary as a function of molecular weight, grafting density, and thickness of the deposited film.[48, 72, 74] To this end, we analyzed the PNIPAM brush layers using advancing and receding contact angle

measurements as a function of temperature, and solvent pre-treatment. The contact angle of the water droplet on the surfaces serves as an effective evaluation of surface energy.[67]

Modified wafers with the grafted layers were rinsed in MEK (good solvent for both blocks), or 25°C water (good solvent for PNIPAM) prior to contact angle analysis. Solvent pre-treatment was carried out in order to study the possibilities of preferential rearrangement of the polymer brush layers. In particular, it is advantageous to have a high concentration of PNIPAM block components located at the air-polymer interface in order to retain brush behavior similar to conventional PNIPAM brushes. ARXPS shows that indeed we have a sufficiently high concentration of PNIPAM at the interface to render thermo-responsive properties.

Firstly, advancing and receding contact angle measurements were performed to confirm SSB films exhibit hydrophilic to hydrophobic transitions when exposed to aqueous media indicative of PNIPAM brush films. The advancing water angle is the angle measured through water at the three-phase contact line when water is advanced over un-wetted surface.[76] Receding angle is defined as the angle measured at the contact line when the liquid is retracted over previously wetted surface.[76] To carry out the measurements, SSB and TSB modified silicon wafers were placed inside a temperature controlled cell. Water was continuously pumped from the syringe that was placed close to the sample surface. As the volume of the droplet increased, the liquid spread and was exposed to new surface (advancing angle). Once the liquid was drawn back into the syringe, the liquid spreads over the surface that already has been wet (receding angle).

Video was taken and individual snapshots were taken where the drops spread or retracted across the surface.

Figure 4.6a-b displays data for advancing and receding contact angles of SSB, TSB, and PNIPAM literature values.[48] Advancing and receding contact angles were measured as a function of temperature, and solvent pre-treatment. **Figure 4.6a** displays advancing contact angle data for pre-treatment in MEK solvent prior to analysis. PGMA block molecular weights of 13.5 (SSB-1) and 24.2k (SSB-2) showed little change in surface wettability as a function of temperature after being rinsed with MEK. These measurements indicate that SSB-1 and -2 had a sufficiently less cross-linking than SSB-3. The good solvent for both block effectively "bloomed" both components to the surface, inhibiting a surface energy change that is indicative of a PNIPAM dominant interface. Conversely, PGMA with the highest block molecular weight showed an increased change upon heating the sample above the LCST of PNIPAM. At 23°C measurements found an advancing contact angle of 57 ± 5 °. As the sample was heated to 40°C the advancing contact was determined to be 75 ± 3°. Thus resulting in an approximately 18° increase in contact angle observed for SSB-3, indicating a decrease in surface energy of the film.

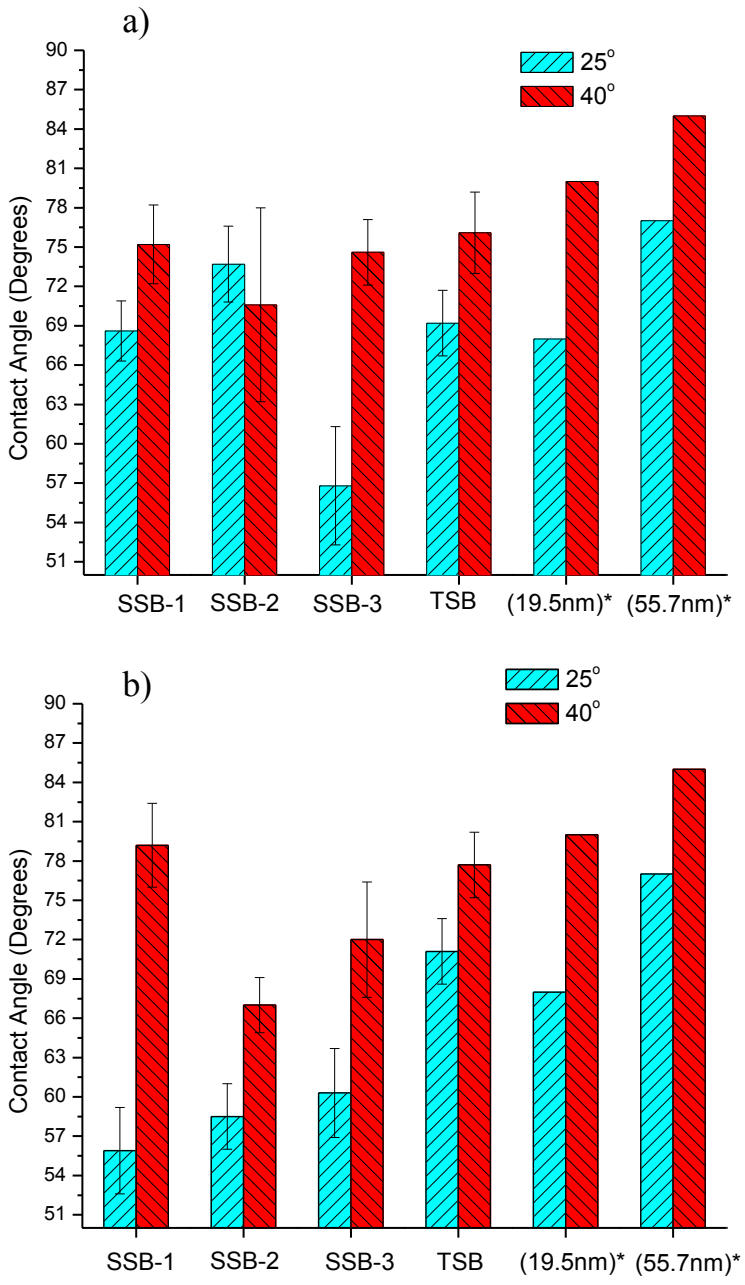

Figure 4.6: Advancing contact angle of all PNIPAM generated films as a function of temperature and pre-solvent treatment. a) advancing contact angle after pre-treatment in MEK b) advancing contact angle after pre-treatment in water. Literature values as published elsewhere.[48]

Similar results have been reported elsewhere.[22, 47-48, 72, 74] It also should be mentioned that homo PGMA thin films result in contact angles approximately 60°.[44, 62-63]

Interestingly, significant changes in advancing contact angles were found upon pre-treatment with a preferential solvent (**Figure 4.6b**) for SSB -1 and -2 prior to contact angle analysis. After rinsing with cold water, SSB-1 and -2 demonstrated substantial changes of advancing contact angle above and below the transition temperature for PNIPAM as compared to values found for MEK treatment. The observed behavior is indicative that indeed SSB-1 and -2 have sufficient mobility for re-orientation of the individual constituents of the block copolymer. In this case, a selective solvent for PNIPAM is used, effectively "blooming" it to the surface inducing a decrease in surface energy upon temperature increase. SSB-1 displayed a variation of contact angle from 56 ± 3° to 79 ± 3°. Roughly a 23° change as compared to 7° change after treatment in MEK. SSB-2 exhibited a 9° change after treatment in water, as opposed to no change after MEK treatment. Conversely, SSB-3, which contains the largest PGMA block, showed approximately the same wettability behavior as a function of temperature independent of solvent treatment.

Receding contact angles were also determined for all samples as function of PGMA block weight, temperature, and solvent treatment (**Table 4.4**). A significant hysteresis was found between the advancing and receding angles independent of temperature, chemical composition, and solvent pre-treatment. Particularly, according to **Table 4.4**, all receding angles were found to be roughly 30°. Observation of this trend has been reported elsewhere.[48, 73] This phenomenon was attributed to exposure of similar

chemical groups in water at temperatures above and below the LCST of PNIPAM. Significant water content in the both the swollen and collapsed layers could also be a contribution to the observed behavior.

Table 4.4: Receding contact angles measured as a function of temperature and solvent pre-treatment. a) Receding contact angle after MEK rinse b) Receding angle after 25°C water rinse.

a	**23°C : Receding Angle**	**40°C : Receding Angle**
SSB-1	33 ± 2.2	29 ± 2.9
SSB-2	31 ± 2.7	26 ± 3.6
SSB-3	27 ± 1.5	26 ± 3.5
Conv. Brush	27 ± 2.0	26 ± 2.2

b	**23°C : Receding Angle**	**40°C : Receding Angle**
SSB-1	30 ± 2.8	28 ± 2.7
SSB-2	30 ± 2.0	29 ± 3.2
SSB-3	28± 3.2	29 ± 1.8
Conv. Brush	25 ± 2.0	26 ± 1.6

To display the relationship and trends observed between the dissimilar PGMA block lengths, solvent treatment, and temperature, the change in wettability ratio (**Figure**

4.7) was plotted for all PNIPAM brush films after MEK and water rinses. The change in wettability ratio (MEK – Water) was taken as advancing contact angle measurements in the collapsed state over the swollen state. It was observed that TSB films showed equal changes in surface wettability behavior after pre treatment with non-selective and selective solvents. A roughly 8° contact angle change was found for both solvent treatments. This is due to the fact that essentially a 2-layer system (**Figure 4.1b**) was fabricated by grafting the carboxy-terminated PNIPAM on top of a PGMA anchoring layer in a second step. Therefore, the PNIPAM layer effectively screens PGMA from any interaction with water droplets placed on the surface. SSB-1 displays the highest change in water contact angle as a function of temperature after water rinse as compared to all other samples. A smaller change in the wettability ratio after water treatment was measured for SSB-2 as compared to SSB-1. Although, after 25°C water treatment, a slightly higher change of WCA was measured. In contrast, SSB-3 was found to have similar WCA values as a function of temperature independent of pre-solvent treatment. However, solvent treatments produced contact angle ratios smaller than that of SSB-1 after treatment in cold water.

We interpreted the observed trends as follows. SSB-1 displayed the highest advancing contact angle trend after exposure to a PNIPAM selective solvent. SSB-1 contains the shortest PGMA block, and therefore, reduced cross-linking density and higher effective grafting density of PNIPAM as compared to other BCPs per unit volume. MEK treatment of SSB-1 and -2 indicate that both PGMA and PNIPAM are present at the polymer-liquid interface, therefore, hindering the ability for PNIPAM block to

undergo a measurable contact angle change. Upon preferential solvent treatment, SSB-1 showed an enhanced ability to preferentially locate at the water-polymer interface due to solvation in 25°C water, confirmed by the greatest contact angle changes. By selectively orienting PNIPAM at the interface we increase the compositional fraction of PNIPAM at the interface. If this is indeed a valid assumption, PNIPAM units located in SSB-1 would feel an increase in energy due to entropic interactions, thus stretching away from the surface, much like the properties observed for a conventional polymer brush.

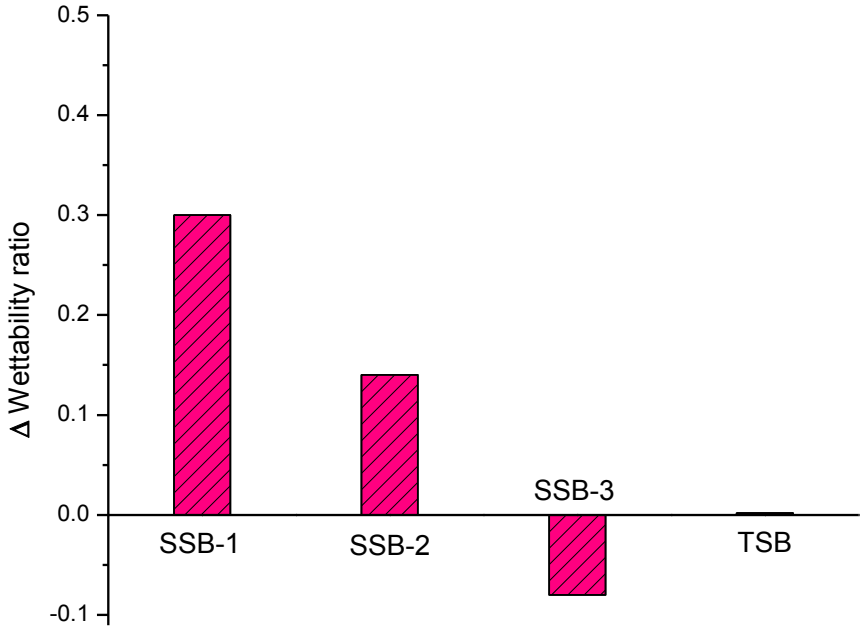

Figure 4.7: Change in wettability ratio (advancing contact angle 55°C/25°C) after MEK pre-treatment and Water Treatment

When looking at block copolymer layers with the largest PGMA fragment, consequently a higher amount of cross-linking per grafted film volume, we see that the layer is practically "locked". There was no change upon exposure to a good solvent for

PNIPAM. This leads to proof that films created from SSB-3 contains layers with increase PGMA units and higher self-cross-linking per unit volume, and decreased grafting density of PNIPAM, hindering PNIPAM fragments ability to swell and collapse to the same extent as SSB-1. Indeed, literature has shown that contact angle measurements of PNIPAM brush layers are affected by molecular weight and grafting density.[48, 77] SSB films with increased PGMA block molecular weight within the BCPs causes a decreased magnitude of change at equal surface coverage which effectively lowers wettability change even after selective "blooming" of PNIPAM to the surface.

Table 4.5: Advancing and receding contact angle measurements for 5nm thick SSB-1 films as a function of temperature and solvent pre-treatment.

SSB-1	**23°C**		**40°C**	
Rinse:	Advancing	Receding	Advancing	Receding
MEK	67 ± 1.7	32 ± 1.7	67 ± 1.3	25.3 ± 3.5
23°C Water	66 ± 4.4	27 ± 1.6	65 ± 2.4	24 ± 1.0

However, all PNIPAM-b-PGMA and conventional brush films showed changes in contact angle data when exposed to 25°C water pretreatment at experimental temperatures. After pre-treatment with cold water, all PNIPAM block copolymers exhibited higher wettability ratios than the TSB films used. It was determined that the highest contact angle changes were found with brushes formed with the least amount of PGMA units. SSB-1 was found to have better temperature contact angle switching behavior as compared to TSB homo brushes.

In conclusion, it is important to note that while thin films (~5nm, **Table 4.5**) were also fabricated by the same technique, no switchability was found for the low PNIPAM grafting density films.

4.3.4:Actuation of Polymer Brush Layers

The thermoresponsive behavior of PNIPAM in the form of homo polymers, copolymers, and hydrogels has been extensively studied. [20, 48, 51, 78-81] Of recent time, surface tethered PNIPAM chains were also investigated for their thermal response in aqueous environments.[20, 72, 81-82] The thermoresponsive nature of PNIPAM brushes is reflected by a transition from a highly swollen and hydrophilic state to a collapsed and more hydrophobic state at elevated temperatures.[20] For this purpose, the responsive nature of PNIPAM SSB fabricated films was investigated by measuring the ellipsometric thickness in-situ as a function of temperature in an aqueous environment. The amount of water contained in the films was determined as a function of SSB chemical composition and temperature.

It is useful to compare swelling of our 1-step brush synthesis to that of a conventional PNIPAM brush synthesis and subsequent in-situ ellipsometric swelling studies by Rahane and co-workers.[20] Combined with the contact angle data (**Figure 4.6a-b, Figure 4.7)** it was expected that PNIPAM brushes from BCPs with more PGMA (decreased grafting density of PNIPAM) mers per unit area would decrease extension of SSB layers, leading to diminished actuation of the polymer brush. It was foreseen that altering the block copolymer ratio (increase PGMA content) would afford control over

the amount of water retained in the polymer films at temperatures above and below the LCST of PNIPAM.

Figure 4.8a shows the results from PNIPAM SSB stretching experiments as a function of temperature. **Figure 4.8a** indicates all three PNIPAM block copolymers exhibit varying changes in thickness at temperatures of 25 and 65°C for all PGMA block molecular weights. The dry layer total thickness is depicted as the dashed line in **Figure 4.8a.** SSB-1 swells from a dry layer thickness of 30nm to roughly 92nm in cold water. As temperature is elevated, thickness decreases to 62nm, roughly a 30nm change in thickness between the two temperatures. As PGMA segment molecular weight is increased, the change in thickness between temperature cycles decreased to 21 and 15nm for SSB-2 and -3 respectively. In fact, the SSB 1-3 films swelled to 96, 82, and 59% of their maximum extension ability in cold solvents. Maximum swelling heights were determined assuming the C-C bond length is 0.154nm, and vinyl repeat units contained two C-C bonds. Therefore, the maximum distance of stretching for SSB PNIPAM segments would be 65, 72, and 78nm respectively for SSB 1-3.

The actuation ratio for each block copolymer was determined as the swollen thickness divided by the collapsed thickness. As PGMA molecular weight is increased, a decrease in actuation ratio from 1.50 to 1.25 was determined. Therefore, it is demonstrated that by changing the symmetry of the block copolymer, we can effectively tune the swelling and collapse thickness change at varying temperatures. Combined with contact angle data, an increase in PGMA molecular weight block segment impacts the ability for PNIPAM to swell and collapse in aqueous conditions.

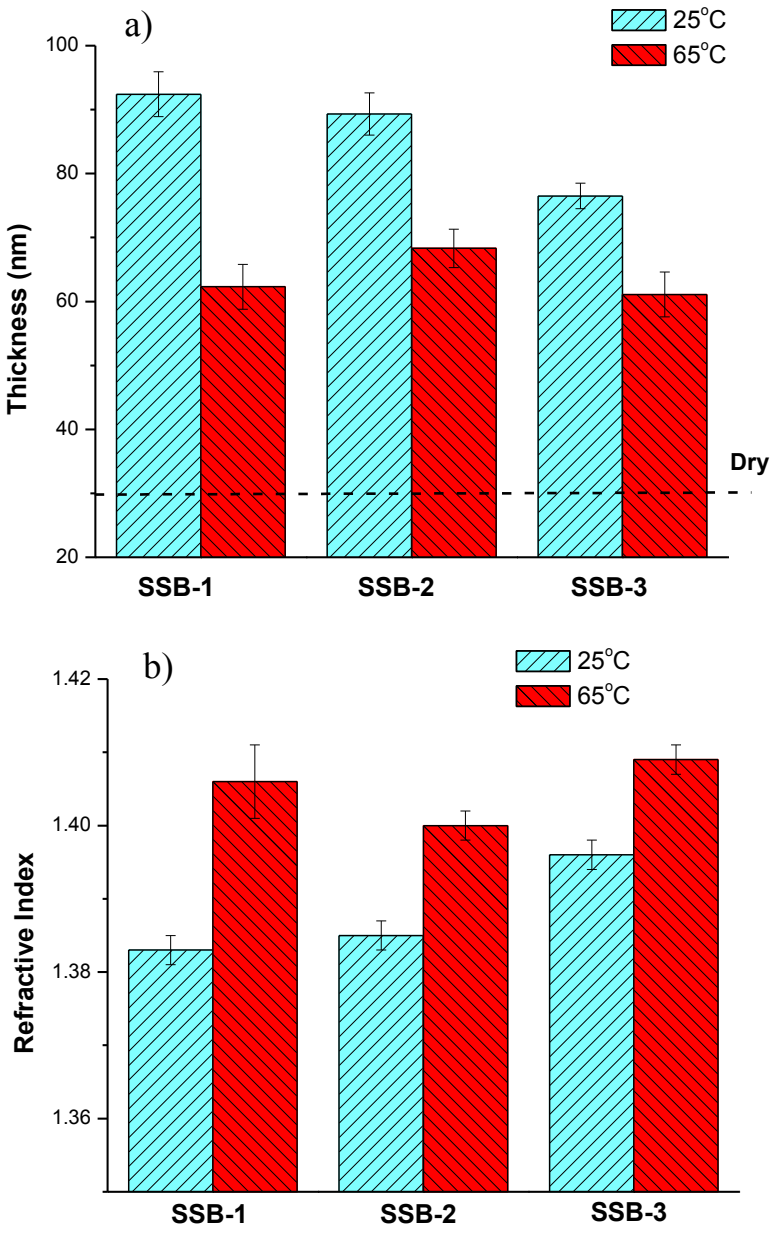

Figure 4.8: Swelling and refractive index results of block copolymer grafted layers using in-situ ellipsometry swelling techniques in an aqueous environment. a) Swelling and collapse for PNIPAM SSB grafted films at 25 and 65^{0}C water. b) Refractive index change.

Refractive index values of the swollen and collapsed states of the layers validate that significant water is contained in the brush layers at different temperatures. In order to utilize the Bruggeman approximation to estimate the percent water content in the layers, the approximation was utilized to calculate the Bruggeman swelling and collapse thicknesses using the apparent refractive index of the "mixed" films. **Figure 4.9** displays the measured layer thickness by Cauchy model fit (closed circles) and Bruggeman approximation thickness values as a function of PGMA and temperature. As **Figure 4.9** displays, the measured ellipsometric values and the calculated Bruggeman values are in close agreement. The average percent deviation for all measured values was 3.3%. Therefore, it is appropriate to use the Bruggeman relationship to estimate the amount of water contained in the SSB films at different temperatures.

Estimations of the volume fraction of water content in the swollen SSB films was conducted using **Equation(4.2).** Swollen block copolymer films with the greatest amount of PNIPAM (SSB-1) were found to contain 70% water at 25°C. The water content as a function of PGMA block length was found to slightly decrease for SSB-2 (69%), and much lower for SSB-3 (62%) at 25°C. **Figure 4.8b** displays the refractive index measurements for the swollen and collapsed conditions in aqueous environments as a function of temperature.

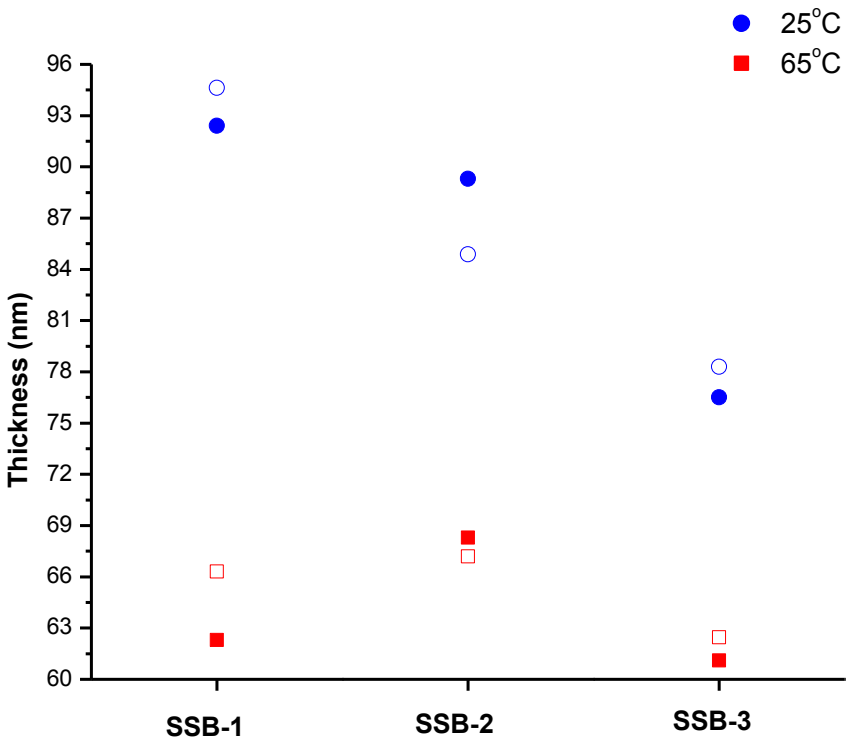

Figure 4.9: Ellipsometric measured thickness values (■ , ●) vs. Bruggeman approximation calculated thickness (□,○) at the experimentally measured temperatures.

In the swollen state, SSB-1 refractive index was determined to be the lowest of all samples, approximately 1.383. Hence, validation that SSB-1 film contains the highest concentration of water within the brush layer, causing an increase in swelling. A general increase in refractive index in cold conditions for longer PGMA block segments was found, validating that the films contained a lower ratio of water in the hydrated state. As temperature was increased, the resulting refractive indexes also increased. Refractive index values for all three polymer layers were found to be slightly above 1.40.

Estimations of water content at 55°C for the collapsed SSB films were found to be 55, 59, and 52% for SSB-1, -2, and -3 respectively. Because the refractive index now approaches that of the dry film, water has been expelled from the polymer layer as PNIPAM collapsed into a more hydrophobic state. Although, a roughly two fold increase in thickness is still apparent for the collapsed brush as compared to the dry state, yielding significant water content even when PINPAM becomes collapsed.

4.3.4.1:Comparison to Previous Reported Data

It is useful to compare the actuation ratios of our polymer brush layers to previously reported experiments carried out in the same manner for homo PNIPAM brushes. Rahane and coworkers reported similar stretching experiments for homo PNIPAM brushes via in-situ ellipsometric thickness measurements as a function of temperature as well. The scientists used surface-initiated photoiniferter-mediated photopolymerization to grow brushes via the "grafting from" technique on the surface of silicon wafers. Their results indicate that actuation ratios in cold and hot water normalized to dry layer thickness was measured to be 2.7 and 1.1 respectively. Comparatively, our results normalized in the same manner for all three block copolymer layers in cold and hot conditions was found to be; 3.1, 2.1 (SSB-1), 3.0, 2.3 (SSB-2), and 2.6, 2.0 (SSB-3). A slight increase in swelling at cold conditions was found for SSB-1 and -2, while SSB-3 was approximately the same as results measured by Rahane at 25°C. At an elevated temperature, Rahane et al. observed a much lower collapsing ratio indicating that the SSB systems contain increased amount of water in the brush films at 55°C.

The observation of increased swelling for the layers containing the least amount of PGMA, follows the switching observed for water contact angles. Previous reported literature indicates that PGMA has a very small magnitude of swelling in water as compared to PNIPAM. Chyasnavichyus et al. determined the swelling ratio of PGMA in water vapor, roughly a 5% increase in the swollen state to that of a dry film.[83] This is much smaller than the roughly 200% swelling from dry to swollen state observed for SSB-1. Therefore, PNIPAM components within the block copolymer film swell independent of the cross-linked PGMA component. However, the block copolymer films contained more water in the swollen and collapsed films than films fabricated by Rahane et al. Also it is apparent that SSB-2 showed the highest water content (59%) of all SSB films at 55°C. This is evidence towards reasons for having the lowest apparent contact angle (67°) at measured temperatures of 40°C. We suggest an increased penetration of the probing liquid into the film would cause the apparent decrease in the contact angle due to an increase in the hydrophillicity of the layer.

4.3.4.2:Comparison to Predicted Behavior By Self Consistent Field Theory

In further analysis, we can utilize *in-situ* ellipsometric swelling experiments to determine the SS brush behavior in comparison to predicted brush behavior in a thermodynamically good solvent, in our case, cold water. We compared the swelling thickness ratio from measured ellipsometric values normalized by initial thickness of the PNIPAM content and compared to predicted swelling ratios by self consistent field theory (SCF).[84] Jordan et al.[85] originally proposed **Equation (4.4)** in order to estimate

the degree of polymerization N, from swollen and dry film measurements via ellipsometry experiments.

$$N = \left[1.074\left(h_{sw}^{*}\right)^{3/2}\right] \Big/ \left[h_{dry}\right]^{1/2} \qquad (4.4)$$

Jordan et al. modified the above equation for analysis of polystyrene brushes assuming a value of 6.7 Å for the Kuhn segment length for a polystyrene monomer unit. In general, polystyrene has a Kuhn value equal to 8 mers while methacrylates contain 6 mers in the Kuhn segment length. Therefore, we can utilize the equation above to approximate the ideal swelling behavior of our brush layers. The formula is based on the analytically determined extended brush thickness from the SCF investigation of grafted polymer brushes presented by Milner et al.[86-87] As Samadi et al.[84] noted, the swollen thickness h_{sw}^{*} predicted by SCF theory result from a parabolic segment density profile. In our measurements, the ellipsometric data was fit using a step-like segment density profile termed a "box like" model. However, the h_{sw}^{*} can be found from the "box like" fits by using the relationship $h_{sw}^{*} = (4/3)\bullet$, implementing the results of the SCF model.

Figure 4.10 displays the swelling ratio as a function of grafting density for the SSB films along with the TSB brush as measured by *in-situ* ellipsometry and compared to values predicted by the SCF theory. The swelling ratio was determined as the swollen thickness, h_{sw}^{*}, normalized by initial dry thickness, h_{dry}. Initial film thicknesses of the SSB films were roughly 30 nm. However, weight fractions of PNIPAM were accounted

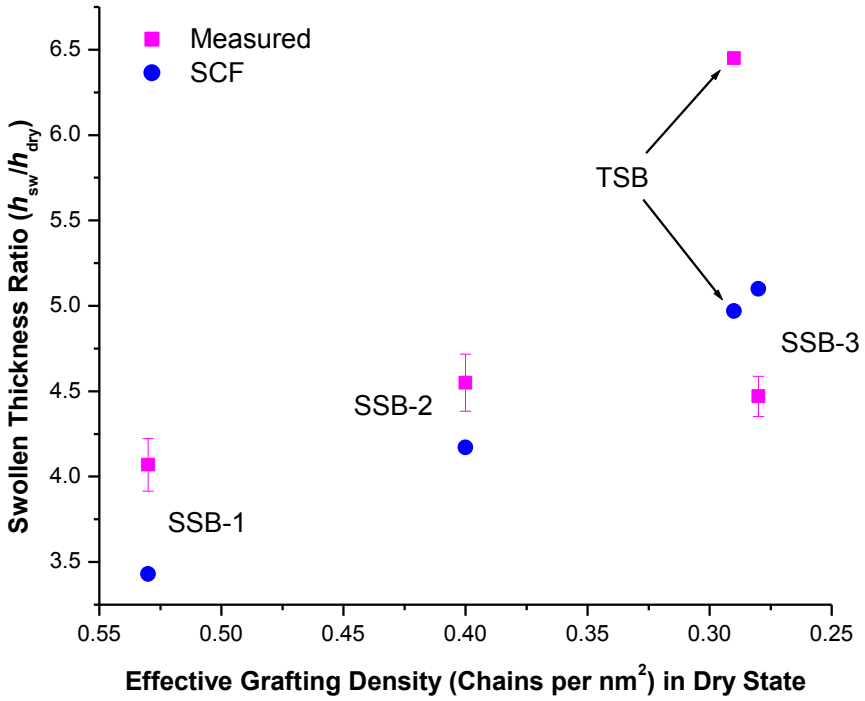

Figure 4.10: Measured values for the swollen thickness ratio vs. effective grafting density calculated from the dry state compared to predicted swelling ratios by SCF theory. Swelling ratio is taken as swollen thickness normalized by dry layer thickness of PNIPAM fraction.

for in the calculation of the actual dry thickness of the PNIPAM fractions, thus subtracting out the PGMA portion of the film from the measurements assuming PGMA does not swell in water. As **Figure 4.10** shows, there is a general increase in swelling ratio moving from SSB-1 to -2. SSB-2 and -3 showed essentially equal swelling ratios within the limits of uncertainty. Interestingly, as a consequence of high grafting density of SSB-1, we observed decreased overall swelling ratio. As grafting density decreases, we see a general increase from SSB-1 to -3. Samadi[84] and Biesalski[88] independently determined the same trends. The authors attributed the observed trend to the fact that at

high grafting densities, chains are already highly stretched, and subsequent treatment with a good solvent does not induce drastic thickness changes. Predicted h_{sw}^{*} values by SCF theory predict an increase in swelling ratio as a function of decreased grafting density.

Interestingly, **Figure 4.10** shows that SSB brush films act as ideal brushes. The measurement values do deviate from predicted swelling ratios, however all differences for SSB brush values are less than 15%. We attribute the differences to the fact that in reality, Milners SCF theory predictions are appropriate for polymers exhibiting weak excluded-volume interactions. In the case of PNIPAM (and PEG in later chapters), hydrogen bonding needs to be accounted for. Hydrogen bonding with water can bring in additional water molecules effectively increasing osmotic pressure within the brush structure causing deviations from expected values for swelling. Also, the derived SCF theory was constructed assuming ideal grafted brushes directly from surfaces. This does not account for the inclusion of PGMA in the brush system. Therefore, due to the inclusion of PGMA, and hydrogen bonding interactions, we conclude that the SSB systems behave as true polymer brush systems.

The TSB grafted film measurements were found to be 23% higher than predicted values. However, the TSB film did not collapse and expel water at the measured temperatures. As a result, the SSB films showed similar swelling ratios, however, SSB films all collapsed at measurement temperatures of 65°C as shown in **Figure 4.8.**

From both dynamic contact angle and in-situ ellipsometric thickness measurements, it was determined that the SSB technique produced PNIPAM brushes that

retained their thermoresponsive nature. The magnitude of property change depends on the amount of PGMA present in the initial BCP. Because we are able to graft varying thicknesses of PNIPAM films via the "grafting to" method while retaining the responsive behavior, wettability properties and magnitude of actuation can be tuned via inclusion of varying amounts of PGMA. This temperature response of the layer in general reflects the behavior of the PNIPAM acting under the influence of higher molecular weights of PGMA. We suggest that this phenomenon is analogous to the grafting density relationship observed for homo PNIPAM brushes.[48] Lastly, the SSB layers perform as ideal brush in terms of extension in a good solvent as predicted by SCF theory.

By effectively controlling the ratio of PNIPAM and PGMA at the interface by block copolymer composition, the switchability of the resulting grafted films can be tuned. However, it is important to determine if the developed relationships persist for biological interaction. Therefore, the relationship of adhesion and adsorption of model protein to PNIPAM containing films (fibrinogen) was studied as a function of block copolymer composition and temperature in **Chapter 5**.

4.4:Conclusions

PNIPAM-b-PGMA diblock copolymers were synthesized via controlled RAFT polymerization yielding a series of block copolymers with varying amounts of PGMA block segment and low polydispersity. The reported experiments demonstrate the fabrication of thermally responsive polymer brushes in a single step fashion. Grafting at 130°C for 16 hours yields 100% retainable films. The 100% self-cross linking was found to be independent of film thicknesses as films from 10-250 nm were found intact in the

same manner. Moreover, the PNIPAM films were deposited via the "grafting to" technique at varying nanoscale thicknesses yielding smooth and full surface coverage indicated by route mean square roughness measurements less than 1 nm for all dry films. The deposited SSB films were found to be well within the "brush regime". It was also observed that block copolymer architecture is necessary in our case due to the macroscopic phase separation observed for films deposited from homo polymer PNIPAM and PGMA blends.

The studied SSB polymer brush films exhibited thermally responsive switching behavior and their surface properties can be tuned by altering the initial block copolymer ratio between PNIPAM and PGMA components. Advancing contact angle measurements after preferential solvent treatment indicated that variations in contact angle values were apparent for SSB films with varying PGMA content. However, SSB-1 which contains the greatest amount of PNIPAM in the block copolymer produced a surface that had greater wettability switching than that of fabricated homo PNIPAM surfaces. Contact angle values at low temperatures were similar within error for all SSB films, however upon increasing the temperature of contact angle measurement, variation was noticed. Interestingly, the contact angles at 55°C, followed trends observed for calculated water content within the collapsed film in aqueous environments. SSB-2 was found to have the greatest amount of water in the collapsed film and subsequently the lowest contact angle at 55°C of all SSB films.

In-situ ellipsometry measurements indicate that tuning of actuation of SSB films is afforded due to variations in PGMA content as well. The overall changes in thickness

as a function of temperature was found to decrease for SSB films with increasing amounts of PGMA. SSB layers were determined to have significant water content in aqueous environments in both the swollen and collapsed films states, however an increased water content percentage was found for SSB films in 25°C as opposed to 65°C water environments.

ARXPS measurements confirmed that PNIPAM is not solely present in the outer 10nm region of the SSB films. On the other hand, as expected the TSB films contain solely PNIPAM dominated interfaces. PNIPAM was found to preferentially organize in greater concentration towards the polymer-air interface for all SSB films. However, as the PGMA content increased, a decreasing amount of PNIPAM at the very outer surface was found.

It is evident that dip-coating and annealing is a suitable technique to avoid the unfavorable arrangement of the polymer layers. From a combination of dip-coating, and a treatment with a PNIPAM specific solvent, it is obvious that thermo responsive properties are retained, and in fact, PNIPAM is preferentially located at the polymer-air interface. We also suggest that the exothermic nature of self cross-linking of the PGMA segment may also aid in delivery PGMA segments to the silicon wafer. Since the layers are annealed above the glass transition of both polymers, it may be that the PGMA reaction nucleation sites occur near the surface of silicon oxide layer. As the reaction proceeds, PGMA is densely cross-linked near the reactive sites on the substrate surface, indeed trapping some PNIPAM block segments near the surface. However, as the layer

cross-linking cascades, and thermosetting proceeds, the upper region of the film yields free PNIPAM chains that are able to effectively bloom to the surface.

This is evidence towards reasons governing the variation in switchability found for the different SSB films and subsequently invokes our ability to generate tunable thermally responsive brush films. By generating coatings at variable thicknesses, with which established "grafting to" procedures cannot, a versatile, simple, and powerful technique has been developed to produce thermally responsive films with tunable surface properties in a single step manner.

4.5:References

1. Kanazawa, H.; Sunamoto, T.; Matsushima, Y., Temperature-responsive chromatographic separation of amino acid phenylthiohydantoins using aqueous media as the mobile phase. *Analytical Chemistry* **2000,** *72* (24), 5961-5966.

2. Kanazawa, H.; Kashiwase, Y.; Yamamoto, K.; Matsushima, Y.; Kikuchi, A.; Sakurai, Y.; Okano, T., Temperature-responsive liquid chromatography .2. Effects of hydrophobic groups in n-isopropylacrylamide copolymer-modified silica. *Analytical Chemistry* **1997,** *69* (5), 823-830.

3. Kanazawa, H.; Yamamoto, K.; Matsushima, Y.; Takai, N.; Kikuchi, A.; Sakurai, Y.; Okano, T., Temperature-responsive chromatography using poly(n-isopropylacrylamide)-modified silica. *Analytical Chemistry* **1996,** *68* (1), 100-105.

4. Kikuchi, A.; Okano, T., Intelligent thermoresponsive polymeric stationary phases for aqueous chromatography of biological compounds. *Progress in Polymer Science* **2002,** *27* (6), 1165-1193.

5. Kushida, A.; Yamato, M.; Konno, C.; Kikuchi, A.; Sakurai, Y.; Okano, T., Temperature-responsive culture dishes allow nonenzymatic harvest of differentiated madin-darby canine kidney (mdck) cell sheets. *Journal of Biomedical Materials Research* **2000,** *51* (2), 216-223.

6. Morikawa, N.; Matsuda, T., Thermoresponsive artificial extracellular matrix: N-isopropylacrylamide-graft-copolymerized gelatin. *Journal of Biomaterials Science-Polymer Edition* **2002,** *13* (2), 167-183.

7. Akiyama, Y.; Kikuchi, A.; Yamato, M.; Okano, T., Ultrathin poly(n-isopropylacrylamide) grafted layer on polystyrene surfaces for cell adhesion/detachment control. *Langmuir* **2004,** *20* (13), 5506-5511.

8. Okano, T.; Yamada, N.; Sakai, H.; Sakurai, Y., A novel recovery-system for cultured-cells using plasma-treated polystyrene dishes grafted with poly(n-isopropylacrylamide). *Journal of Biomedical Materials Research* **1993,** *27* (10), 1243-1251.

9. Shimizu, T.; Yamoto, M.; Kikuchi, A.; Okano, T., Two-dimensional manipulation of cardiac myocyte sheets utilizing temperature-responsive culture dishes augments the pulsatile amplitude. *Tissue Engineering* **2001,** *7* (2), 141-151.

10. Bittrich, E.; Burkert, S.; Muller, M.; Eichhorn, K. J.; Stamm, M.; Uhlmann, P., Temperature-sensitive swelling of poly(n-isopropylacrylamide) brushes with low molecular weight and grafting density. *Langmuir 28* (7), 3439-3448.

11. Okano, T.; Yamada, N.; Okuhara, M.; Sakai, H.; Sakurai, Y., Mechanism of cell detachment from temperature-modulated, hydrophilic-hydrophobic polymer surfaces. *Biomaterials* **1995,** *16* (4), 297-303.

12. Jones, D. M.; Smith, J. R.; Huck, W. T. S.; Alexander, C., Variable adhesion of micropatterned thermoresponsive polymer brushes: Afm investigations of poly (n-isopropylacrylamide) brushes prepared by surface-initiated polymerizations. *Advanced Materials* **2002,** *14* (16), 1130-1134.

13. Kaholek, M.; Lee, W. K.; Ahn, S. J.; Ma, H. W.; Caster, K. C.; LaMattina, B.; Zauscher, S., Stimulus-responsive poly(n-isopropylacrylamide) brushes and nanopatterns prepared by surface-initiated polymerization. *Chemistry of Materials* **2004,** *16* (19), 3688-3696.

14. Ito, Y.; Chen, G. P.; Guan, Y. Q.; Imanishi, Y., Patterned immobilization of thermoresponsive polymer. *Langmuir* **1997,** *13* (10), 2756-2759.

15. Harmon, M. E.; Kuckling, D.; Frank, C. W., Photo-cross-linkable pnipaam copolymers. 2. Effects of constraint on temperature and ph-responsive hydrogel layers. *Macromolecules* **2003,** *36* (1), 162-172.

16. LeMieux, M. C.; Peleshanko, S.; Anderson, K. D.; Tsukruk, V. V., Adaptive nanomechanical response of stratified polymer brush structuresвђ *Langmuir* **2006,** *23* (1), 265-273.

17. Benetti, E. M.; Zapotoczny, S.; Vancso, G. J., Tunable thermoresponsive polymeric platforms on gold by "photoiniferter"-based surface grafting. *Advanced Materials* **2007,** *19* (2), 268-+.

18. Burkert, S.; Bittrich, E.; Kuntzsch, M.; Mueller, M.; Eichhorn, K.-J.; Bellmann, C.; Uhlmann, P.; Stamm, M., Protein resistance of pnipaam brushes: Application to switchable protein adsorption. *Langmuir 26* (3), 1786-1795.

19. Cole, M. A.; Voelcker, N. H.; Thissen, H.; Griesser, H. J., Stimuli-responsive interfaces and systems for the control of protein-surface and cell-surface interactions. *Biomaterials* **2009,** *30* (9), 1827-1850.

20. Rahane, S. B.; Floyd, J. A.; Metters, A. T.; Kilbey, S. M., Swelling behavior of multiresponsive poly(methacrylic acid)-block-poly (n-isopropylacrylamide) brushes synthesized using surface-initiated photoiniferter-mediated photopolymerization. *Advanced Functional Materials* **2008,** *18* (8), 1232-1240.

21. Huang, X.; Misra, G. P.; Vaish, A.; Flanagan, J. M.; Sutermaster, B.; Lowe, T. L., Novel nanogels with both thermoresponsive and hydrolytically degradable properties. *Macromolecules* **2008,** *41* (22), 8339-8345.

22. Seeber, M.; Zdyrko, B.; Burtovvy, R.; Andrukh, T.; Tsai, C. C.; Owens, J. R.; Kornev, K. G.; Luzinov, I., Surface grafting of thermoresponsive microgel nanoparticles. *Soft Matter 7* (21), 9962-9971.

23. Kuckling, D.; Vo, C. D.; Wohlrab, S. E., Preparation of nanogels with temperature-responsive core and ph-responsive arms by photo-cross-linking. *Langmuir* **2002,** *18* (11), 4263-4269.

24. Crespy, D.; Rossi, R. N., Temperature-responsive polymers with lcst in the physiological range and their applications in textiles. *Polym. Int.* **2007,** *56* (12), 1461-1468.

25. Dimitrov, I.; Trzebicka, B.; Muller, A. H. E.; Dworak, A.; Tsvetanov, C. B., Thermosensitive water-soluble copolymers with doubly responsive reversibly interacting entities. *Progress in Polymer Science* **2007,** *32* (11), 1275-1343.

26. Nagase, K.; Kobayashi, J.; Okano, T., Temperature-responsive intelligent interfaces for biomolecular separation and cell sheet engineering. *Journal of the Royal Society Interface* **2009,** *6*, S293-S309.

27. Dai, S.; Ravi, P.; Tam, K. C., Ph-responsive polymers: Synthesis, properties and applications. *Soft Matter* **2008,** *4* (3), 435-449.

28. Richter, A.; Paschew, G.; Klatt, S.; Lienig, J.; Arndt, K. F.; Adler, H. J. P., Review on hydrogel-based ph sensors and microsensors. *Sensors* **2008,** *8* (1), 561-581.

29. Jeong, B.; Gutowska, A., Lessons from nature: Stimuli-responsive polymers and their biomedical applications. *Trends in Biotechnology* **2002,** *20* (7), 305-311.

30. Tsyalkovsky, V.; Burtovyy, R.; Klep, V.; Lupitskyy, R.; Motornov, M.; Minko, S.; Luzinov, I., Fluorescent nanoparticles stabilized by poly(ethylene glycol) containing shell for ph-triggered tunable aggregation in aqueous environment. *Langmuir* **2010,** *26* (13), 10684-10692.

31. Ercole, F.; Davis, T. P.; Evans, R. A., Photo-responsive systems and biomaterials: Photochromic polymers, light-triggered self-assembly, surface modification, fluorescence modulation and beyond. *Polymer Chemistry* **2010,** *1* (1), 37-54.

32. Katz, J. S.; Burdick, J. A., Light-responsive biomaterials: Development and applications. *Macromolecular Bioscience* **2010,** *10* (4), 339-348.

33. He, D. M.; Susanto, H.; Ulbricht, M., Photo-irradiation for preparation, modification and stimulation of polymeric membranes. *Progress in Polymer Science* **2009,** *34* (1), 62-98.

34. Bohmer, M. R.; Klibanov, A. L.; Tiemann, K.; Hall, C. S.; Gruell, H.; Steinbach, O. C., Ultrasound triggered image-guided drug delivery. *European Journal of Radiology* **2009,** *70* (2), 242-253.

35. Meng, H.; Hu, J. L., A brief review of stimulus-active polymers responsive to thermal, light, magnetic, electric, and water/solvent stimuli. *Journal of Intelligent Material Systems and Structures* **2010,** *21* (9), 859-885.

36. Brazel, C. S., Magnetothermally-responsive nanomaterials: Combining magnetic nanostructures and thermally-sensitive polymers for triggered drug release. *Pharmaceutical Research* **2009,** *26* (3), 644-656.

37. Liu, H. X.; Wang, C. Y.; Gao, Q. X.; Liu, X. X.; Tong, Z., Magnetic hydrogels with supracolloidal structures prepared by suspension polymerization stabilized by fe_2o_3 nanoparticles. *Acta Biomaterialia* **2010,** *6* (1), 275-281.

38. Yang, J.; Yamato, M.; Okano, T., Cell-sheet engineering using intelligent surfaces. *Mrs Bulletin* **2005,** *30* (3), 189-193.

39. Kawaguchi, H.; Fujimoto, K.; Mizuhara, Y., Hydrogel microspheres .3. Temperature-dependent adsorption of proteins on poly-n-isopropylacrylamide hydrogel microspheres. *Colloid and Polymer Science* **1992,** *270* (1), 53-57.

40. Luzinov, I.; Minko, S.; Tsukruk, V. V., Responsive brush layers: From tailored gradients to reversibly assembled nanoparticles. *Soft Matter* **2008,** *4* (4), 714-725.

41. Zhao, B.; Brittain, W. J., Polymer brushes: Surface-immobilized macromolecules. *Prog. Polym. Sci.* **2000,** *25* (5), 677-710.

42. ten Cate, A. T.; Reinders, S. A. F.; Turkenburg, D. H.; Bruin, A.; D'Souza, F.; Donnelly, G. T.; Willemsen, P. R.; Maas, J. H.; van Bommel, K. J. C., High density hydrophilic and hydrophobic brush coatings using a polymeric primer layer. *Progress in Organic Coatings* **2009,** *64* (2-3), 221-224.

43. Iyer, K. S.; Zdyrko, B.; Malz, H.; Pionteck, J.; Luzinov, I., Polystyrene layers grafted to macromolecular anchoring layer. *Macromolecules* **2003,** *36* (17), 6519-6526.

44. Zdyrko, B.; Iyer, K. S.; Luzinov, I., Macromolecular anchoring layers for polymer grafting: Comparative study. *Polymer* **2006,** *47* (1), 272-279.

45. Jones, R. A. L.; Lehnert, R. J.; Schonherr, H.; Vancso, J., Factors affecting the preparation of permanently end-grafted polystyrene layers. *Polymer* **1999,** *40* (2), 525-530.

46. Xue, C. Y.; Choi, B. C.; Choi, S.; Braun, P. V.; Leckband, D. E., Protein adsorption modes determine reversible cell attachment on poly(n-isopropyl acrylamide) brushes. *Advanced Functional Materials 22* (11), 2394-2401.

47. Xue, C. Y.; Yonet-Tanyeri, N.; Brouette, N.; Sferrazza, M.; Braun, P. V.; Leckband, D. E., Protein adsorption on poly(n-isopropylacrylamide) brushes: Dependence on grafting density and chain collapse. *Langmuir 27* (14), 8810-8818.

48. Plunkett, K. N.; Zhu, X.; Moore, J. S.; Leckband, D. E., Pnipam chain collapse depends on the molecular weight and grafting density. *Langmuir* **2006,** *22* (9), 4259-4266.

49. Cheng, X. H.; Canavan, H. E.; Stein, M. J.; Hull, J. R.; Kweskin, S. J.; Wagner, M. S.; Somorjai, G. A.; Castner, D. G.; Ratner, B. D., Surface chemical and mechanical properties of plasma-polymerized n-isopropylacrylamide. *Langmuir* **2005,** *21* (17), 7833-7841.

50. Reed, J. A.; Lucero, A. E.; Hu, S.; Ista, L. K.; Bore, M. T.; Lopez, G. P.; Canavan, H. E., A low-cost, rapid deposition method for "smart" films: Applications in mammalian cell release. *Acs Applied Materials & Interfaces 2* (4), 1048-1051.

51. Nakayama, M.; Yamada, N.; Kumashiro, Y.; Kanazawa, H.; Yamato, M.; Okano, T., Thermoresponsive poly(n-isopropylacrylamide)-based block copolymer coating for optimizing cell sheet fabrication. *Macromolecular Bioscience 12* (6), 751-760.

52. Loh, X. J.; Cheong, W. C. D.; Li, J.; Ito, Y., Novel poly(n-isopropylacrylamide)-poly[(r)-3-hydroxybutyrate]-poly(n-isopropyl acrylamide) triblock copolymer surface as a culture substrate for human mesenchymal stem cells. *Soft Matter* **2009,** *5* (15), 2937-2946.

53. Zdyrko, B.; Klep, V.; Luzinov, I., Universal platform for surface modification employing grafted polymer layers. *Material Matters* **2008,** *3* (2), 44-47.

54. Burtovyy, O.; Klep, V.; Turel, T.; Gowayed, Y.; Luzinov, I., *Polymeric membranes: Surface modification by "grafting to" method and fabrication of multilayered assemblies, in nanoscience and nanotechnology for chemical and biological defense, editors: Nagarajan, r.; zukas, w.; hatton, t. A.; lee, s.* ACS Symposium Series 1016, Washington DC: 2009; p 289-305.

55. Zdyrko, B.; Varshney, S. K.; Luzinov, I., Effect of molecular weight on synthesis and surface morphology of high-density poly(ethylene glycol) grafted layers. *Langmuir* **2004,** *20* (16), 6727-6735.

56. Zdyrko, B.; Luzinov, I., Polymer brushes by the "grafting to" method. *Macromolecular Rapid Communications 32* (12), 859-869.

57. Luzinov, I. A.; Swaminatha Iyer, K. L.; Klep, V. Z.; Zdyrko, B. V. Surface graft modification of substrates, us patent 7,026,014 b2, apr. 11, 2006.

58. Henn, G.; Bucknall, D. G.; Stamm, M.; Vanhoorne, P.; Jerome, R., Chain end effects and dewetting in thin polymer films. *Macromolecules* **1996,** *29* (12), 4305-4313.

59. Bruggeman, D. A. G., Berechnung verschiedener physikalischer konstanten von heterogenen substanzen. I. Dielektrizitätskonstanten und leitfähigkeiten der mischkörper aus isotropen substanzen. *Annalen der Physik* **1935,** *416* (7), 636-664.

60. Prevo, B. G.; Hwang, Y.; Velev, O. D., Convective assembly of antireflective silica coatings with controlled thickness and refractive index. *Chemistry of Materials* **2005,** *17* (14), 3642-3651.

61. Pantelic, N.; Seliskar, C. J., Anomalous diffusion in poly(vinyl alcohol)-poly(acrylic acid) thin films. *Journal of Physical Chemistry C* **2007,** *111* (5), 2054-2062.

62. Zdyrko, B.; Hoy, O.; Kinnan, M. K.; Chumanov, G.; Luzinov, I., Nano-patterning with polymer brushes via solvent-assisted polymer grafting. *Soft Matter* **2008,** *4* (11), 2213-2219.

63. Burtovyy, O.; Klep, V.; Chen, H. C.; Hu, R. K.; Lin, C. C.; Luzinov, I., Hydrophobic modification of polymer surfaces via "grafting to" approach. *Journal of Macromolecular Science Part B-Physics* **2007,** *46* (1), 137-154.

64. Fleer, G. J. C. S., M. A.; Scheutjens, J. M. H. M.; Cosgrove, T.; Vincent, B. , *Polymers at interfaces*. Chapman & Hall: London, 1993.

65. Lokitz, B. S.; Wei, J.; Hinestrosa, J. P.; Ivanov, I.; Browning, J. F.; Ankner, J. F.; Kilbey, S. M., II; Messman, J. M., Manipulating interfaces through surface confinement of poly(glycidyl methacrylate)-block-poly(vinyldimethylazlactone), a dually reactive block copolymer. *Macromolecules* **2012,** *45* (16), 6438-6449.

66. Brittain, W. J.; Minko, S., A structural definition of polymer brushes. *Journal of Polymer Science Part a-Polymer Chemistry* **2007,** *45* (16), 3505-3512.

67. Sperling, L. H., *Physical polymer science*. 3rd edition ed.; Wiley&Sons Inc.: 2001.

68. Liu, Y.; Klep, V.; Zdyrko, B.; Luzinov, I., Synthesis of high-density grafted polymer layers with thickness and grafting density gradients. *Langmuir* **2005,** *21* (25), 11806-11813.

69. Song, W.; So, S. K.; Cao, L., Angular-dependent photoemission studies of indium tin oxide surfaces. *Applied Physics a-Materials Science & Processing* **2001,** *72* (3), 361-365.

70. Eaton P, W. P., *Atomic force microscopy*. Oxford University Press: 2010.

71. Luzinov, I.; Tsukruk, V. V., Ultrathin triblock copolymer films on tailored polymer brushes. *Macromolecules* **2002,** *35* (15), 5963-5973.

72. Balamurugan, S.; Mendez, S.; Balamurugan, S. S.; O'Brien, M. J.; Lopez, G. P., Thermal response of poly(n-isopropylacrylamide) brushes probed by surface plasmon resonance. *Langmuir* **2003,** *19* (7), 2545-2549.

73. Liang, L.; Feng, X. D.; Liu, J.; Rieke, P. C.; Fryxell, G. E., Reversible surface properties of glass plate and capillary tube grafted by photopolymerization of n-isopropylacrylamide. *Macromolecules* **1998,** *31* (22), 7845-7850.

74. Burdukova, E.; Li, H. H.; Ishida, N.; O'Shea, J. P.; Franks, G. V., Temperature controlled surface hydrophobicity and interaction forces induced by poly (n-isopropylacrylamide). *Journal of Colloid and Interface Science 342* (2), 586-592.

75. Reed, J. A.; Love, S. A.; Lucero, A. E.; Haynes, C. L.; Canavan, H. E., Effect of polymer deposition method on thermoresponsive polymer films and resulting cellular behavior. *Langmuir 28* (4), 2281-2287.

76. Gao, L.; McCarthy, T. J., Wetting 101 degrees. *Langmuir* **2009,** *25* (24), 14105-14115.

77. Halperin, A.; Kroger, M., Collapse of thermoresponsive brushes and the tuning of protein adsorption. *Macromolecules 44* (17), 6986-7005.

78. Rzaev, Z. M. O.; Dincer, S.; Piskin, E., Functional copolymers of n-isopropylacrylamide for bioengineering applications. *Progress in Polymer Science* **2007,** *32* (5), 534-595.

79. Alarcon, C. D. H.; Pennadam, S.; Alexander, C., Stimuli responsive polymers for biomedical applications. *Chemical Society Reviews* **2005,** *34* (3), 276-285.

80. Schilli, C. M.; Zhang, M. F.; Rizzardo, E.; Thang, S. H.; Chong, Y. K.; Edwards, K.; Karlsson, G.; Muller, A. H. E., A new double-responsive block copolymer synthesized via raft polymerization: Poly(n-isopropylacrylamide)-block-poly(acrylic acid). *Macromolecules* **2004,** *37* (21), 7861-7866.

81. Yim, H.; Kent, M. S.; Mendez, S.; Balamurugan, S. S.; Balamurugan, S.; Lopez, G. P.; Satija, S., Temperature-dependent conformational change of pnipam grafted chains at high surface density in water. *Macromolecules* **2004,** *37* (5), 1994-1997.

82. Yim, H.; Kent, M. S.; Satija, S.; Mendez, S.; Balamurugan, S. S.; Balamurugan, S.; Lopez, G. P., Evidence for vertical phase separation in densely grafted, high-molecular-weight poly(n-isopropylacrylamide) brushes in water. *Physical Review E* **2005,** *72* (5), 7.

83. Chyasnavichyus, M.; Tsyalkovsky, V.; Zdyrko, B.; Luzinov, I., Tuning fluorescent response of nanoscale film with polymer grafting. *Macromolecular Rapid Communications 33* (3), 237-241.

84. Samadi, A.; Husson, S. M.; Liu, Y.; Luzinov, I.; Kilbey, S. M., Low-temperature growth of thick polystyrene brushes via atrp. *Macromol. Rapid Commun.* **2005,** *26* (23), 1829-1834.

85. Jordan, R.; Ulman, A.; Kang, J. F.; Rafailovich, M. H.; Sokolov, J., Surface-initiated anionic polymerization of styrene by means of self-assembled monolayers. *Journal of the American Chemical Society* **1999,** *121* (5), 1016-1022.

86. Milner, S. T., Compressing polymer brushes - a quantitative comparison of theory and experiment. *Europhysics Letters* **1988,** *7* (8), 695-699.

87. Milner, S. T.; Witten, T. A.; Cates, M. E., Theory of the grafted polymer brush. *Macromolecules* **1988,** *21* (8), 2610-2619.

88. Biesalski, M.; Ruhe, J., Scaling laws for the swelling of neutral and charged polymer brushes in good solvents. *Macromolecules* **2002,** *35* (2), 499-507.

CHAPTER 5:DETERMINATION OF BIOLOGICAL INTERACTION AND SWITCHING RESILIANCY OF PNIPAM-b-PGMA BRUSH FILMS

5.1:Introduction

Intensive research has gone into the application of thin polymeric coatings to tailor surface properties of bulk materials for regulation of biological interaction. [1-4] The control of bio-interfacial interactions between coatings and biomolecules is extremely important for fabrication of next generation biotechnological devices.[5-10] Therefore, detailed characterization of the interfacial interaction between the coating and biomolecules is essential for development of bio-controllable surfaces. Recently, polymeric coatings have been developed to garner bio-interfacial properties that can be switched between adhesive and non-adhesive states in response to a change in environmental stimuli.[5, 11] The discussion in **Chapter 4** gives evidence that block copolymer (BCP) architecture affords us the ability to not only create switchable adhesion states, but control the magnitude of change in biological interfacial interactions in a simplistic single step method. Therefore, the quantitative study of adhesion becomes an important property to determine for each coating as a function of temperature and chemical architecture.

Over the past decade, well-defined PNIPAM brush films have emerged as candidates for temperature manipulated surfaces used in applications such as control of protein absorption and cell adhesion. [10, 12-14] Due to a transition near physiological conditions, PNIPAM has broad and practical potential for applications in biotechnology.[10-12, 15-17] It has been demonstrated that PNIPAM brush layers in the

extended swollen state are practically protein adsorption resistant. [3, 16, 18] On the contrary, reports suggest a sizable increase in protein absorption to collapsed PNIPAM brush layers. [1, 3, 19]

PNIPAM films are successfully used for cell-sheet engineering. [10, 15-16] Cells adhere to PNIPAM at 37°C to form converging cell sheets, and as temperature is decreased, cell sheets may be detached without harming the cell sheet monolayer. [10, 16, 20-22] The creation of smart surfaces for the responsive attachment-detachment of cells is most often carried out by the use of PNIPAM grafted tissue culture dishes. Cells are seeded on the modified culture dish at 37°C. After the cells form a continuous monolayer, they can be detached by lowering the temperature of the culture dish, usually by exchange of the culture medium with fresh medium with temperature less than the LCST.[23] This assumption manifests itself from the idea that above the LCST of PNIPAM, cells are adsorbed on the more hydrophobic PNIPAM layer. When temperature is lowered, and PNIPAM becomes more hydrated and swollen, hydrophobic interaction between cells and PNIPAM surface decrease, enabling detachment of the material.[16] **Chapter 4** demonstrated that PNIPAM SSB films could garner films with pre-defined grafting density and thickness, thus being strong candidates as a material for biotech applications.

PNIPAM has also been used for the creation of switchable protein adsorption surfaces.[11, 15, 18-19, 24] It is well known that the transition phenomenon associated with PNIPAM is affected by molecular weight, grafting density, and thickness. Therefore,

care must be taken in designing thermoresponsive coatings to effectively manipulate protein interaction.

However, literature on protein adsorption to PNIPAM grafted layers is controversial. [3, 16] A major assumption is that when PNIPAM chains are collapsed and more hydrophobic in nature, protein adsorbs to the surface, while layers in the swollen state tends to repel protein adsorption. Although, contradictory reports suggest that this is not always the case. PNIPAM brushes have been shown to not exhibit enhanced protein adsorption above the LCST. Additionally, it was demonstrated that proteins do not adsorb to all PNIPAM coatings.[16, 18]

Yu and coworkers observed increased levels of protein adsorption on thick grafted films of PNIPAM.[3] In contrast, Xue et al.[16] showed that the transition of PNIPAM brushes depended on the grafting density and molecular weight, and concluded that reversible protein adsorption does not occur under all conditions. In fact they found enhanced protein adsorption above the LCST of PNIPAM at intermediate grafting densities. They indicated the reversible and temperature dependent protein adsorption to PNIPAM films actually depends on the film architecture. [18, 21, 25]

Collectively from contact angle data, swelling experiments, and angle-resolved X-ray photoelectron spectroscopy (ARXPS), it was determined that thermally responsive single step PNIPAM brush films (SSB) formed from reactive block copolymers (BCP) effectively afford control over surface behavior at temperatures above and below the

LCST of PNIPAM generated by different ratios of components in the block copolymer. Control of surface wettability is necessary to regulate protein interaction.

In this chapter the interaction between fibrinogen and PNIPAM brushes was studied via atomic force microscopy (AFM) colloidal probe technique, and protein (Bovine fibrinogen) adsorption experiments. Fibrinogen was used as a model protein to investigate the protein adhesion and adsorption on the modified surfaces. Globular proteins are very good prospects for the study of protein adsorption onto polymeric surfaces because of their relatively geometrical simplicity and broad abundance in living organisms.[26-27] The molecular weight of the fibrinogen is 330 kDa. Another advantage of using fibrinogen lies in the fact that an adsorbed monolayer has a height of 3.5-4nm, thus easily detected by ellipsometry.[28] Also there is ample amount of fibrinogen in blood plasma, and it plays a major role in coagulation processes.[4] Therefore, forces of adhesion between the PNIPAM grafted layers and fibrinogen as well as the amount of fibrinogen adsorbed to the surfaces was studied in order to verify that SSB grafted layers are an effective method to generate films with pre-defined and thermally responsive, controllable protein interaction.

The primary goal of the reported work in **Chapter 4** is the single step robust fabrication of thermally responsive thin films with accurate control over surface properties and biological interaction. Interestingly, it was found that protein adsorption could be controlled in an on off manner, and further, the magnitude of the change could be altered or arrested altogether.

Further, a method was developed to study how adhesion properties between protein and PNIPAM films changed after the coatings were subjected to abrasion. Abrasion of the modified substrates was done via contact mode AFM with applied voltages such that 24-90% of the film thickness was removed from the intact layer. The resiliency characteristics of the SSB-1 films were evaluated as a function of amount of abrasion as well as a direct comparison to TSB brush films subjected to abrasion. In order to evaluate adhesion properties of the damaged regions, AFM colloidal probe technique was employed in the same manner as intact surfaces.

5.2:Experimental

Dry grafted layer thickness was determined by ellipsometry (**Section 3.3.3.**1). In order to confirm that protein readily adsorbed to the surface of the PGMA modified bead used for AFM colloidal probe technique, Rhodamine-labeled fibrinogen was adsorbed to the colloidal probe as discussed below, and imaged under fluorescent microscopy (**Figure 5.2a).**

Adhesion measurements were carried out using MultiMode AFM equipped with a temperature controlled stage in a liquid cell. Measurements were run at set stage temperatures of 25 and 55°C to ensure the sample was heated above the LCST of PNIPAM. Several force-distance curves were collected over the wafers' areas. The obtained results for each curve were averaged. Regions of constant compliance of approaching curve at high deflection values were used to determine sensitivity

coefficient. Protein adsorption experiments were carried out as described in **Section 3.3.6.**

In order to estimate the work of adhesion ($\Delta\gamma$) per unit contact area from the measured pull-off force values, the Johnson-Kendall-Roberts (JKR)[29] , and Derjaguin-Muller-Toporov (DMT)[30] models were employed. The JKR model was used to determine work of adhesion (ω) by **Equation(3.6).** The DMT model was utilized in the same manner to determine the work of adhesion values utilizing the **Equation(5.1)**:

$$F_{DMT} = 2\pi R_{tip}\omega \tag{5.1}$$

the only difference being the constant of 2 vs. 1.5 with the JKR model.

All abrasion experiments were carried out on a Dimension 3100 AFM (Veeco Inc.) equipped with a Nanoscope IIIa controller in contact mode. Deflection set-points were set at 0.50-0.75V. Samples lines were set at 512 with a scan speed of 1 Hz with a scan area of 50 x 50 μm. Samples were scanned repeatedly, 4-6 times. After the completion of scanning 1 time at 0°, the scan angle was changed to 90° for the next scan, following the same pattern for the entire experiment. After abrasion, samples were washed in MEK and scanned in tapping mode in order to evaluate the amount of material that was removed. Next, abraded samples were measured for pull off force values and subsequently work of adhesion values at temperatures of 25 and 55°C as described above inside of the abraded areas in fresh PBS buffer.

5.3:Results and Discussion

5.3.1:Study of Protein-Brush Interaction by AFM Colloidal Probe Technique

Adhesion is defined as the molecular attraction or repulsion applied between surfaces of bodies in contact.[31] Both long range and short range interactions may be present when two surfaces are brought in and out of contact.[31] However, in our experimental PNIPAM based system, mainly physical interactions such as Van der Waals interaction and hydrophobic forces are important.[31-33] Utilizing AFM, we can perform quantitative studies of adhesion between two contacting surfaces. AFM is an advantageous technique over other methods such as surface force apparatus (SFA) because we can easily measure samples in air, liquid, or vacuum with high lateral resolution.[31]

Therefore, to demonstrate control over protein surface interaction using SSB films, forces of adhesion, also known as "pull off force" between the grafted polymer layers and fibrinogen was measured by the AFM colloidal probe technique. Specifically, the effect of PGMA block length of the SSB layers on protein adhesion at temperatures above and below the LCST of PNIPAM were studied.[8, 34] Adhesion force, which is defined as the maximum force required for pulling apart two surfaces after initial contact was studied as a function of temperature. In brief, hollow glass spheres were modified with PGMA and fibrinogen proteins and subsequently attached to the end of AFM cantilevers.[8, 34] Modified beads were brought into contact with polymer grafted surfaces in a PBS environment via AFM force volume mode in order to generate force distance curves.

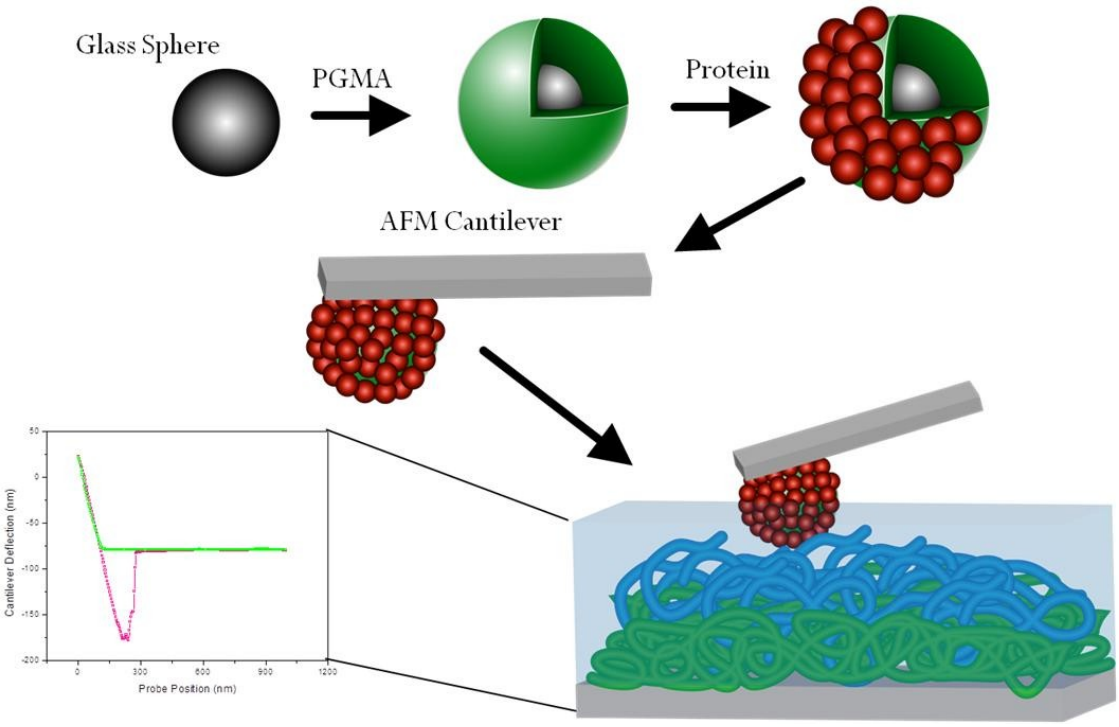

Figure 5.1: Schematic of AFM colloidal probe fabrication procedure.

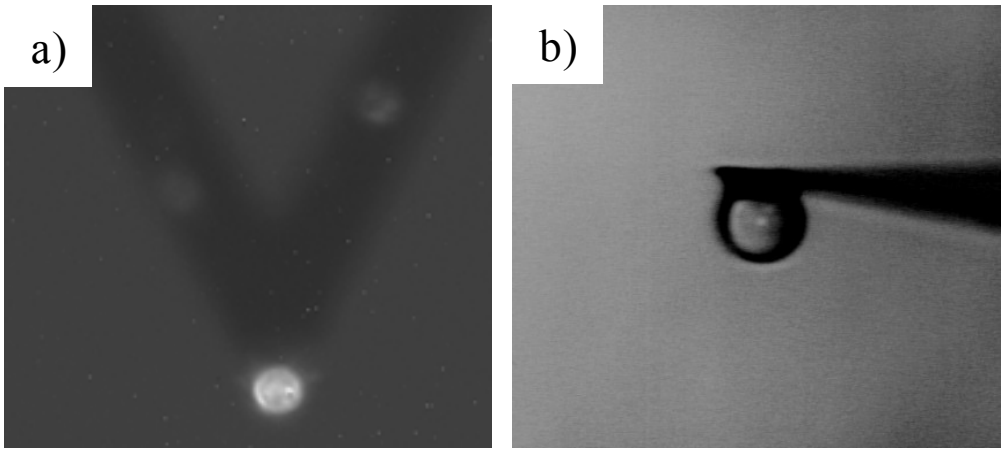

Figure 5.2: Modified glass sphere attached to AFM cantilever of a) Fluorescent imaging of adsorbed Rhodamine-B labeled fibrinogen. b) As modified bead glued to AFM cantilever

An overall schematic of the experimental protocol is displayed by **Figure 5.1.** To validate that indeed fibrinogen successfully attached to the PGMA modified glass beads, Rhodamine-B labeled fibrinogen was attached to the bead and imaged under fluorescent microscopy. **Figure 5.2a** shows a fluorescent microscopy image of labeled protein adsorbed to the glass bead. The results confirm that fibrinogen protein was successfully adsorbed to the PGMA modified bead. Modified spheres were then attached to the end of cantilevers (**Figure 5.2b)** using epoxy glue in order to carry out force distance measurements by AFM contact mode (force volume).[35] The AFM colloidal probe was then brought into contact with the PNIPAM surfaces in PBS environment at either 25 or 55°C.

Figure 5.3 exhibits typical AFM retraction curves as function of temperature for all SSB layers. The retracting curves reflect the level (nm) of deflection the AFM cantilever undergoes while pulling the protein covered probe from the polymer grafted surface. The larger the value of cantilever deflection measured, the higher the adhesion force present. PGMA grafted films were probed as a reference as well. PGMA does not exhibit temperature responsive surface properties, and therefore, should be represented by comparable pull off forces at both measured temperatures. As seen in **Figure 5.3e**, PGMA films were measured to have roughly 160nm of deflection at both temperatures measured. The measured cantilever deflection values for the films under consideration were then multiplied by the measured force constant (0.093 N/m) of the AFM cantilever providing pull off force values.

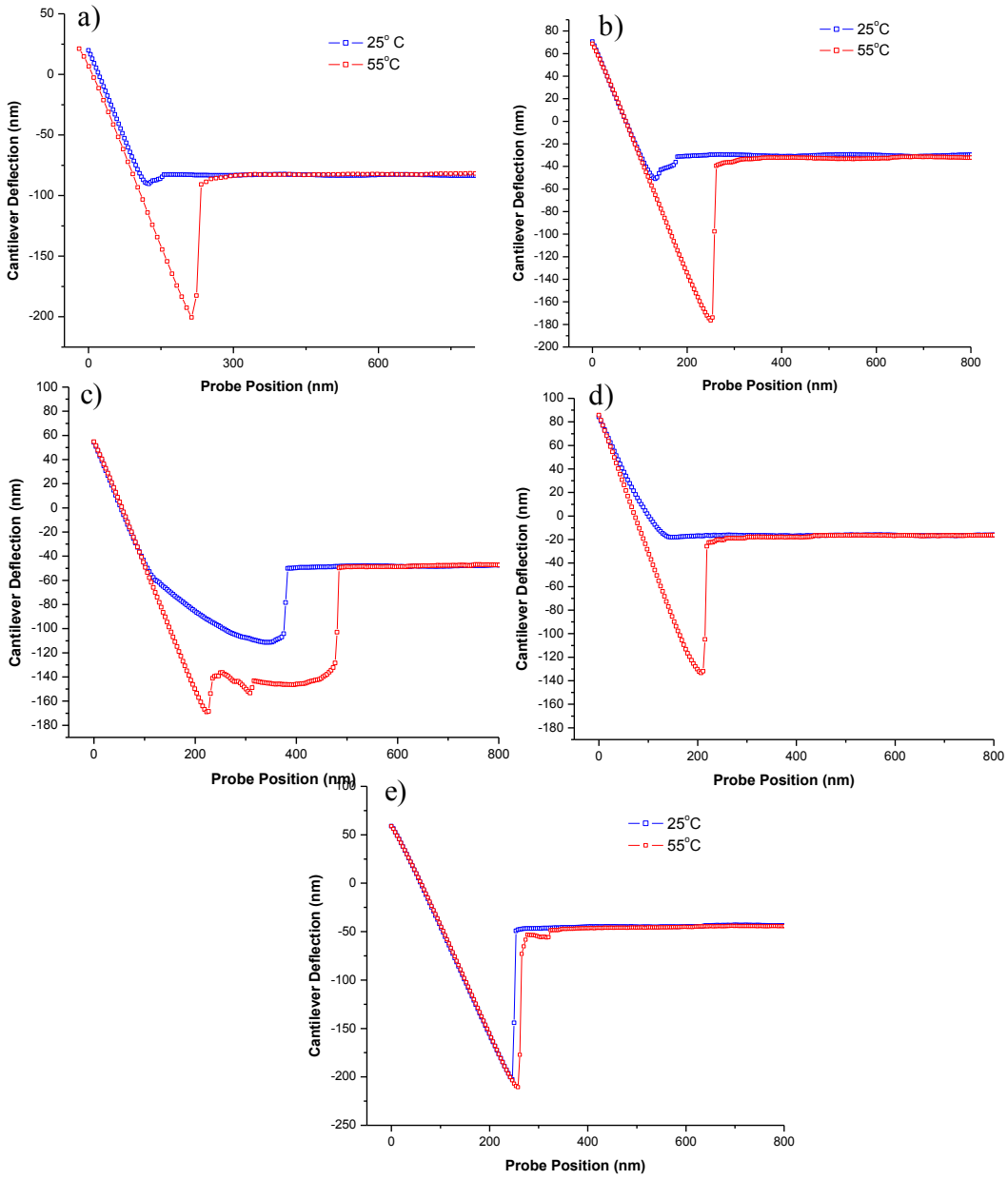

Figure 5.3: AFM force-distance retracting curves as a function of temperature for a) SSB-1 b) SSB-2 c) SSB-3 d) TSB e) PGMA reference.

Figure 5.4 displays values for the effective pull off force for all SSB and TSB grafted films at temperatures of 25 and 55°C. All PNIPAM containing coatings showed significant thermally responsive surface behavior. At temperatures below the LCST, all PNIPAM films showed low adhesion force (< 6.0×10^{-6} mJ/m). At temperature above the LCST, SSB-1 exhibited an approximately 14-fold increase in adhesion force. As the amount of PGMA in the block copolymer increased, the total change in pull-off force from 25-55°C decreased. SSB-2 exhibited a 7.4-fold increase while SSB-3 exhibited a 3-fold increase in the adhesion force upon change of temperature to 55°C. For comparison, the TSB traditional PNIPAM brush film exhibited a 6.3-fold increase in adhesion from 25-55°C.

Significant differences in the magnitude of pull off forces were observed for each PNIPAM film. At temperatures of 25°C, PNIPAM SSBs exhibited an increase from ~7.7 x 10^{-7} to ~5.6 x 10^{-6} mJ/m force for decreasing amounts of PNIPAM in the block copolymer. This is due to fact that increased amounts of PGMA are present in the top most (10nm) dry nano region of the film as shown by ARXPS (**Table 4.3**) results. PNIPAM is swollen and hydrated in PBS at 25°C, consequently yielding a film that is soft and penetrable by the AFM probe. Penetration by the AFM probe induces an increased contact area with PGMA units, with which fibrinogen strongly adheres to, resulting in an increase of pull off force.

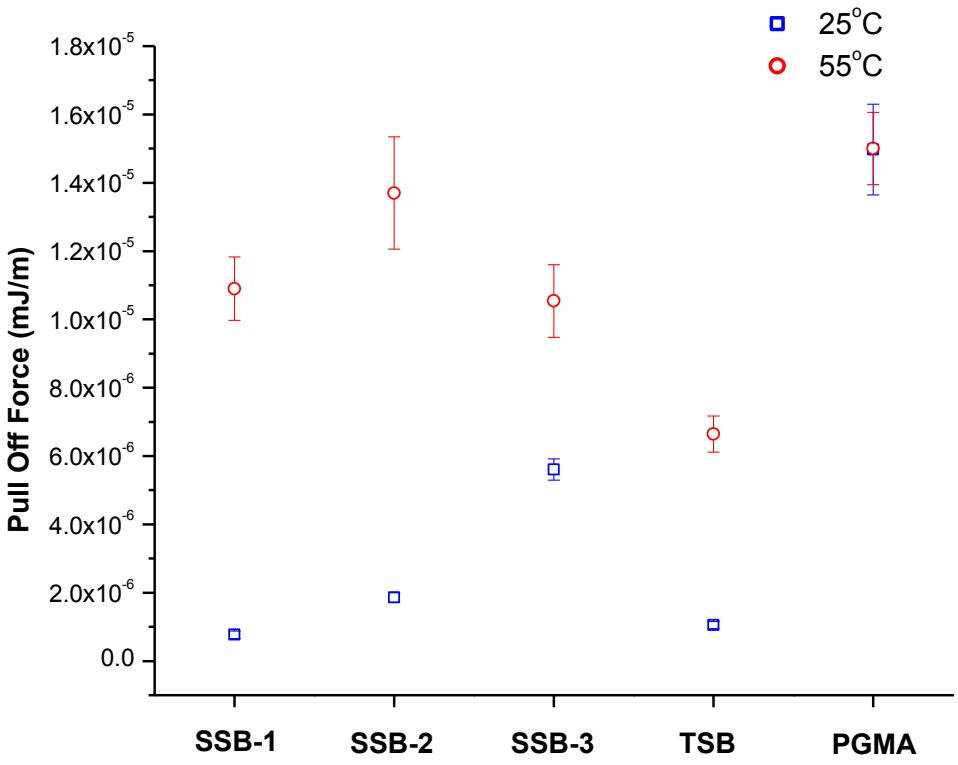

Figure 5.4: Effective pull of Force or *adhesion force* measured as a function of temperature.

At temperatures (55°C) above the LCST of PNIPAM, the SSB adhesion values follow trends observed for measured amounts of PNIPAM (**Table 4.3**) in the block copolymer films at the outer most nano-region of the film. As observed from ellipsometry measurements, PNIPAM arranges into a collapsed and dehydrated layer at 55°C. The surface becomes less dominated by PNIPAM, inducing a synergistic adhesion affect due to hydrophobic interaction with collapsed PNIPAM layers and an increase of PGMA content, indicated by increased adhesion forces to values in between pure PNIPAM (TSB

films) in the collapsed state and pure PGMA. TSB systems which contain a solely dominate PNIPAM interface at 55°C display roughly 6.6 x 10^{-6} mJ/m of force as compared to 1.5 x 10^{-5} mJ/m of pure PGMA. All three PNIPAM SSB films displayed adhesion force values above the homopolymer block constituent reference values at 55 °C, but less than pure PGMA. Interestingly, symmetric SSB-2 showed the highest value (1.37 x 10^{-5} mJ/m) of adhesion at elevated temperature. PNIPAM-2 contains the most water in the layer at 55°C. Therefore we suggest that as the water content of the layer increases there will be deeper penetration of the probe, resulting in increased interaction with PGMA in the SSB-2 layer.

In order to quantitatively discuss the effective control over biological interaction, the work of adhesion (ω) was determined by the JKR and DMT models.

5.3.2:Work of Adhesion as a Function of Block Copolymer Composition and Temperature: JKR vs. DMT models.

The amount of force required to separate fibrinogen covered probes and PNIPAM grafted surfaces is termed the pull of force, or "adhesive force" as displayed by **Figure 5.4**. [31] Therefore, we can define what is known as work of adhesion (ω), the amount of work done or free energy change from separating two surfaces per unit area to infinity. Since surface energy is the free energy change when the surface area of our sample is increased by some area, this parameter is also known as surface tension.[31] Therefore, we can relate the work of adhesion to surface tension by the **Equation (5.2)**:

$$\omega_{adhesion} = \gamma_A + \gamma_B - \gamma_{AB} \qquad (5.2)$$

where γ_A and γ_B are the surface tensions of the individual materials before contact.

Original work in contact mechanics in the late 1800s by Hertz, found that the contact force was a function of the reduced elastic modulus, the radius of the contacting bodies, and the contact radius.[29, 31, 36-37] However, his theory assumed no adhesive forces. For a number of systems, especially protein-polymer systems, adhesive forces do exist. Therefore, Hertz model cannot be used to describe the forces of interaction between fibrinogen protein and PNIPAM brush modified substrates in our case.

In the 1970's two groups of scientists provided relationships between adhesive forces within contact mechanics. [29-30] Johnson, Kendall Roberts, and Derjaguin, Muller, and Toporov found that work of adhesion is related to the force of adhesion (pull-off force) through their respective models which became known as JKR[29] and DMT[30] models for contact mechanics.

The JKR model modified Hertz's original work to include surface forces.[29] In short, interacting forces are short ranged and act only inside the contact area between the tip and surface.[29, 31] . In general the JKR model is used when larger probes are utilized with materials of higher surface energies. [36, 38]

On the other hand, the DMT model is generally employed for rigid systems with smaller radii of curvature and low work of adhesion.[31, 38] The only difference between the JKR and DMT models being the constant of 3/2 vs. 2 for the DMT model. In the present work, both models are utilized to relate the maximum pull off force as measured by the AFM, to the work of adhesion for the quantitative comparison of adhesion switching capability of PNIPAM SSB, TSB, and PGMA reference films.

Figure 5.5a displays the quantitative JKR work of adhesion values for all PNIPAM brush and PGMA reference films. Typical trends as seen by pull off forces in **Figure 5.4** were followed. SSB-1 and -2, as well as TSB films showed significant protein repelling properties at 25°C. The work of adhesion values were less than 0.04 mJ/m^2. An increase from 0.02 to 0.12 mJ/m2 was observed as the PGMA content was increased in the PNIPAM diblock copolymers, a roughly 6 fold increase in work of adhesion at 25°C. SSB-1 and TSB showed practically identical work of adhesion values (0.02 mJ/m^2) at 25°C. To establish a work of adhesion value sufficient enough to adsorb a complete monolayer of protein to the surface, PGMA work of adhesion values were determined. PGMA work of adhesion at both measured temperatures was found to be 0.32 mJ/m^2. At experimental temperatures of 55°C, all SSB brush films showed higher work of adhesion values than the TSB films, but lower than pure PGMA. SSB-1 and -3 were found to have similar values, roughly 0.23 mJ/m2, almost 2x larger than the TSB film. As observed from pull off force measurements, SSB-2 films showed the highest value of all PNIPAM films at 55°C (0.29 mJ/m^2).

Figure 5.5b displays the relationship between the JKR and DMT work of adhesion values. As it should be from mathematical considerations, all calculated DMT values were less than their JKR counterparts. However, irrespective of the model and tip radii curvature, the DMT and JKR models indicated the same trends for work of adhesion as a function of block copolymer composition and temperature.

Interestingly, SSB-1 showed characteristics as the best material towards a complete protein and cell switchable surface, ranging from complete protein repelling

and high energy surface (0.02 mJ/m^2), to 0.23 mJ/m^2, and thus significantly protein adhering. This was a more effective "protein switch" than observed for the comparison film, TSB (0.02 to 0.14 mJ/m^2). Interestingly, the characteristics of the switchable surface could be easily tuned by increasing the amount of PGMA which effectively decreased the overall magnitude of change. Such changes created surfaces with increased work of adhesion values at 25°C.

However, trends in work of adhesion measurements indicate that the colloidal probe technique is not a solely interfacial interaction measurement in our case. Deformation of the swollen "gel like" surfaces may not represent protein and cell adsorption, especially to densely grafted brushes. Therefore, assuming protein adsorption events are limited to adsorption at the outer regions of the film, the amount of protein adsorption to the grafted layers may not strictly follow work of adhesion level.

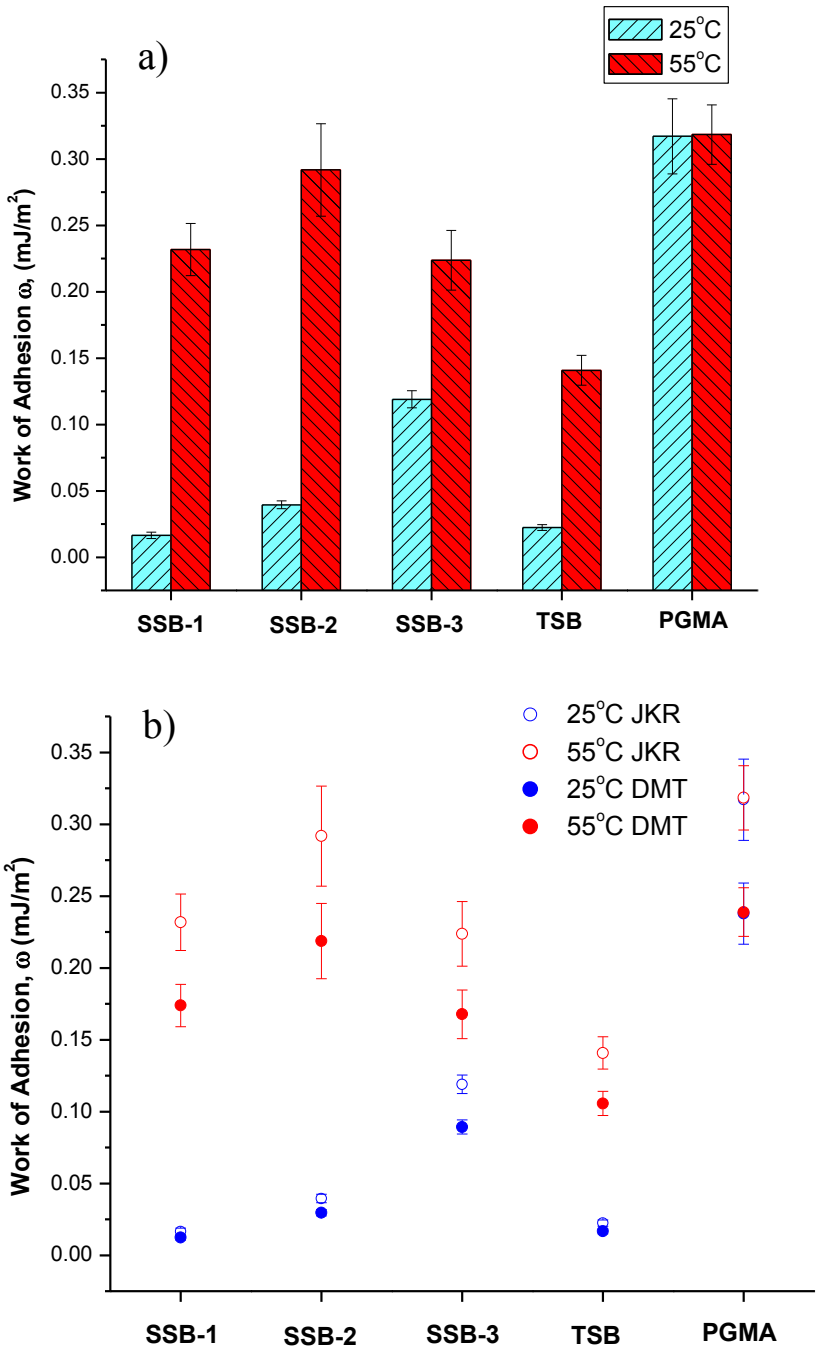

Figure 5.5: Work of adhesion values determined from JKR and DMT models as a function of temperature. a) JKR b) JKR vs. DMT**.**

5.3.3:Adsorption of Protein onto PNIPAM fabricated Films

The adsorption of protein was studied through the introduction of modified silicon wafers into an agitated solution of fibrinogen (1mg/mL) in phosphate buffered saline (pH 7.4) solution for 30 minutes. An overall schematic of the experimental protocol is displayed in **Figure 5.6**. The amount of protein adsorption was characterized by measuring the ellipsometric dry layer thickness before and after protein adsorption experiments. 1nm of adsorbed fibrinogen corresponds to 3 x 10^{-9} mol/m^2. The protein and polymer layer refractive index was set at 1.5 for all systems. TSB PNIPAM brush films were again used as comparison. Thin films of pure PGMA showed protein adsorption behavior of roughly 5nm thickness.

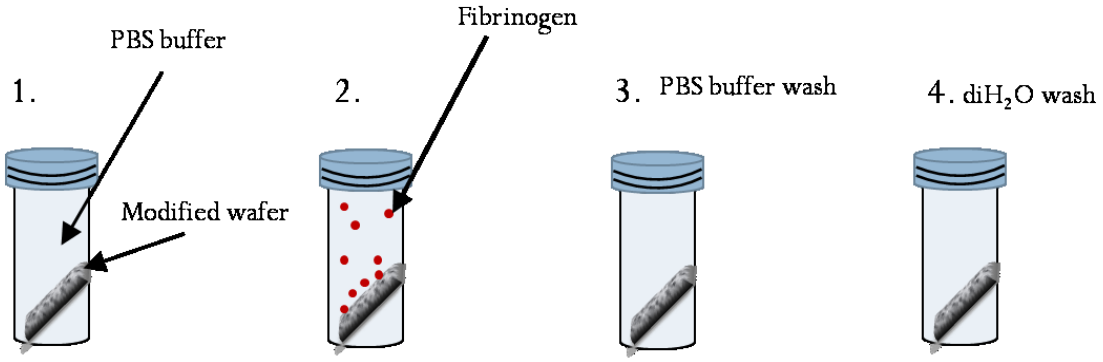

Figure 5.6: Schematic overview of Fibrinogen adsorption procedure.

Under these experimental conditions, PNIPAM SSB brushes with varying amounts of PGMA block segment showed distinct levels of protein adsorption behavior (**Figure 5.7**). SSB layer with the least amount of PGMA present in the film (SSB-1) showed the greatest change in amount of protein adsorbed at 25 and 41°C. A change from

0.1 ± 0.5nm at 25°C to 3.8 ± 0.7nm in thickness of the adsorbed protein layer was determined, roughly a 3.7nm thickness change. As PGMA block molecular weight was increased to 24.2k (SSB-2), the magnitude of thermally responsive adsorption decreased. Interestingly, there was a slight increase at 25°C (0.4 ± 0.3nm), and a slight decrease in the thickness of the protein layer (2.7 ± 0.5nm) at temperatures above the LCST of PNIPAM, resulting in an overall thickness change of roughly 2.3nm.

Finally, as the PGMA molecular weight is increased to 43.9k (SSB-3), again, the same trend is observed. For SSB-3 samples, an increase in protein adsorption at cold temperatures (1.5 ± 0.4nm) was determined, while a decrease of adsorption at high temperatures (1.4 ± 0.8nm) was observed as compared to SSB-1 and -2 layers.

The trend follows the amount of change in work of adhesion values of SSB-3 at the different temperatures. SSB-3 showed the smallest change in adhesion values as a function of temperature. As a result, no change in adsorption levels with temperature variation was measured for SSB-3. In comparison, TSB films showed a change in protein adsorption magnitude at the experimental temperatures. However SSB-1 and -2 showed higher switchability threshold than TSB films. The presence of PGMA in the collapsed state enhances the amount of fibrinogen adsorbed at high temperatures, while swelling of PNIPAM at temperatures below the LCST preserves protein repelling behavior.

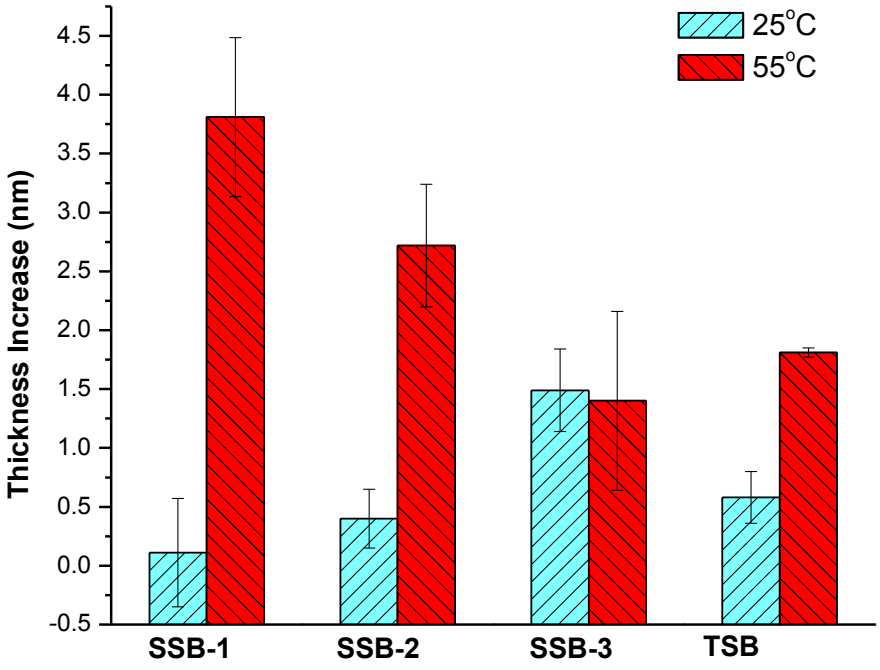

Figure 5.7: Fibrinogen absorption to PNIPAM brush layers as a function of temperature as measured by ellipsometry. Error was calculated as standard error. 1nm of fibrinogen corresponds to 3 x 10^{-9} mol/m^2, or 21% of a monolayer of protein adsorbed to PGMA layer.

To complement the observed results, AFM phase imaging was utilized to reveal the morphology of the films after protein adsorption (**Figure 5.8**). **Figure 5.8a-b** show phase images of pure PGMA films before (**Figure 5.8a)** and after (**Figure 5.8b**) protein adsorption. It is clearly seen that prior to fibrinogen adsorption to PGMA, a smooth film is present. After the protein adsorption, a dense monolayer of fibrinogen was observed on the surface, as noticed by the globular structures now present. Similar results were seen for SSB-1 films. **Figure 5.8c** shows the SSB-1 film prior to protein adsorption. A smooth and homogenous surface is present. Protein adsorption at 25°C (**Figure 5.8c**),

exhibited phase images with sparse fibrinogen molecules on the surface. Ellipsometric measurements gave practically no significant increase in film thickness in cold conditions; however AFM indicates there are sparse proteins adsorbed on the surface. Very low levels (10-15 molecules) of adsorption are within the 0.5nm sensitivity of the ellipsometer used in our experiments. Lastly, **Figure 5.8e** exhibits a 1 x 1 μm phase image of SSB-1 films after fibrinogen adsorption in hot conditions. It is evident that a similar mono-layer is present similar to pure PGMA layers. Fibrinogen practically forms a monolayer at high temperatures on SSB-1 brushes, as seen by the appearance of globular like structures present on the surface much like pure PGMA films.

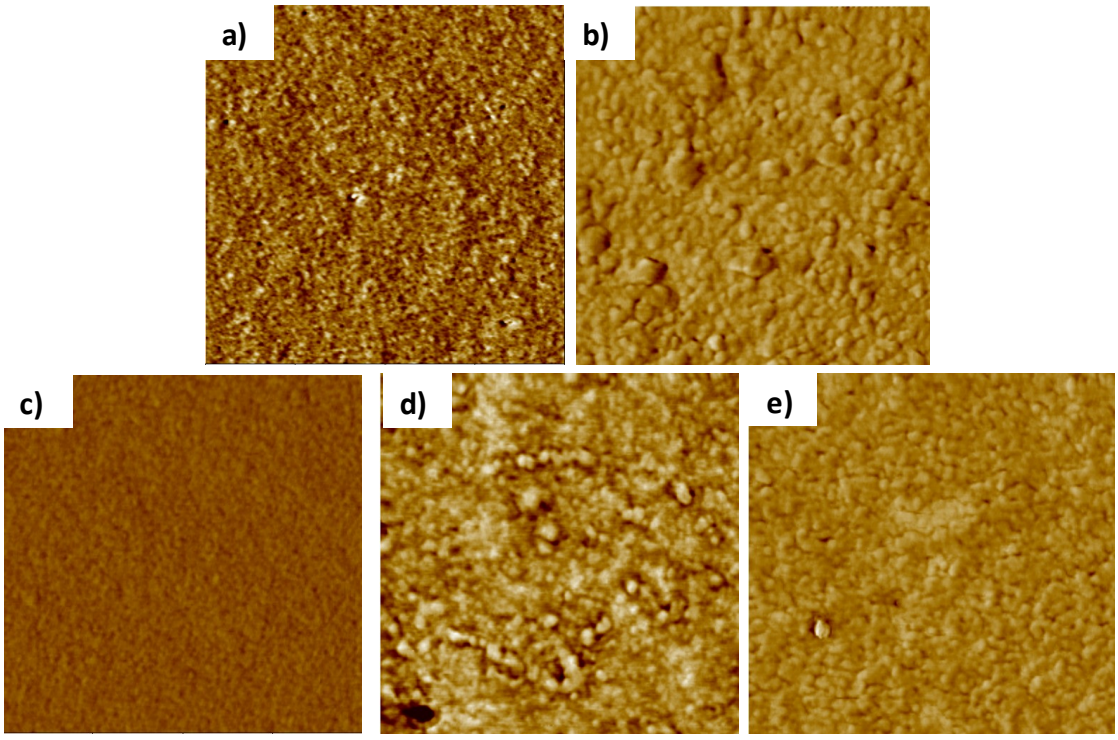

Figure 5.8: 1 x 1 μm AFM phase images. a) PGMA before protein adsorption b) PGMA after protein adsorption c) SSB-1 before protein adsorption d) SSB-1 after protein adsorption at room temperature e) SSB-1 protein adsorption at 41^0C. Vertical scale: 30^0.

Ellipsometric thickness measurements and AFM phase imaging determined that indeed, manipulation of protein adsorption is achieved through careful control of block copolymer chemical composition. Asymmetric PNIPAM dominated BCPs deliver protein switchable layers that surpass that of traditional brush approaches produced in our laboratory. By increasing the PGMA content, one can manipulate the amount of protein adsorption change, or produce films that show no preferential adsorption to temperature (SSB-3). Most importantly, these films also show the ability to actuate and undergo the volume phase transition, producing unique wettability property changes for each individual BCP composition. We attributed the observed adsorption behavior as follows.

Although PNIPAM brush systems are formed from block copolymers, films created with PNIPAM dominated BCP segments retain sufficient mobility to concentrate at the polymer-water interface (as shown by ARXPS results), hence the 3-fold increase in thickness at the lower water temperatures. Moreover, increased PGMA content consequently causes an increase in cross-linking density and a decrease in the apparent grafting density of PNIPAM. This effectively decreases the amount of swelling/collapse thickness and contact angle measurement changes with changing temperature. It was found that when PNIPAM is in a dehydrated and collapsed state, the presence of PGMA creates a synergistic interaction effect, creating differences in adsorption amounts for the series of block copolymers. As SSB-1 films show, at low temperatures, if there is a sufficiently high enough PNIPAM to PGMA ratio, it can exhibit protein repellent properties. In the collapsed state, increase adsorption is due to the hydrophobic nature of

PNIPAM, and the synergistic effect of PGMA at the polymer water interface, increasing the protein-polymer interaction.[6]

5.3.4:Switching Resiliency of SSB and TSB Brush Films.

We envisioned that a major drawback to the single step fabrication method could be SSB responsive properties would depreciate after wear as compared to traditional synthetic approaches. ARXPS showed an appreciable amount of PGMA deeper in the film as compared to the polymer air interface region. Consequently, abrading the surface may expose additional PGMA domains causing a depletion of thermal response towards protein adhesion.

With this is mind, we developed a method to abrade polymer brush layers as a function of damage depth (nm). The PNIPAM brush layers were then characterized for fibrinogen-polymer adhesion forces inside the damaged areas as function of temperature and compared to their intact layer values. The experimental protocols were carried out via a combination of two AFM techniques. For this purpose, the surface in 50 x 50 μm areas was abraded and damaged by AFM tip using contact mode AFM. Amplitude set-point and number of scans was optimized in order to achieve different amounts of abrasion. Fibrinogen modified AFM colloidal probe technique was used to elucidate the change in adhesion forces post abrasion.

Two experiments were conducted to study film performance after abrasion. A comparison of the TSB films vs. SSB-1 films after similar abrasion (7-10nm) was performed. Second, SSB-1 films (28nm initial thickness) were subjected to 3 varying levels of abrasion. Profile changes via AFM confirmed that the SSB-1 films experienced

a decrease in film thickness of 7, 17, and 24nm after abrasion. The work of adhesion values were measured at all resulting depths and compared to the initial undamaged films.

Figure 5.9a-c displays the resulting JKR work of adhesion values of non abraded areas vs. abraded areas for both SSB-1 and TSB films, and typical 20 x 20 μm AFM topography images of the abraded regions of the films. Abrasion to the SSB-1 film resulted in a 7nm decrease from the original 28nm layer. The TSB PNIPAM brush exhibited a 10 nm decrease from the intact 22nm layer. **Figure 5.9a** shows that both surfaces experience a decrease in switchability properties after abrasion as compared to the intact films. The actual magnitude of decrease in adhesion switchability is less for the TSB approach. However, the initial properties of the non abraded SSB-1 system show a greater magnitude of adhesion switchability than the traditional brush approach. Consequently, the damaged area (0.02 mJ/m^2 at 25°C and ~0.12 mJ/m^2 at 55°C) of the SSB-1 film exhibits properties resembling non-damaged traditional brush films (0.02 mJ/m^2 at 25°C and ~0.14 mJ/m^2 at 55°C).

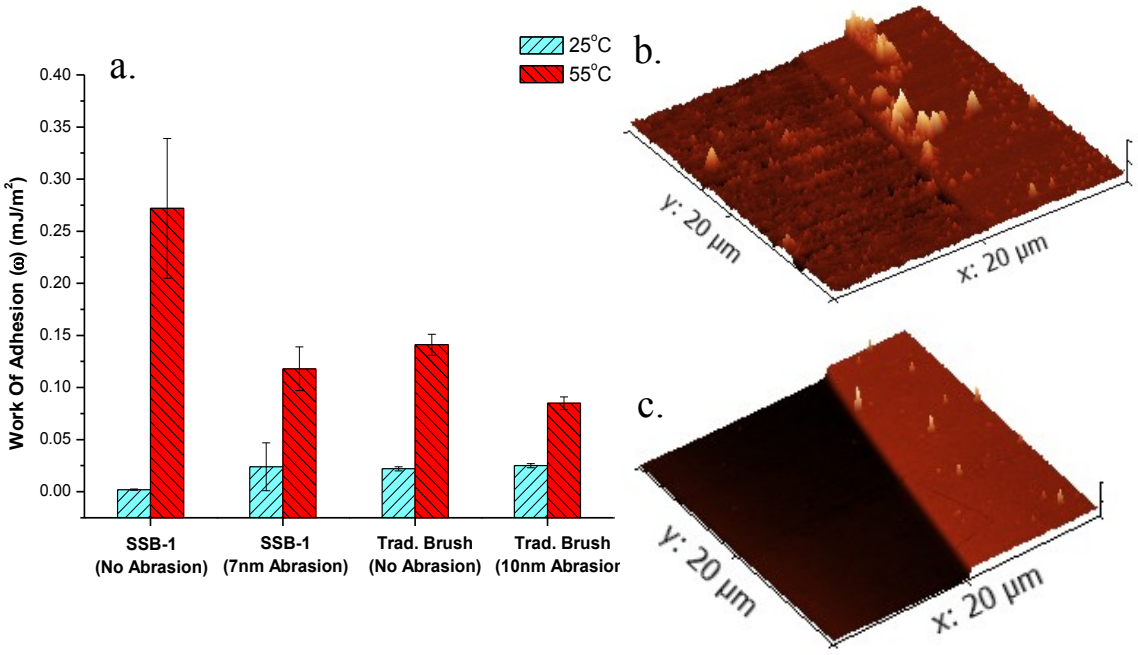

Figure 5.9:a) Work of adhesion determined for to damaged brush layers as compared to intact films b-c) 20 x 20 µm AFM topography images of abraded brush layers in SSB-1 and TSB films respectively.

We expect that this would be highly desirable in situations where coatings would be used for extended periods of time, and it is likely that the SSB systems may exhibit more wear resistant coating qualities than that of the traditional approach due to better initial performance. The reason behind the decrease in switchability and overall increase in surface energy is discussed in the next paragraph. However, more detailed studies are needed in order to determine the exact mechanism behind preserved switchability of the abraded BCP films.

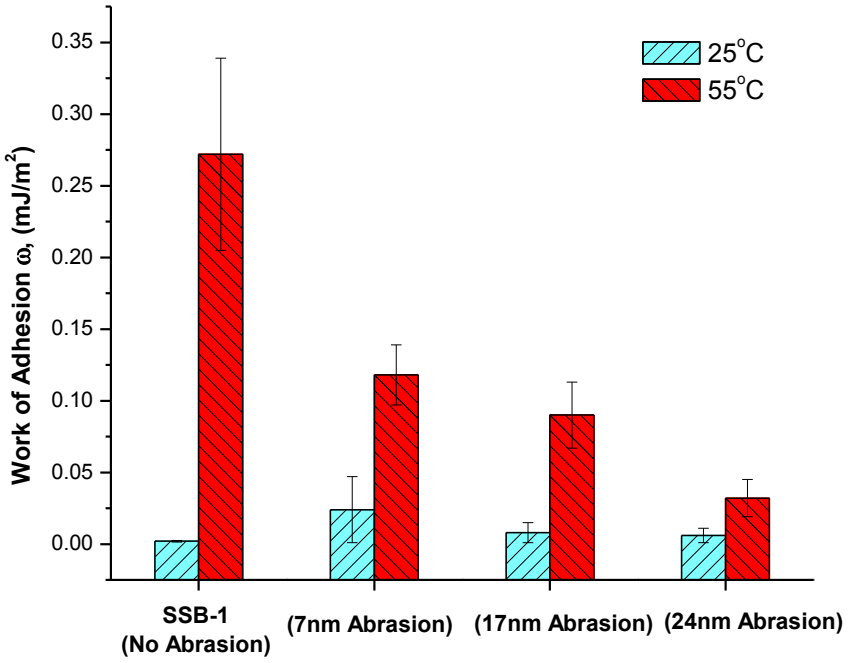

Figure 5.10: Work of adhesion values of SSB-1 films (initial thickness of 30nm) as a function of abraded depth. Measurements were performed at 25 and 55°C.

Figure 5.10 displays the work of adhesion values as a function of temperature and abrasion depth. As observed, the intact film shows the greatest amount of change in adhesion at the measured temperatures. As the depth of abrasion is increased (7-24nm) it is apparent that the magnitude of switching is greatly reduced. Interestingly, the films become overall higher surface energy coatings after damage, independent of temperature. At 25°C, the work of adhesion remains relatively constant for all abrasion depths, less than 0.02 mJ/m^2, indicating protein repelling surfaces regardless of damage. However, an interesting trend is observed at 55°C. Here we see a roughly exponential decrease in work of adhesion as a function of abrasion depth. A decrease from 0.27 (intact) to 0.12

(7nm), 0.09 (17nm) and 0.03 mJ/m^2 at 24nm depth is observed. Adhesion properties at 7 and 17nm still show changes in adhesion with temperature, however at 24nm the film becomes practically non-active, and fully protein repelling at both temperatures.

The trends observed for adhesion values at different temperatures as a function of abrasion depth is consistent with studies previously published on PNIPAM chain collapse as a function of molecular weight.[6, 39-40] It was shown that optimal grafting conditions to show the largest switchability change in PNIPAM films was determined to be at high molecular weight chains and intermediate grafting density.[39] Plunket et al. showed that their contact angles at low molecular weights were lower than that of thicker more densely grafted films.[6] Zhu et al. found that low molecular weight PNIPAM end grafted films(Mw = 10k) do not collapse, and that low molecular weight brushes remain swollen and extended in aqueous environments regardless of temperature.[40] Indeed, what occurs during abrasion is the breaking and ripping of the diblock copolymer chains. As we break chains, we predict that the PNIPAM and PGMA chains are severed, resulting in PNIPAM chains of decreased effective molecular weight. As seen from Zhu et al.[40] films of low molecular weight still become highly swollen with water, however, once the temperatures are raised above the LCST, the film remains highly swollen and does not have the ability to collapse. This is the reason why at 25°C, the work of adhesion remains constant and low. Indeed the films are highly swollen with water creating hydrophilic materials. However, at 55°C, damaged PNIPAM chains become lower molecular weight and, therefore, cannot collapse and expel water. This is why a decrease in work of adhesion is noticed as the amount of damage to film is increased.

5.4:Conclusions

The most important achievement of the research lies in the ability to manipulate surface properties, and thus interaction with proteins. Independent of thickness, the PNIPAM brush layers can undergo surface wettability changes by changes in temperature (films over 15nm in thickness), and can be tuned to the amount of change desired.

Work of adhesion determined for all SSB diblock copolymer films were found to be unique at each chemical composition. By effectively altering the amount of PGMA in the initial block copolymer, the protein interaction was effectively changed. Therefore, we demonstrated the ability to construct surfaces with varying changes in adhesion states versus temperature. SSB-1 films showed practically no adhesion at 25°C, and adhesion values approaching 0.30 mJ/m^2 at 55°C. When the amount of PGMA was increased (SSB-2 and -3), the adhesion values at 55°C were relatively constant. However, a decrease in surface energy was found at 25°C for increasing amounts of PGMA. SSB-3 films had much less change in adhesion states versus temperature compared to SSB-1. This effectively leads towards films that undergo small changes in adhesion states irrespective of temperature. Therefore, based on the work of adhesion, we successfully created films that went from highly switchable, to very low switching ability by effectively controlling the amount of each component in the block copolymer prior to deposition. This surpasses conventional techniques because surfaces are garnered in a very simplistic singe step manner.

Additionally, protein adsorption can be manipulated in much the same way. Interfacial interaction between protein and polymer are constrained through adhesion

interactions between the two surfaces. However, the ability to modulate the adhesion states at temperatures above and below the LCST allows us to generate on-demand surfaces that repel and adsorb protein in a predictable manner. All three SSB films showed unique temperature dependent protein adsorption. Adsorption with fibrinogen was determined to follow similar trends as work of adhesion measurements by AFM. At low molecular weight blocks of PGMA, the ability to completely turn on and off protein adsorption was demonstrated. As PGMA molecular weight increased, the magnitude of protein absorption change decreased, up to a point where constant adsorption was observed independent of temperature. This provides a novel technique for the design of synthetic material surfaces for interaction with biological materials.

The switching resiliency of the polymer layers was also studied. In comparison to TSB films, SSB-1 films depreciated at a faster rate at roughly the same abrasion depth, however, due to the significantly better performance of the intact films, the SSB-1 damaged films approached thermoresponsive adhesion behavior of intact TSB films.

Work of adhesion as a function of the amount of abrasion (7-24nm layer removal) was determined for SSB-1 films at temperatures of 25 and 55°C as well. Overall, the properties of PNIPAM block copolymer adhesion switchability decreases with increasing amounts of abrasion. It was found that work of adhesion was constant independent of abrasion at 25°C. However at 55°C, work of adhesion decreased from a protein adsorbing surface to practically total protein repelling at deep levels of abrasion. This trend was found to be consistent with behavior of low molecular weight PNIPAM. The intact films contain PNIPAM at high enough molecular weight to exhibit very obvious

thermally responsive behavior, however as the polymer chains are damaged and broken, the effective molecular weight is decreased, leading to films that can no longer collapse and expel water creating higher energy surfaces. Therefore, at deep abrasion levels, PNIPAM remains swollen and hydrated creating hydrophilic and protein repelling properties irrespective of temperature.

5.5:References

1. Yin, Z. Z.; Zhang, J. J.; Jiang, L. P.; Zhu, J. J., Thermosensitive behavior of poly(n-isopropylacrylamide) and release of incorporated hemoglobin. *Journal of Physical Chemistry C* **2009,** *113* (36), 16104-16109.

2. Yu, Q.; Zhang, Y.; Chen, H.; Zhou, F.; Wu, Z.; Huang, H.; Brash, J. L., Protein adsorption and cell adhesion/detachment behavior on dual-responsive silicon surfaces modified with poly(n-isopropylacrylamide)-block-polystyrene copolymer. *Langmuir 26* (11), 8582-8588.

3. Mori, N.; Horikawa, H.; Furukawa, H.; Watanabe, T., Temperature-induced changes in the surface wettability of sbr plus pnipa films. *Macromolecular Materials and Engineering* **2007,** *292* (8), 917-922.

4. Yu, Q.; Zhang, Y. X.; Chen, H.; Zhou, F.; Wu, Z. Q.; Huang, H.; Brash, J. L., Protein adsorption and cell adhesion/detachment behavior on dual-responsive silicon surfaces modified with poly(n-isopropylacrylamide)-block-polystyrene copolymer. *Langmuir 26* (11), 8582-8588.

5. Cole, M. A.; Voelcker, N. H.; Thissen, H.; Horn, R. G.; Griesser, H. J., Colloid probe afm study of thermal collapse and protein interactions of poly(n-isopropylacrylamide) coatings. *Soft Matter* **2010,** *6* (12), 2657-2667.

6. Plunkett, K. N.; Zhu, X.; Moore, J. S.; Leckband, D. E., Pnipam chain collapse depends on the molecular weight and grafting density. *Langmuir* **2006,** *22* (9), 4259-4266.

7. Rzaev, Z. M. O.; Dincer, S.; Piskin, E., Functional copolymers of n-isopropylacrylamide for bioengineering applications. *Progress in Polymer Science* **2007,** *32* (5), 534-595.

8. Schmidt, S.; Zeiser, M.; Hellweg, T.; Duschl, C.; Fery, A.; Mohwald, H., Adhesion and mechanical properties of pnipam microgel films and their potential use as switchable cell culture substrates. *Advanced Functional Materials* **2010,** *20* (19), 3235-3243.

9. Stuart, M. A. C.; Huck, W. T. S.; Genzer, J.; Muller, M.; Ober, C.; Stamm, M.; Sukhorukov, G. B.; Szleifer, I.; Tsukruk, V. V.; Urban, M.; Winnik, F.; Zauscher, S.; Luzinov, I.; Minko, S., Emerging applications of stimuli-responsive polymer materials. *Nature Materials* **2010,** *9* (2), 101-113.

10. Yang, J.; Yamato, M.; Okano, T., Cell-sheet engineering using intelligent surfaces. *Mrs Bulletin* **2005,** *30* (3), 189-193.

11. Cole, M. A.; Voelcker, N. H.; Thissen, H.; Griesser, H. J., Stimuli-responsive interfaces and systems for the control of protein-surface and cell-surface interactions. *Biomaterials* **2009,** *30* (9), 1827-1850.

12. Bittrich, E.; Burkert, S.; Muller, M.; Eichhorn, K. J.; Stamm, M.; Uhlmann, P., Temperature-sensitive swelling of poly(n-isopropylacrylamide) brushes with low molecular weight and grafting density. *Langmuir 28* (7), 3439-3448.

13. Akiyama, Y.; Kikuchi, A.; Yamato, M.; Okano, T., Ultrathin poly(n-isopropylacrylamide) grafted layer on polystyrene surfaces for cell adhesion/detachment control. *Langmuir* **2004,** *20* (13), 5506-5511.

14. Kawaguchi, H.; Fujimoto, K.; Mizuhara, Y., Hydrogel microspheres .3. Temperature-dependent adsorption of proteins on poly-n-isopropylacrylamide hydrogel microspheres. *Colloid and Polymer Science* **1992,** *270* (1), 53-57.

15. Xue, C. Y.; Choi, B. C.; Choi, S.; Braun, P. V.; Leckband, D. E., Protein adsorption modes determine reversible cell attachment on poly(n-isopropyl acrylamide) brushes. *Advanced Functional Materials 22* (11), 2394-2401.

16. Xue, C. Y.; Yonet-Tanyeri, N.; Brouette, N.; Sferrazza, M.; Braun, P. V.; Leckband, D. E., Protein adsorption on poly(n-isopropylacrylamide) brushes: Dependence on grafting density and chain collapse. *Langmuir 27* (14), 8810-8818.

17. Halperin, A.; Kroger, M., Collapse of thermoresponsive brushes and the tuning of protein adsorption. *Macromolecules 44* (17), 6986-7005.

18. Burkert, S.; Bittrich, E.; Kuntzsch, M.; Mueller, M.; Eichhorn, K.-J.; Bellmann, C.; Uhlmann, P.; Stamm, M., Protein resistance of pnipaam brushes: Application to switchable protein adsorption. *Langmuir 26* (3), 1786-1795.

19. Huber, D. L.; Manginell, R. P.; Samara, M. A.; Kim, B. I.; Bunker, B. C., Programmed adsorption and release of proteins in a microfluidic device. *Science* **2003,** *301* (5631), 352-354.

20. Takagi, R.; Murakami, D.; Kondo, M.; Ohki, T.; Sasaki, R.; Mizutani, M.; Yamato, M.; Nishida, K.; Namiki, H.; Yamamoto, M.; Okano, T., Fabrication of human oral mucosal epithelial cell sheets for treatment of esophageal ulceration by endoscopic submucosal dissection. *Gastrointestinal Endoscopy 72* (6), 1253-1259.

21. Takahashi, H.; Nakayama, M.; Yamato, M.; Okano, T., Controlled chain length and graft density of thermoresponsive polymer brushes for optimizing cell sheet harvest. *Biomacromolecules 11* (8), 1991-1999.

22. Tsuda, Y.; Kikuchi, A.; Yamato, M.; Nakao, A.; Sakurai, Y.; Umezu, M.; Okano, T., The use of patterned dual thermoresponsive surfaces for the collective recovery as co-cultured cell sheets. *Biomaterials* **2005,** *26* (14), 1885-1893.

23. Cooperstein, M. A.; Canavan, H. E., Biological cell detachment from poly(n-isopropyl acrylamide) and its applications. *Langmuir* **2010,** *26* (11), 7695-7707.

24. Alarcon, C. D. H.; Pennadam, S.; Alexander, C., Stimuli responsive polymers for biomedical applications. *Chemical Society Reviews* **2005,** *34* (3), 276-285.

25. Mizutani, A.; Nagase, K.; Kikuchi, A.; Kanazawa, H.; Akiyama, Y.; Kobayashi, J.; Annaka, M.; Okano, T., Thermo-responsive polymer brush-grafted porous polystyrene beads for all-aqueous chromatography. *Journal of Chromatography A 1217* (4), 522-529.

26. Hoy, O. Synthesis and characterisation of polymer brushes for controlled protein adsorption. Clemson University 2008.

27. Allison, A. C., *Structure and function of plasma proteins vol 1*. 1974; p VIII-316.

28. Toscano, A.; Santore, M. M., Fibrinogen adsorption on three silica-based surfaces: Conformation and kinetics. *Langmuir* **2006,** *22* (6), 2588-2597.

29. Johnson, K. L.; Kendall, K.; Roberts, A. D., Surface energy and contact of elastic solids. *Proceedings of the Royal Society of London Series a-Mathematical and Physical Sciences* **1971,** *324* (1558), 301-&.

30. Derjaguin, B. V.; Muller, V. M.; Toporov, Y. P., Effect of contact deformations on adhesion of particles. *Journal of Colloid and Interface Science* **1975,** *53* (2), 314-326.

31. Thoreson, E. J. From nanoscale to macroscale, using atomic force microscope to quantify the role of few-asperity contacts in adhesion. Worcester Polytechnic Institute, 2006.

32. Bhushan, B., Adhesion and stiction: Mechanisms, measurement techniques, and methods for reduction. *Journal of Vacuum Science & Technology B* **2003,** *21* (6), 2262-2296.

33. Cappella, B.; Dietler, G., Force-distance curves by atomic force microscopy. *Surface Science Reports* **1999,** *34* (1-3), 1-+.

34. Synytska, A.; Svetushkina, E.; Puretskiy, N.; Stoychev, G.; Berger, S.; Ionov, L.; Bellmann, C.; Eichhorn, K. J.; Stamm, M., Biocompatible polymeric materials with switchable adhesion properties. *Soft Matter* **2010,** *6* (23), 5907-5914.

35. Jones, R.; Pollock, H. M.; Cleaver, J. A. S.; Hodges, C. S., Adhesion forces between glass and silicon surfaces in air studied by afm: Effects of relative humidity, particle size, roughness, and surface treatment. *Langmuir* **2002,** *18* (21), 8045-8055.

36. Nalaskowski, J.; Drelich, J.; Hupka, J.; Miller, J. D., Adhesion between hydrocarbon particles and silica surfaces with different degrees of hydration as determined by the afm colloidal probe technique. *Langmuir* **2003,** *19* (13), 5311-5317.

37. Hertz, H., Über die berührung fester elastischer körper (on the contact of rigid elastic solids). *Miscellaneous Papers* **1896**, p 156 English Translation.

38. Kafi, A. A.; Magniez, K.; Fox, B. L., Measuring the adhesion force on natural fibre surface using scanning probe microscopy. *Journal of Adhesion Science and Technology* **2012,** *26* (1-3), 175-187.

39. Yim, H.; Kent, M. S.; Mendez, S.; Lopez, G. P.; Satija, S.; Seo, Y., Effects of grafting density and molecular weight on the temperature-dependent conformational change of poly(n-isopropylacrylamide) grafted chains in water. *Macromolecules* **2006,** *39* (9), 3420-3426.

40. Zhu, X.; Yan, C.; Winnik, F. M.; Leckband, D., End-grafted low-molecular-weight pnipam does not collapse above the lcst. *Langmuir* **2007,** *23* (1), 162-169.

CHAPTER 6:SYNTHESIS AND CHARACTERIZATION OF MIXED BRUSH FILM BY SINGLE STEP PROCESS

6.1:Introduction

Recent research towards development of stimuli responsive surfaces has progressed through the grafting of mixed polymer brushes.[1] The two most common approaches towards fabrication of such mixed polymer brush layers is using "grafting to" and "grafting from" methods. Utilizing the "grafting to" technique, mixed polymer brushes can be prepared by grafting of end-functionalized chains to a surface simultaneously or in subsequent steps.[1] Both fabrication techniques first require a surface activation step or attachment of anchoring layers. Minko et al. found that mixed brushes attached simultaneously using "grafting to", formed patchy and non-uniform layers.[1] Grafting of mixed polymer brushes via "grafting to' by subsequent steps was shown to garner more uniform brushes, however the process is more labor intensive.[2] Typically, scientists carried out such a process by grafting of first polymer, extraction of unbound chains, grafting of second layer, and finally removal of unbound polymer layers.

The "grafting from" approach is carried out firstly by attachment of initiator species on the substrate of interest. Mixed polymer brushes are fabricated by polymerization of the first monomer species followed by the subsequent initiation of the second monomer species. Brushes obtained by "grafting from" have been shown to have broader polydispersities than "grafting to".[3] Due to advances in polymerization technology, various techniques have been employed to build mixed brush films via "grafting from" such as; atom transfer radical polymerization (ATRP)[4], nitroxide

mediated radical polymerization[4], free radical polymerization[5], and reversible addition chain transfer polymerization (RAFT).[6] Wu et al. found that similar to "grafting to", mixed polymer brushes by "grafting from" produced "patchy" films if immiscible polymers were grafted.[7]

The grafting of mixed polymer brushes essentially creates nano-structured heterogeneous layers where each component has a unique role.[8] Mixed brush layers possess distinctive surface behavior in that morphology of the resulting films can be directly influenced by functionality of the polymer constituents and choice of solvent treatment.[8-9]. When a mutually good solvent for the system is used, both polymers are present at the surface and the resulting properties are affected by both segments. However, utilizing a selective solvent, one can specifically "bloom" the soluble polymer to the surface, while the resulting polymer in a "bad" solvent environment will pin to the surface of the substrate, effectively becoming screened from interaction. The resulting surface properties will be affected by the polymer "bloomed" to the surface.[9] A schematic demonstrating the effect of solvent treatment on mixed polymer brushes is displayed in **Figure 6.1**.

Mixed brushes containing PNIPAM are of high interest of late due to the transition of PNIPAM (hydrophilic to hydrophobic) occurring within physiological tolerable environments.[10] In addition poly ethylene glycol (PEG), has also garnered research interest due to the known protein and cell repellency of the layer, and high biocompatibility.[11-12] Therefore PEG has been heavily studied from a biomedical application standpoint.[13-14]

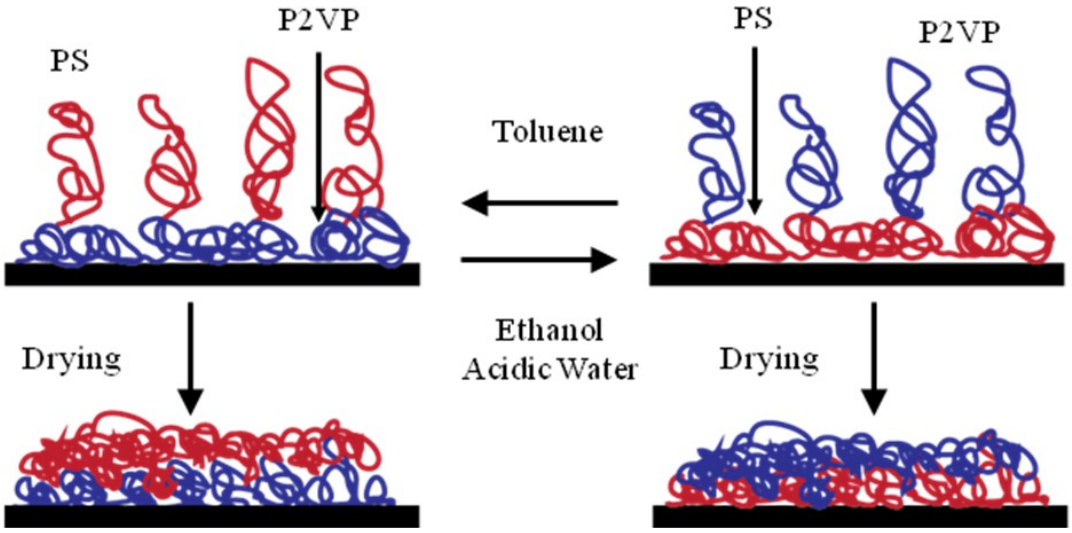

Figure 6.1: Schematic diagram illustrating the switching behavior of mixed polymer brushes after treatment with different solvents. The polymer chains collapse after drying. Redrawn from Stamm et al.[15]

The current work is the application of the single step brush (SSB) fabrication technique formed from reactive block copolymers (BCP), towards a next generation of mixed brush films. Mixed brush films were fabricated from two reactive block copolymers consisting of PEG-PGMA (PEG 1-3) and PNIPAM-PGMA. PEG was chosen as a secondary constituent due to possibilities to better control protein interaction (**Chapter 5)** by implementation of a matrix biocompatible polymer. Literature has shown PEGlyation of such responsive surfaces give rise to future possibilities as cell-culture carriers that can deliver biomacromolecules on-demand, such as growth factors.[16-17] As PNIPAM can effectively swell and collapse, attachment of biomolecules to the end of PNIPAM chains, can effectively create a scaffold for "delivery" or "hiding" the

fragments on demand, within a biocompatible matrix of PEG. Therefore, **Chapter 6** will lay the foundational work towards smart surfaces that can deliver active ligands on demand.

The generation of MB of PNIPAM-PEG was formed from two different block copolymers. PNIPAM-b-PGMA (**Chapter 4,** BCP-2) was combined within a mixed solution with PEG-b-PGMA (**Table 6.1,** PEG-3). Firstly, before SS MB of PNIPAM and PEG were grafted to model substrates, both constituent BCP were characterized individually (PNIPAM block segments, **Chapter 4, Chapter 5**). PEG1-3 surface properties and morphology where characterized by advancing and receding contact angle and AFM imaging. The swelling and collapse of the PEG layers were studied as a function of temperature by monitoring changes of thickness by *in-situ* ellipsometry.

MB films consisting of SSB-2 and PEG-3 were prepared at varying w/v ratios in MEK and subsequently dip-coated and annealed, forming films via the SS approach. The resulting thermally responsive properties of MB films were monitored in aqueous solutions at different temperatures by *in*-situ ellipsometry and contact angle measurements. The modified surfaces at varying w/v ratios of PNIPAM and PEG were also evaluated for their propensity for control over biological interaction. Work of adhesion values were measured for varying ratios of PNIPAM-PEG MBs films as a function of temperature by the AFM colloidal probe technique. Fibrinogen adsorption experiments were carried out as a function of temperature and resulting thickness changes were measured before and after protein adsorption in the dry state by ellipsometry.

Finally, for comparison, two step (TS) MB films of PNIPAM-PEG were fabricated. SSB-1 primary layers were fabricated as discussed in **Chapter 4**. Carboxy terminated PEG was grafted in a second step to the primary layers as a function of time at 100°C, therefore creating films with varying amounts of PEG. The changes in morphology and protein interaction were studied via AFM and fibrinogen adsorption experiments. The versatility of the approach was validated by the secondary grafting of low molecular PS instead of PEG, creating a hydrophobic matrix. The resulting films were studied via advancing and receding contact angle as a function of solvent pre-treatment, and AFM imaging.

6.2:Experimental

6.2.1:Synthesis of PEG-b-PGMA Block Copolymers at ORNL

The synthesis of the *PGMA-b*-PEG diblock copolymers was carried out as followed. PGMA *MacroCTA* reactions were formulated in a single-neck 100 mL Airfree® round bottom reaction flask equipped with a Teflon-coated magnetic stir bar. In a typical reaction, GMA (7.11 g, 5.00 x 10^{-2} mol) was combined with CPDT (245.71 mg, 7.11 x 10^{-4} mol; GMA: CPDT = 352), V-70 (43.85 mg; molar ratio of CPDT:V-70 = 5:1) and benzene (50.0 mL). The reaction vessel was capped with a rubber septum and the solution was sparged with dry argon for approximately 30 min. The reaction vessel was then placed in a heated oil bath thermostatted at 30°C and allowed to react for a predetermined time, after which the reaction vessel was immersed in liquid nitrogen to quench the polymerization.

PEO MacroCTA. PEO-monomethylether 4-Cyano-4-[(dodecylsulfanylthiocarbonyl)sulfanyl]pentanoic acid (PEO-CTA) was prepared according the procedure reported by Bottcher and coworkers.[18] PEO monomethyl ether (10.0 g, 2 mmol) in 200 g of toluene was dried by azeotropic distillation (65 mL of toluene was distilled off). After adding 4-Cyano-4-[(dodecylsulfanylthiocarbonyl)sulfanyl]pentanoic acid (4.04 g, 10 mmol) and p-toluenesulfonic acid (38 mg, 0.2 mmol), the mixture was refluxed for 2 days. Water was removed using a Soxhlet extractor with dry molecular sieves (3 A). The crude product was precipitated into diethyl ether (500 mL) and filtered. The PEO MacroCTA was redissolved into warm acetone and precipitated into hexane.

PEO-b-PGMA. Reactions were formulated in a single-neck 50 mL Airfree® round bottom reaction flask equipped with a Teflon-coated magnetic stir bar. In a typical reaction, GMA (2.84 g, 2.00×10^{-2} mol) was combined with the PEO macroCTA (511.85 mg, 9.48×10^{-5} mol; PGMA:PEO macroCTA = 211), V-70 (9.74 mg; molar ratio of PEO macroCTA:V-70 = 3:1) and benzene (20.0 mL). The reaction vessel was capped with a rubber septum and the solution was sparged with dry argon for approximately 30 min. The reaction vessel was then placed in a heated oil bath thermostatted at 30°C and allowed to react for a predetermined time, after which the reaction vessel was immersed in liquid nitrogen to quench the polymerization. The final product was washed with water to remove un-reacted PEO.

6.2.2:Grafting of Block Copolymer Layers

Silicon wafers were used as a model substrate for all films discussed in the **Chapter 3**. The study and characterization of PEG BCPs were grafted in the same manner as PNIPAM block. (**Chapter 4)**. Highly polished single-crystal silicon wafers (Semiconductor Processing Co.) were used as the model substrate (**Section 5.2)**. PEG block co-polymers (PEG 1-3) were dissolved in MEK (0.75% w/v) and thin films (30 ± 5nm) were deposited on the substrate by dip-coating (Mayer Feintechnik D-3400, speed 240 mm/min) and annealed at 130°C for 16 hours. To be consistent with all experiments, all samples were rinsed three times in fresh MEK for 30 minutes respectively.

Single-step mixed brushes of PEG-b-PGMA (PEG-3) and PNIPAM-b-PGMA (SSB-2) were grafted to silicon wafers as described above. A 0.75 w/v% solution of either 50/50 or 75/25 SSB-2:PEG-3 weight ratios in MEK were dip-coated onto clean silicon wafers. Dip-coated films were annealed under vacuum at 130°C for 16 hours. To be consistent with all prior experiments, grafted films were washed in fresh MEK 3 times for 10 minutes each.

Two-step mixed brushes were fabricated as followed. Poly(ethylene glycol) monomethyl ether with Mn of 5,000 g/mol was modified with succinyl anhydride (Aldrich) to give carboxy end functionalized PEG (PEG-COOH). The acylation was carried out by refluxing poly(ethylene glycol) monomethyl ether methacrylate with a 20 fold excess of succinyl anhydride in THF. PEG-COOH (latter in the text will be referred to as just PEG) was purified by multiple precipitations from THF into diethyl ether.

SSB-1 films were dipcoated from a roughly 0.75 w/v% solution onto clean silicon wafers. Diblock copolymer films were annealed under vacuum for 16 hours at 130°C and rinsed in fresh MEK for 10 minutes three times. Following, PEG polymer was deposited onto the surface of a clean glass slide at 100°C, and subsequently brought between vacuum and standard pressure to remove any air bubbles. Modified silicon wafers were then placed on the melted PEG powder and brought under vacuum until all air bubbles were removed between the two surfaces. The surfaces were annealed at 100°C for 12 hours to enable the PEG end groups to react with the un-reacted epoxy units from the PNIPAM block copolymer layer. Unbound PEG was removed with multiple rinsings in methanol.

Two-step mixed brushes containing polystyrene (PS, Mn 2,000 g/mol) were prepared in the same manner as PEG. Carboxy terminated PS was dip-coated onto SSB-1 layers from a 1% solution in MEK. Samples were annealed under vacuum at 120°C for 12 hours. Un-bound polystyrene was removed by rinsing in fresh aliquots of toluene for 30 min.

6.2.3:Characterization of Block Copolymer Layers

Dry grafted layer thickness was determined as discussed in **Section 3.3.3.1**. Advancing and receding contact angle data was performed as described in **Section 3.3.4.**

6.2.4:Protein interaction with Block Copolymer Layers

All adhesion measurements were carried out in accordance to experimental procedure as discussed in **Section 5.2.**[19-20] Additionally, all protein adsorption

experiments to PEG and mixed brush layers were carried out as mentioned in **Section 5.2** as well.

6.2.5:Equations used for Characterization of Brush Layers

To characterize the polymer layers, several parameters have been evaluated.[21] The surface coverage (adsorbed amount), Γ (mg/m^2), was calculated from the ellipsometry thickness of the layer h (nm) using **Equation (3.1)** The chain density, σ ($chain/nm^2$) was determined by **Equation (3.2)** The distance between grafting sites, D (nm), was calculated using the following **Equations (3.3)**: The radius of gyration for the macromolecules was estimated using **Equation (3.4)**: The end-to-end distance for PNIPAM and PGMA were calculated by **Equation (3.5).** C_∞ was calculated as 5.0 and 9.8 for PEG and PGMA respectively utilizing the Polymer Design Tools Software.

In order to determine the amount of water entering the films during swelling and collapse of the films determined by *in-situ* ellipsometry, Bruggemans effective medium approximation was applied according to **Equation.(4.1)** and **Equation (4.2)**[22]

In order to estimate the work of adhesion (Δγ) per unit contact area from the measured pull-off force values, the Johnson-Kendall-Roberts (JKR)[23] model was employed (**Equation (4.3)**.

6.3:Results and Discussion

6.3.1:Characterization of Second Component of Mixed Brush: PEG Block Copolymer

6.3.1.1:Synthesis of PEG-b-PGMA diblock copolymers

Poly ethylenglycol (PEG) containing diblock copolymers were synthesized by reversible-addition fragmentation chain transfer (RAFT) polymerization at Oak Ridge National Lab by Dr. Bradley Lokitz. Similar to PNIPAM block copolymers described in **Chapter 4**, a series of diblocks were synthesized bearing two chemically unique segments, PEG and poly(glycidyl methacrylate) (PGMA) with varying molecular weight values. A PEG macro chain transfer agent was synthesized and employed to build PGMA block segments with varying molecular weights. The diblock copolymers were fabricated in such a way to create three distinct block copolymers with varying ratios of degree of polymerization by holding the PEG block segment constant while varying the PGMA unit, similarly as PNIPAM in **Chapter 4.**

The targeted weights and degrees of polymerization were chosen in order to study the effects of increasing PGMA content on PEG SS homo brushes solution properties, and as a constituent as a second component of a mixed brush. The block copolymers (BCP) were characterized by GPC. Chromatography was utilized for estimation of the molecular weights of individual and entire block copolymer molecules. **Table 6.1** displays the molecular weight characteristics of the series of PEG block copolymers. PEG-1 was found to have a copolymer number average molecular weight of 11,580

g/mol. The molecular weight of the PEG block for all three block copolymers was held constant at 7,500 (degree of polymerization (N) 170). However, PEG-1 BCP was found to contain a PGMA segment with a number average molecular weight (Mn) of 4,080 g/mol resulting in a degree of polymerization ratio of PEG:PGMA of 6:1.

The molecular weight of PGMA was increased to 8,500 and 19,400 yielding degree of polymerization ratios of roughly 3:1 and ~1:1 for PEG-2 and PEG-3 respectively. The total copolymer number average molecular weight ranged from 11,580 to 26,900 for the series of PEG-PGMA diblock copolymers. Moreover, **Table 6.1** shows that the block copolymers exhibited low polydispersity, (<1.23). The PEG block copolymers here on out will be referred to by sample names given in **Table 6.1**

Table 6.1: Molecular weights and polydispersity of SSB PEG-b-PGMA diblock copolymers.

	Block Copolymer Mn	Mw	PDI	PEG Mn	Mw	PDI	PGMA Mw
PEG-1	11,580	13,200	1.14	7,500	8,200	1.08	5,000
PEG-2	16,000	19,600	1.18	7,500	8,200	1.08	11,400
PEG-3	26,900	33,200	1.23	7,500	8,200	1.08	25,000

6.3.1.2: **Fabrica*tion of Single Step PEG Brush Films***

The series of PEG BCPs were deposited onto silicon wafers substrates via dipcoating from ~0.75 w/v solution in MEK. All samples had film thicknesses of

approximately 25-35 nm in order to compare film properties. As described in **Chapter 4**, the surface modification arises from the epoxy groups located in each glycidyl methacrylate unit in the diblock copolymers. Our group has used PGMA as an anchoring layer and subsequent attachment of end-functionalized polymers.[24-28] The approach utilized by attachment of PGMA to a substrate of interest and the subsequent reaction of end-functionalized macromolecules is termed "grafting to".[29-31] Among the advantages of the "grafting to" technique, the attachment of highly characterized polymers and simplistic experimental procedure are attractive for future industrial high volume production. However, the self limiting nature of this approach has limited grafting densities and layer thicknesses of the resulting films after modification.[25-26] In **Chapter 4** we utilized the listed advantages and overcame the self-limiting nature of the film formation by creation of films with tunable thickness (30-250nm) and, therefore, controlling the resulting properties of the film. We aimed to achieve the same results utilizing PEG BCP system, and further, the creation of complex mix block copolymer systems all in a single step process.

MEK was chosen as a solvent for deposition of the PEG block copolymers in order to achieve complete solubility of the copolymer. **Figure 4.1a** displays the overall schematic of our single step (SS) BCP film generation technique. Block copolymers were annealed at 130°C for 16 hours and rinsed in fresh solvents with varying polarity to confirm that indeed PEG block copolymers bearing epoxy functionality could be attached to clean silicon wafers.

To substantiate the PEG 1-3 brush system are indeed polymer brush surfaces, the distance between grafting sites should be smaller than two radii of gyration.[32] Accordingly, the surface grafted PEG BCP surfaces can be assigned to the "brush" or "mushroom" regimes for the single-step (SS) process based on **Figure 6.2a**. The dashed line in **Figure 6.2a** corresponds to the approximate border point between the brush and mushroom regimes for the PEG BCP systems. The radius of gyration, end-to-end distance, and grafting density of the SS PEG brushes were calculated assuming an end-tethered nature of PEG to the PGMA scaffold. The effective radius of gyration for the SS PEG brush films was calculated as 3.25nm, yielding a 2Rg of approximately 6.5nm. Therefore, as exhibited in **Figure 6.2a**, the distance between grafting sites for all PEG BCP systems is less than two radii of gyration, yielding end-tethered molecules that when contacting solvent, are in the brush regime.

When taking the block copolymer as a single entity in a mutually good solvent, the incorporation of different molecular weights of PGMA alter the overall apparent radius of gyration. The apparent radii of gyration for the series of PEG BCP were found to be 4.7, 5.4, and 6.5 nm for PEG1-3 respectively. Therefore, when all block copolymers are normalized to 30nm thick films, we effectively create three surfaces with unique grafting densities. **Figure 6.2b** shows the apparent grafting density of the SS PEG films normalized to 30nm thick films as a function of PGMA molecular weight in the diblock copolymer. PEG-1 effective grafting density (PEG chains) at 30nm thick films was found to be 1.6 chains/nm^2 while, PEG-2 and -3 were calculated to be 1.2 and 0.7 chains/nm^2 respectively.

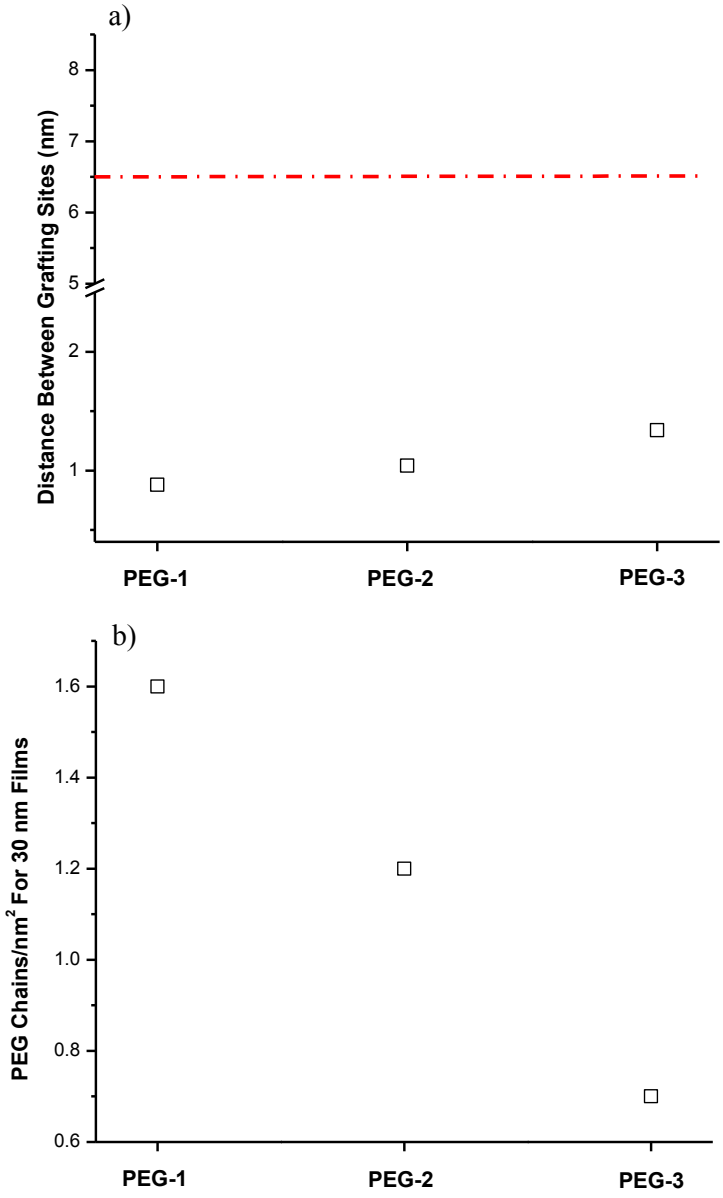

Figure 6.2: Parameters of PEG 1-3 SSBs a) Distance between grafting sites vs. PGMA block length. Dashed line corresponds to the border between the mushroom (above line) regime and brush (below) regime. b) Grafting density (chains/nm^2) for PEG SSB brush films normalized to 30nm films.

Thirty nanometer films were designated for reasons as described in **Chapter 4**, in order to study the brush behavior of "single" layer films of the SSB layers. We assume layer formation because AFM images did not reveal cylindrical or spherical formation (See **3.3.1.3**). Therefore we calculated the thickness of the lamellae size of each PEG and PGMA component of PEG 1-3 films depending on the molecular weights of the block substituents.[33] To do so, we used the **Equation(6.1):**

$$R = 1.4\alpha \bar{K} M^{1/2} \tag{6.1}$$

where $\bar{K}$ is the experimental constant relating the root mean square end-to-end distance to the molecular weight and is taken as 0.565 (poly (methyl methacrylate), R is the half thickness of the lamella, α values were taken as 1.25 since α varies between 1.0 and 1.5 for most polymers and M is the number average molecular weight.[33] **Table 6.2** displays the calculated values for the full thickness of the resulting lamellae structures found from PEG PGMA phase separation.

Table 6.2: Theoretical calculated thickness values for lamellae structures formed from BCP phase separation depending on molecular weight.

	PEG Lamellae Thickness (nm)	**PGMA Lamellae Thickness (nm)**	**Total Thickness (nm)**
PEG-1	17.1	12.6	29.8
PEG-2	17.1	18.2	35.4
PEG-3	17.1	27.5	44.7

As observed, with increasing PGMA molecular weight, the total lamellae formation for one complete layer ranges approximately from 30-45nm for PEG 1-3 respectively. If PEG layers were deposited at thickness above values listed in **Table 6.2**, multi-layer structures would start to form. Therefore, we can conclude that film thickness studied in this chapter (~30 nm) are not multi-layer structures, and more closely resemble a single layer system much like conventional polymer brush films.

6.3.1.3:Characterization of SS PEG Brush Layers

To investigate the effect of PGMA block length on film formation and morphology, AFM imaging (**Figure 6.3a-d**) was utilized to image the top most surface of the films. **Figure 6.3b-d** shows 1 x 1 μm images of PEG 1-3 films after annealing at 130°C for 16 hours. The block copolymer films all formed smooth and homogenous surfaces. The root mean square roughness, evaluated for each image was found to less than 1 nm for PEG films. Zdyrko et al. found 5,000 g/mol PEG grafted to PGMA films formed crystal formations as similarly seen here in **Figure 6.3b-c**.[34] However, as the PGMA block reached a molecular weight of 19,400 g/mol, (1:1 ratio of chemical repeat units) the crystal formation was not observed.

Interestingly, AFM images before annealing of PEG-1 gives way to large crystal formation. However, after annealing and rinsing, PEG-1 forms smooth and homogenous surfaces that indicate a large presence of PEG at the polymer air interface. PEG-2 and -3 (data not shown) looked identical pre- and post anneal, however PEG-2 displayed crystal like spherical domains similar to PEG-1 after annealing (**Figure 6.3b**).

In order to validate the presence of PEG at the interface, advancing and receding contact angle was carried at temperatures of 25° and 40°C. At the measurement temperatures, PEG copolymers are not expected to be temperature responsive. It has been shown that homo-PEG undergoes a volume phase transition in water at ~120°C.[35-36]

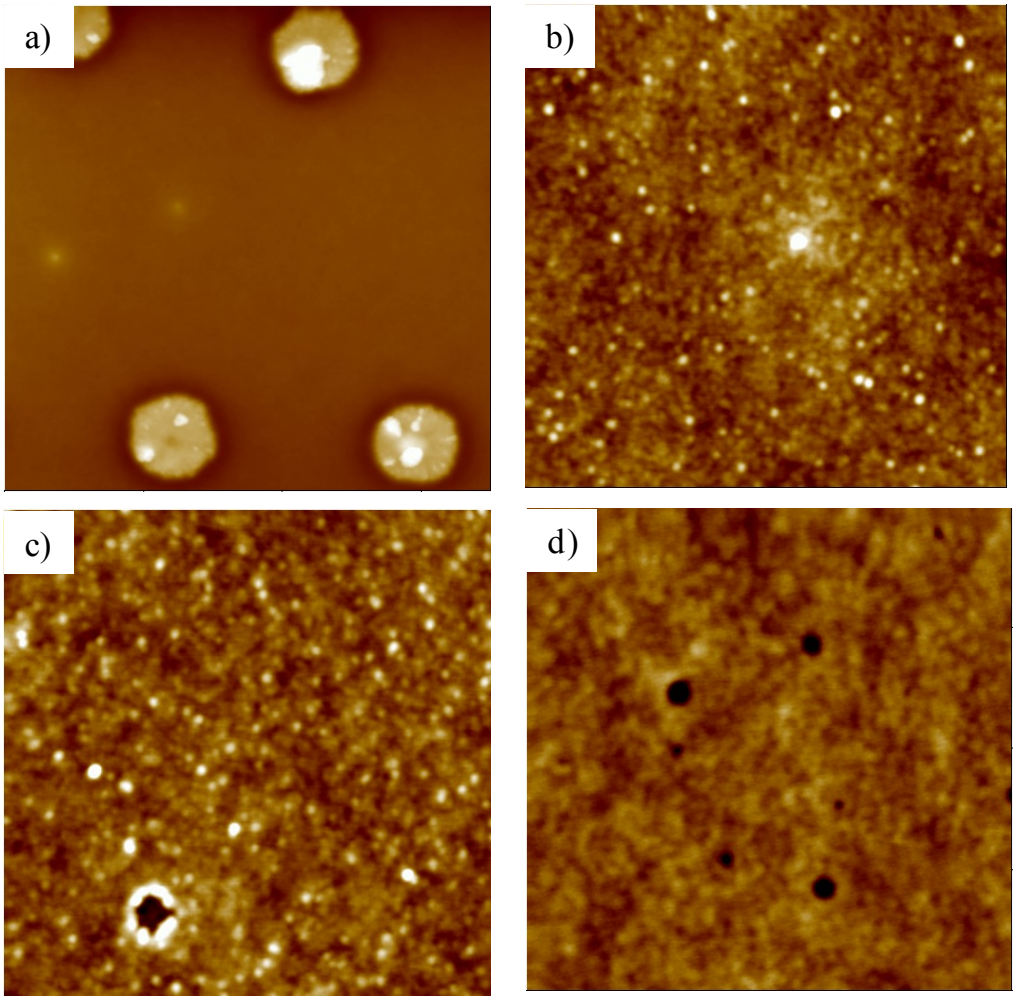

Figure 6.3: AFM topographical images (b-d: 1 x 1 µm, a: 7 x 7 µm) of grafted PEG SSB layers on silicon wafers, vertical scale for b-c: 7nm, a: 40nm a) PEG-1 pre anneal b) PEG-1 post anneal c) PEG-2 post anneal d) PEG-3 post anneal.

To this end, we analyzed the SS PEG BCP brush layers using advancing and receding contact angle measurements as a function of temperature. To carry out the measurements, the SS PEG films were placed inside the temperature controlled cell. Water was continuously pumped from the syringe that was placed close to the sample surface. When the volume of the drop increased and liquid spread, new surface was exposed (advancing). As the liquid was drawn back into the syringe, the liquid spread over previously wet surface (receding). Videos of the liquid delivery were cut at individual frames and analyzed for the advancing and receding angles.

Table 6.3: Advancing and receding contact angle of all PEG SSB generated films as a function of temperature after pre-water rinse. Two step PEG films and PGMA contact angles were also measured for comparison.

	23^{0}C		**40^{0}C**	
	Advancing	Receding	Advancing	Receding
PEG-1	52.9 ±1.9	29.3 ± 1.7	52.7 ± 2.0	31.3 ± 2.6
PEG-2	65.1 ± 1.7	41.1 ± 2.4	62.5 ± 2.4	41.7 ± 3.3
PEG-3	65.2 ± 2.5	35.2 ± 2.3	64.4 ± 2.2	33.1 ± 3.0
TSB (5K PEG)	33.2 ± 1.8	25.1 ± 2.1	35.2 ± 2.4	28.8 ± 3.1
PGMA Film	62.2 ± 3.4	45.0 ± 1.8	58.7 ± 1.3	42.2 ± 2.2

Table 6.3 displays the data for advancing and receding contact angles for the SS PEG films, as well as conventional PEG films (5000 g/mol end functionalized PEG grafted to PGMA films) and pure PGMA films as references. As displayed in **Table 6.3**

all films exhibited constant advancing and receding angles independent of measurement temperature. Since the SS PEG block copolymers are fabricated from PGMA and PEG components, pure PEG (Mn 5000 g/mol) and PGMA (Mn 176k g/mol) were analyzed. Pure PEG layers produced advancing contact angles of approximately 34° at 25 and 40°C. This is consistent with prior literature values.[24-25, 34] On the other hand, PGMA films yielded advancing contact angle values of approximately 61°, which is also consistent with prior literature values.[31, 37-38]

Furthermore, as seen from **Table 6.3,** PEG 1-3 yielded varying advancing and receding contact angles. PEG-1 displayed advancing (52°) and receding (30°) contact angles between both the PEG and PGMA reference samples. However, PEG-2 and -3 yielded advancing angles similar to pure PGMA angles (~62°). Although, PEG-2 and -3 receding angles were measured to be in between PEG/PGMA reference samples.

In order to estimate the fractional area of PEG at the three phase contact line of the water-air-polymer surface, we can treat the SS PEG BCP films as non-rough chemically inhomogeneous surfaces. Since we have nano structured surface of PEG and PGMA present, the surface is considered macroscopically uniform as compared to the droplet size used for contact angle measurements. Therefore, we can employ the Cassie relation as written as **Equation (6.2)**:[39]

$$\cos\theta_{CB} = f\cos\theta_{PEG} + (1-f)\cos\theta_{PGMA} \qquad (6.2)$$

where θ_{CB} is the Cassie apparent contact angle, f and $(1-f)$ are the fractional area of PEG and PGMA respectively, θ_{PEG} and θ_{PGMA} is the contact angle of pure PEG and PGMA references samples taken from **Table 6.3** respectively. **Figure 6.4** displays

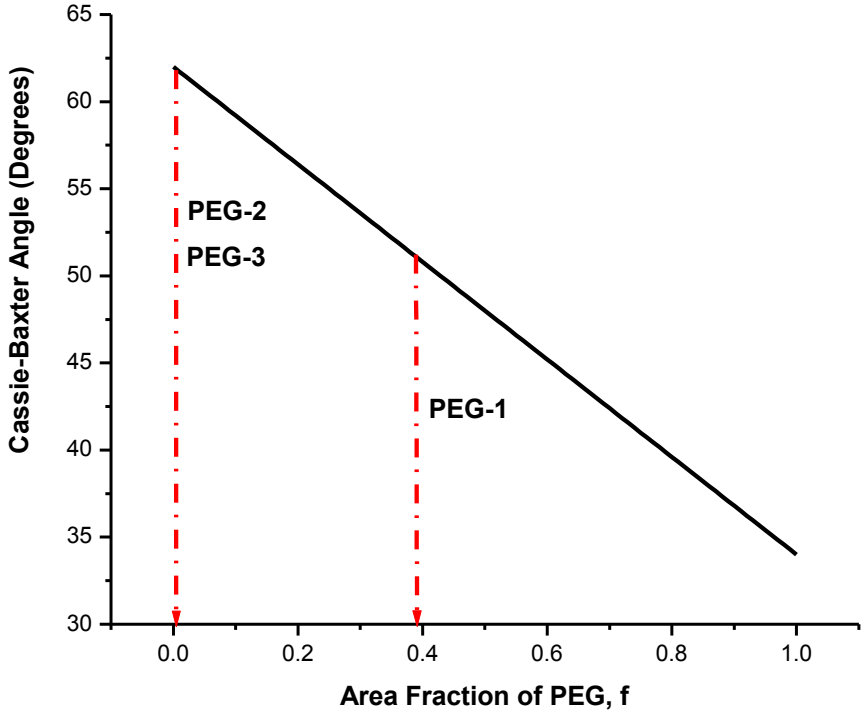

Figure 6.4: Apparent Cassie-angle vs. fractional area of PEG in the films.

the calculated Cassie apparent contact angle relationship (black line) as a function of fractional area of PEG. The red dashed tie lines indicate the calculated values for the amount of PEG for SS PEG 1-3 films as measured by advancing contact angle. Interestingly, PEG-1 was the only films to display a significant amount of PEG (~39%) at

the three phase contact line. PEG-2 and -3 all displayed values associated with 100% PGMA. However, further examination is needed to characterize the actuation behavior of the SS PEG BCP films completely in aqueous environment.

6.3.1.4:Actuation of SS PEG Brush Layers

To study the swelling and collapse behavior of SS PEG BCP grafted films, *in-situ* ellipsometry was employed to measure the layer thicknesses in aqueous environments at temperatures of 25 and 65°C. From the layer thickness, utilizing the Bruggerman Approximation relationships, we can estimate the extent of water intake of each SS PEG film as a function of temperature and PGMA block length. It is well known that pure PEG (Mn-5000 g/mol) exhibits LCST behavior around 120°C. However, the recent discovery that copolymers of oligo(ethylene glycol) methacrylate (OEGMA) which contain vinyl backbones and varying lengths of PEG side chains are also thermally responsive in the same manner as PNIPAM.[14, 40-43] The LCST of OEGMA based copolymers are extremely tunable (26-90°C°) depending on the OEGMA content.[40] Much like PNIPAM's amide groups, ethylene glycol groups can have various hydrogen bonding interactions with water at different temperatures.[14] The vinyl backbone of OEGMA gives ethylene glycol units a platform to collapse around. Therefore, we have designed a new type of material consisting of end-tethered PEG chains to a hydrophobic second block segment, rendering thermally responsive brushes in its own right.

Figure 6.5a-b displays the results from the SS PEG stretching experiments as a function of temperature. **Figure 6.5a** indicates that all SS PEG layers exhibit stretching

away from surface much like end-tethered macromolecules in the "brush" regime.[44] **Figure 6.5a** also indicates that PEG-1 and -2 exhibit thermally responsive behavior between the temperatures of 25 and 65°C. All samples were measured to be approximately 30nm in the dry state. PEG-1 showed the largest change in thickness values between the temperatures measured. At 25°C, the measured thickness determined to be roughly 90nm, and when temperature was raised to 65°C, the layer collapsed to roughly 60nm, similarly to SSB-1 values determined in **Chapter 4**. As PGMA block molecular weight was increased from 4,080 to 8,500 g/mol, a decrease in the magnitude of swelling and collapse was observed as function of temperature. PEG-2 swollen layer thickness was measured to be roughly 82nm and 62nm at 25 and 65°C respectively, a 20% decrease in swelling at low temperatures. PEG-3 exhibited strong extension in aqueous conditions (78 and 69nm at 25 and 65°C), however lower thermally responsiveness was noticed. The high swelling ratios of SS PEG films indicate that significant PEG units are free and mobile at the polymer interface, validated by PGMA low swelling (5%) in water.[45] In fact, the maximum stretching (assuming polymer chain is stretched to 180° bond angle) for PEG chains with number average molecular weight and degree of polymerization 7,500 g/mol and 170, was found to be 75 nm. This was calculated assuming the C-C and C-O bond length to be 0.154 and 0.143nm respectively multiplied by the appropriate number of bonds and bond type in the backbone of the polymer. Therefore, in the swollen state PEG-1 effectively extended to 83% of the maximum value. PEG-2 and 3 extended to 70 and 63% respectively.

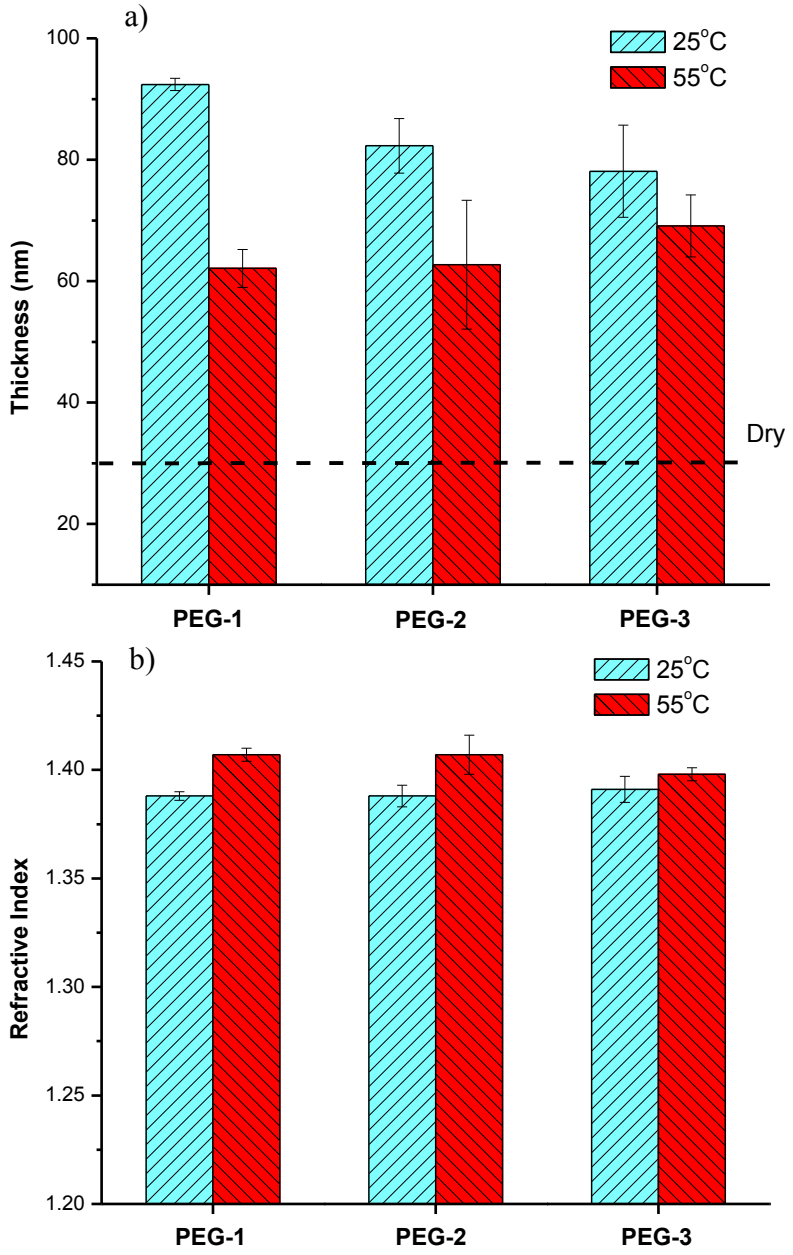

Figure 6.5: Swelling and refractive index results of block copolymer grafted layers using in-situ ellipsometry swelling techniques in an aqueous environment. a) Swelling and collapse for PEG SSB grafted films at 25 and 65^{0}C water b) Refractive index change.

In fact, a linear relationship was found between apparent grafting density of the SS PEG brush films and changes in thickness between the swollen and collapsed states. **Figure 6.6** displays the change in thickness vs. effective grafting density of the SS PEG films. The change in thickness was taken as swollen thickness in 25°C water conditions minus collapse thickness at 65°C, as measured by in-situ ellipsometry measurements. It is apparent that with increasing the effective grafting density, the overall magnitude of swelling change increases. Stronger extension occurs when the interaction energy

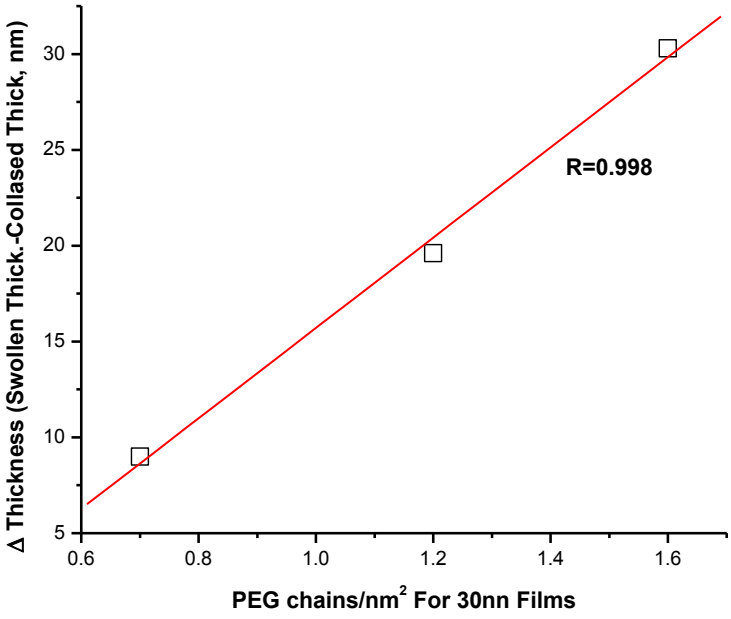

Figure 6.6: Dependence of actuation behavior on effective grafting density of SS PEG brush films. Actuation behavior is displayed as swollen thickness minus collapse thickness as measured by *in-situ* ellipsometry.

between PEG chains increases and thus stretching increases due to effectively decreasing the tethering distances between neighboring chains.

This is contrast to amount of PEG determined at the polymer liquid interface by Cassie relationship. We attribute this to the long equilibration time of the modified wafer surface in the liquid ellipsometer cell. Samples were equilibrated in the temperature controlled water for 15 minutes prior to measurements giving the macromolecules time to reorient within the films, whereas contact angle samples were equilibrated in air at the desired temperature. Macromolecules in the dry state are collapsed on each other when in the amorphous state. Therefore, PEG molecules buried under the top most layer of the surface would not have time to reorient during contact angle measurements.

Estimations of the volume fraction of water content in the swollen SS PEG films were conducted using **Equation (4.2)**, taking the average values of film thicknesses from **Figure 6.5a**. PEG-1 contained 69.8 and 55.1% of water in the film at 25 and 65°C respectively. When increasing the size of the PGMA block, the volume fraction of water contained in the PEG-2 film at 25°C decreased to 67.4%, while the water content in the collapsed film was constant at 57.3% to that of PEG-1. As discussed above, PEG-3 showed low temperature responsiveness at the measurement temperatures, and this is reflected by a relatively constant water content of 64.3 and 59.6% at 25 and 65°C respectively.

In further analysis, we can utilize *in-situ* ellipsometric swelling experiments to determine the SS brush behavior in comparison to predicted brush behavior in a

thermodynamically good solvent, in our case, cold water. We compared the swelling thickness ratio from measured ellipsometric values normalized by initial thickness of the PEG content and compared to predicted swelling ratios by self consistent field theory (SCF)[46], as was done in **Chapter 4.** Utilizing **Equation (6.3),** we can estimate the swollen thickness h_{sw}^{*}, from dry film measurements via ellipsometry experiments and degree of polymerization found from GPC measurements. [47]

$$N = \left[1.074\left(h_{sw}^{*}\right)^{3/2}\right] \Big/ \left[h_{dry}\right]^{1/2} \tag{6.3}$$

As was done in **Chapter 4,** the ellipsometric data was fit using a step-like segment density profile termed a "box like" model, however, the h_{sw}^{*} can be found from the "box like" fits by using the relationship $h_{sw}^{*} = (4/3)\bullet$, implementing the results of the SCF model. **Equation 6.3** was developed for polystyrene chains. The Kuhn segment is assumed close to 6.7Å.

Figure 6.7a-b displays the measured and predicted swollen layer thickness vs. PGMA block length (**Figure 6.7a**), and swelling ratio as a function of grafting density (**Figure 6.7b**). As observed in **Figure 6.7a**, as PGMA block length is increased, the overall swollen thickness values decrease for both measured and predicted values for 30nm layers. All SCF predicted values show similar trends to experimental values and are within roughly 25% error, suggesting that the PEG layers act as ideal swollen brushes as predicted by SCF theory. **Figure 6.7b** displays the apparent swelling ratio, which was found by swollen thickness normalized by the dry layer thickness of the PEG fraction vs.

the calculated grafting density. As observed, with decreasing grafting density, the overall swelling ratio increases for both predicted and experimental values. The same trends were found with PNIPAM block in **Chapter 4**. As grafting density increases, chain stretching increases, and upon entrance of a good solvent, polymer chains are already stretched significantly and a decrease in overall swelling ratio is observed. Again, predicted and experimental values exhibit the same trends, and data is within roughly 28%, suggesting predictable polymer brush behavior. As discussed in **Chapter 4**, the SCF model accounts for polymer brushes exhibiting weak excluded-volume interactions and ideal grafted brushes from the surface. However, like PNIPAM, PEG experiences hydrogen bonding with water molecules. Hydrogen bonding is not accounted for and is likely a large reason the deviation from SCF is seen. Additionally, the model does not account for the inclusion of PGMA within the layer.

In conclusion, smooth homogenous PEG based films were successfully grafted in a single step fashion from reactive/responsive block copolymers. Cassie relationship estimated that PEG-1 contained 39% of PEG units at the polymer-liquid-air boundary, however PEG-2 and -3 was estimated to be 100% PGMA. However, at long equilibration times in aqueous environments, SS PEG proved to be highly thermally responsive when PGMA block segment molecular weight was <8,500 g/mol. The successful grafting of PEG based block copolymers render the macromolecules promising constituents for single step grafting of mixed brush films.

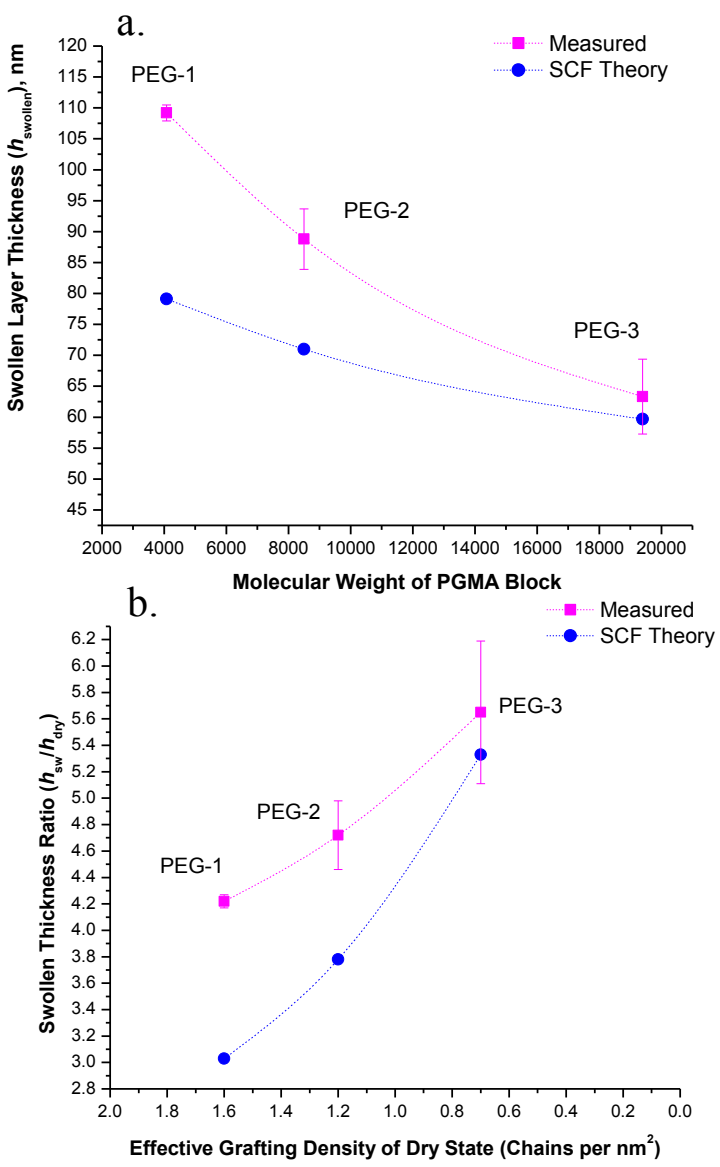

Figure 6.7: a) Swollen thickness ratios normalized by initial PEG composition of dry 30 nm films vs effective grafting density calculated from dry state. PEG content was calculated by weight fraction percent of BCP. Square values are determined swelling ratios as measured by *in-situ* ellipsometric values, and closed blue circles are the theoretical predicted swelling ratios normalized by initial dry layer fraction of PEG.

6.3.2:Characterization of Single Step Synthesis of Mixed Brush

Employing the same strategy as discussed in **Chapter 4**, **Section 4.3.3.1**, we can create more complex systems via the single step process. Furthermore, a mixed brush (MB) system containing PNIPAM and PEG was created by mixing the SSB-2 BCP and PEG-3 BCPs in a known weight/volume ratio in MEK. By designation of specific weight/volume ratio solutions we can effectively control the composition of the resulting mix brush film. An overall schematic of the mix brush technique is displayed in the upper half of **Figure 6.8**.

Advancing and receding contact angles and *in-situ* ellipsometry were conducted on films deposited from a 50/50 w/v % solution in MEK. **Table 6.4** displays advancing

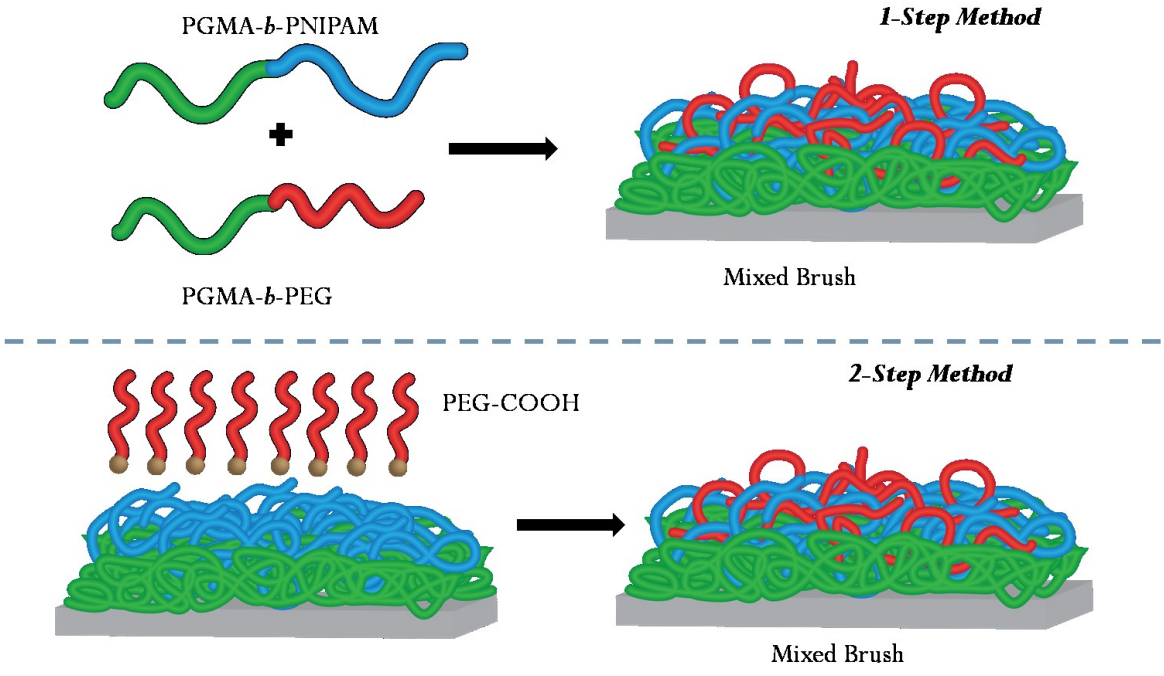

Figure 6.8: Single Step and two step fabrication method for PNIPAM-PEG mixed brush films.

Table 6.4: Advancing and receding contact angle of 50/50 PNIPAM-PEG MB by SS method.

	22°C		43°C	
	Advancing	Receding	Advancing	Receding
Mixed Brush CA	69.9 ± 1.4	34.6 ± 3.0	77.0 ± 2.6	31.2 ± 3.2

and receding contact angles of 50/50 MB films deposited via SS methods as a function of temperature. At 22°C the mixed brush exhibits an advancing contact angle of roughly 70°, while at 43°C an increase to 77° was observed. Indeed, MBs of PNIPAM-PEG at 50/50 deposition ratio produces thermally responsive wettability properties similar as seen for the PNIPAM TSB (**Figure 4.1b)** films from **Chapter 4**.

However, differences were observed when measuring the level of brush swelling and collapsing via *in-situ* ellipsometry. **Figure 6.9a-b** reveals the extent of switchability via thickness and refractive index measurements as a function of three different temperatures. As seen in **Figure 6.9a**, the 50/50 MB films exhibit relatively decreased switchability as compared to pure PNIPAM SSB-2 films. At 25°C, 50/50 MB films swelled from a dry layer measured 30nm to a thickness of approximately 89nm. At temperatures above the LCST of PNIPAM (44°C), a median collapsed thickness of 84nm was measured. Furthermore, at 65°C, a final collapsing thickness of 82nm was determined, roughly a total of only 8% collapse in layer thickness. As previously calculated, utilizing Bruggemans approximation allows us to determine the extent of water contained in the mix brush films as a function of temperature. At 25°C it was

determined that the swollen film contained 68.4% of water. At temperatures of 44 and 65°C, the water content was found to be 66.5 and 65.7% respectively.

While contact angle data suggests that PNIPAM renders surface energy changes as a function of temperature, it is noticed via ellipsometry thickness and refractive index (**Figure 6.9a-b**) measurements that the swelling and collapse of PNIPAM-PEG MB 50/50 films experience a decrease in actuation behavior. We suggest the observed behavior is due to specific hydrogen bonding interactions between PEG and water which interfere with PNIPAM interaction with water and itself. It has been shown that PEG effectively repels hydrophobically driven protein adsorption due to a protective hydration shell due to PEG-water hydrogen bonding.[11, 48-49] Virtenan et al. found that solution behavior of graft copolymers of PEG and PNIPAM was determined by the competition of PNIPAM hydrophobic interactions and solubilizing effect of PEG at the temperatures measured.[11] Therefore for our SS MB films, as PNIPAM collapses, we suggest soluble PEG chains extend outward and sustain solubility, decreasing the extent of total collapse of the layer. To further characterize the surface characteristics of the PNIPAM-PEG films, the SS MB films were studied in terms of biological interaction and compared with their two-step MB counterparts.

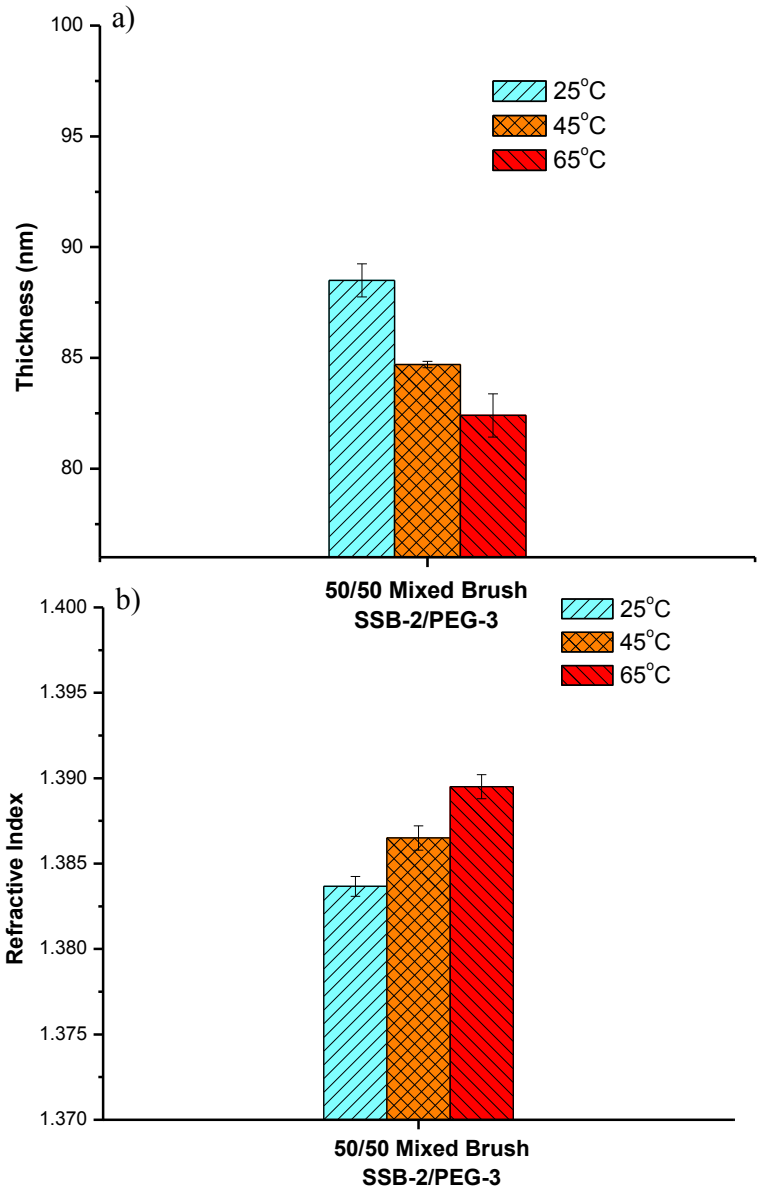

Figure 6.9: Swelling and refractive index results of 50/50 PNIPAM-PEG mixed brush grafted layers in SS method using in-situ ellipsometry swelling techniques in an aqueous environment. a) Swelling and collapse for PNIPAM-PEG SSB grafted films at 25 and 65^{0}C water. b) Refractive index change.

6.3.3: Protein Interaction of Single Step Mixed Brush

To study the effect of varying amounts of PEG in MB films with PNIPAM and the resulting effects on biological interaction, AFM colloidal probe, fibrinogen adsorption, and AFM imaging techniques were utilized. It is well known that PEG films provide non-specific protein interaction resistance in biological environments.[11, 48] PEG is also a highly desirable material for biological devices due to its low toxicity and nonimmunogenic properties.[14, 48] Interestingly, Gan et al. found that copolymer crosslinked microgels composed of PNIPAM and PEG reduced bovine serum albumin (BSA) adsorption to particles even at temperatures above the LCST of PNIPAM.[48] Further, even when the PEG is "buried" within the particle core, BSA adsorption was suppressed at temperatures above the LCST of PNIPAM.

Firstly, AFM colloidal probe technique involving a fibrinogen modified bead (**Figure 5.2**) and JKR relationship was utilized to determine the work of adhesion values for SS PNIPAM-PEG MB in ratios of 75/25 (PNIPAM-PEG) and 50/50 w/v deposition ratios. Values were compared to their single BCP substituent's (SSB-2 and PEG-3). **Figure 6.10** displays work of adhesion values (mJ/m^2) for MB and BCP constituents as a function of temperature. As measured in **Chapter 5**, SSB-2 brushes show distinct work of adhesion value changes as function of temperature.

6.3.3.1:Protein-Brush Interaction by AFM Colloidal Probe Technique

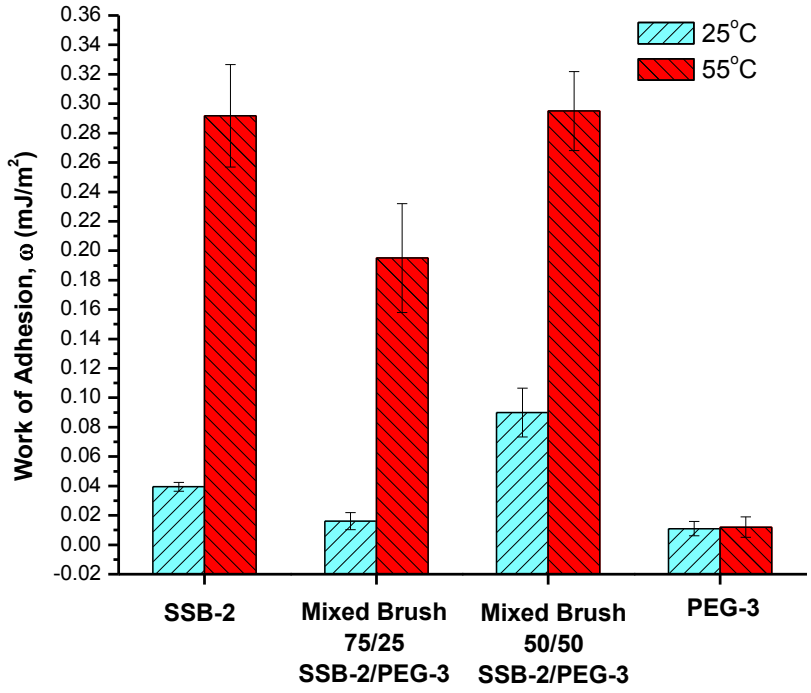

Figure 6.10: Work of adhesion measured by AFM colloidal probe technique for SS PNIPAM-PEG mixed brushes.

At 25°C, protein repelling surface adhesion value of 0.04 mJ/m^2 was measured, while at 55°C an increase to approximately 0.29 mJ/m^2 was seen. PEG-3 films, which showed non-thermally responsive properties via contact angle and *in*-situ ellipsometry, exhibited constant protein repelling films at both temperatures measured, 0.01 mJ/m^2.

Interestingly, PNIPAM-PEG MB films in 75/25 w/v deposition ratios, an overall decrease in work of adhesion values for polymer-fibrinogen were found. At 25°C,

complete protein repelling (0.01 mJ/m^2) properties were observed, while a large increase (0.19 mJ/m^2) was noticed at 55°C, however both values being less than pure SSB-2 films. This is indicative of the hydrophilic effect of the addition of PEG. As temperature is increased and PNIPAM collapses, the PEG remains solubilized and extended in solution, decreasing the work of adhesion at 55°C as compared to SSB-2 films. However, enough PNIPAM is present in the film to retain large changes in overall work of adhesion as a function of temperature.

Increasing the amount of PEG-3 in the deposition solution of PNIPAM-PEG MB films (50/50 w/v ratio) create thermally switchable and less protein repellent surfaces in terms of work of adhesion. At 25°C, the work of adhesion value increased as compared to the 75/25 MB films to 0.08 mJ/m^2. At 55°C, the work of adhesion also increased (0.30 mJ/m^2) in comparison to 75/25 MB films as well. This is counter intuitive to fact that adding additional PEG to the film yields surfaces that overall, have increase in work of adhesion values as compared to 75/25 deposited MB films. However, when adding additional PEG-3 to the deposition solution, we are also adding a significant amount of PGMA (19,400 g/mol block segment) in the film. At high water contents of the film (>55%) the large probe can penetrate the softened film and experience the synergistic effect of PGMA within the film.

6.3.3.2:Protein-Brush Interaction by Fibrinogen Adsorption

To further validate and study the effect of PEG in PNIPAM-PEG MB films, adsorption of fibrinogen (**Figure 6.11**) to modified wafers was studied. The adsorption

of fibrinogen was carried out through the introduction of grafted silicon wafers into an agitated solution of 1mg/mL fibrinogen in 0.01M phosphate buffered saline (PBS) as a function of temperature.

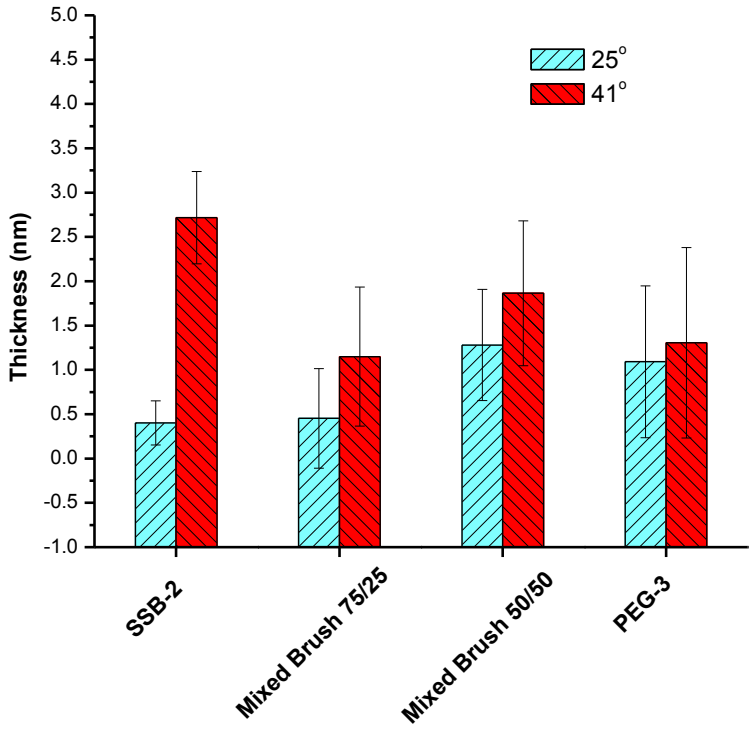

Figure 6.11: Protein adsorption to SS PNIPAM-PEG mixed brush films.

The amount of adsorbed protein was characterized by measuring the dry layer thickness before and after protein adsorption in the dry state. The polymer and protein-polymer layer was measured with a set refractive index 1.5. The single BCP constituents were also measured as reference values.

As reported in **Chapter 5**, SSB-2 films showed protein adsorption switchability. At 25°C, thickness increase was measured as less than 0.5nm, while a roughly 2.7nm increase in thickness after adsorption at 41°C was found. PEG-3 films exhibited protein repelling properties, however slightly increased values as compared to pure PEG brush layers in literature.[34] Zydrko et al. showed that 5000 g/mol molecular weight PEG grafted to PGMA via the traditional "grafting to" approach showed protein adsorption thickness increases of 0.2-1nm with decreasing grafting density of PEG.[34] PEG-3 films in our case showed thickness level increases of roughly 1nm, similar to PEG films fabricated by "grafting to" methods with grafting densities ≤ 0.5 chains/nm[234]. Apparent grafting density for 30nm films of PEG-3 was calculated to be approximately 0.7 chains/nm^2.

75/25 and 50/50 PNIPAM-PEG MB films were measured for change of thickness values after protein adsorption as well. Overall, 75/25 MB showed more protein repelling properties than 50/50, however both surfaces were within each other's error limits. Both films approximated values close to that of pure PEG-3. MB 50/50 showed slightly higher protein adsorption capabilities at the upper error limitations measured. In general though, films with PEG both decreased the overall protein adsorption, and decreased the switchability of the single step mixed brush films composed of reactive-responsive block copolymers. The introduction of PEG into the film increases the overall hydrophillicity of the resulting film towards protein adsorption events.

To further elucidate the effect of PEG in PNIPAM MB films, AFM imaging was utilized to image the top most surface of the PNIPAM-PEG MB films before and after protein adsorption. **Figure 6.12a-c** displays 1 x 1 μm images of 75/25 PNIPAM-PEG films before (**Figure 6.12a**) and after protein adsorption at temperatures of 25°C (**Figure 6.12b**) and 41°C (**Figure 6.12c**). As observed in **Figure 6.12a**, before protein adsorption, 75/25 MB films exhibit the absence of the 3-nodal fibrinogen structure on the film surface. However, at temperatures of 25°C, very sparse adsorption is seen as highlighted by the dashed red circle. At temperatures of 41°C, sparse adsorption is also noticed, resulting in films with protein adsorption that is repellent at both temperatures measured, validating dry layer ellipsometry measurements. Indeed, the introduction of PEG causes an overall increase in hydrophillicity and protein repelling properties independent of temperature.

Comparatively, 50/50 PNIPAM-PEG MB films were imaged via AFM in tapping mode. **Figure 6.13a-c** shows 1 x 1 μm films before and after fibrinogen adsorption as a function of temperature. As seen in **Figure 6.13a**, no nodular protein structures are found prior to adsorption. However, at temperatures of 25°C (**Figure 6.13b**), sparse adsorption is noticed as highlighted by the red dashed circles. Interestingly, at 41°C (**Figure 6.13c**), an

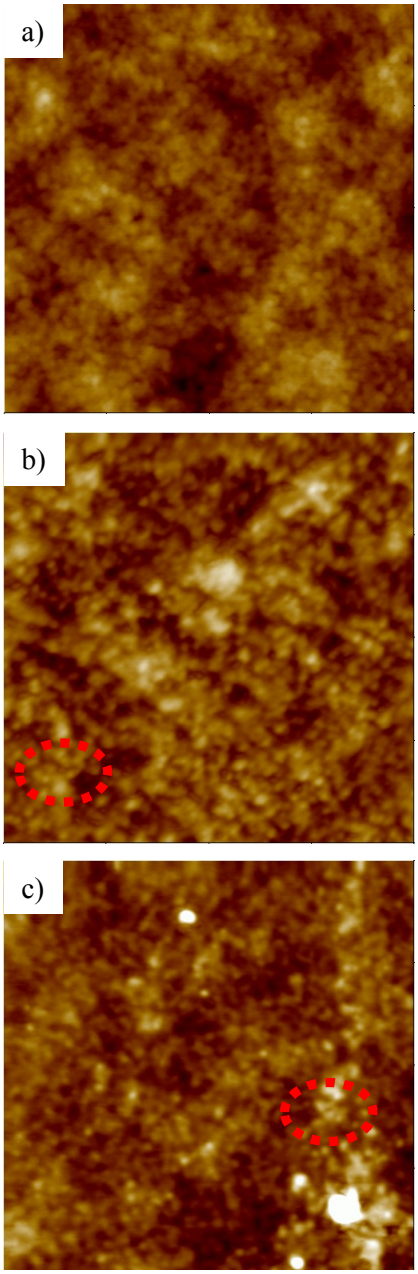

Figure 6.12: AFM topography images (1 x 1 um) of 75/25 SS PNIPAM-PEG mixed brushes. a) 75/25 MB before protein adsorption b) after protein adsorption at 25°C c) after protein adsorption at 41°C.

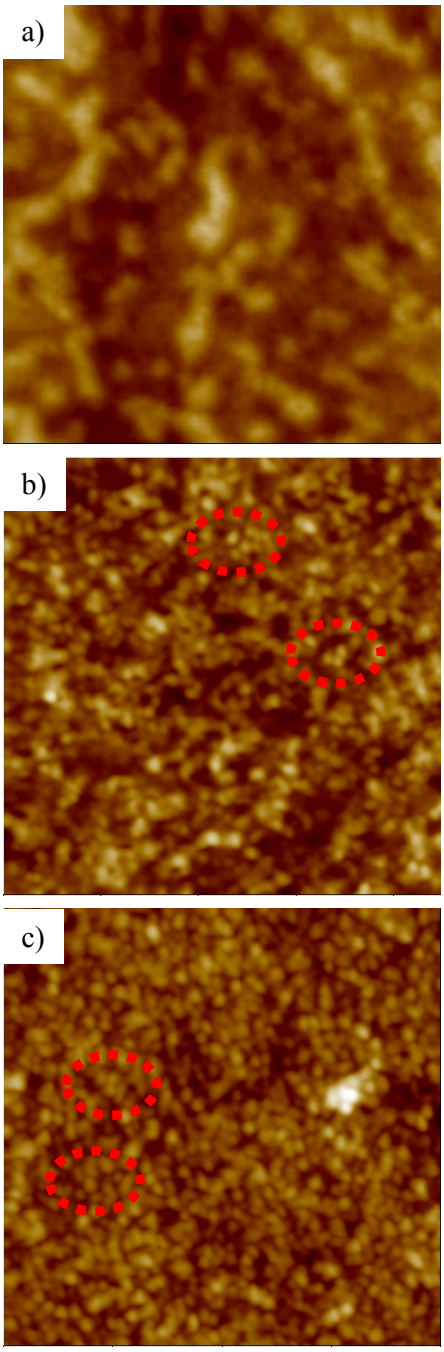

Figure 6.13: AFM topography images (1 x 1 um) of 50/50 SS PNIPAM-PEG mixed brushes. a) 50/50 MB before protein adsorption b) after protein adsorption at 25°C c) after protein adsorption at 41°C.

increase in the amount of globular structures is noticed on the top most surface of the MB films, which can indicate an increase in the amount of protein adsorption; however both ratios of PEG in the MB films display relatively sparse adsorption independent of temperature, and a general loss of films that effectively turn protein adsorption on and off.

6.3.4:Comparison to Mix Brush by Two Step Method: Versatility and Evaluation of Towards Biological Control

6.3.4.1:Fabrication of Mixed Brush Films by Two-Step Method

The adaptability of the SS brush formation from reactive responsive block copolymers provides straightforward routes to create mix brush in a two-step (TS) method as well. After deposition and annealing of PNIPAM-b-PGMA (SSB) films, un-reacted epoxy groups remain available for further reaction with macromolecules end functionalized with complimentary functional groups. Therefore, we can create a wide variety of MB systems in a TS manner. Herein, we utilized carboxy terminated PEG (Mn 5000 g/mol) for post grafting to SSB-1 films deposited as discussed in **Chapter 4** as a comparison to SS PNIPAM-PEG MB systems. The amount of PEG grafted to the SSB-1 films was varied as a function of grafting time. To validate the universal nature of the approach, a hydrophobic second component, namely carboxy terminated polystyrene (PS, Mn-2000) was in turn grafted to the SSB-1 films. The resulting films were characterized via AFM imaging, contact angle, measurements, and evaluated for biological interaction as a function of temperature in the subsequent section (**3.3.5**).

Firstly, carboxy terminated PEG was grafted to SSB-1 films from the melt, as a function of time at 100°C. The overall schematic of the TS fabrication technique is pictured in the lower half of **Figure 6.8**. Subsequent films were rinsed in methanol to remove un-bound PEG chains from the surface of the modified wafers. **Figure 6.14** displays the thickness increase to the SSB-1 films after grafting of PEG at the designated time intervals. **Figure 6.14** shows the amount of PEG grafted to the SSB-1 films increases with grafting time.

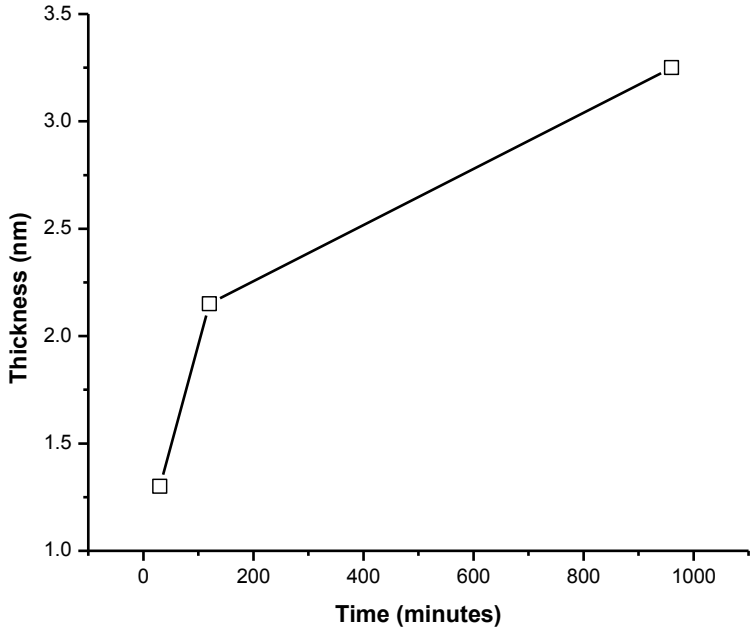

Figure 6.14: Grafting of PEG to SSB-1 layers vs. time. Layers were grafted at 100°C.

After 30 min of grafting, approximately 1.3nm increase of film thickness was noticed. Upon increasing the grafting time to 960 min, an average thickness increase of

3.2 nm was measured. A maximum of 3.2nm increase in film thickness was noticed, indicating that after grafting of SSB-1 films for 16 hours at 130°C, much of the free epoxy units noticed for pure PGMA films were indeed reacted. However, we can create films with small variations in PEG thickness grafted in a second step.

6.3.4.2:Characterization and Biological Interaction of Mixed Brush Films by Two-Step Method

6.3.4.2.1: Grafting of Two-step Mixed Brush Films

To validate grafting of PEG in a TS manner, AFM imaging via tapping mode (**Figure 6.15**) was conducted on 30, 120 and 960 min PEG grafting films. As observed in **Figure 6.15a**, smooth homogenous layers are still apparent, practically identical to pure SSB-1 films (**Figure 4.4**). However, upon grafting PEG for 120 min, the onset of globular PEG crystal domains is apparent. This is indicative of PEG brushes in low grafting density[34], creating isolated domains of PEG. We associate the isolated domains with PEG crystals being formed by a fraction of the grafted macromolecules due to the low surface coverage and resulting low grafting density of the films.[13] At grafting times of 960 min, **Figure 6.15c**, it is apparent that the size and surface concentration of PEG crystals increased with the extent of grafting. Zdyrko et al. found similar results for PEG grafted films.[34] Scientists found similar surface concentration of isolated domains for surface coverage from 1.59-3.64 mg/m^2. However, as the grafting density and surface coverage increased, the disappearance of isolated domains was observed, and the resulting development of larger crystals covering 15-50% of the sample surface.

6.3.4.2.2: Protein Adsorption to Two-step Mixed Brush Films

Figure 6.16 displays fibrinogen adsorption experiments for TS PNIPAM-PEG MB surfaces grafted at 30, 120, and 960 min to pre prepared SSB-1 films. SSB-1 protein measurements and PEG-3 films are included as references. As discussed previously, SSB-1 produces highly switchable protein surfaces as function of temperature.

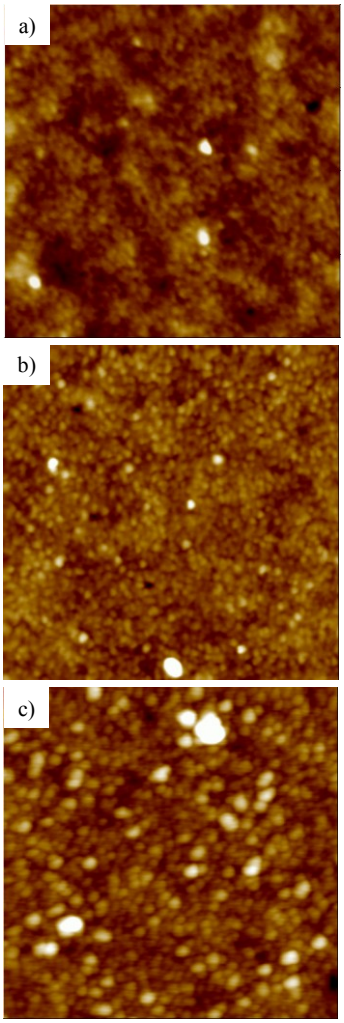

Figure 6.15: AFM topography images (1 x 1 um) of TS MB PNIPAM-PEG grafted layers. a) PEG grafted for 30 min b) 120min c) 960min. Vertical scale; a) 8nm b) 10nm c) 13nm.

At 25°C, SSB-1 film thickness increase after fibrinogen adsorption exhibits almost no increase in thickness, indicative of highly protein repelling surfaces. At 41°C, SSB-1 film thickness increases were measured at nearly 4nm. PEG-3 brushes on the other hand, display constant thickness increase after protein adsorption (~1-1.2nm) independent of temperature.

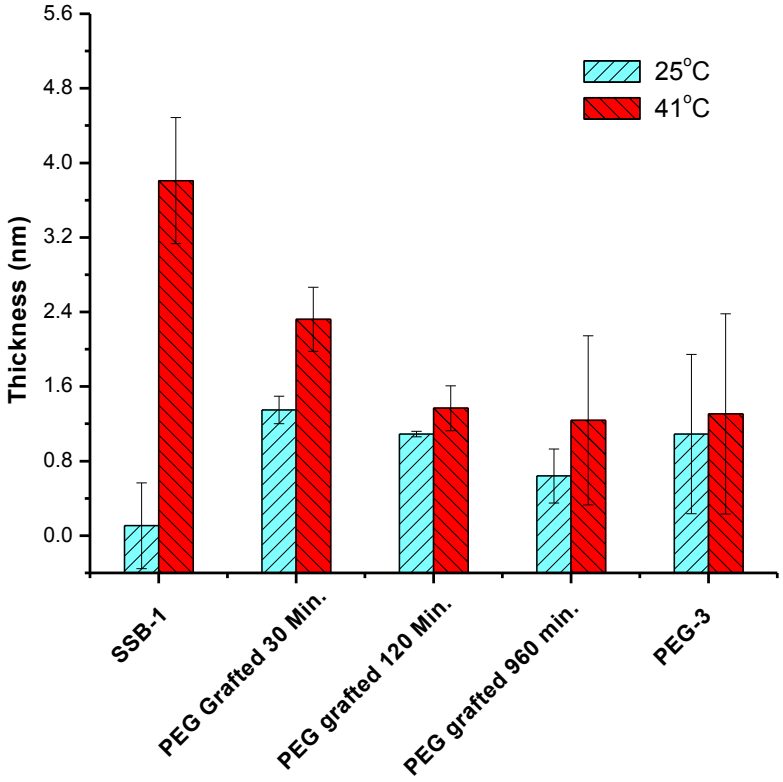

Figure 6.16: Protein adsorption to TS PNIPAM-PEG mixed brush at different grafting times of PEG.

Interestingly, at 30 min grafting time of end functionalized PEG, an immediate effect is noticed after protein adsorption. An increase of thickness at 25°C (1.3nm), and a decrease at 41°C (2.2 nm) is observed. Overall the surface became much less responsive with grafting of roughly only 1 nm of PEG in a second step. Protein adsorption levels

start to resemble amounts measured for pure PEG-3 films. As seen in **Figure 6.16**, when grafting time is increased to 120 and 960 minutes, films became practically non-responsive to protein adsorption at 25 and 41°C. Both systems become practically "locked" resembling what was measured for PEG-3 thicknesses after fibrinogen adsorption experiments. It is evident that even small amounts of PEG (1-3nm thickness increases), have a strong effect on the ability of PNIPAM to render thermally responsive properties in biological media, indeed creating an increased hydrophilic surface. Protein adsorption was suppressed even at temperatures above the LCST of PNIPAM.

Significantly, the mixed brush systems have demonstrated behavior for potential on-demand delivery of active ligands. **Figure 6.17** displays a schematic detailing the idea behind active delivery. Small active ligands such as growth factors can be attached to the terminus of the PNIPAM block fragments. By utilizing PEG as the second component of the MB system, we can effectively create a biocompatible matrix for the coating. Therefore, we can utilize the thermally responsive behavior of PNIPAM to actively deliver or hide (**Figure 6.17**) the growth factors within the biocompatible matrix. Protein adsorption experiments demonstrate the foundational groundwork towards fabrication of such coatings. Both the SS and TS MB approaches show an overall hydrophilic increase in the layers upon addition of PEG into the MB films. Moreover, at temperatures below

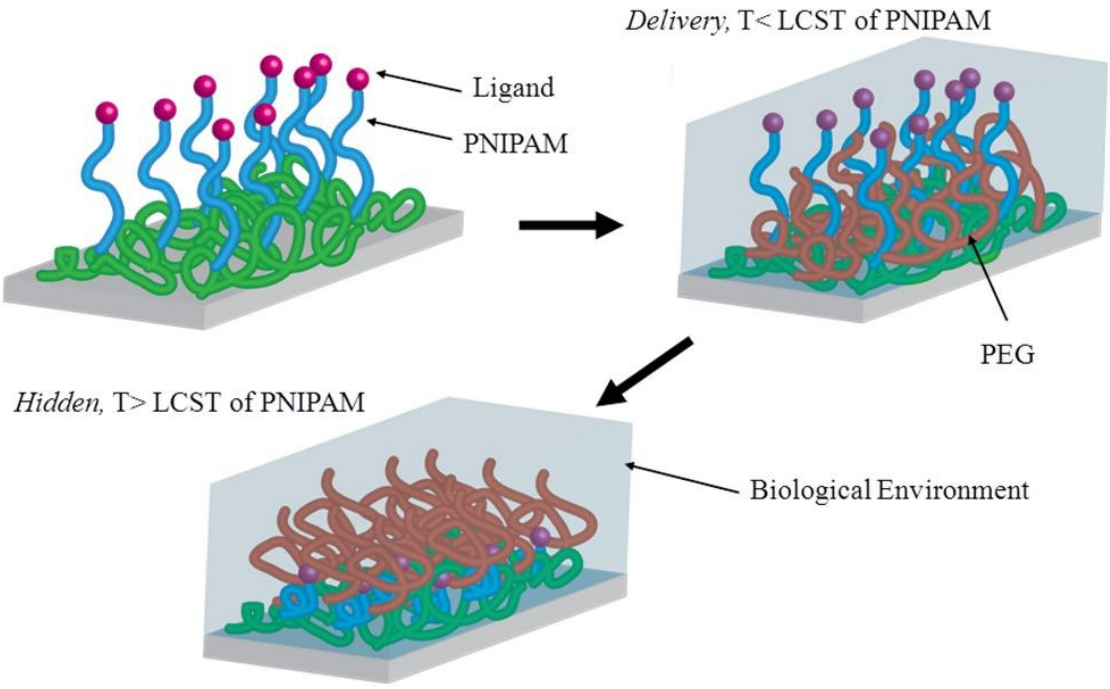

Figure 6.17: Schematic of delivery on-demand by MB systems containing PNIPAM and PEG.

the LCST of PNIPAM, the layers are subsequently protein resistant. However, at temperatures above the LCST of PNIPAM (~40°C), but below the LCST of the PEG component, PNIPAM chains will collapse while PEG chains remain extended. Protein adsorption experiments demonstrate such behavior at the measurement temperatures of 41°C. For all PNIPAM-PEG MB systems, the layers remain more protein resistant than that of the pure PNIPAM SSB component, approaching measurements of the pure PEG layer component. We foresee the observed behavior due to the collapsing of PNIPAM at 41°C and the subsequent extension of PEG.

6.3.4.3:Secondary Grafting of Hydrophobic Component via TS method

To illustrate the adaptability and universal nature of the approach, hydrophobic second components were attached to SSB-1 films in a second step. Static contact angle measurements of pure PS and PEG films were found to be roughly 90[50] and 32°[24] respectively. Therefore, different resulting surface energy components can be fabricated by grafting the end functionalized polymer in a second step to thermally responsive PNIPAM SSB-1 films. Herein, we discuss the secondary grafting of PS to create PNIPAM-PS MB films via the TS method. A 1% w/v solution in toluene of carboxy terminated PS with number average molecular weight of 2,000 g/mol was utilized to deposit layers of PS via dip-coating to SSB-1 films. Non end-functionalized PS (Mn 280,000 g/mol) was added to the solution to increase the viscosity and subsequently prevent de-wetting upon grafting of low molecular weight PS. The initial SSB-1 dry layer thickness was measured at 28nm by ellipsometry. PS layers were grafted for 4 hours at 130°C. Subsequent films were rinsed with fresh aliquots of MEK and toluene to remove any unbound low molecular weight or adsorbed high molecular weight PS chains. The subsequent grafting produced films with roughly 7 nm of PS.

Resulting PNIPAM-PS MB films where characterized by advancing and receding contact angles and imaged via AFM as a function of pre solvent treatment. MEK was utilized as a mutually good solvent for both blocks. Toluene was utilized as a selective solvent for PS, a non-solvent for PNIPAM, effectively "blooming" PS to the outer region of the polymer film.

Table 6.5a-b displays advancing and receding contact angle measurements as a function of solvent pre-treatment of the modified PNIPAM-PS MB substrates.

Table 6.5: Advancing and receding contact angles for PS-PNIPAM mixed brush system via 2-step process as a function of pre-solvent treatment a) MEK b) Toluene

MEK Rinse	**22°C**		**40°C**	
	Advancing	Receding	Advancing	Receding
Average	84.1	32.2	88.8	36.8
STDEV	1.4	2.8	1.5	1.4

Toluene Rinse	**22°C**		**40°C**	
	Advancing	Receding	Advancing	Receding
Average	91.8	55.0	91.0	47.8
STDEV	0.9	2.5	1.1	2.9

As observed in **Table 6.5a**, pre-treatment with a non-selective solvent yields films with retained thermoresponsive behavior, however, less switchability is noticed as compared to pure PNIPAM films. At 22°C, the advancing contact angle was roughly 84°, while at 40°C the advancing angle increased to ~89°. The receding angles were similar at both temperatures, 32 and 37° at 22 and 40°C respectively. This indicates that PNIPAM is at the three phase boundary line rendering the surface slightly more hydrophilic than pure PS. However, when rinsed with toluene (good solvent for PS), temperature dependent advancing contact angles disappear, and the surface yields contacts angles (92 and 91°) identical to pure PS brush films independent of temperature.

Toluene effectively "blooms" PS to the top most region of the surface, screening interaction of PNIPAM.

To validate the changes in advancing contact angle, the surface morphology and smoothness of the grafted PNIPAM-PS MB films were determined with tapping mode AFM as a function of pre-solvent treatment. **Figure 6.18a-c** displays 800 x 800 nm AFM topography images of the PNIPAM-PS TS MB films, before PS grafting (**Figure 6.18a**), after PS grafting and MEK rinse (**Figure 6.18b**), and after PS grafting and toluene rinse (**Figure 6.18c**). As seen in **Figure 6.18a**, before PS grafting, smooth surfaces are present with little to no globular structures observed. After grafting of PS and rinsing in a non-selective solvent, surfaces remain smooth and practically identical to surfaces prior to PS grafting, however a very small onset of globular domains become apparent, indicative of PS surfaces attached to PGMA anchoring layers as published by Iyer et al. for Mn 4500 g/mol PS.[50] However, after rinsing grafted PS surfaces with toluene (**Figure 6.18c**), a large concentration of defined globular structures are present on the surface, indicating a PS dominated layer. We attribute the globular domain phenomenon as follows. Roughly 7nm of PS was grafted; therefore as PS chains concentrate at the interface, they effectively create areas of isolated structures due to chains collapsing on one another after evaporation of the solvent.

Indeed, the versatility of the TS MB fabrication technique was confirmed via the grafting of both a hydrophilic (PEG) and hydrophobic (PS) secondary component. The grafting of PS allowed for an overall low surface energy film as compared to PEG, and a

slight thermally responsive layer after rinsing in a good solvent for both PNIPAM and PS. However, thermally responsive behavior is suppressed after rinsing in a selective solvent for PS.

6.4:Conclusions

The utilization of reactive and responsive BCP approach has led to the synthesis of MB systems via single and two step approaches. The utilization of PGMA block segment has proved to be a very versatile approach in creating next generation polymer brush surfaces. Complex MB brush systems can be produced in a very straightforward manner. Block copolymers consisting of PGMA-PNIPAM and PGMA-PEG are mixed in known ratios, dipcoated and annealed, forming MB surfaces of tunable thickness utilizing the simplistic “grafting to” approach all in a single step. Traditional MB fabrication techniques utilize multiple steps and acquire more complex grafting chemistry

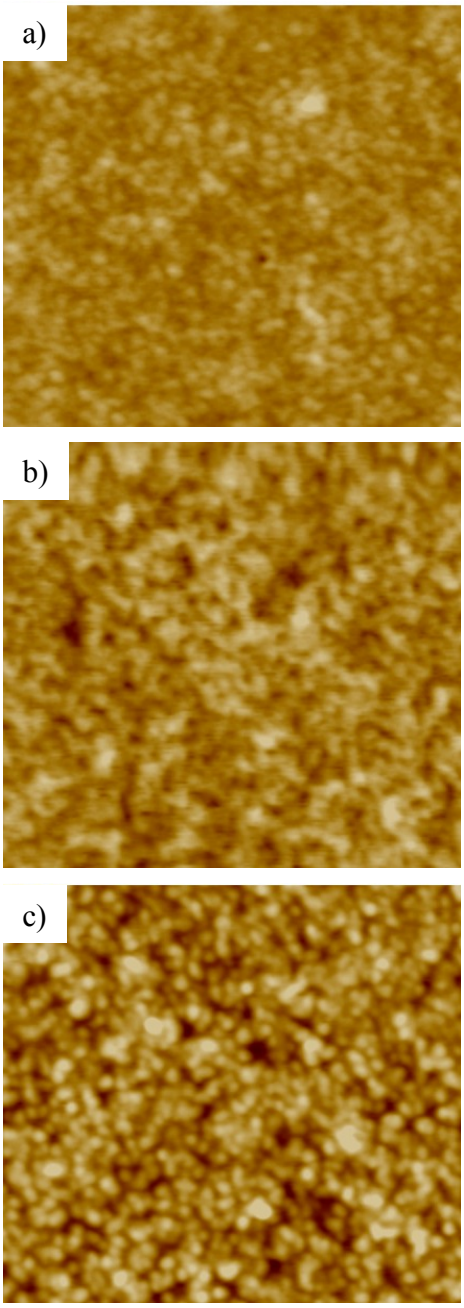

Figure 6.18: AFM topography images (800 x 800 nm) of PS grafted TS brush to SSB-1 films. a) no PS grafting b) PS grafted film after MEK rinse c) PS grafted film after toluene rinse. Vertical scale: a-c) 15nm.

Firstly, pure PEG 1-3 BCP systems formed smooth homogenous layers that were found to be well within the "brush" regime. PEG 1-3 layers were found to undergo thermally responsive swelling and collapse in aqueous environments between the temperatures of 25 and 65°C due to hydrogen bonding interactions between water and PEG units, however the PGMA block segment provided a platform for PEG to collapse upon above its LCST. Hence, the new BCP systems were strong potential candidates for MB films towards the generation of on-demand delivery of active ligands within a biocompatible matrix.

SSB-2 and PEG-3 mixed brush systems in a 50/50 ratio proved to undergo a swelling and collapse, however much smaller in magnitude than their pure BCP constituents. However, advancing contact angle data measurements indicate that the SS PNIPAM-PEG MB could still undergo surface wettability changes as a function of temperature. This was also validated by the work of adhesion values as measured by AFM colloidal probe technique with a labeled fibrinogen tip. MB ratios of 75/25 and 50/50 proved to be thermally switchable at measurement temperatures of 25 and 55°C. The 75/25 mixed brush proved to be more hydrophilic at both temperatures than pure SSB-2 brush films, however when additional PEG-3 BCP was added, the system became slightly more hydrophobic. This was attributed to the large amounts of PGMA present per unit area, due to both PGMA chain segments approaching 20k for the BCP constituents. However, when fibrinogen adsorption experiments were conducted, surfaces became practically protein repelling independent of temperature. Interestingly, the MB SS films can effectively swell and collapse, while suppressing protein adsorption.

We attributed the observed effect to the collapse of PNIPAM while PEG chains remained extended in the film and suppressing protein adsorption.

End-functionalized polymer molecules were grafted in a second step to pure SSB-1 films to generate PNIPAM-PEG MB in a two step process as well. Varying amounts of PEG within the MB system was fabricated by varying time of the secondary grafting step. However, even at the lower limits of 1.2nm of PEG grafting, surfaces became more protein repelling, however still slightly thermally switchable. However, upon increasing the amount of thickness increase after PEG grafting to 2nm, suppression of protein switchable surfaces was noticed. Similar effects were observed for both SS and TS MB approach, indicating the potential for both methods for the fabrication of on-demand delivery coatings.

The versatility of the TS MB approach was validated by the secondary grafting of a hydrophobic PS component. Interestingly, the surface energy of the film could be controlled via solvent pre-treatment. Non-selective solvents rendered low energy surfaces with slight temperature dependence on contact angle. However, washing with a selective solvent for PS, the surface became practically identical to pure PS layers grafted to PGMA, and non temperature dependent.

Overall, MB from reactive/responsive BCP are a very interesting and versatile approach in creating MB surfaces. With the recent advantages in living polymerization techniques, namely RAFT, there is practically an unlimited number of combinations of various polymers one can chose in designing polymer brush surfaces. Also, by creating

mixed polymer brush films between PNIPAM-PEG MB, we observed interesting interactions between PEG and PNIPAM. The smallest introductions of PEG into the MB layer alter the films interaction with protein to a large extent, and practically diminish any thermo responsive nature of the films towards fibrinogen. In the future, we hope to shed some light on the interaction by utilizing IR spectroscopic ellipsometry measurements in order to study the interaction between PEG and PNIPAM within biological environments.

6.5:References

1. Minko, S.; Ionov, L.; Sydorenko, A.; Houbenov, N.; Stamm, M.; Zdyrko, B.; Klep, V.; Luzinov, I., Gradient stimuli-responsive polymer grafted layers. In *Stimuli-responsive polymeric films and coatings*, Urban, M. W., Ed. 2005; Vol. 912, pp 68-83.

2. Draper, J.; Luzinov, I.; Minko, S.; Tokarev, I.; Stamm, M., Mixed polymer brushes by sequential polymer addition: Anchoring layer effect. *Langmuir* **2004,** *20* (10), 4064-4075.

3. Nagase, K.; Kobayashi, J.; Kikuchi, A.; Akiyama, Y.; Annaka, M.; Kanazawa, H.; Okano, T., Influence of graft interface polarity on hydration/dehydration of grafted thermoresponsive polymer brushes and steroid separation using all-aqueous chromatography. *Langmuir* **2008,** *24* (19), 10981-10987.

4. Zhao, B., Synthesis of binary mixed homopolymer brushes by combining atom transfer radical polymerization and nitroxide-mediated radical polymerization. *Polymer* **2003,** *44* (15), 4079-4083.

5. Usov, D.; Gruzdev, V.; Nitschke, M.; Stamm, M.; Hoy, O.; Luzinov, I.; Tokarev, I.; Minko, S., Three-dimensional analysis of switching mechanism of mixed polymer brushes. *Macromolecules* **2007,** *40* (24), 8774-8783.

6. Rungta, A.; Natarajan, B.; Neely, T.; Dukes, D.; Schadler, L. S.; Benicewicz, B. C., Grafting bimodal polymer brushes on nanoparticles using controlled radical polymerization. *Macromolecules* **2012,** *45* (23), 9303-9311.

7. Wu, D.; Yang, Y.; Cheng, X.; Liu, L.; Tian, J.; Zhao, H., Mixed molecular brushes with plla and ps side chains prepared by aget atrp and ring-opening polymerization. *Macromolecules* **2006,** *39* (22), 7513-7519.

8. Vrlinic, T. Development of new anti-bioadhesive surfaces for specific neurodegenerative agents. L'UNIVERSITE DU MAINE Le Mans 2011.

9. Sidorenko, A.; Minko, S.; Schenk-Meuser, K.; Duschner, H.; Stamm, M., Switching of polymer brushes. *Langmuir* **1999,** *15* (24), 8349-8355.

10. Cole, M. A.; Voelcker, N. H.; Thissen, H.; Griesser, H. J., Stimuli-responsive interfaces and systems for the control of protein-surface and cell-surface interactions. *Biomaterials* **2009,** *30* (9), 1827-1850.

11. Virtanen, J.; Tenhu, H., Thermal properties of poly(n-isopropylacrylamide)-g-poly(ethyl oxide) in aqueous solutions: Influence of the number and distribution of the grafts. *Macromolecules* **2000,** *33* (16), 5970-5975.

12. Hoy, O. Synthesis and characterization of polymer brushes for controlled adsorption of proteins. Clemson University, 2008.

13. Sanderson, L. A. W.; Emoto, K.; Van Alstine, J. M.; Weimer, J. J., Characterization of grafted poly(ethylene glycol) on si wafers using scanning probe microscopy. *Journal of Colloid and Interface Science* **1998,** *207* (1), 180-183.

14. Gao, X.; Kucerka, N.; Nieh, M.-P.; Katsaras, J.; Zhu, S.; Brash, J. L.; Sheardown, H., Chain conformation of a new class of peg-based thermoresponsive polymer brushes grafted on silicon as determined by neutron reflectometry. *Langmuir* **2009,** *25* (17), 10271-10278.

15. Vyas, M. K.; Schneider, K.; Nandan, B.; Stamm, M., Switching of friction by binary polymer brushes. *Soft Matter* **2008,** *4* (5), 1024-1032.

16. Schmaljohann, D.; Beyerlein, D.; Nitschke, M.; Werner, C., Thermo-reversible swelling of thin hydrogel films immobilized by low-pressure plasma. *Langmuir* **2004,** *20* (23), 10107-10114.

17. von Recum, H.; Okano, T.; Kim, S. W., Growth factor release from thermally reversible tissue culture substrates. *Journal of Controlled Release* **1998,** *55* (2-3), 121-130.

18. Skrabania, K.; Laschewsky, A.; Berlepsch, H. v.; BoÌˆttcher, C., Synthesis and micellar self-assembly of ternary hydrophilicâˆ’lipophilicâˆ’fluorophilic block copolymers with a linear peo chain. *Langmuir* **2009,** *25* (13), 7594-7601.

19. Burtovyy, R.; Tregub, A.; Moinpour, M.; Buehler, M.; Luzinov, I., Measurement of interactions between abrasive silica particles and copper, titanium, tungsten and tantalum. In *Advances and challenges in chemical mechanical planarization*, Zwicker, G.; Borst, C.; Economikos, L.; Philipossian, A., Eds. Materials Research Society: Warrendale, 2007; Vol. 991, pp 133-137.

20. Jones, R.; Pollock, H. M.; Cleaver, J. A. S.; Hodges, C. S., Adhesion forces between glass and silicon surfaces in air studied by afm: Effects of relative humidity, particle size, roughness, and surface treatment. *Langmuir* **2002,** *18* (21), 8045-8055.

21. Henn, G.; Bucknall, D. G.; Stamm, M.; Vanhoorne, P.; Jerome, R., Chain end effects and dewetting in thin polymer films. *Macromolecules* **1996,** *29* (12), 4305-4313.

22. Bruggeman, D. A. G., Berechnung verschiedener physikalischer konstanten von heterogenen substanzen. I. Dielektrizitätskonstanten und leitfähigkeiten der mischkörper aus isotropen substanzen. *Annalen der Physik* **1935,** *416* (7), 636-664.

23. Johnson, K. L.; Kendall, K.; Roberts, A. D., Surface energy and contact of elastic solids. *Proceedings of the Royal Society of London Series a-Mathematical and Physical Sciences* **1971,** *324* (1558), 301-&.

24. Zdyrko, B.; Varshney, S. K.; Luzinov, I., Effect of molecular weight on synthesis and surface morphology of high-density poly(ethylene glycol) grafted layers. *Langmuir* **2004,** *20* (16), 6727-6735.

25. Zdyrko, B.; Luzinov, I., Polymer brushes by the "grafting to" method. *Macromolecular Rapid Communications 32* (12), 859-869.

26. Seeber, M.; Zdyrko, B.; Burtovvy, R.; Andrukh, T.; Tsai, C. C.; Owens, J. R.; Kornev, K. G.; Luzinov, I., Surface grafting of thermoresponsive microgel nanoparticles. *Soft Matter 7* (21), 9962-9971.

27. Luzinov, I. A.; Swaminatha Iyer, K. L.; Klep, V. Z.; Zdyrko, B. V. Surface graft modification of substrates, us patent 7,026,014 b2, apr. 11, 2006.

28. Lokitz, B. S.; Wei, J.; Hinestrosa, J. P.; Ivanov, I.; Browning, J. F.; Ankner, J. F.; Kilbey, S. M., II; Messman, J. M., Manipulating interfaces through surface confinement of poly(glycidyl methacrylate)-block-poly(vinyldimethylazlactone), a dually reactive block copolymer. *Macromolecules* **2012,** *45* (16), 6438-6449.

29. Bittrich, E.; Burkert, S.; Muller, M.; Eichhorn, K. J.; Stamm, M.; Uhlmann, P., Temperature-sensitive swelling of poly(n-isopropylacrylamide) brushes with low molecular weight and grafting density. *Langmuir 28* (7), 3439-3448.

30. Luzinov, I.; Minko, S.; Tsukruk, V. V., Responsive brush layers: From tailored gradients to reversibly assembled nanoparticles. *Soft Matter* **2008,** *4* (4), 714-725.

31. Zdyrko, B.; Iyer, K. S.; Luzinov, I., Macromolecular anchoring layers for polymer grafting: Comparative study. *Polymer* **2006,** *47* (1), 272-279.

32. Brittain, W. J.; Minko, S., A structural definition of polymer brushes. *Journal of Polymer Science Part a-Polymer Chemistry* **2007,** *45* (16), 3505-3512.

33. Sperling, L. H., *Physical polymer science*. 3rd edition ed.; Wiley&Sons Inc.: 2001.

34. Zdyrko, B. Thin polymer films for biomedical applications: Synthesis and characterization. Clemson University 2005.

35. Saeki, S.; Kuwahara, N.; Nakata, M.; Kaneko, M., Upper and lower critical solution temperatures in poly (ethylene glycol) solutions. *Polymer* **1976,** *17* (8), 685-689.

36. Malcolm, G. N.; Rowlinson, J. S., The thermodynamic properties of aqueous solutions of polyethylene glycol, polypropylene glycol and dioxane. *Transactions of the Faraday Society* **1957,** *53* (0), 921-931.

37. Zdyrko, B.; Klep, V.; Luzinov, I., Universal platform for surface modification employing grafted polymer layers. *Material Matters* **2008,** *3* (2), 44-47.

38. Burtovyy, O.; Klep, V.; Turel, T.; Gowayed, Y.; Luzinov, I., *Polymeric membranes: Surface modification by "grafting to" method and fabrication of multilayered assemblies, in nanoscience and nanotechnology for chemical and biological defense, editors: Nagarajan, r.; zukas, w.; hatton, t. A.; lee, s.* ACS Symposium Series 1016, Washington DC: 2009; p 289-305.

39. Cassie, A. B. D., Contact angles. *Transactions of the Faraday Society* **1948,** *44* (3), 11-16.

40. Jonas, A. M.; Glinel, K.; Oren, R.; Nysten, B.; Huck, W. T. S., Thermo-responsive polymer brushes with tunable collapse temperatures in the physiological range. *Macromolecules* **2007,** *40* (13), 4403-4405.

41. Hu, T. J.; Wu, C., Grafting density induced stretching and collapse of tethered poly(ethylene oxide) chains on a thermally sensitive microgel. *Macromolecules* **2001,** *34* (19), 6802-6805.

42. Laloyaux, X.; Mathy, B.; Nysten, B.; Jonas, A. M., Surface and bulk collapse transitions of thermo responsive polymer brushes. *Langmuir* **2010,** *26* (2), 838-847.

43. Das, S.; Samanta, S.; Chatterjee, D. P.; Nandi, A. K., Thermosensitive water-soluble poly(ethylene glycol)-based polythiophene graft copolymers. *Journal of Polymer Science Part a-Polymer Chemistry* **2013,** *51* (6), 1417-1427.

44. Minko, S., Responsive polymer brushes. *Polymer Reviews* **2006,** *46* (4), 397-420.

45. Chyasnavichyus, M.; Tsyalkovsky, V.; Zdyrko, B.; Luzinov, I., Tuning fluorescent response of nanoscale film with polymer grafting. *Macromolecular Rapid Communications 33* (3), 237-241.

46. Samadi, A.; Husson, S. M.; Liu, Y.; Luzinov, I.; Kilbey, S. M., Low-temperature growth of thick polystyrene brushes via atrp. *Macromol. Rapid Commun.* **2005,** *26* (23), 1829-1834.

47. Jordan, R.; Ulman, A.; Kang, J. F.; Rafailovich, M. H.; Sokolov, J., Surface-initiated anionic polymerization of styrene by means of self-assembled monolayers. *Journal of the American Chemical Society* **1999,** *121* (5), 1016-1022.

48. Gan, D.; Lyon, L. A., Synthesis and protein adsorption resistance of peg-modified poly(n-isopropylacrylamide) core/shell microgels. *Macromolecules* **2002,** *35* (26), 9634-9639.

49. Virtanen, J.; Baron, C.; Tenhu, H., Grafting of poly(n-isopropylacrylamide) with poly(ethylene oxide) under various reaction conditions. *Macromolecules* **2000,** *33* (2), 336-341.

50. Iyer, K. S.; Zdyrko, B.; Malz, H.; Pionteck, J.; Luzinov, I., Polystyrene layers grafted to macromolecular anchoring layer. *Macromolecules* **2003,** *36* (17), 6519-6526.

CHAPTER 7:DEVELOPMENT OF THERMALLY RESPONSIVE BRUSH LIKE LAYERS FROM GRAFTABLE NANOGELS: PART 1

7.1:Introduction

Recent studies in the area of responsive surfaces/interfaces show their importance for prospective applications in micro- and nanofluidics, biocompatible materials, controlled drug release, nano- and biotribology, controlled cell growth and proliferation, and bio- and chemosensing.[1-2] As discussed in the previous chapters, PNIPAM exhibits a temperature-sensitive phase transition in water, known as a lower critical solution temperature (LCST), at temperatures within the tolerances of human metabolism (~32 °C).[3] This is due primarily to the coil-to-globule transition at the critical temperature.[4] At temperatures below the LCST, PNIPAM macromolecules arrange into a swollen and hydrated conformation. Conversely, at temperatures above the LCST, PNIPAM chains collapse and arrange into a non-hydrated, collapsed conformation. Consequently, PNIPAM has been utilized in various forms, such as thermoresponsive hydrogels, particles, brushes, spheres and micelles.[1-2, 5-9]

To this end, **Chapter 4** reports an additional modification to the "grafting to" method that now allows the straightforward formation of much thicker, thermoresponsive PNIPAM-grafted layers. In essence, the proposed approach includes grafting of PNIPAM microgel nanoparticles containing reactive carboxyl (acrylic acid) groups to a surface. The straightforward nature and the facility of the "grafting to" approach is preserved in this case and the thickness of the grafted layer can be tuned by changing the size of the nanoparticles that are to be grafted. Microgels are typically nano- or microparticles made

of a cross-linked, hydrogel-forming polymer.[6-7] We chose microgel particles because they are an intermediate between grafted polymer layers and macroscopic gels, thus combining some of the advantages of both. These advantages include: rapid phase transition, robustness, and having an easily tunable composition.[10] We compared the behavior of the synthesized grafted layers with the (reported in literature[11-14]) behavior of PNIPAM brushes (densely end-grafted layers). This comparison demonstrates that the microgel-grafted layer is comparable to PNIPAM brushes with respect to its thermoresponsive properties. Therefore, the microgel-grafted layer can be considered as a system capable of competing with the PNIPAM brushes.

Microgel submicron particles, made of temperature-responsive polymers, have been widely researched for carrying out separations, as substrates for bioreactors, for enzyme and cell immobilization, as biosensors, and for *in vivo* drug delivery.[4-5, 7, 15-19] PNIPAM-containing microgels have been synthesized and functionalized using various techniques, such as emulsion non-surfactant or surfactant stabilized precipitation radical polymerization.[4-5, 7, 20-21] Complex microgel structures have also been fabricated. For example, PNIPAM hydrogels containing ferromagnetic nanoparticles have been synthesized.[22] Additionally, Huang et al. synthesized thermoresponsive and biodegradable microgels by copolymerizing NIPAM with dextran–lactate–2-hydroxyethyl methacrylate using an emulsion polymerization technique.[3]

In spite of the many potential applications for thin films made from microgels, most published work is devoted to the multilayered assemblies obtained by layer-by-layer

techniques.[7] Only a few articles describe fabrication and investigation of microgel monolayers on a surface.[10, 23-24] These studies describe the adsorbed layers and not the chemically anchored layers of microgel nanoparticles. The primary focus of the work reported in **Chapter 4** is the synthesis and characterization of covalently grafted PNIPAM-containing microgel monolayers. To the best of our knowledge, fabrication of this type of grafted layer has not yet been reported in the scientific literature.

The synthesis of the microgels was conducted via a surfactant-stabilized free-radical-precipitation polymerization in an aqueous environment, in the presence of acrylic acid as a co-monomer and *N,N'*-methylenebisacrylamide (BIS) as a cross-linker. The available carboxyl groups were then utilized to attach the microgels to the surface of various substrates, including silicon wafers, glass slides, tungsten wires, and poly(vinylidene fluoride) (PVDF) fibers. Surfaces were formerly activated by depositing a thin layer of poly(glycidyl methacrylate) (PGMA) as an anchoring layer.[25-27] This type of surface activation brings a significant number of epoxy groups to the substrate surface. Therefore, the microgel grafting was made possible through the reaction between epoxy groups from the PGMA anchoring layer and the carboxyl groups from acrylic acid.[25] The swelling and collapsing of the grafted microgel monolayers were investigated using atomic force microscopy (AFM) while scanning samples underwater at temperatures above and below the LCST. Scanning electron microscopy (SEM), AFM, contact angle measurements, elemental analysis, and proton NMR analyses were conducted to elucidate the structure, morphology, and surface characteristics of the synthesized microgels and the grafted layers.

7.2:Experimental

7.2.1:Fabrication of PVDF fibers

PVDF fibers were fabricated by electrospinning using PVDF (M_n=350–450,000 g/mol, purchased from Goodfellow) and poly(ethylene oxide) (PEO, M_n=1,000,000 g/mol from Sigma–Aldrich), by Dr. Konstatin Kornev research group, Clemson University. For this purpose, 2–3 mL of the polymer solution (0.2 g of PEO and 2 g of PVDF in 10g of DMA (Spectrum)) was loaded into a 10-mL plastic syringe. The syringe was covered with a flexible heater (Watlow) (to maintain a constant temperature of 55°C) and was attached to a syringe-type infusion pump. The syringe needle and the spinneret needle were connected using a Teflon tube. A stainless-steel spinneret needle was connected to a high-voltage device and the system was grounded to a collector. Nanofibers were collected with a copper fork and woven into yarns.

7.2.2:Characterization techniques

A Veeco Dimensions 3100 AFM, equipped with a Nanoscope 3A controller, was used to image the morphology of the grafted monolayers of the PNIPAM microgels in tapping mode. A silicon cantilever, with force constant of 40 N/m, was used for the samples scanned in ambient air. Swelling and collapsing studies were conducted (in contact mode under water) using a Veeco Multimode AFM (with a Nanoscope 3A controller and a liquid cell) and silicon nitride cantilevers with force constant of 0.24 N/m. Monomer concentrations were monitored throughout the synthesis using a Bruker 300-MHz NMR. Elemental analyses of the synthesized nanogels were conducted using a Perkin–Elmer Series II-2400 CHNS/O Analyzer. Advancing and receding contact angle

data was performed as described in **Section 3.3.4.** Scanning electron microscopy was conducted using a Field Emission Hitachi S4800 SEM. Ellipsometry measurements were used to measure dry layer thickness (**Section3.3.3.1**). Harrick Scientific Corporation (Model PDC-32G) plasma cleaner/sterilizer was used in the current study to treat PVDF fibers and tungsten wires prior to the grafting.

To investigate change in the surface energy of the substrate as a function of temperature, we ran two different experiments (Taras Andrukh, Kornev Group, Clemson University) using tungsten wire modified with the grafted microgel layer. In the first experiment, the modified tungsten wire (130 μm) was placed into a thermo-insulated box with controllable humidity and temperature. Two alligator clips were attached to the wire ends thus closing the circuit when the device was connected to the power supply. The current and, therefore, the Joule heating of the wire can be controlled by adjusting the voltage. A different tungsten wire with a smaller (100 μm) diameter was used for the droplet delivery and deposition on the test wire. The delivery wire, droplet, and modified tungsten wire altogether were maintained at the same temperature. In order to confirm that the heat exchange played no role in the contact-angle analysis, we (Andrukh, Kornev) made the following estimates. The time of heat exchange between the drop and the wire in question is estimated using **Equation(7.1)**:

$$\tau = \rho c_p R^2 / \mathrm{k} \qquad (7.1)$$

where ρ is the water density, c_p is the specific heat, k is thermoconductivity, and R is the droplet radius. Approximating R as 150 μm and $k/(\rho c_p)$= 1.4 x 10^{-7} m^2/s, we

obtained t ~ 0.2s, which is much smaller than the time of observation of the change of contact angle.

To make additional contact angle measurements a second experiment was carried out. The grafted wire was attached to the 1D manipulator–positioner stage (VT-21, MICOS USA) and gently dipped and held in the container with deionized water. A K-type thermocouple (30 gauge) was used to monitor and control water temperature. The experimental setup (**Figure 7.1**) also consisted of a water pump that aided in the circulation of water through the jacket while also controlling the temperature. The thermocouple was used to accurately determine the temperature of the water. A 1D manipulator was used to move the modified substrate up or down. Lastly, a camera (Dalsa Falcon 1.4) was used to record the shape of the meniscus. To avoid diffraction from the edge of the water-jacketed condenser, the water was slightly overfilled.

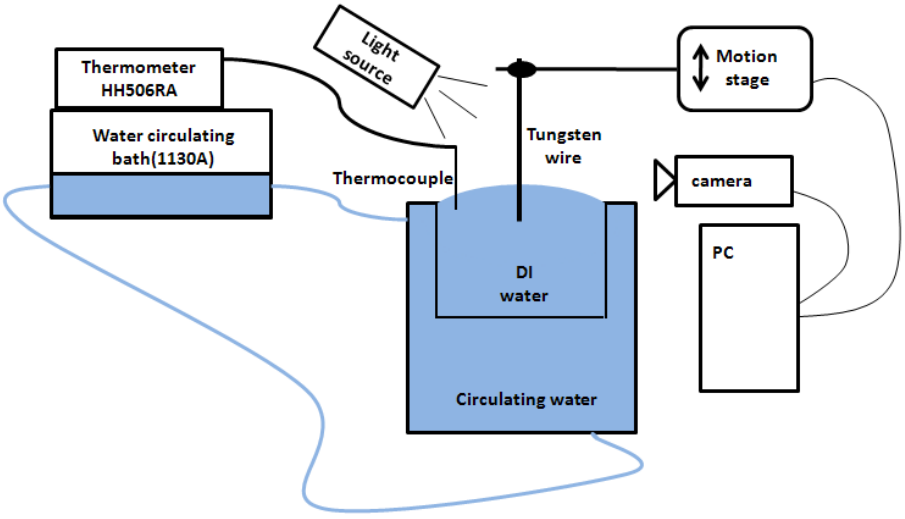

Figure 7.1: Schematic of the experimental setup for the analysis of the change of meniscus shape with temperature.

7.2.3:Synthesis of Microgels

The synthesis of carboxy functionalized PNIPAM nanogels was carried out as follows. The overall schematic of the synthetic procedure is shown in **Figure 7.2**[28]. In general, we followed the modified procedure reported by Li et al., [29] so that 0.65 g (0.006 mol) of NIPAM, 5 mol% ($2.87x10^{-4}$ mol) of AAc, 5 mol% ($2.87x10^{-4}$ mol) of BIS, and 0.075 g ($2.84x10^{-4}$ mol) of Dodecyltrimethylammonium chloride(DTAC) were dissolved in 60 mL of deionized H_2O and placed in a 100-mL three-necked round-bottom flask. The flask was equipped with an overhead mechanical stirrer set at 250 rpm, a nitrogen inlet and outlet, and a water-jacketed condenser. The monomer solution was placed in a water bath, thermostatted at 70ºC and bubbled with nitrogen for 1 hour to remove any dissolved oxygen. To initiate the polymerization, 0.03 g of AAPH was dissolved in 5 mL of water and charged into the flask. The solution was left to react for 6 hours under a nitrogen blanket. The reaction vessel was then submerged in an ice bath to arrest the polymerization. To purify the product, aliquots were centrifuged, decanted, and re-dispersed, first in fresh H_2O, and then three times in tetrahydrofuran (THF, OmniSolv).

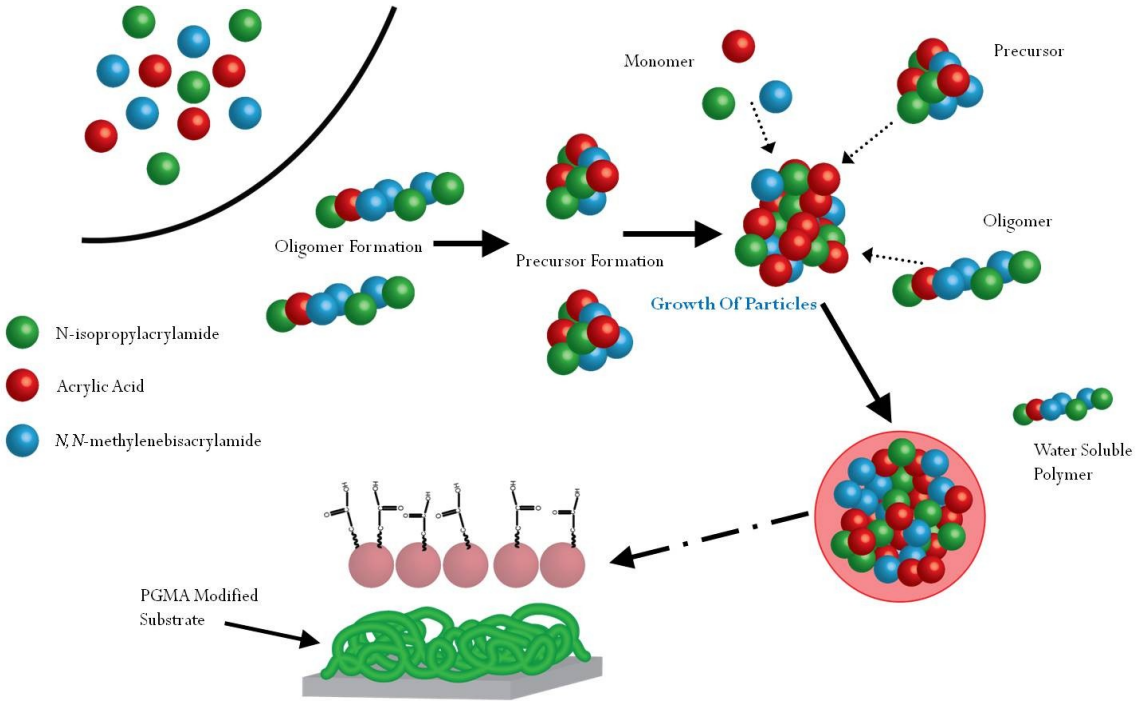

Figure 7.2: General schematic of PNIPAM nanogels made by surfactant stabilized precipitation polymerization.

Characterization of the chemical composition of the resulting PNIPAM particles was carried out using proton NMR (H-NMR). For the NMR experiments, microgel particle synthesis was repeated using deuterium oxide (D_2O) as a solvent. Changes in the monomer concentration during synthesis were monitored. As an internal reference,[21] 40 μL of DMAC was added to the reaction mixture. Next, 1-mL aliquots were collected at time intervals of 0, 5, 10, 20, 40, 80, 120, and 240 min. This was accomplished by withdrawing approximately 1-mL of the reaction solution at each given time interval and quenching it in an ice bath to halt the polymerization. The monomer concentration was calculated from the integrated area of the peaks that are individually unique to each

monomer, as opposed to the peaks observed for the DMAC. Concentration values were calculated as a ratio of initial concentration and the area under the respective bands.

7.2.4:Surface Grafting of Microgels

The covalent grafting of thermally responsive PNIPAM containing nanogels was performed as follows. Highly polished single-crystal silicon wafers were prepared as discussed in **Section 4.2.1**. To deposit a thin layer of PGMA on the surface of the wafer, a 0.14% w/v solution of PGMA in chloroform (Spectrum) was made, and clean wafers were then coated by being dipped into the solution. Dip-coated wafers were annealed under vacuum at 120 °C for 20 min. After annealing, the wafers were rinsed three times for 10 minutes in fresh chloroform to remove any unattached polymer. Generally, this procedure produces a PGMA layer approximately 6 nm in thickness, as determined by ellipsometric measurements. A solution of approximately 6 mg/mL PNIPAM microgels in THF was used to deposit microgels onto the PGMA layer via the dip-coating procedure (Mayer Feintechnik D-3400, speed 240 mm/min). Typically, three consecutive dips were necessary to create a monolayer. Upon dip-coating, samples were annealed under vacuum at 120ºC for 2 hours. Samples were then rinsed three times for 10 minutes in fresh THF to remove any unattached particles from the surface. In an additional experiment, modified silicon wafers were left overnight in the solvent and it was determined that no grafted particles were lost. The procedure described above was also used to modify glass slides (VWR micro slides, 25 x 75 mm, 1.0 mm thick). The only difference was that in the modification of glass slides, the microgel nanoparticles were deposited onto the surface prior to the grafting by spin-coating (Headway Research) from

THF suspension.

The modification of complex surfaces was carried out by attaching to both metallic and organic substrates. Firstly, tungsten wires (130 μm in diameter) were treated with air plasma for 10 minutes. The wires were then immersed in deionized water for 5 minutes (to develop surface hydroxyl groups) and air dried before deposition of the PGMA layer. Next, PGMA was drop-casted onto the wires from a 0.14% solution by weight of PGMA in chloroform. The wires were subsequently annealed at 120°C under vacuum for 20 minutes. Following the annealing step, the wires were rinsed three times in fresh chloroform for 10 minutes to remove any unattached polymer from the surface. PNIPAM microgels were deposited onto the PGMA-modified tungsten wire from an approximately 0.4 weight % solution in THF by drop-casting. Following this deposition, wires were then annealed for 12 hours at 120°C under vacuum. Finally, the wires were rinsed three times in fresh THF for 10 minutes to remove any unattached particles from the wire surfaces.

In order to modify complex organic polymeric substrates we followed the procedure reported for modification of PVDF membranes with a PGMA anchoring layer[30]. To activate the surface of PVDF the fibers were plasma treated for 3 minutes. Treated fibers were rinsed in MEK three times for 10 minutes and dried before deposition of the PGMA layer. For this purpose the fibers were first placed in a 0.14 % w/v solution of PGMA in MEK. A round-bottom flask used in the experiment was equipped with a single-arm, screw-top vacuum attachment. Fibers in the PGMA solution were kept under

vacuum until the solution boiled. This procedure was repeated three times. The vacuum procedure was used to fill the fiber/yarn pores with the PGMA solution. After drying, the fibers were annealed under vacuum at 60ºC for 2 hours. The PGMA-modified fibers were rinsed three times in fresh MEK to remove any unattached polymer from the surface. Fibers were then placed into a suspension of microgel nanoparticles in THF (6 mg/mL) and treated in the same fashion as they were for the PGMA modification. Modified fibers were then annealed under vacuum at 120ºC for 2 hours. The annealed fibers were again washed three times for 10 minutes in fresh THF to remove any free particles. All fibers used for SEM imaging were sputter-covered for one minute with platinum.

7.2.5:Actuation of Grafted Microgels

Actuation of PNIPAM nanogel layer was carried out via AFM. Silicon wafers (1x1 cm) were grafted with PNIPAM-containing microgel nanoparticles and placed inside an AFM liquid cell mounted on a temperature-controllable stage. Samples were scored with a razor blade to locally remove particles from the surface. To observe conformational changes, scanning was conducted across the scratch to view the profile of the changing layer. Temperatures were fixed at 22°C and 40°C for the swelling and collapsing experiments, respectively. The AFM scanning was conducted using a force as small as possible, to minimize any lateral compression of the microgels. Image J freeware was used to extract the profile heights from the various scans.

7.3:Results and Discussion

7.3.1:Synthesis and Characterization of PNIPAM microgel nanoparticles

Upon gentle heating of the nanoparticle suspensions a transition of the microgel particles from transparent at room temperature to opaque was observed as the suspension reached 35–40 °C. This transition was the first indicator that the nanoparticles exhibit thermoresponsive properties, since this transition occurred at just above the LCST temperature of pristine PNIPAM, which is typically 32 °C. **Figure 7.3** shows the SEM images of a drop-casted (from a 6–8 mg/mL particle suspension in THF) layer of microgels on a silicon wafer.

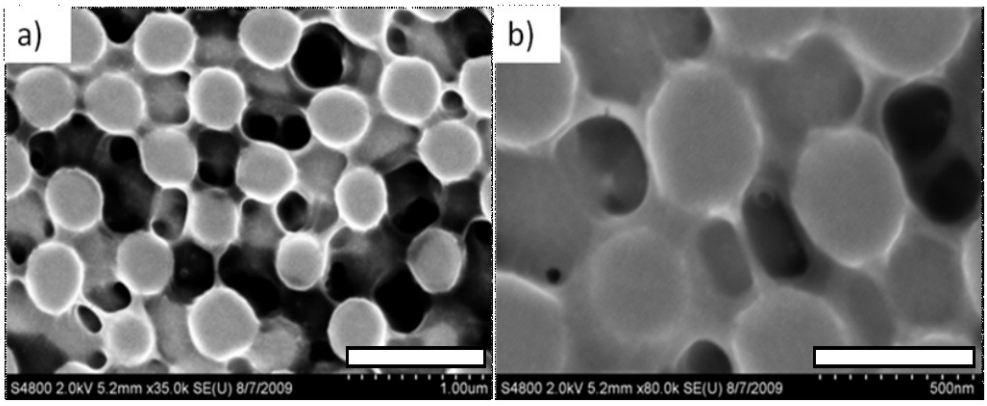

Figure 7.3: SEM images of PNIPAM microgel nanoparticles drop-casted on a silicon wafer from diluted solution. Scale bar: 1 μm (a) and 500 nm (b).

The images confirm that, indeed, nanoparticles with a spherical shape were synthesized. The size of the particles, estimated from the image, is approximately 250±20 nm. The tentacle-like substance surrounding and connecting the particles indicates that the nanoparticles possess a core–shell structure. Scientific literature[24, 31-38] well-documents the core–shell morphology of microgels prepared by precipitation–copolymerization of

NIPAAM and a BIS cross-linker. The phenomenon is associated with the dissimilar copolymerization rates of BIS and NIPAAM. Specifically, the rate is higher for BIS, which is depleted early in the polymerization process. This situation causes formation of the highly cross-linked BIS-enriched cores of the microgel particles. Data on distribution of the AAc units in NIPAAM–BIS–AAc microgel nanoparticles are controversial.[31] Some researchers reported enrichment of the core with AAc fragments, whereas other scientists suggested that the shell contains higher concentration of AAc monomeric units.

To estimate distribution of the components in the particles synthesized in this work, we have determined consumption rates for the monomers during the polymerization. For this purpose, the composition of the polymerizing media was analyzed with proton NMR as a function of polymerization time. The results of the experiment are shown in **Figure 7.4**. It is evident that, in our case, AAc and BIS monomers are consumed much more rapidly than NIPAM. In fact, AAc and BIS are fully consumed at approximately the 20-minute interval. Consequently, we can suggest that the cores of the particles are much more densely cross-linked with BIS and contain a higher ratio of AAc. Moreover, it can be assumed that, even though the nanoparticle synthesis was conducted for 6 hours, the formation of the microgels was practically complete in approximately 40 min.

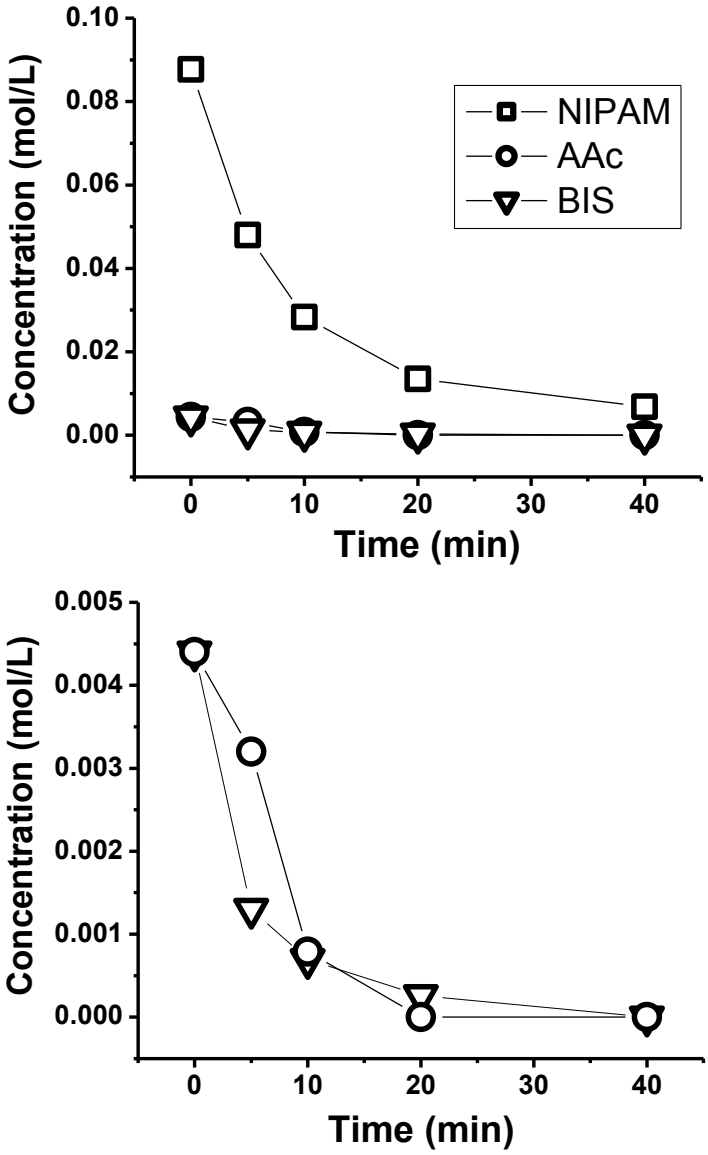

Figure 7.4: Change in concentrations of monomers during the synthesis of microgel nanoparticles. a) Change for NIPAM, AAc, and BIS; b) Change for AAc and BIS only. The concentrations were determined by NMR.

Elemental analysis measurements were taken on the final microgels to estimate the amount of each monomer contained in the particles. From percentages of C, N, H and O, simultaneous mol fraction equations were used to determine the approximate weight percents of the individual monomers present in the microgel particles. Elemental analysis confirmed that NIPAM was the most abundant monomer in the final co-polymer (55 %), and AAc and BIS comprised 21% and 24%, respectively. Coupled with the NMR results, this also suggested the presence of a densely cross-linked core with a high ratio of AAc and BIS and a shell with mostly NIPAM "hairs." Additionally, the obtained NMR and elemental analysis results indicated that, at the end of the polymerization, a PNIPAM homopolymer was formed.

7.3.2:Grafting of PNIPAM Nanogel Layers.

A thin layer of PGMA was deposited onto the surfaces of silicon wafers, glass slides, PVDF fibers, and tungsten wires for the initial surface modification. PGMA, which contains an epoxy group in every repeating unit, has been used extensively as a macromolecular anchoring layer for the grafting of polymers to surfaces.[39] A study of the deposition of PGMA onto various surfaces revealed that a uniform and homogeneous epoxy-containing layer can be obtained on surfaces using either adsorption, spin-coating, or dip-coating. The anchoring layer can be employed to modify various polymeric and inorganic surfaces. Therefore, procedures developed in this work for silicon, glass, PVDF, and tungsten surfaces can be readily adapted to other materials.

In our work, suspension in THF was used to deposit microgel nanoparticles onto

substrates prior to the grafting. The organic solvent was employed instead of an aqueous environment to ensure the formation of a densely packed monolayer of the particles on a surface.

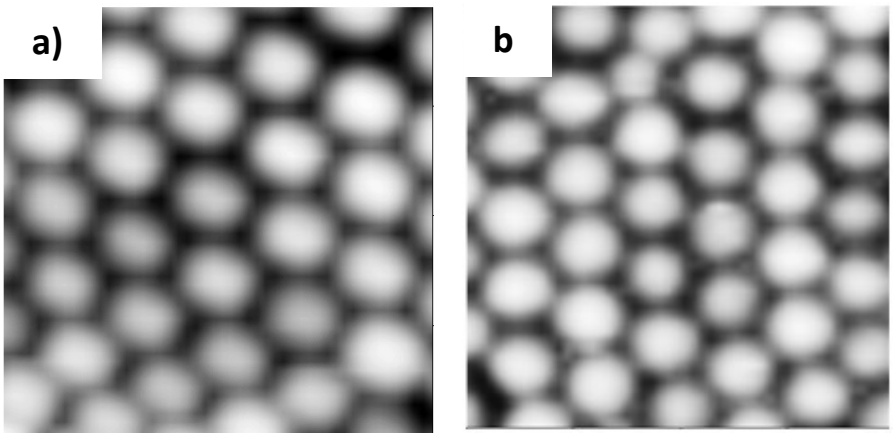

Figure 7.5: AFM topography images (2x2 μm) of microgel nanoparticle monolayer on a silicon wafer: a) before grafting and b) after grafting. Vertical scale 100 nm.

Indeed, previous studies for microgels containing acrylic acid units suggested that close-packed microgel monolayers cannot be formed from water because of the strong ionic inter-particle repulsion originating from the dissociated AAc units.[10, 24, 40-41] **Figure 7.5a** shows an AFM topography image for the "as deposited" monolayer of nanoparticles on the silicon wafer. The particles in the microgel monolayer are nearly monodisperse and close-packed into a periodic hexagonal-like structure. Next, the monolayer samples were annealed at 120 ºC for 2 hours to conduct a reaction between the carboxylic groups of the AAc and the epoxy groups of the PGMA. Previously we demonstrated that, at this temperature, carboxy-terminated PNIPAM macromolecules can be readily grafted onto a

surface via the PGMA anchoring layer.[42] The thickness of the grafted layer measured by ellipsometry was 58 ±2 nm. After the grafting, the structure of the layer remained practically unchanged (**Figure 7.5b**).

Figure 7.6 shows that the grafted layer covers the silicon substrate uniformly at the microscopic level. The root mean square (RMS) roughness of the layer, evaluated from the topographical 10x10 μm AFM image (**Figure 7.6a**), is 5.4 nm. The roughness, which is much lower than the layer thickness, confirmed the formation of a complete monolayer. **Figure 7.6c** shows an SEM image taken at the edge of a silicon wafer to visualize a cross-sectional view of the surface. It is evident that the particles are attached to the surface and assume a "pancake" type of conformation.

The particle density of the grafted layer, estimated from counting the particle surface population, is ~9 particles per μm^2 (**Figure 7.6a**). The center-to-center distance for the particles in the monolayer, measured from the main peak of the 2D Fourier transform of the AFM 10x10 μm topographical image (**Figure 7.6a**), is 300±25 nm. Since the thickness of the layer measured by ellipsometry is only 58 nm, the obtained data confirm that, in the grafted layer, the particles are flattened because of their interaction with the surface. Specifically, the nanoparticles in the dry monolayer adopt this morphology when the horizontal diameter is larger than the vertical. We measured the height of the 30 nanoparticles at the edge of the monolayer and found them to be 70±7 nm. This result corroborates the conclusion drawn from the ellipsometric measurements, i.e., that the particles are squashed towards the surface in a "pancake-like"

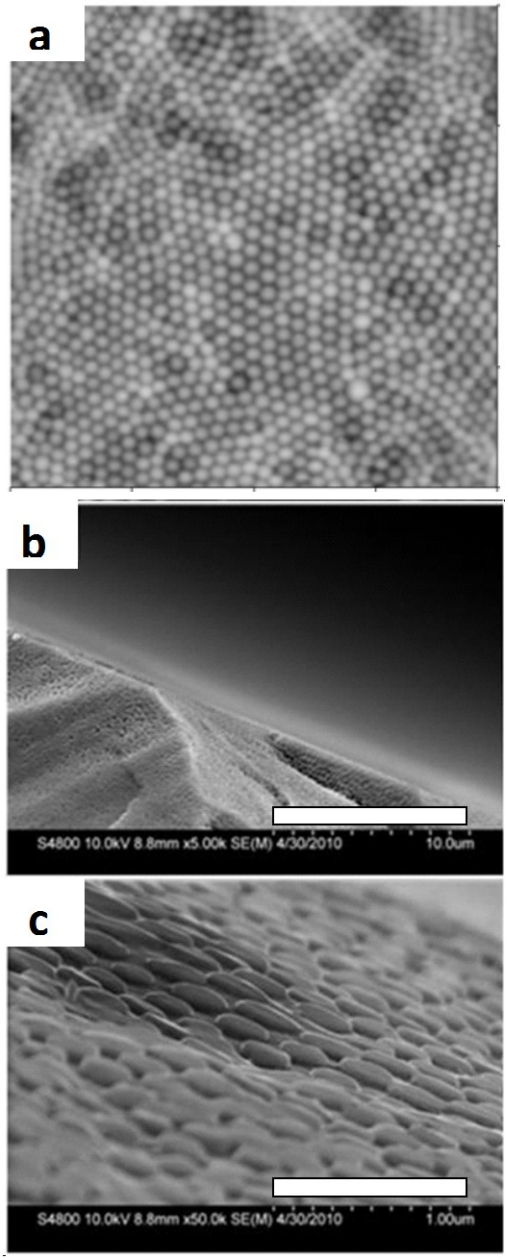

Figure 7.6: a) AFM topographical image (10 x 10 µm) of grafted microgel layer on silicon wafer, vertical scale: 150 nm. SEM images of grafted microgel layer on silicon wafer: b) rough edge of the wafer, scale bar 10 µm; c) close to the wafer edge, scale bar 1 µm.

morphology. AFM data on the particle's height (h) and diameter (center-to-center distance, d) allowed for the estimation of the dry unperturbed particle size, using the volume of the spherical cap-shaped particles (V):[24, 43]

$$V = \frac{1}{6}\pi h\left(3\left(\frac{d}{2}\right)^2 + h^2\right) \tag{7.2}$$

After the volume was found, the diameter of a spherical particle having the same volume was calculated. In this fashion, the dry-state diameter of the microgel particles was determined to be ~163 nm.

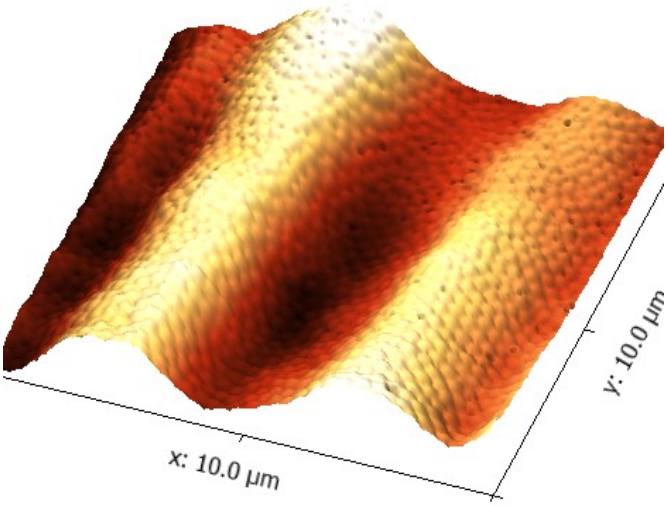

Figure 7.7: AFM topographical image (10 x 10 µm) of grafted microgel layer on tungsten wire, vertical scale: 200 nm.

Figure 7.6b, illustrating the rough edge of the silicon wafer covered with the grafted layer, indicates that the monolayer of particles can be attached to shapes more complex than simple flat silicon wafers and glass slides. In fact, we effectively modified

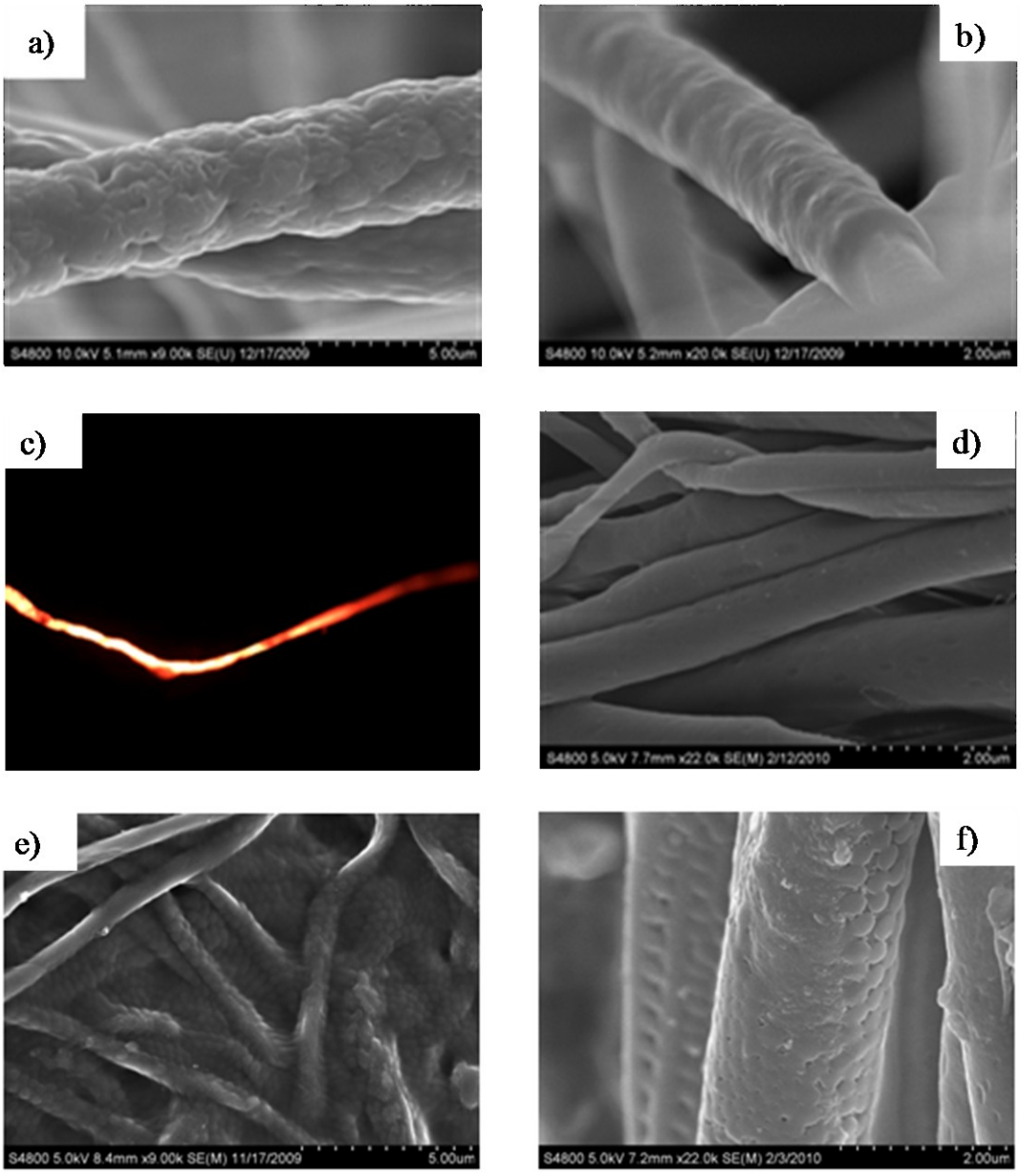

Figure 7.8: a,b) SEM images of virgin PVDF fibers; c) Fluorescent microscopy image of fibers modified with Rhodamine-B-labeled PGMA; d) SEM image of the PGMA-modified fibers; e,f) SEM images of the fibers grafted with microgels. Scale bar: a, e) 5 μm; b,d,f) 2 μm

tungsten wires with the microgel monolayer. The grafted layer covered the surface evenly and possessed virtually the same morphology as the layer grafted to the Si wafer (**Figure 7.7**). Yarns of PVDF fibers (**Figure 7.8a and b**) were covered with the microgel layer as well. In this case, we used Rhodamine B-labeled PGMA to visualize the attachment of the anchoring polymer layer to the fiber surface. Fluorescent microscopic imaging of the fibers confirmed PGMA attachment to the surface (**Figure 7.8c**). A comparison of SEM images for the unmodified (**Figure 7.8a and b**) and modified (**Figure 7.8d**) fibers show as well that the deposition of the anchoring layer was achieved. After the activation of the fibers, the nanoparticles were grafted onto their surface. SEM images of the fibers, after the modification with the particles, are shown in **Figure 7.8e-f**. The images confirm the successful grafting of microgels to the surface. These images clearly show that the particles completely cover the curved surfaces of the fibers, as well as the crevices and pores created between fibers in a monolayer fashion.

7.3.3:Swelling and Collapse of Nanogel Layers as a Function of Temperature

Due to surface confinement, microgel particles can display different switching behavior than do free particles. Toward this end, AFM underwater studies were conducted to determine if the particles in the grafted monolayer demonstrate the ability to swell and collapse with temperature change. In this experiment, the layer was scratched with an ultra-sharp needle to delaminate the layer down to the Si-wafer. The sample was then scanned over the area with the scratch to observe the quality and thickness of the grafted monolayer. **Figure 7.9** shows AFM topographical images of the microgel layer near the scratch recorded at temperatures below (25 ºC) and above (40 ºC) the LCST of

the PNIPAM in water. It is evident that the monolayer swells and collapses at the lower and higher temperature, respectively. The difference in the layer thicknesses when the microgels were collapsed and swollen was measured. For the grafted layer in the collapsed state (**Figure 7.9b**), this thickness was calculated to be ~214 nm and, while in its swollen state, the thickness was calculated to be ~468 nm (**Figure 7.9**). Therefore, the thickness of the grafted microgel layer increases ~2.2 times in the cold water. Since the grafted films extend only in the vertical direction upon crossing the LCST, the volume of the layer changed by a factor of ~2.2. The result indicates that ~272 mg/m^2 of water can be absorbed and released by the layer upon swelling and collapsing, respectively.

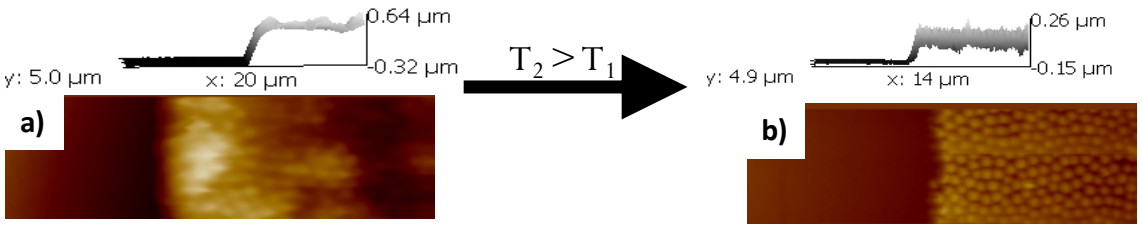

Figure 7.9: AFM topographical images of the scratched grafted-microgel layer under water at temperatures below (a) and above (b) the LCST of PNIPAM.

A significant difference exists between the AFM thicknesses of the dry-grafted layer and the collapsed/swollen layer in water. In fact, the thickness of the dry-grafted layer, estimated from ellipsometry, is ~58 nm. The thickness of the collapsed layer is ~3.5 times higher. Therefore, the water content in the collapsed layer is ~156 mg/m^2 or on the order of 67%. For the swollen layer the water content is ~410 mg/m^2 or 88%. The results obtained for the fractional water content are close to the data reported for

PNIPAM microgel layers that are electrostatically adsorbed on a silicon surface modified with poly(ethyleneimine).[10]

Interestingly, the amount of thickness increase at 25°C the particle layer undergoes can be tuned by the amount of AAc contained in the polymerization feed. **Figure 7.10** displays the layer thickness upon swelling and collapse for particles containing 5 and 10 mol% AAc in the feed. The results show that by increasing the acrylic acid content to 10 mol%, the thickness of the swollen layer effectively increased to 600nm as compared to 468nm in 5 mol% particles. However, the collapsed particle thickness was roughly equal, 200nm. Therefore the effective swelling ratio is increased for 10 mol% particles (2.9) as compared to 5 mol% particles (2.2). Increasing amounts of AAc induce increased amounts of electrostatic repulsion effectively increasing the thickness of the swollen layer.

It is appealing to compare the swelling capacity of the grafted microgel layer synthesized in this work with the swelling capacity of PNIPAM brushes. Kaholek et al. demonstrated that PNIPAM brushes, anchored by the "grafting from" approach to a flat surface, swelled ~3 times in room temperature water compared to the dry state thickness of ~200 nm.[11] For the thinner (15 nm dry thickness) PNIPAM brush, obtained using the "grafting to" method, ~5 times swelling was reported.[12] Conversely, in room-temperature water, the microgel-grafted layer extended ~8 times in the vertical direction from the dry state.

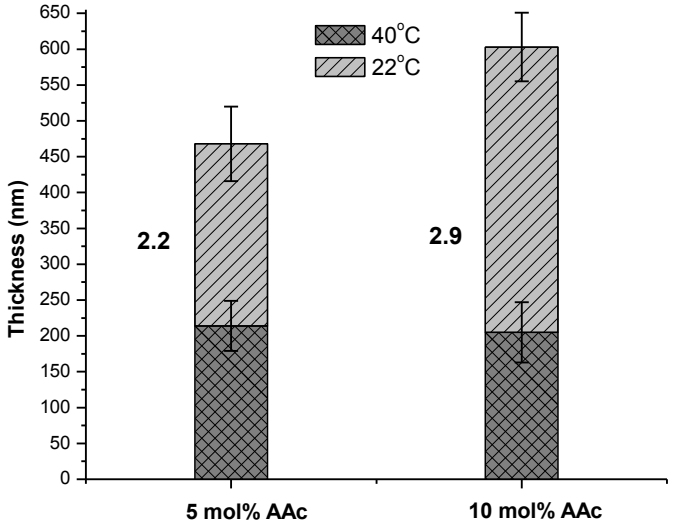

Figure 7.10: AFM thickness of grafted microgel layer under water at different temperatures for PNIPAM containing nanogels with 5 and 10 mol% of AAc.

Therefore, in terms of reversibility and capacity, temperature-induced swelling of microgel-grafted layers can be considered, as a system, comparable to linear PNIPAM brushes with respect to their thermoresponsive properties

Figure 7.11 exhibits the repeatability of the swelling and collapsing of the grafted microgel layer. Three cycles of heating and cooling were performed. Cycles 1 and 2 at 25 ºC were essentially equivalent. However, an increase in thickness was observed during the third cycle, which suggests that the equilibrium time for complete swelling might not have been reached within the first two cycles. At elevated temperatures, a general decrease in thickness was observed from Cycle 1 to Cycle 3. This also suggests that not enough time was given for the complete collapse and expelling of the water. To evaluate

the robustness of the microgel layer upon the swelling−deswelling cycles, we subjected glass slides grafted with a PNIPAM nanoparticle layer, to six heating–cooling cycles in water. The duration of each cycle was two hours: 1 hour at 20 °C and 1 hour at 50 °C. The experiment confirmed the noteworthy robustness of the layers, since no particle removal was observed via AFM imaging.

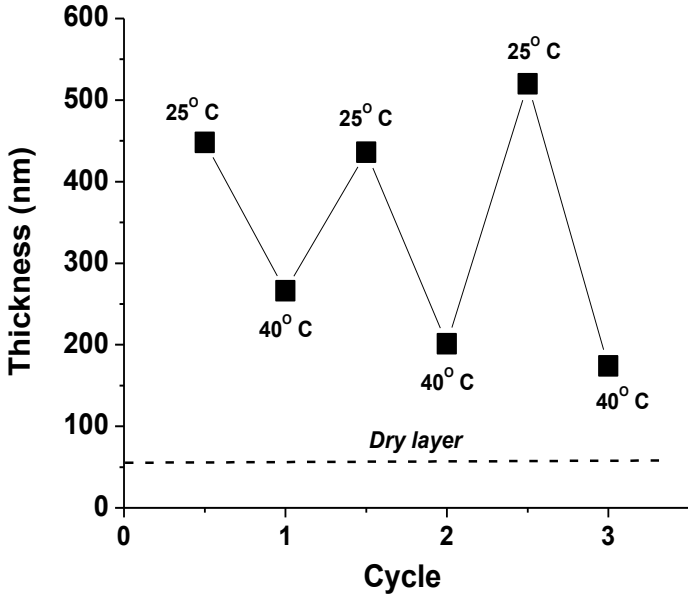

Figure 7.11: AFM thickness of grafted microgel layer under water at different temperatures.

7.3.4:Wettability Switching of Grafted Nanogel Layers

An important property of the grafted PNIPAM layers is their ability to demonstrate temperature-dependant wettability.[13-14, 44] Therefore, we further analyzed the microgel-grafted layer using contact angle measurements taken as a function of temperature. First, advancing contact angles were determined, to confirm the transition of the surface covered with microgels from more hydrophilic to more hydrophobic in

nature. For the measurements, silicon wafers grafted with the nanoparticles were placed inside a temperature-controlled sample cell. Water was continuously fed onto the surface from a needle close to the surface. As the volume of the drop increased, the drop spread and, therefore, it was exposed to the new surface. Video was taken and individual snapshots were captured at points where the drop spread (**Figure 7.12a-b**).

At 23 ºC, the advancing contact angle was measured to be 71 ±2º (**Figure 7.12a**). Upon heating to 50 ºC, the advancing contact angle was determined to be 90.0 ±2º (**Figure 7.12b**). Hence, an approximately 20º increase in the contact angle is observed upon heating above the LCST of PNIPAM. Advancing angle temperature transitions in the similar range were found for the PNIPAM brushes.[13-14] This emphasizes that, analogous to the brushes made of end-grafted linear PNIPAM chains, cross-linked microgel nanoparticles, constituting the grafted layer, also have the ability to rearrange their conformation across the LCST and exhibit a wettability change due to a change in temperature.

We also determined receding contact angles for the surface modified with the grafted microgels **(Figure 7.12c-d**). A significant hysteresis was found to exist between the advancing and receding angles. Namely, the receding contact angles were measured to be 13±2º. The angles were virtually independent from the temperature.

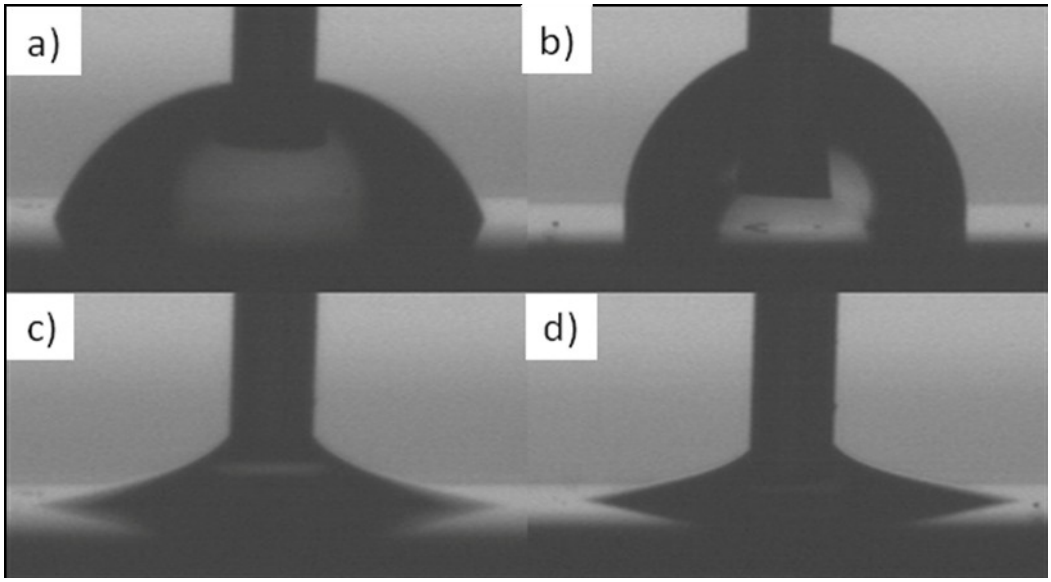

Figure 7.12: Advancing (a,b) and receding (c,d) contact angle snapshots. a) Image taken at 23 °C. Advancing contact angle was calculated to be 71 ± 2°. b) Image was taken at 50 °C. Advancing contact angle was calculated to be 90 ± 2°. c) Image was taken at 23 °C

The phenomenon was already reported for surfaces modified with PNIPAM-grafted layers.[14, 44] The observed result indicates that the PNIPAM-containing microgel particles expose similar chemical groups to the water both below and above the LCST. This effect is also connected with significant water content in the swollen and the collapsed grafted layers.

Wettability measurements were conducted on the tungsten wires modified with the microgel-grafted layers. **Figure 7.13** shows two images of water droplets placed on the modified wire at temperatures above and below the LCST of the microgels. At 20 °C, the water droplet adopts a barrel-like configuration (**Figure 7.13a**). Barrel-like configurations indicate a more hydrophilic surface in nature.[45]

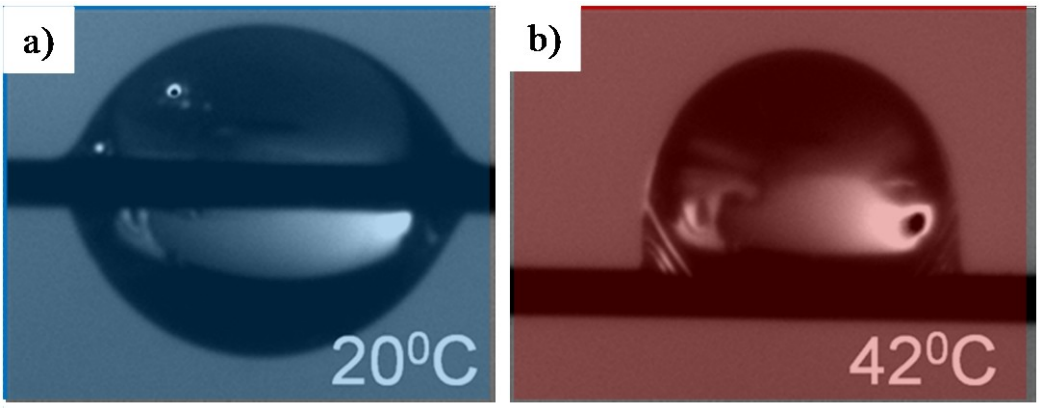

Figure 7.13: Optical images of the water droplet on the tungsten wire modified with grafted microgel layer at different temperatures: a): barrel-like configuration; b): clamshell-like configuration.

This is because the liquid has a greater affinity to the surface, which creates a larger area of interaction between the water and modified wire. Using the image analysis based on the Carroll formulas [46] the contact angle was estimated as ~40°. Contrarily, the drop adopts a clam-shell configuration when placed on the warm wire maintained at 42 °C (**Figure 7.13b**). This is a manifestation of its weak wettability. Typically, the drop forms the clam-shell-like configuration at contact angles of greater than 70°, which indicates that the surface is less hydrophilic.[45] It was also established that the quantitative wetting data significantly depends on the method of measurements. **Figure 7.14a** shows the meniscus formed when a modified tungsten wire is immersed perpendicularly into the 20 °C water. Again, we observe a meniscus that crawls up the side of the wire confirming that the wire surface is wettable. Using the image analysis based on the Lo formulas [47], the contact angle was estimated to be ~ 14°, i.e. it is much smaller than that found for a

droplet. When the temperature was increased to 40°C which is above the LCST of the PNIPAM microgels, the meniscus configuration changed significantly, **Figure 7.14b**.

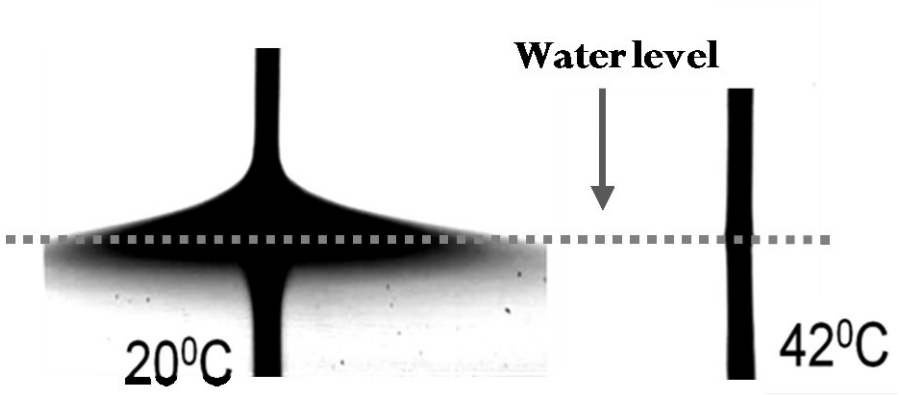

Figure 7.14: Change of the wettability of the tungsten wire grafted with a microgel layer, inserted in water of different temperature.

It became virtually flat, practically perpendicular to the immersed wire. This change directly indicates a change in the surface energy, as this configuration suggests a more hydrophobic surface. The results obtained for the tungsten wires suggest that the grafted microgel layer retains its ability to change morphologically when exposed to external temperature variations on both flat and more complex, curved surfaces.

7.4:Conclusions

The PNIPAM-containing thermoresponsive microgels with carboxy functionalities were synthesized via a surfactant-stabilized, free-radical, precipitation polymerization in an aqueous environment in the presence of acrylic acid as a co-monomer, and BIS as a cross-linker. Analyses indicated that the particles were composed

of a densely cross-linked core containing a high ratio of AAc and BIS, and a shell comprising mostly NIPAM "hairs." A monolayer of the thermoresponsive microgel PNIPAM nanoparticles was grafted onto the surface of silicon wafers, glass slides, PVDF fibers, and tungsten wires. Particle anchoring was conducted by the "grafting to" approach using a PGMA anchoring layer. AFM and SEM studies demonstrated that the grafted layer covered the surfaces uniformly at the microscopic level. The grafted monolayer swelled and collapsed reversibly at temperatures below and above the LCST of the PNIPAM. For the flat silicon substrate, a wettability study of the grafted layer showed ~20º increase in the water advancing contact angle upon heating above the LCST of the PNIPAM. A significant hysteresis exists between the advancing and receding angles, and wettability experiments indicated that the receding angle is virtually independent of temperature for this system. The wettability data obtained for the tungsten wires show that the grafted microgel layer retains its ability to undergo morphological changes when exposed to external temperature variations on complex curved surfaces. Overall, the results obtained demonstrate that, in many aspects, the grafted microgel layer, as a system, is comparable in performance to a PNIPAM brush system with respect to their thermoresponsive properties

7.5:References

1. Luzinov, I.; Minko, S.; Tsukruk, V. V., Responsive brush layers: From tailored gradients to reversibly assembled nanoparticles. *Soft Matter* **2008,** *4* (4), 714-725.

2. Cohen Stuart, M. A.; Huck, W. T. S.; Genzer, J.; Muller, M.; Ober, C.; Stamm, M.; Sukhorukov, G. B.; Szleifer, I.; Tsukruk, V. V.; Urban, M.; Winnik, F.; Zauscher, S.; Luzinov, I.; Minko, S., Emerging applications of stimuli-responsive polymer materials. *Nature Materials* **2010,** *9* (2), 101-113.

3. Huang, X.; Misra, G. P.; Vaish, A.; Flanagan, J. M.; Sutermaster, B.; Lowe, T. L., Novel nanogels with both thermoresponsive and hydrolytically degradable properties. *Macromolecules* **2008,** *41* (22), 8339-8345.

4. Kuckling, D.; Vo, C. D.; Wohlrab, S. E., Preparation of nanogels with temperature-responsive core and ph-responsive arms by photo-cross-linking. *Langmuir* **2002,** *18* (11), 4263-4269.

5. Zhang, J. T.; Liu, X. L.; Fahr, A.; Jandt, K. D., A new strategy to prepare temperature-sensitive poly(n-isopropylacrylamide) microgels. *Colloid and Polymer Science* **2008,** *286* (10), 1209-1213.

6. Kuckling, D., Responsive hydrogel layers-from synthesis to applications. *Colloid and Polymer Science* **2009,** *287* (8), 881-891.

7. Lyon, L. A.; Meng, Z. Y.; Singh, N.; Sorrell, C. D.; John, A. S., Thermoresponsive microgel-based materials. *Chem. Soc. Rev.* **2009,** *38* (4), 865-874.

8. Tokarev, I.; Minko, S., Stimuli-responsive hydrogel thin films. *Soft Matter* **2009,** *5* (3), 511-524.

9. Luzinov, I.; Minko, S.; Tsukruk, V. V., Adaptive and responsive surfaces through controlled reorganization of interfacial polymer layers. *Progress in Polymer Science* **2004,** *29* (7), 635-698.

10. Schmidt, S.; Zeiser, M.; Hellweg, T.; Duschl, C.; Fery, A.; Mohwald, H., Adhesion and mechanical properties of pnipam microgel films and their potential use as switchable cell culture substrates. *Advanced Functional Materials* **2010,** *20* (19), 3235-3243.

11. Kaholek, M.; Lee, W. K.; Ahn, S. J.; Ma, H. W.; Caster, K. C.; LaMattina, B.; Zauscher, S., Stimulus-responsive poly(n-isopropylacrylamide) brushes and nanopatterns prepared by surface-initiated polymerization. *Chemistry of Materials* **2004,** *16* (19), 3688-3696.

12. Bittrich, E.; Kuntzsch, M.; Eichhorn, K. J.; Uhlmann, P., Complex ph- and temperature-sensitive swelling behavior of mixed polymer brushes. *Journal of Polymer Science Part B-Polymer Physics* **2010,** *48* (14), 1606-1615.

13. Balamurugan, S.; Mendez, S.; Balamurugan, S. S.; O'Brien, M. J.; Lopez, G. P., Thermal response of poly(n-isopropylacrylamide) brushes probed by surface plasmon resonance. *Langmuir* **2003,** *19* (7), 2545-2549.

14. Plunkett, K. N.; Zhu, X.; Moore, J. S.; Leckband, D. E., Pnipam chain collapse depends on the molecular weight and grafting density. *Langmuir* **2006,** *22* (9), 4259-4266.

15. Ying, L.; Kang, E. T.; Neoh, K. G., Synthesis and characterization of poly(n-isopropylacrylamide)-graft-poly(vinylidene fluoride) copolymers and temperature-sensitive membranes. *Langmuir* **2002,** *18* (16), 6416-6423.

16. Da Silva, R. M. P.; Mano, J. F.; Reis, R. L., Smart thermoresponsive coatings and surfaces for tissue engineering: Switching cell-material boundaries. *Trends in Biotechnology* **2007,** *25* (12), 577-583.

17. Jagur-Grodzinski, J., Polymeric gels and hydrogels for biomedical and pharmaceutical applications. *Polymers for Advanced Technologies* **2010,** *21* (1), 27-47.

18. Hamidi, M.; Azadi, A.; Rafiei, P., Hydrogel nanoparticles in drug delivery. *Advanced Drug Delivery Reviews* **2008,** *60* (15), 1638-1649.

19. Kim, S.; Kim, J. H.; Jeon, O.; Kwon, I. C.; Park, K., Engineered polymers for advanced drug delivery. *European Journal of Pharmaceutics and Biopharmaceutics* **2009,** *71* (3), 420-430.

20. Zhang, Q. S.; Zha, L. S.; Ma, J. H.; Liang, B. R., A novel route to prepare ph- and temperature-sensitive nanogels via a semibatch process. *Journal of Colloid and Interface Science* **2009,** *330* (2), 330-336.

21. Rieger, J.; Grazon, C.; Charleux, B.; Alaimo, D.; Jerome, C., Pegylated thermally responsive block copolymer micelles and nanogels via in situ raft aqueous dispersion polymerization. *Journal of Polymer Science Part a-Polymer Chemistry* **2009,** *47* (9), 2373-2390.

22. Liu, H. X.; Wang, C. Y.; Gao, Q. X.; Liu, X. X.; Tong, Z., Magnetic hydrogels with supracolloidal structures prepared by suspension polymerization stabilized by fe_2o_3 nanoparticles. *Acta Biomaterialia* **2010,** *6* (1), 275-281.

23. FitzGerald, P. A.; Dupin, D.; Armes, S. P.; Wanless, E. J., In situ observations of adsorbed microgel particles. *Soft Matter* **2007,** *3* (5), 580-586.

24. Horecha, M.; Senkovskyy, V.; Synytska, A.; Stamm, M.; Chervanyov, A. I.; Kiriy, A., Ordered surface structures from pnipam-based loosely packed microgel particles. *Soft Matter* **2010,** *6* (23), 5980-5992.

25. Zdyrko, B.; Iyer, K. S.; Luzinov, I., Macromolecular anchoring layers for polymer grafting: Comparative study. *Polymer* **2006,** *47* (1), 272-279.

26. Zdyrko, B.; Hoy, O.; Kinnan, M. K.; Chumanov, G.; Luzinov, I., Nano-patterning with polymer brushes via solvent-assisted polymer grafting. *Soft Matter* **2008,** *4* (11), 2213-2219.

27. Burtovyy, O.; Klep, V.; Chen, H. C.; Hu, R. K.; Lin, C. C.; Luzinov, I., Hydrophobic modification of polymer surfaces via "grafting to" approach. *Journal of Macromolecular Science Part B-Physics* **2007,** *46* (1), 137-154.

28. Meunier, E., *Colloidal particles: Synthesis and chracterization* CRC Press: 2003.

29. Li, X.; Zuo, J.; Guo, Y. L.; Yuan, X. H., Preparation and characterization of narrowly distributed nanogels with temperature-responsive core and ph-responsive shell. *Macromolecules* **2004,** *37* (26), 10042-10046.

30. Singh, N.; Husson, S. M.; Zdyrko, B.; Luzinov, I., Surface modification of microporous pvdf membranes by atrp. *Journal of Membrane Science* **2005,** *262* (1-2), 81-90.

31. Christensen, M. L.; Keiding, K., Study of the compositional heterogeneity in poly (n-isopropylacrylamide-acrylic acid) microgels by potentiometric titration experiments. *Colloid Surf. A-Physicochem. Eng. Asp.* **2005,** *252* (1), 61-69.

32. Pelton, R. H.; Chibante, P., Preparation of aqueous lattices with n-isopropylacrylamide. *Colloids and Surfaces* **1986,** *20* (3), 247-256.

33. Rodriguez, B. E.; Wolfe, M. S.; Fryd, M., Nonuniform swelling of alkali swellable microgels. *Macromolecules* **1994,** *27* (22), 6642-6647.

34. Saunders, B. R., On the structure of poly(n-isopropylacrylamide) microgel particles. *Langmuir* **2004,** *20* (10), 3925-3932.

35. Mason, T. G.; Lin, M. Y., Density profiles of temperature-sensitive microgel particles. *Physical Review E* **2005,** *71* (4), 040801.

36. Stieger, M.; Pedersen, J. S.; Lindner, P.; Richtering, W., Are thermoresponsive microgels model systems for concentrated colloidal suspensions? A rheology and small-angle neutron scattering study. *Langmuir* **2004,** *20* (17), 7283-7292.

37. Fernandez-Barbero, A.; Fernandez-Nieves, A.; Grillo, I.; Lopez-Cabarcos, E., Structural modifications in the swelling of inhomogeneous microgels by light and neutron scattering. *Physical Review E* **2002,** *66* (5), 10.

38. Wu, X.; Pelton, R. H.; Hamielec, A. E.; Woods, D. R.; McPhee, W., The kinetics of poly(n-isopropylacrylamide) microgel latex formation. *Colloid and Polymer Science* **1994,** *272* (4), 467-477.

39. Zdyrko, B.; Luzinov, I., Polymer brushes by the "grafting to" method. *Macromolecular Rapid Communications* **2011,** *32* (12), 859-869.

40. Schmidt, S.; Hellweg, T.; von Klitzing, R., Packing density control in p(nipam-co-aac) microgel monolayers: Effect of surface charge, ph, and preparation technique. *Langmuir* **2008,** *24* (21), 12595-12602.

41. Schmidt, S.; Motschmann, H.; Hellweg, T.; von Klitzing, R., Thermoresponsive surfaces by spin-coating of pnipam-co-paa microgels: A combined afm and ellipsometry study. *Polymer* **2008,** *49* (3), 749-756.

42. Klep, V.; Zdyrko, B.; Luzinov, I., Pnipaam gradient polymer brushes. *PMSE Preprints* **2005,** ***93***, 462.

43. Hofl, S.; Zitzler, L.; Hellweg, T.; Herminghaus, S.; Mugele, F., Volume phase transition of "smart" microgels in bulk solution and adsorbed at an interface: A combined afm, dynamic light, and small angle neutron scattering study. *Polymer* **2007,** *48* (1), 245-254.

44. Liang, L.; Feng, X. D.; Liu, J.; Rieke, P. C.; Fryxell, G. E., Reversible surface properties of glass plate and capillary tube grafted by photopolymerization of n-isopropylacrylamide. *Macromolecules* **1998,** *31* (22), 7845-7850.

45. McHale, G.; Newton, M. I., Global geometry and the equilibrium shapes of liquid drops on fibers. *Colloids and Surfaces a-Physicochemical and Engineering Aspects* **2002,** *206* (1-3), 79-86.

46. Carroll, B. J., The accurate measurement of contact angle, phase contact areas, drop volume, and la place excess pressure in drop-fiber systems. *Journal of Colloid and Interface Science* **1976,** *57* (3), 488-95.

47. Lo, L. L., The meniscus on a needle - a lessson in matching. *Journal of Fluid Mechanics* **1973,** *132*, 65-78.

CHAPTER 8:DEVELOPMENT OF THERMALLY RESPONSIVE BRUSH LIKE LAYERS FROM GRAFTABLE NANOGELS: PART 2

8.1:Introduction

In **Chapter 7**, we presented a "grafting to" approach that produced much thicker, thermoresponsive PNIPAM grafted layers, while preserving the straightforward and simplistic manner of the "grafting to" approach. Namely, PNIPAM cross-linked particles containing small amounts of acrylic acid were synthesized with the idea to utilize the carboxyl group functionality of acrylic acid monomer to covalently attach the particles to the macromolecular (PGMA) anchoring layer. The behavior of the grafted layer was comparable to prior data published on linear PNIPAM grafted brushes[1-4] with respect to their thermoresponsive properties. Additionally, it was possible to tune the size of the synthesized particles, while simultaneously tuning the thickness of the grafted layer. Cross-linked nano and microgels of PNIPAM bridge the gap between grafted polymer layers and macroscopic gels, while also bringing their own set of advantages. Advantages found include; rapid phase transition, robustness, and straightforward tunablilty in relation to chemical composition.[5] While most published results regarding thin films of microgel particles have dealt with layer-by-layer formation[5-6] of the particle layer, our efforts deliver a more robust approach with the chemical anchoring of particle layers.

Dating back, PNIPAM particles have been commonly synthesized using conventional free radical polymerization techniques such as; emulsion polymerization without the use of surfactant, or more commonly surfactant stabilized precipitation

polymerization.[7-12] Recent advances in living polymerization techniques, specifically reversible-addition fragmentation chain transfer (RAFT) polymerization, have given rise to large variety of possible synthetic polymers with well defined and complex architectures.[13] Rieger et al. developed a technique to synthesize nanometric pegylated thermoresponsive core-shell particles directly in water. They conducted a RAFT-controlled radical crosslinking mechanism, where the macro-RAFT agent served for both the stabilization and polymerization control mechanism. It was found that the stability and size of the resulting particles were dependent on the concentration of the monomer, cross-linker, and the length of the macro-RAFT agent used. This technique allows the possibility towards functional groups located on the shell of the particle by copolymerizing these particles with functional monomers.[13]

Wenqing et al. used macro-RAFT polymerization method to synthesize a core-shell nanogel directly in water using poly(ethylene glycol) and/or nonlinear polymers using oligo(ethylene glycol). They were able to efficiently synthesize particles with tunable sizes and thermosensitivities with the idea to create biocompatible and antifouling nanogels.[14] Pegylated amphilic macro-RAFT agents were also used in one pot synthesis to create cationic nanogels at sizes sub 30nm in diameter. The amphiphilic RAFT agent was used to stabilize the resulting micelles formed of pegylated poly(N,N'-Dimethylaminoethyl methacrylate), and control the subsequent cross-linking.[15] The adaptability in using the macro-RAFT aqueous dispersion technique was exhibited by Sun and colleagues, by carrying out the RAFT polymerization of N,N-Dimethylacrylamide and NIPAM in moderately frozen aqueous conditions. Researchers

created chemically degradable "cryogels" by incorporating disulfide branching agents throughout the polymerization.[16]

The aim of the work presented in **Chapter 8** is the synthesis and characterization of covalently graftable thermally responsive nanogels obtained by the macro-RAFT aqueous dispersion polymerization resulting in smaller particle diameter size compared to the ones reported results in **Chapter 7**. Coatings in the ranges of 250-600nm were observed (**Chapter 7)**, however, we wanted to create particle coatings smaller than 250nm but thicker (>30nm) than films produced by traditional "grafting to" procedures. This was achieved via diblock copolymers in **Chapter 4**, however, we aimed to preserve the advantages of brush like particle coatings, including rapid phase transition and ease of chemical composition tunability.[17]

Polymerizations were conducted in the presence of N,N'-methylenebisacrylamide (BIS) and a macro-RAFT agent functionalized with carboxylic acid groups throughout the backbone. Prior work has shown that this method produces functional groups that are located throughout the core-shell structure of the resulting nanogels.[13] The newly prepared nanogels remained stable in aqueous dispersions due to electrostatic repulsion of the covalently attached hairy polyelectrolyte shell. The present strategy is predicated on the utilization of acrylic acid macroRAFT agents for the direct synthesis of PNIPAM containing thermally responsive nanogels particles in water, similar to published results for pegylated nanogel derivatives.[13, 18 19]

Rieger and coworkers determined that the synthesis utilizing macro RAFT agents produced thermally responsive PNIPAM containing nanogels with functional units having a homogenous composition throughout the particle, in contrast to our previous work where functional groups where located internally in the core of the particle.[17] Pegylated responsive particles synthesized by Rieger et al. were smaller than 100nm, the target size range for the current work.[13] Acrylic acid was incorporated chemically to introduce carboxylic acid groups in order to generate thermally responsive and graftable nanogels with which the acrylic acid will be located throughout the particle, and thus, on the exterior of the nanogels.

The one-pot particle formulation is synthesized and cross-linked in the absence of surfactant forming auto-stabilized particles coated with hairy like acrylic acid shells.[13] As Rieger et al.[13] found with pegylated versions of responsive nanoparticles, the straightforward approach relies on the fact that the macroRAFT agent acts as the chain transfers agent and particle stabilizer.

The available carboxylic acid groups on the particle surface were used to covalently attach the particles to surfaces pre modified with an epoxy containing polymer anchoring layer.[17] Particles were attached to silicon wafers and PVDF yarns. The layers were imaged by atomic force microscopy (AFM) and scanning electron microscopy (SEM). Inclusion of PNIPAM and the presence of carboxyl groups were investigated using infrared spectroscopy techniques. Swelling and collapsing of particles in aqueous solutions at different temperatures was monitored by dynamic light scattering (DLS).

Interestingly, it was found that particle layer thickness of the initial deposited layer could be manipulated by different solvents used for dip-coating.

8.2:Experimental

8.2.1:Synthesis and Fabrication of Macromolecules and Fibers

All reagents were used without further purification. 2,2'-Azobis (2-methylpropionamide) dihydrochloride 97% (AAPH) and N,N'-methylenebisacrylamide 98% (BIS) were purchased from Aldrich. N-Isopropylacrylamide 99% (NIPAM) was purchased from Aldrich. Water (pH-6.0) was deionized at a resistivity of 18 MΩ using a Millipore Milli-Q water purification system. Glycidyl methacrylate (Sigma Aldrich) was polymerized free radically to produce PGMA, M_n = 135 000 g mol^{-1}, PDI = 2.97.[20] The polymerization was conducted in methyl ethyl ketone (MEK, VWR) at 60°C. Polymerization initiation was carried out using Azobisisobutyronitrile, AIBN (Sigma Aldrich). The polymer product was purified by multiple precipitations from diethyl ether. Rhodamine –B was used to label PGMA via a reaction between the epoxy groups of PGMA and the carboxyl groups of the dye as described elsewhere.[21] Macromolecular RAFT agents containing AAc units (PAAc-macroRAFT, Mn = 7800, g/mol, PDI = 1.66) in the backbone were synthesized by Rieger group at CERM (Paris, France) according to procedures published elsewhere.[13] PVDF fibers were produced as discussed in **Section 7.2.1** by Kornev Group (Clemson University).

Morphology of grafted layers of PNIPAM nanogel films were imaged using a Veeco Dimensions 3100 Atomic Force Microscopy (AFM) in tapping mode. A silicon

cantilever with a force constant of 40 N m^{-1} was used. Ellipsometry measurements were acquired as written in **Section 3.3.3.1.** Scanning electron microscopy imaging was carried out using a Field Emission Hitachi S4800 SEM. To investigate the hydrodynamic diameter of synthesized PNIPAM nanogels above and below the LCST, dynamic light scattering measurements were conducted on a Malvern Nanosizer Nano-ZS DLS. To confirm the inclusion of the carboxylic acid functionalized RAFT agent within the PNIPAM particles, Fourier-transfer infrared spectroscopy (FT-IR) was performed using a Thermo Nicolet Magna 550 FT-IR Spectrometer equipped with a Thermo Spectro-Tech endurance diamond ATR. Data was analyzed with Omnic software.

8.2.2:Synthesis of Nanogels

The *in-situ* RAFT aqueous dispersion polymerization of PNIPAM functionalized nanogels was carried out as follows (**Figure 8.1**). Overall, we followed a modified procedure reported by Rieger et al.[13] To a 15 ml round bottom flask, 178 mg (.0016mol) of NIPAM, 68 mg ($1.33x10^{-5}$mol) of the PAAc-macroRAFT agent, 6 mg ($3.89 x10^{-5}$) of BIS, and 1.0 mL from a stock solution of 1.4 X 10^{-3}M aqueous solution of AAPH. Reactants were dissolved in 10 mL of deionized water. The round bottom flask was septum sealed and equipped with a nitrogen inlet, outlet, and a magnetic stir bar. The reaction solution was purged with nitrogen for 45 minutes in an ice bath to remove any dissolved oxygen, and subsequently placed in a water bath held constant at 70°C to initiate polymerization, while under a continuous nitrogen blanket. The reaction was allowed to proceed for 90 minutes at a stir speed of 250 rpm.

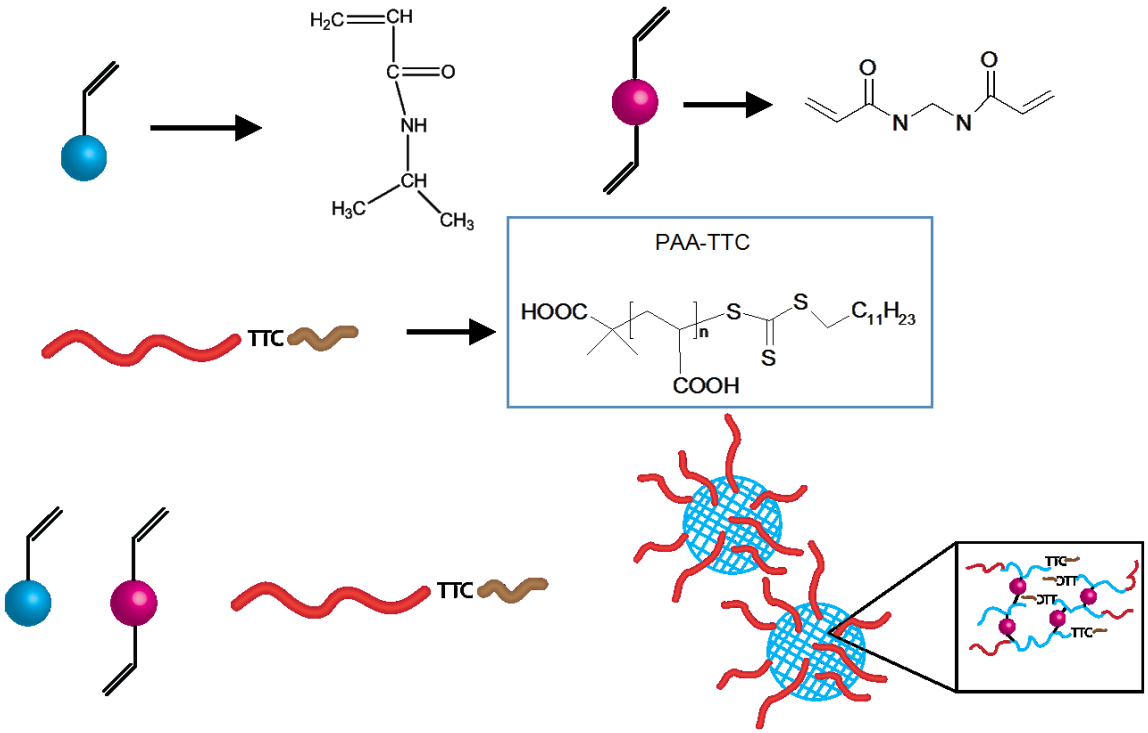

Figure 8.1: Overall synthetic schematic of carboxy functionalized PNIPAM nanogels by in-situ RAFT aqueous dispersion polymerization. Redrawn from Ref.[13]

To halt the polymerization, the reaction vessel was submerged in an ice bath. To purify the product, aliquots were centrifuged, decanted, and re-dispersed in fresh H_20 three times, followed by three cycles in fresh tetrahydrofuran (THF, OmniSolv). Although, Rieger et al. showed in previous synthesis that reactions had little to no contaminants due to total inclusion of the macro-RAFT agent, and bringing the polymerization to completion[13].

8.2.3:Grafting of Nanogels

Grafting of RAFT-nanogels to model silicon wafers was executed as described here. Polished single-crystal wafers (Semiconductor Processing Co.) were prepared as described in **Chapter 3**. Before attachment of PNIPAM nanogels to the silicon wafers, a thin layer of PGMA was attached. To do so, a 0.14% w/v solution of PGMA in chloroform (Spectrum) was made, and clean wafers were then dip-coated (Mayer Feintechnik D-3400, speed 240 mm min^{-1}) into the polymer solution. Dip-coated wafers were annealed under vacuum at 120°C for 20 min. Following annealing, wafers were rinsed three times for 10 minutes in fresh chloroform to remove any unattached polymer. Typically, this procedure produces PGMA film thickness approximately 6nm in thickness, as determined by ellipsometry measurements. A solution of approximately 6-8 mg mL^{-1} of PNIPAM nanogels dispersed in THF was used to deposit nanogel particles on the surface of PGMA modified wafers. Usually, 2-3 subsequent (multiple dip-coatings were performed before annealing) dips were needed to create a monolayer. Following dip-coating, samples were annealed under vacuum at 120°C for 2 hours. Samples were then rinsed 3 times for 10 minutes in fresh THF to remove any unattached particles from the surface of the wafers. Surface attachment to electrospun PVDF fibers was carried out as described in **Section 7.2.4**.

8.2.4:Thermoresponsive Behavior of Nanogels

To study the temperature responsive behavior and size of the as synthesized RAFT-nanogels, dynamic light scattering (DLS) was employed. A Malvern Zetasizer nanoZS particle analyzer (Malvern Intruments Ltd, Malvern UK) was used (Mefford

Group, Clemson University) to monitor the hydrodynamic diameter change of PNIPAM particles at varying temperatures in ultrapure deionized water (pH = 6.0). A 4.0mW, solid state He-Ne laser at a wavelength of 633nm was used as the light source. The NanoZS measures at a scattering angle of 173° to reduce the effect of multiple scattering due to any contaminants.[22] Zetasizer Nano 4.2 software (Malvern) was utilized to calculate intensity, volume, and number average diameters. PNIPAM particle solutions were run from 25-38C° at 2 degree intervals.

8.3:Results and Discussion

8.3.1:Characterization of RAFT Synthesized Nanogels

At polymerization temperature of 70°C, the reaction solution was opaque. Upon quenching the reaction to temperatures below the LCST of pristine PNIPAM, the solution undertook a transition from opaque at elevated temperatures to transparent below the critical temperature. This observation was the first indication that the nanogel particles exhibited thermally reversible properties in an aqueous environment. **Figure 8.2a-b** displays AFM scans of grafted nanogels to a silicon wafer dip-coated from a solution in THF. The image verifies that nanogels of spherical shape were synthesized.

To validate the inclusion of PNIPAM (amide peaks) and AAc (carboxyl peaks) chemical functionalities into the resulting particles, infrared spectroscopy was used. A solution PNIPAM nanogels was deposited and dried on a Zn-Se crystal. **Figure 8.3** shows

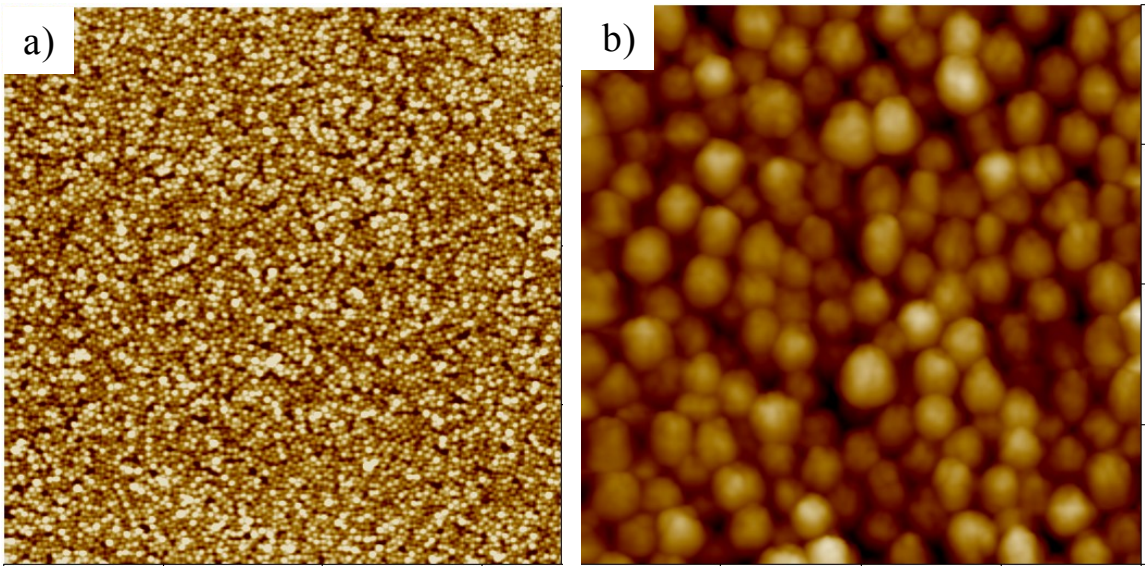

Figure 8.2: AFM topography image of the RAFT-nanogel layer on a silicon wafer after dip-coating and grafting from THF. a) 7 x 7 µm; vertical scale 25nm. b) 1x1 µm; vertical scale 70nm

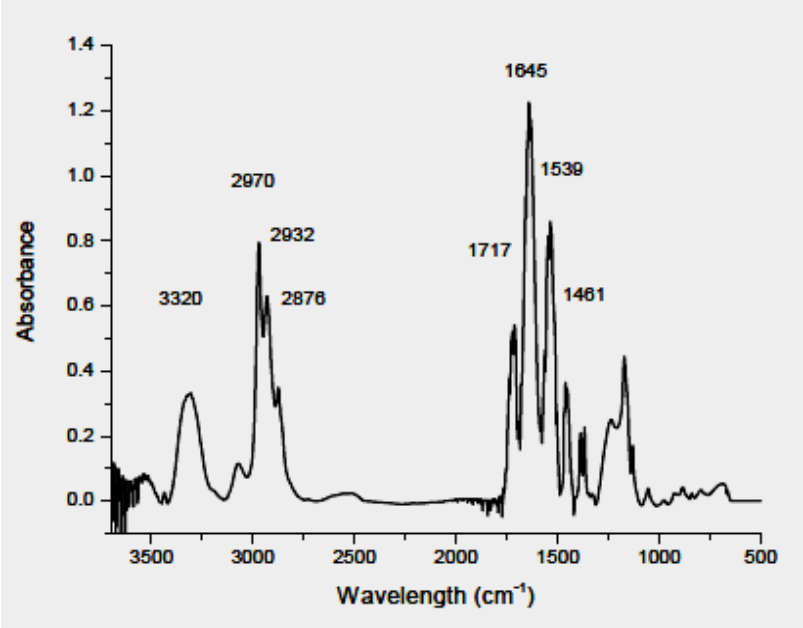

Figure 8.3: FT-IR spectra of carboxy functionalized PNIPAM nanogels.

ATR FT-IR spectrum of the particle layer deposited on the crystal. On the spectrum, characteristic peaks of PNIPAM, bands at; 1644 cm^{-1} and 1535 cm^{-1} (Amide I and II bands respectively) are present. The spectrum also shows characteristic peaks for acrylic acid; bands at; 1717 cm^{-1} (C=O stretching from free carboxylic peak) and 3200 cm^{-1} (O-H stretch). Indeed, successful inclusion of thermo responsive entity PNIPAM, and reactive AAc units was achieved.

8.3.2:Thermo-Responsive Behavior of PNIPAM RAFT-Nanogels

To confirm the ability for the synthesized particles to undergo a volume phase transition with changes in temperature, DLS measurements were conducted above and below the LCST for PNIPAM linear macromolecules. To do so, a solution of PNIPAM nanogels (6-8 mg/mL) in deionized water (pH=6) was used to fill a cuvette and placed into the DLS temperature chamber. At this pH, acrylic acid should be in the deprotonated form and provide electrostatic stability for the nanogels in solution, therefore, resulting in higher quality correlation functions due to lower multiple scattering and decreased polydispersity from agglomeration. DLS measurements were taken at temperatures from 25ºC -38ºC in 2º step intervals. **Figure 8.4** displays the hydrodynamic diameter in nm vs. temperature. Values for the diameter were taken as z-average diameters. Although not a sharp transition is observed, the curve indicates that there is swelling and collapsing relationship vs. temperature for the synthesized particles. Beginning at 25ºC, the hydrodynamic diameter is approximately 103nm. At 29ºC, a decrease in the diameter to around 93nm is seen. From 32-38 ºC the diameter decreased and stayed constant at

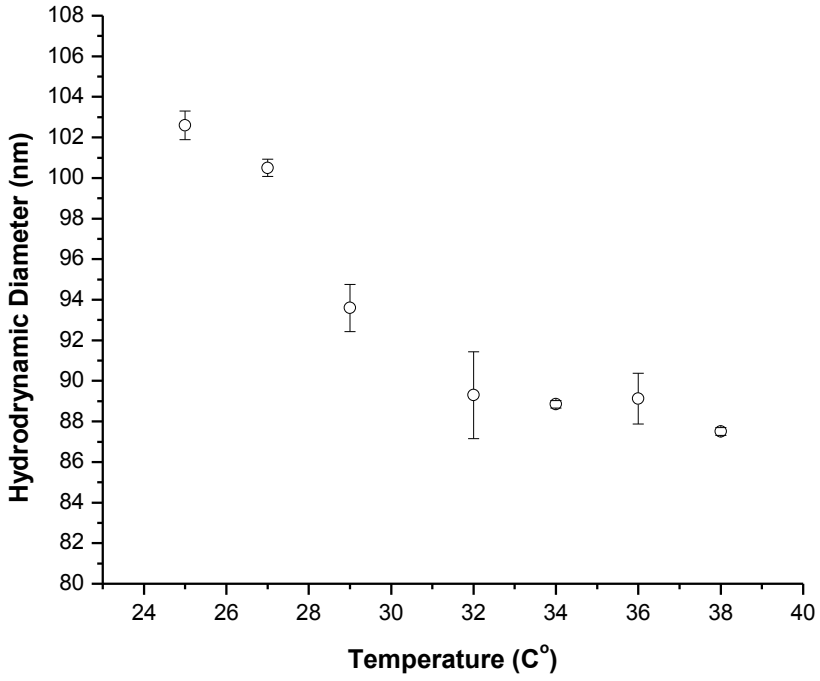

Figure 8.4: Hydrodynamic diameter vs. temperature as measured by DLS. Diameter values were taken as Z-average.

approximately 88nm. Although it is not a sharp volume phase transition similar to that of linear PNIPAM, there is a change in about 15nm in diameter across the LCST, roughly a 15% decrease in size. Increased error is observed through the transition temperature range (**Figure 8.4**). We foresee that this effect comes from the amount of equilibration time at the different temperatures. Temperatures were equilibrated for 15 minutes at each temperature prior to analysis. Therefore, the equilibrium time for complete swelling may have exceeded the time allowed for temperature equilibration.

Interestingly, the synthesized RAFT-nanogels did not exhibit traditional trends seen with copolymerization of PNIPAM and AAc in terms of temperature responsive solution behavior. Literature has shown that such copolymerizations, depend on the amount of AAc in the polymerization feed, led to an increase in the LCST temperature of the PNIPAM and AAc copolymers upwards towards 50°C.[23-26] Bokias et al. attributed the observation to influences from intrachain hydrogen bonding between AAc and NIPAM units effectively altering the phase behavior.[23] However, in our case DLS data revealed that while the LCST transition was broad (27-32°C), no dramatic increases in the transition temperature of the RAFT-nanogels was observed. Presumably, since the AAc units are located in periphery of the particle, intrachain hydrogen bonding between deprotonated carboxy units and amide units are not prevalent which would cause a noticeable increase in transition temperature.

The nanogel diameter increases ~ 1.2 times in cold water. Assuming the particles take on a perfect sphere in solution, the change in volume upon decreasing temperature below the LCST was determined to be $3.9 \times 10^{-4} \mu m^3$, ~32% increase in volume. Therefore, it can be concluded that the water content of the swollen particles (below LCST) is 3.9×10^{-11} ng, thus 68% of the volume of the expanded particle is due to water absorption. This is roughly a ~1.3 times decrease in water content found from our previous results for PNIPAM particle water composition when attached to a substrate.[17] This leads to the observation that the macroRAFT synthesis produced a denser crosslinked core. This has lead to the smaller overall decrease in diameter upon raising

the temperature over the LCST of RAFT-nanogels (~15% decrease) as compared to nanogels synthesized (~ 70% decrease) in **Chapter 7.**

8.3.3:Grafting of RAFT-Nanogel Particles to Silicon Wafer

Prior to deposition of PNIPAM nanogels, a thin layer of PGMA was deposited onto flat silicon wafers and PVDF fibers. PGMA is used as a macromolecular anchoring layer for the covalent attachment of polymers due to the epoxy group located in the repeat unit of the monomer.[20, 27-31] In prior publications, it was found that PGMA can be deposited onto various surfaces forming uniform and homogenous epoxy containing layers by dip-coating, spin-coating, or adsorption. We have shown in **Chapter 7** that this method can be readily adapted to different surfaces for grafting of polymeric nanoparticles. A suspension of the synthesized particles in THF was used for the deposition. An organic solvent was used to help the formation of tightly packed, dense monolayers of particles. Reason being, in water AAc (pKa = 4.2) becomes ionic in nature resulting in a colloidal stabilization effect. Literature has shown that particular PNIPAM particles copolymerized with AAc has proved to be difficult in forming tightly packed layers due to the ionic inter-particle interactions formed in an aqueous environment.[5, 32-34]

Annealing at 120°C has proved to be sufficient to create a covalent bond between the carboxylic groups from AAc and the epoxy groups from PGMA[35]. After the annealing, particle layers were rinsed in a series of solvents of varying polarity to confirm complete grafting. **Figure 8.2a-b** shows AFM topography (7 x7 and 1 x 1 μm

respectively) images for a layer of nanogels dip-coated from THF and grafted to a PGMA modified silicon wafer. The AFM images demonstrate that substrates can be completely and uniformly covered by the macro-RAFT synthesized particles. The particles appear to be nearly mono-disperse, but do not seem to pack in a hexagonal fashion as conventional free radical synthesized particles have.[17] **Figure 8.2b** shows that slight stacking occurs in the layer, however mostly a monolayer of particles is present.

The average vertical distance (diameter) of the "dry" particles as deposited from THF was found to be about 45 nm, while the average horizontal distance was about 98 nm according to AFM profile measurements. Again, it is evident that particles form an interaction with the surface of the wafer. Due to the fact that the horizontal distance is much larger than the vertical, a "pancake" type morphology is created. From the AFM data of the horizontal and vertical distances of the grafted particle, the dry unperturbed particle size was calculated using the volume of a spherical cap-shaped particle **Equation(7.2)**[32, 36]:

Using the volume found from the equation above, the diameter of a spherical particle having the same volume was calculated. The dry-state apparent diameter of the nanogel particles deposited from THF was found to be ~75nm. This is roughly a 2.2 times decrease in diameter from particles synthesized by free radical surfactant stabilized precipitation polymerization (163nm) reported in **Chapter 7**. Indeed the macroRAFT polymerization technique was successful in generating smaller PNIPAM functionalized nanogels.

Interestingly, it was found that by changing the solvent used for dip-coating, the vertical height or thickness of the resulting particle layer could be altered. **Figure 8.5a-b** displays RAFT-nanogel layers deposited on silicon wafers from dimethyl sulfoxide (DMSO). **Figure 8.5a** displays the 7 x 7 μm AFM topography image, showing that indeed a smooth homogenous monolayer can be deposited from DMSO and subsequently grafted.

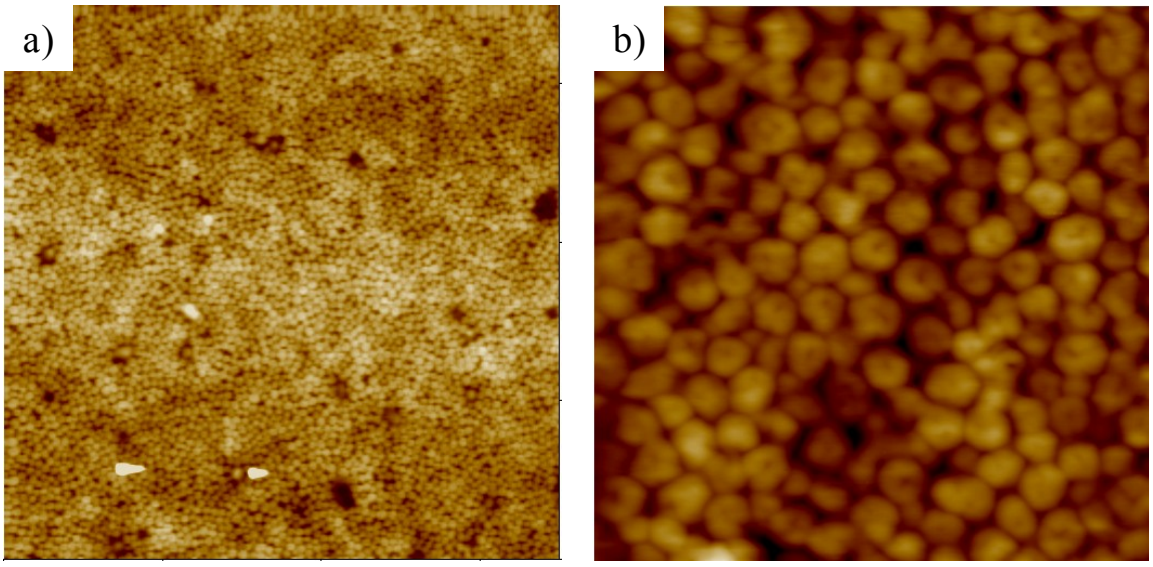

Figure 8.5: AFM topography images of the RAFT-nanogel layer on a silicon wafer after deposition and annealing from DMSO. a) 7 x 7 μm; vertical scale 22nm. B) 1x1 μm; vertical scale 20nm.

However, the major difference that is observed is that the particle height via AFM profile measurements, indicate that the vertical height of the layer is much smaller than for particles deposited from THF. In fact, the measured height of the particles deposited from DMSO was measured to be approximately 10-12 nm. Therefore, the dry state apparent diameter of a perfect spherical particle calculated from the volume from **Equation (7.2)** was found to be 44nm. However, the horizontal distance was measured

to be roughly equal to that of THF deposited layers (~97nm), leading to similar particle densities, ~139 particles per μm^2. Due to the diameter decrease of the RAFT-nanogels, there was an apparent 15 fold increase in the amount of particles per μm^2 area as compared to the free radical precipitation polymerization as observed in **Chapter 7**.

It is apparent that the shapes of the particles are different after deposition in THF or DMSO. We attribute this to the large difference in vapor pressures (THF – 143mmHg at 20°C, and DMSO – 0.417mmHg at 20°C) of the respective solvents and the solubility of polyacrylic acid components of the RAFT agent. The slow evaporation rate of DMSO allows the soft particles to interact and spread on the surface much like the pancake structures found from nanogels synthesized in **Chapter 7.** Indeed the horizontal distance of the individual particles are independent of solvent choice, however the DMSO deposited particles vertically collapse, resembling a biconcave shape with a thin disc like center, increasing the surface area to volume ratio.

Additionally, the polyacrylic acid moiety in the RAFT agent causes solubility differences between solutions casted from THF and DMSO. The RAFT agent was synthesized to contain approximately 103 AAc repeat units within the macroRAFT agent. THF is known to be a relatively poor solvent for poly(acrylic acid). Therefore, when the particles are deposited from THF, we foresee the poly(acrylic acid) chains collapsing around the perimeter of the gels causing swelling of the interior gel and the immergence of an AAc shell on outer edge of the nanogel. An overall illustration is displayed in **Figure 8.6**. This is evidence towards the observation of spherical particles deposited on

the surface of silicon wafers from THF. However, DMSO is a good solvent for poly(acrylic acid) and PNIPAM. Therefore, the particles are completely swollen, and absent of an outer collapsed shell of AAc. The deposition of gels in such a state, coupled with low vapor pressures gives the particles time to orient and interact with the surface. The low vapor pressure and subsequently slower evaporation rate of solvent from the particle layers, coupled with high solubility of nanogels causes a collapse of the soft particles leading to different conformation of grafted particles. We foresee this being an interesting topic of further exploration in the future, as creating particles with increased surface area to volume may be beneficial for diffusion and gas permeability applications.

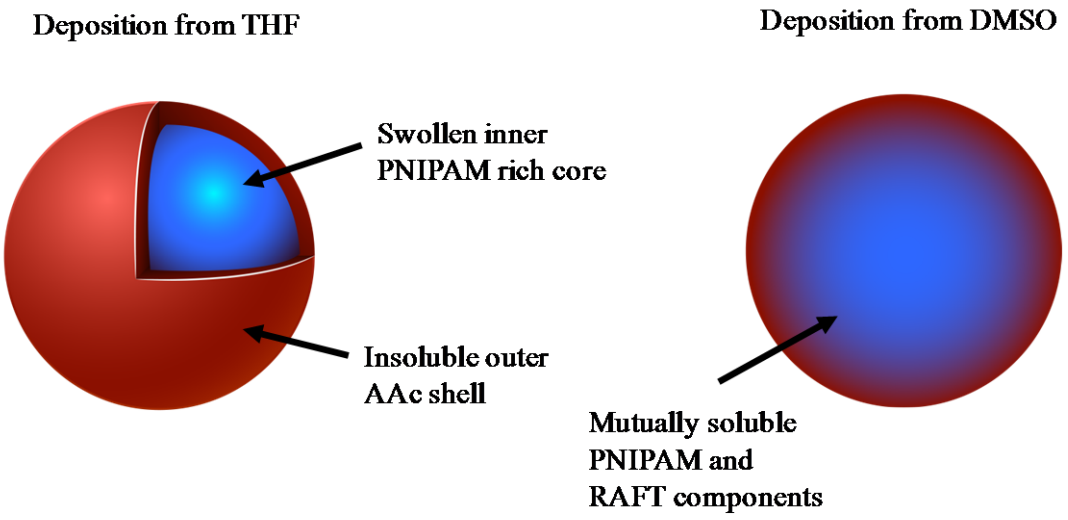

Figure 8.6: Schematic illustration of nanogels deposited from THF and DMSO. Deposition from THF creates a collapsed outer shell while deposition of DMSO induces a complete swollen particle.

8.3.4:Grafting of Nanogels to PVDF Fibers

Complex surfaces of yarns of PVDF fibers (**Figure 8.7a-d**) were modified with the synthesized particles as well. To first verify the original attachment of PGMA, we used Rhodamine B-labeled PGMA to visualize the attachment of the anchoring layer to the yarns. To confirm this, fluorescent microscopy was used to image the fibers (**Figure 8.7b**).

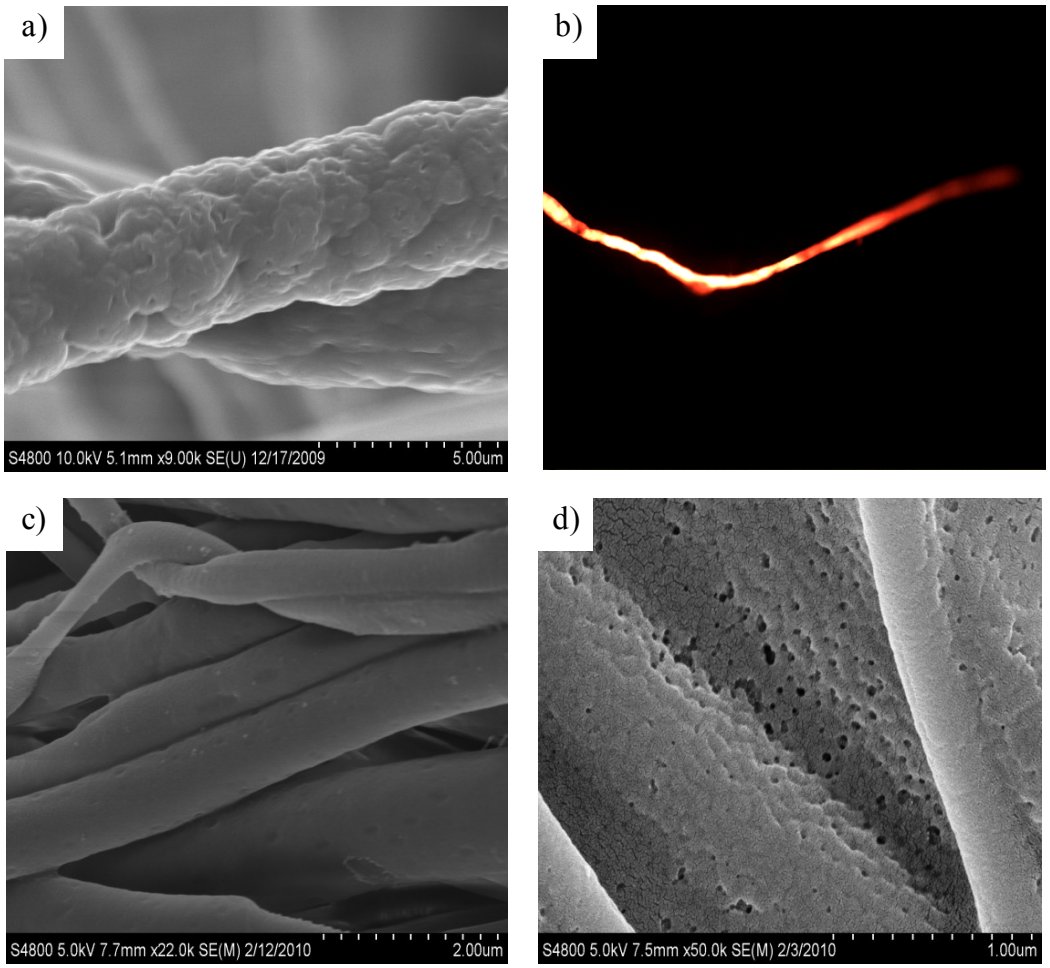

Figure 8.7: a) SEM images of virgin PVDF fibers; (b) fluorescent microscopy image of PVDF fiber modified with Rhodamine-B-labeled PGMA; (c) SEM image of PGMA-modified fibers; (d) SEM image fibers grafted with PNIPAM nanogels. Scale bar: (a) 5 μm; (c) 2 μm; (d) 1 μm

Before and after SEM images (**Figure 8.7a and c**) confirms that there was attachment of the anchoring layer to PVDF yarns. After the surface attachment of PGMA was confirmed, nanogels were deposited and grafted to the surface of the PVDF fibers. SEM imaging of the particle modified fiber is shown in **Figure 8.7d**. The image confirms the successful attachment of particles to the surface of the PVDF fibers. The image clearly shows that these particles cover the curved and complex substrate, not only on the surface, but the crevices and pores created between subsequent single fibers.

8.4:Conclusion

The PNIPAM-containing nanogels were successfully synthesized *via* a RAFT aqueous dispersion polymerization. The Macro-RAFT agent served as the species contributing the carboxy functionalities, but also as the stabilizing agent of the polymerization. FT-IR analysis demonstrated the inclusion of the free carboxylic groups from the macro-RAFT agent along with amide bands due to PNIPAM. Moreover, the macro-RAFT synthesis allows for more control over the reaction resulting in smaller diameter particles compared with previous free radical approaches undertook in **Chapter 7.** AFM topography images confirmed that indeed smaller nanogels were synthesized. Morphology of particles deposited on substrate surfaces demonstrated "pancake" morphology, similarly seen in prior results within **Chapter 7**, whereas the vertical and horizontal height was measured as 45 and 98nm respectively by AFM.

Dry grafted layer thickness was found to be tunable via choice of solvent for dip-coating. DMSO, a low vapor pressure solvent for dip-coating, and a good solvent for the

PAAc RAFT moiety, created particles that exhibited a biconcave structure with a thin disc like center. The AFM vertical and horizontal height was found to be 12 and 97nm respectively. However, only the vertical height differed from layers deposited from THF. The resulting decrease in vertical height and similar horizontal diameter created particles with a biconcave structure. The dry-state calculated diameter of perfect spherical particles was found to be 44 and 75nm deposited from DMSO and THF respectively. Although, both diameters were smaller than nanogels synthesized by free radical polymerization.

Analysis indicated that a monolayer of thermoresponsive PNIPAM nanogels synthesized in this fashion were grafted to the surface of silicon wafers and PVDF yarns successfully. This was achieved by utilizing the "grafting to" approach using PGMA as a macromolecular anchoring layer. AFM and SEM studies demonstrate the ability to cover various substrates in a monolayer fashion. DLS studies show that particles exhibit a volume phase transition within the temperature region of 27-32°C. In our case, the copolymerization of AAc and NIPAM did not cause a markedly increase in the LCST of the nanogels, due to expected low intrachain hydrogen bonding of AAc and NIPAM units. We attribute this to the mechanism of synthesis, resulting in a core of PNIPAM and an outer hairy shell rich AAc region.

Overall, the results obtained show that placement of the carboxy groups do not seem to play an important role on grafting to the surface. It also is possible to gain flexibility in choosing different functional species one can introduce into the formed

particles. Researchers have the ability to tune the size and functionality of nano- or microgels, with the opportunity to graft thermally responsive polymer layers that can overcome thickness limitations associated with conventional "grafting to' methods, but also retain the ease and straightforwardness of the technique with a comparable modified approach.

8.5:References

1. Kaholek, M.; Lee, W. K.; Ahn, S. J.; Ma, H. W.; Caster, K. C.; LaMattina, B.; Zauscher, S., Stimulus-responsive poly(n-isopropylacrylamide) brushes and nanopatterns prepared by surface-initiated polymerization. *Chemistry of Materials* **2004,** *16* (19), 3688-3696.

2. Bittrich, E.; Kuntzsch, M.; Eichhorn, K. J.; Uhlmann, P., Complex ph- and temperature-sensitive swelling behavior of mixed polymer brushes. *Journal of Polymer Science Part B-Polymer Physics 48* (14), 1606-1615.

3. Balamurugan, S.; Mendez, S.; Balamurugan, S. S.; O'Brien, M. J.; Lopez, G. P., Thermal response of poly(n-isopropylacrylamide) brushes probed by surface plasmon resonance. *Langmuir* **2003,** *19* (7), 2545-2549.

4. Plunkett, K. N.; Zhu, X.; Moore, J. S.; Leckband, D. E., Pnipam chain collapse depends on the molecular weight and grafting density. *Langmuir* **2006,** *22* (9), 4259-4266.

5. Schmidt, S.; Zeiser, M.; Hellweg, T.; Duschl, C.; Fery, A.; Mohwald, H., Adhesion and mechanical properties of pnipam microgel films and their potential use as switchable cell culture substrates. *Advanced Functional Materials* **2010,** *20* (19), 3235-3243.

6. FitzGerald, P. A.; Dupin, D.; Armes, S. P.; Wanless, E. J., In situ observations of adsorbed microgel particles. *Soft Matter* **2007,** *3* (5), 580-586.

7. Kuckling, D.; Vo, C. D.; Wohlrab, S. E., Preparation of nanogels with temperature-responsive core and ph-responsive arms by photo-cross-linking. *Langmuir* **2002,** *18* (11), 4263-4269.

8. Zhang, J. T.; Liu, X. L.; Fahr, A.; Jandt, K. D., A new strategy to prepare temperature-sensitive poly(n-isopropylacrylamide) microgels. *Colloid and Polymer Science* **2008,** *286* (10), 1209-1213.

9. Lyon, L. A.; Meng, Z. Y.; Singh, N.; Sorrell, C. D.; John, A. S., Thermoresponsive microgel-based materials. *Chemical Society Reviews* **2009,** *38* (4), 865-874.

10. Ying, L.; Kang, E. T.; Neoh, K. G., Synthesis and characterization of poly(n-isopropylacrylamide)-graft-poly(vinylidene fluoride) copolymers and temperature-sensitive membranes. *Langmuir* **2002,** *18* (16), 6416-6423.

11. Da Silva, R. M. P.; Mano, J. F.; Reis, R. L., Smart thermoresponsive coatings and surfaces for tissue engineering: Switching cell-material boundaries. *Trends in Biotechnology* **2007,** *25* (12), 577-583.

12. Jagur-Grodzinski, J., Polymeric gels and hydrogels for biomedical and pharmaceutical applications. *Polymers for Advanced Technologies 21* (1), 27-47.

13. Rieger, J.; Grazon, C.; Charleux, B.; Alaimo, D.; Jerome, C., Pegylated thermally responsive block copolymer micelles and nanogels via in situ raft aqueous dispersion polymerization. *Journal of Polymer Science Part a-Polymer Chemistry* **2009,** *47* (9), 2373-2390.

14. Shen, W. Q.; Chang, Y. L.; Liu, G. Y.; Wang, H. F.; Cao, A. N.; An, Z. S., Biocompatible, antifouling, and thermosensitive core-shell nanogels synthesized by raft aqueous dispersion polymerization. *Macromolecules 44* (8), 2524-2530.

15. Yan, L.; Tao, W., One-step synthesis of pegylated cationic nanogels of poly(n,nâ€²-dimethylaminoethyl methacrylate) in aqueous solution via self-stabilizing micelles using an amphiphilic macroraft agent. *Polymer 51* (10), 2161-2167.

16. Sun, X.-L.; He, W.-D.; Li, J.; Li, L.-Y.; Zhang, B.-Y.; Pan, T.-T., Raft cryopolymerizations of n,n-dimethylacrylamide and n-isopropylacrylamide in moderately frozen aqueous solution. *Journal of Polymer Science Part A: Polymer Chemistry* **2009,** *47* (24), 6863-6872.

17. Seeber, M.; Zdyrko, B.; Burtovvy, R.; Andrukh, T.; Tsai, C.-C.; Owens, J. R.; Kornev, K. G.; Luzinov, I., Surface grafting of thermoresponsive microgel nanoparticles. *Soft Matter*.

18. Zheng, Q.; Zheng, G.-h.; Pan, C.-y., Preparation of nano-sized poly(ethylene oxide) star microgels via reversible addition-fragmentation transfer polymerization in selective solvents. *Polymer International* **2006,** *55* (9), 1114-1123.

19. McLeary, J. B.; Klumperman, B., Raft mediated polymerisation in heterogeneous media. *Soft Matter* **2006,** *2* (1), 45-53.

20. Burtovyy, O.; Klep, V.; Chen, H. C.; Hu, R. K.; Lin, C. C.; Luzinov, I., Hydrophobic modification of polymer surfaces via "grafting to" approach. *Journal of Macromolecular Science Part B-Physics* **2007,** *46* (1), 137-154.

21. Tsyalkovsky, V.; Klep, V.; Ramaratnam, K.; Lupitskyy, R.; Minko, S.; Luzinov, I., Fluorescent reactive core-shell composite nanoparticles with a high surface concentration of epoxy functionalities. *Chemistry of Materials* **2008,** *20* (1), 317-325.

22. Miles, W. C.; Goff, J. D.; Huffstetler, P. P.; Mefford, O. T.; Riffle, J. S.; Davis, R. M., The design of well-defined pdmsâ€“magnetite complexes. *Polymer 51* (2), 482-491.

23. Bokias, G.; Staikos, G.; Iliopoulos, I., Solution properties and phase behaviour of copolymers of acrylic acid with n-isopropylacrylamide: The importance of the intrachain hydrogen bonding. *Polymer* **2000,** *41* (20), 7399-7405.

24. Qiu, X. P.; Kwan, C. M. S.; Wu, C., Laser light scattering study of the formation and structure of poly(n-isopropylacrylamide-co-acrylic acid) nanoparticles. *Macromolecules* **1997,** *30* (20), 6090-6094.

25. Shibayama, M.; Tanaka, T., Small-angle neutron-scattering study on weakly charged poly(n-isopropyl acrylamide-co-acrylic acid) copolymer solutions. *Journal of Chemical Physics* **1995,** *102* (23), 9392-9400.

26. Chen, G. H.; Hoffman, A. S., Graft-copolymers that exhibit temperature-induced phase-transitions over a wide-range of ph. *Nature* **1995,** *373* (6509), 49-52.

27. Zdyrko, B.; Iyer, K. S.; Luzinov, I., Macromolecular anchoring layers for polymer grafting: Comparative study. *Polymer* **2006,** *47* (1), 272-279.

28. Zdyrko, B.; Hoy, O.; Kinnan, M. K.; Chumanov, G.; Luzinov, I., Nano-patterning with polymer brushes via solvent-assisted polymer grafting. *Soft Matter* **2008,** *4* (11), 2213-2219.

29. Burtovyy, O.; Klep, V.; Turel, T.; Gowayed, Y.; Luzinov, I., *Polymeric membranes: Surface modification by "grafting to" method and fabrication of multilayered assemblies, in nanoscience and nanotechnology for chemical and biological defense, editors: Nagarajan, r.; zukas, w.; hatton, t. A.; lee, s.* ACS Symposium Series 1016, Washington DC: 2009; p 289-305.

30. Zdyrko, B.; Klep, V.; Luzinov, I., Universal platform for surface modification employing grafted polymer layers. *Material Matters* **2008,** *3* (2), 44-47.

31. Luzinov, I. A.; Swaminatha Iyer, K. L.; Klep, V. Z.; Zdyrko, B. V. Surface graft modification of substrates, us patent 7,026,014 b2, apr. 11, 2006. 2006.

32. Horecha, M.; Senkovskyy, V.; Synytska, A.; Stamm, M.; Chervanyov, A. I.; Kiriy, A., Ordered surface structures from pnipam-based loosely packed microgel particles. *Soft Matter* **2010,** *6* (23), 5980-5992.

33. Schmidt, S.; Hellweg, T.; von Klitzing, R., Packing density control in p(nipam-co-aac) microgel monolayers: Effect of surface charge, ph, and preparation technique. *Langmuir* **2008,** *24* (21), 12595-12602.

34. Schmidt, S.; Motschmann, H.; Hellweg, T.; von Klitzing, R., Thermoresponsive surfaces by spin-coating of pnipam-co-paa microgels: A combined afm and ellipsometry study. *Polymer* **2008,** *49* (3), 749-756.

35. Klep, V.; Zdyrko, B.; Luzinov, I., Pnipaam gradient polymer brushes. *PMSE Preprints* **2005,** ***93***, 462.

36. Hofl, S.; Zitzler, L.; Hellweg, T.; Herminghaus, S.; Mugele, F., Volume phase transition of "smart" microgels in bulk solution and adsorbed at an interface: A combined afm, dynamic light, and small angle neutron scattering study. *Polymer* **2007,** *48* (1), 245-254.

CHAPTER 9:SUMMARY

The dissertation provides the work on synthesis of thermally responsive polymer layers via well defined block copolymers and functionalized cross-linked nanogels. The outline provides the basis for future development for the design of polymer layers towards surfaces with well defined and controllable properties toward protein adsorption, temperature triggered on-demand delivery coatings, and variable thicknesses of polymer coatings on complex surfaces for temperature controllable surface wetting properties.

9.1:Synthesis of thermally responsive polymer layers via reactive block copolymers in one-step (SSB layers):

Well defined block copolymers (BCP) consisting of Poly (*N*-isopropylacrylamide) (PNIPAM) and the surface reactive monomer glycidyl methacrylate (GMA) were deposited in a single step method. The reported experiments demonstrated that 100% retainable films can be achieved through annealing as-deposited films at 130°C. The anchoring was found to be independent of film thickness. Atomic force microscopy imaging revealed that the resulting morphology of the single step brush (SSB) films of PNIPAM were smooth and fully covered the substrate. In fact, calculations showed that the PNIPAM brush layers were well within the brush regime. By regulating the length of the GMA block, it is possible to pre-define the grafting density of the films, yielding controllable properties as a function of temperature in aqueous environments.

Advancing contact angle measurements indicated variations in the magnitude of contact angle change at the measurement temperatures for different GMA block lengths in the BCPs. Interestingly, SSB-1 layers (highest ratio of PNIPAM to PGMA in the

BCP) showed greater contact angle switchabilty between the measurements temperatures as compared to PNIPAM brush layers fabricated by the conventional "grafting to" technique. In-situ ellipsometry measurements showed that all three PNIPAM SSB layers reversibly swelled and collapsed in aqueous environments as function of temperature. However, by tuning the amount of GMA in the BCP, the grafting density was changed, as well as the overall magnitude of swelling and collapse thicknesses measured as a function of temperature. Angle resolved x-ray photon spectroscopy (ARXPS) revealed that PNIPAM was preferentially located at the polymer air interface of the film, giving evidence as to why thermally-responsive properties were retainable by our methods.

9.2:Studies of protein adhesion and adsorption on SSB layers:

The interaction of fibrinogen protein and the PNIPAM SSB layers where characterized by AFM colloidal probe technique and protein adsorption experiments. Work of adhesion values for all PNIPAM SSB layers was found to be unique at each BCP composition. By changing the GMA content in the initial BCP, the protein adhesion values were altered, yielding an effective method for the creation of well-defined layers with controllable protein interaction properties. SSB-1 films showed practically no adhesion towards fibrinogen below the LCST of PNIPAM. However with increasing GMA content in the film, the adhesion (< LCST) increased. At temperatures above the LCST, the three PNIPAM films showed a significant increase in work of adhesion values.

Protein adsorption behavior was manipulated in much the same way as adhesion. Again, all three PNIPAM SSB films showed unique protein adsorption behavior at

temperatures above and below the LCST of PNIPAM. The highest ratio of PNIPAM in the BCP garnered films that effectively repelled protein (T < LCST) or adsorbed a monolayer (T >LCST). As the content of GMA in BCP was increased, the change in protein adsorption as a function of temperature decreased. In fact, at the highest amount of GMA in the BCP, protein adsorption was constant within the uncertainties of the experiment, at both measurement temperatures.

The switching resiliency of the highly switchable SSB-1 was evaluated for protein adhesion properties after being subjected to layer abrasion. In fact, the SSB damaged film was found to have comparable properties to intact conventional PNIPAM brush films. However, the SSB brush films showed a larger decrease in properties after wear as compared to the conventional surfaces. When the SSB-1 layer switching resiliency was studied as a function of abrasion depth, it was found that after high levels of wear, the layer becomes non-switchable and totally protein repellent. This was found to be typical of low molecular weight PNIPAM layers.

9.3:Synthesis of Poly(ethylene glycol) layers via one-step method:

The deposition of well defined GMA containing reactive block copolymers proved to be a universal approach towards the creation of well defined polymer brush layers. Further, block copolymers containing GMA and poly(ethylene glycol) (PEG) were deposited at varying ratios of GMA. The PEG layers were found to form smooth and homogenous layers. Interestingly, the PEG BCP layers displayed their own thermo-responsive actuation behavior at 23 and 65°C. It was found that the PGMA block segment provided a hydrophobic platform for the PEG chains to collapse upon. By

subsequently changing the ratio of GMA in the BCP film, the overall magnitude of layer thickness change decreased with increasing GMA. In conclusion, the single-step method for the formation of polymer brush films proved to be a candidate for the fabrication of mixed brush films as well.

9.4:Extension of one-step layer formation for mixed brush films:

The single step layer approach for the formation of responsive block copolymer films was extended to the fabrication of mixed brush films. Mixed brush films containing two reactive BCPs, namely PNIPAM-*b*-PGMA, and PEG-*b*-PGMA were deposited onto silicon substrates from a single solution containing known ratios of both block copolymers. SSB-1 and PEG-3 BCP were firstly mixed in a 50:50 weight by volume solution in MEK, and studied for their swelling/collapse, and protein interaction behavior. In-situ ellipsometry showed that the mixed brush film indeed underwent a thermally responsive layer thickness change, however, the magnitude was smaller that of PNIPAM layers.

Work of adhesion values as measured by AFM colloidal probe technique was used to study single step mixed brush films in 50:50 and 75:25 PNIPAM to PEG films. Both mixed brush films showed thermally responsive layer thickness change as a function of temperature. The 75/25 film proved to be more hydrophilic at both measurements temperatures than pure SSB-2 films. Interestingly, as more PEG was added via the one-step method, the surface became slightly more adhering toward fibrinogen at both measurement temperatures due to the increase in GMA in the block copolymer films.

However, fibrinogen adsorption experiments displayed trends toward the future goal of on-demand active delivery coatings. The mixed brush films became practically totally protein repelling at both temperatures. We foresee this is due to the fact that at temperatures below the LCST of PNIPAM, both PEG and PNIPAM are extended and hydrated, creating a hydrophilic and protein repellent properties. When the temperature is increased above the transition temperature of PNIPAM (~42°C), the PNIPAM chains collapse towards the substrate while PEG chains remain swollen and stretched away from the substrate surface. This type of behavior effectively retains the protein repelling properties of the film.

9.5:Synthesis and characterization of thermally responsive polymer film formed from functionalized nanogels:

PNIPAM containing thermoresponsive nanogels were synthesized in the presence of acrylic acid in order to provide carboxyl functionalities for the attachment to PGMA anchoring layers. Monolayers of the polymeric particles was successfully deposited on silicon wafers, glass slides, poly(vinylidene fluoride) (PVDF) fibers, and tungsten wires. The particles were deposited on the different substrates by the "grafting to" procedure. AFM and SEM imaging demonstrated the uniform and monolayer formation.

Akin to conventional PNIPAM films, the grafted nanogel monolayer demonstrated reversible swelling collapsing behavior at temperatures below and above the transition temperature for PNIPAM. Further, the amount of swelling and collapse could be tuned by the amount of acrylic acid contained in the nanogel particles. On the flat model substrates, contact angle measurements displayed a 20° change between the

measurement temperatures. Wettability testing results on the tungsten wire demonstrated that the PNIPAM nanogels retain their ability to undergo morphological changes on complex curves surfaces.

Overall, the results demonstrated that PNIPAM nanogel layers grafted to surfaces are comparable in performance to conventional PNIPAM brush layers with respect to their thermo-responsive behavior.

9.6:Synthesis and characterization of thermally responsive films fromed from nanogels by reversible addition fragmentation chain transfer (RAFT) polymerization technique:

PNIPAM containing nanogels were successfully synthesized utilizing a RAFT aqueous dispersion polymerization. The macroRAFT agent was designed to contain acrylic acid units in the backbone of the chain transfer agent. This was done in order to provide the carboxyl functionality for the attachment of particles to a PGMA anchoring layer. The macroRAFT agent serves as the stabilizing agent and polymerization control agent for the reaction. AFM and DLS measurements indicated the particle diameter was approximately 100nm in low temperature aqueous conditions. This was a significant size decrease as compared to our previous work where particles had a diameter of approximately 250 nm in the same conditions. AFM demonstrated a similar pancake morphology of the particle layers bound to a substrate, similar to our PNIPAM nanogel layers synthesized by the free radical precipitation polymerization.

Interestingly, it was found that the layer thickness could be tuned by the deposition solvent used. High vapor pressure solvents like THF created particle layers

with thicknesses close to 97 nm. However when using a low vapor pressure solvent like DMSO, the particle thickness decreased to roughly 12nm. The RAFT nanogel particles were also successfully grafted in a monolayer fashion to PVDF yarns, validated by SEM imaging. Dynamic light scattering (DLS) studies indicated the LCST was in the 27-32°C range. Particles underwent a roughly 20nm change in diameter in aqueous conditions as a function of temperature.

9.7:Publications and Presentations

The above mentioned research resulted in publications and presentations listed below from August 2008 to August 2013.

9.7.1:Publications

1. **M. Seeber,** Zydrko,B; Burtovvy, R; Andrukh, T. "Surface grafting of thermoresponsive microgel nanoparticles." Soft Matter, **2011**, 21, 9962-9971
2. Lovingood, D, Owens, J; **Seeber, M**; Kornev, K; Luzinov, I. "Controlled Microwave-Assisted Growth of Silica Nanoparticles under Acid Catalysis". ACS Appl. Mater. Interfaces, 2012, **DOI:** 10.1021/am3020247
3. **Seeber**, **Michael J**.; Zdyrko, Bogdan; Rieger, Jutta; Boisse, Stephanie; Tsai, Chen-Chih; Kornev, Konstantin; Luzinov, Igor. Characterization and surface grafting of thermally responsive carboxy functionalized PNIPAM nanogels synthesized via RAFT aqueous dispersion polymerization. Polymer Preprints **2010**, 51(2), 578-579.
4. **Seeber, Michael J**.; Lokitz, B; Burtovyy, R., Kilbey II, S.M., Luzinov, I. "One-step synthesis of thermally responsive polymer brushes". *(Prepared for Submission, Expected 6/13)*
5. **Seeber, Michael J**.; Lokitz, B; Burtovyy, R., Kilbey II, S.M., Luzinov, I. "Tuning the properties of thermally responsive polymer brush films by one-step synthetic process." *(Prepared for Submission, 8/13)*

9.7.2:Presentations

1. **M. Seeber,** et al., "One-step synthesis of thermally responsive polymer brushes for control of surface properties and biological interaction." American Chemical Society National Meeting, New Orleans, LA, 2013, oral.
2. **M. Seeber,** et al., "One-step synthesis of thermally responsive mixed polymer brushes." American Chemical Society National Meeting, New Orleans, LA, 2013, poster.
3. **M. Seeber,** et. al., "Using PNIPAM nanogels in controlling the wettability properties of nano-probing devices." American Chemical Society National Meeting, Anaheim, CA, 2011, oral presentation.
4. **M. Seeber,** et. al., "Surface Modification with PNIPAM containing nanogels." American Chemical Society National Meeting, Boston, MA, August 2010, oral presentation.
5. **M. Seeber,** et. al., "Surface Modification with PNIPAM containing nanogels." American Chemical Society National Meeting, San Diego, CA, March 2012, poster presentation.
6. **M. Seeber,** et. al., "Characterization and surface grafting of thermally responsive carboxy functionalized PNIPAM nanogels synthesized via RAFT aqueous dispersion polymerization." American Chemical Society National Meeting, Boston, MA, March 2010, poster presentation.
7. **M. Seeber,** et. al., "Surface Modification with PNIPAM containing nanogels." American Chemical Society National Meeting, Washington DC, August 2009, poster presentation.

CHAPTER 10:FUTURE WORK

The work presented here provided the results on the synthesis and characterization of thermally responsive polymer layers by modified "grafting to" procedures. Reactive block copolymers gave a basis for future modification of different substrates for biomedical devices with controllable protein adsorption by changing the initial composition of the PGMA block segment. However, there are number of questions that should be addressed in future work:

1) Further evaluation of protein adsorption on block copolymer brush films as a function of temperature and block segment length.

In this work only a single protein, bovine fibrinogen, was used for protein adsorption studies to the various reactive block copolymers discussed. However, there are a large variety of various proteins with different size, shape, and surface charge in human blood. Therefore, it is likely that different proteins will have different interactions with the polymer brush layers and mixed polymer brush layers. Moreover, various proteins, and mixtures of proteins will be studied *in-situ* under static and dynamic conditions. The work will be done utilizing *in-situ* spectroscopic (ATR-IR) ellipsometry measurements. Therefore, the brush swelling, and liquid intake into the film can be monitored as well as any adsorption band changes in the mid-infrared spectrum due to adsorption or desorption of proteins. We can also investigate whether preferential protein adsorption is apparent from biological media. We can additionally utilize quartz micro balance measurements to further deduce a more accurate

investigation into the amount of protein adsorbed onto various PNIPAM brush layers formed from reactive block copolymers.

2) Study the effect of poly(*N*-isopropylacrylamide) (PNIPAM) actuation behavior when grafted in a matrix of polyethylene glycol matrix.

In this work, we measured the overall swelling and collapse of the mixed brush layers as a function of temperature. From protein adsorption and *in-situ* ellipsometry measurements in this work, we observed evidence that the PNIPAM-PEG mixed brush systems is a strong candidate for an active on demand delivery coating. However, utilizing the spectroscopic (ATR-IR) ellipsometry we can observe the changes in the adsorption bands of the polymer layers during the swelling and collapse. The beam will be reflected from the underside of the substrate, therefore we can effectively observe the amide bands in PNIPAM and ether bands in PEG during the swelling and collapse. As PNIPAM swells above the PEG layer, the amide bands should decrease in intensity. When the PNIPAM collapses down on the substrate with increased temperature, amide bands will subsequently increase in intensity. We can compare the actuation at the same temperature changes of PEG (intensity of the ether band), in order to confirm that PEG stays in the swollen state at moderate temperature changes.

3) Attach active ligands to the end of PNIPAM chain fragments and evaluate the ability for PNIPAM chains to deliver and hide fragments within the biocompatible matrix.

As discussed above, in this work, we have laid the foundation for the design of an active on demand delivery coating to facilitate biological processes by mixed brush layers

from reactive block copolymers. As discussed in **Chapter 4** of this work, the PNIPAM block copolymers were synthesized by reversible addition fragmentation chain transfer (RAFT) polymerization. It is well documented in literature that dormant RAFT agents capable of re-activation remain on the end of synthesized macromolecule chains. Therefore, we will utilize the dormant RAFT agents present on the end of the PNIPAM chains in order to initiate the polymerization of short polystyrene (PS) components. Water is a bad solvent for PS, therefore, the PS fragment will collapse into a globule confirmation. With small PS fragments at the terminus of the block copolymer chains, we can further attach ligands such as growth factors to the PS fragments through hydrophobic interactions. Growth factors are a class of naturally occurring substances that can stimulate cell growth, cell proliferation, as well as various other cellular processes. They typically trigger signals between neighboring cells in the human body. Therefore we foresee an on-demand delivery coating being very important for future application towards the on and off signaling of cellular processes from a coating capable of sustaining biological environments. We can monitor the actuation behavior of the delivery ligands by spectroscopic ellipsometry experiments as discussed above.